CONTRACT NUMBER: NAS 9-13004
DRL NUMBER: T-825
DRD NUMBER: MA-129TA
REPORT: MDC E0886

HIGH TEMPERATURE ANTENNA DEVELOPMENT FOR SPACE SHUTTLE

FINAL REPORT

VOLUME II

30 APRIL 1974

MCDONNELL DOUGLAS ASTRONAUTICS COMPANY - EAST

MCDONNELL DOUGLAS CORPORATION

CONTRACT NUMBER: NAS 9-13004
DRL NUMBER: T-825
DRD NUMBER: MA-129TA
REPORT: MDC E0896

COPY NO. 2

HIGH TEMPERATURE ANTENNA DEVELOPMENT FOR SPACE SHUTTLE

FINAL REPORT

VOLUME II
30 APRIL 1974

Prepared by E A Kuhlman
E.A. Kuhlman
Group Engineer, Electronics

Approved by
A.L. Furfine
Manager, Advanced Electronic Techniques

Approved by H L Hotchan
H.L. Hotchan
Director, Avionics Engineering

MCDONNELL DOUGLAS ASTRONAUTICS COMPANY - EAST

Saint Louis, Missouri 63166 (314) 232-0232

MCDONNELL DOUGLAS CORPORATION

ABSTRACT

An S-band antenna system and a group of off-the-shelf aircraft antenna were exposed to temperatures simulating shuttle orbital cold soak and entry heating. Radiation pattern and impedance measurements before and after exposure to the thermal environments were used to evaluate the electrical performance.

The S-band antenna system was exposed to predicted temperature histories (peak 1533 K (2300°F)) at the outer surface of the thermal protection system (TPS) which resulted in antenna and structural skin temperatures of 422 K (300°F). The off-the-shelf antennas, with no TPS, were exposed to predicted entry temperature histories (peak 450 K (350°F)) of the structural skin line.

The results of the electrical and thermal testing are given. The test data showed minor changes in electrical performance and established the capability of these antenna to withstand both the low temperatures of space flight and the high temperatures of entry.

PRECEDING PAGE BLANK NOT FILMED

CONTENTS

PRECEDING PAGE BLANK NOT FILMED

LIST OF PAGES

Title

ii thru xiii
1-1 thru 1-2
2-1 thru 2-2
3-1 thru 3-2
4-1 thru 4-2
5-1 thru 5-64
6-1 thru 6-74
7-1 thru 7-32
8-1 thru 8-2

LIST OF FIGURES

FIGURE

LIST OF FIGURES (CONT.)

FIGURE

LIST OF FIGURES (CONT.)

FIGURE

LIST OF FIGURES (CONT.)

FIGURE

LIST OF TABLES

SUMMARY

The S-band antenna system (designed, fabricated and tested under the original contract) and selected off-the-shelf antennas were subjected to cold temperatures of 172 K (-150°F) and 117 K (-250°F) followed by simulated entry heating which was supplied by a radiant heat source. Preliminary tests were run with the breadboard S-band antenna system to establish the test setup and control procedures required to meet the study objectives.

Test setups and techniques are discussed for simulating both cold space and hot entry environments.

The breadboard unit test results are compared to the results of the plasma heating tests at NASA-JSC. This correlation shows that both types of heating are satisfactory for evaluating antenna and structural integrity. However, the radiant heating technique can match predicted flight surface temperature and pressure history more accurately, but plasma heating gives more realistic flow and gap-heating.

On the first simulated entry heating test of an untested prototype S-band antenna system, a black carbonaceous substance was deposited on the LI-1500 HRSI (high temperature reusable surface insulation) tiles of the antenna window and TPS (thermal protection system). This deposit, which was observed in only trace amounts during the plasma heating tests at NASA-JSC, resulted in significant degradation in antenna pattern shape, gain, axial ratio, and impedance. The prototype unit used in the test at NASA-JSC was substituted and the S-band antenna system tests successfully completed.

The electrical performance of the off-the-shelf antennas, when covered with simulated antenna windows and surrounded by TPS, is discussed and evaluated.

The test results demonstrate that: (1) the S-band antenna system design approach results in hardware which is adequate for surviving both the orbital cold and entry heating environments; and (2) the off-the-shelf antennas electrical performance is satisfactory when covered by an antenna window, and after being subjected to the cold and hot temperatures predicted for orbital and entry flight. Although some post curing of the filler foam in the off-the-shelf antennas occurred when the respective design temperatures were exceeded, the electrical test results for this condition were satisfactory.

CONCLUSIONS

The conclusions reached from an evaluation of the tests results obtained during this study are:

(a) The antenna system design approach developed in the original contract is satisfactory for both the orbital cold and entry heating environments.

(b) Off-the-shelf antennas protected by HRSI antenna windows are capable of withstanding the Space Shuttle Orbiter orbital cold and the entry heating environments.

(c) The effects of the antenna window over the off-the-shelf antenna are minor and can be compensated for in the respective antenna design, if required by overall system consideration.

(d) Entry heating simulation by radiant heating gives results comparable to plasma heating for antennas and basic structural members.

(e) A radiant heat source can be controlled to give a more accurate surface temperature response than a plasma heat source, but temperature distribution differs somewhat between the HRSI surface and structural-skin (e.g., at insulation gaps) due to the different modes of heat transfer.

(f) The ambient pressure can be controlled over a wide range during radiant heating, since the pressure is not a factor in sustaining the heat source process, as it is in a plasma heating facility.

(g) A better temperature control could be obtained on the surface of the OTS antennas by covering this antenna with a thin layer of insulation, attaching a metallic sheet to the insulation, and controlling the temperature of the metallic sheet.

(h) The LI-1500 tile coating showed more cracks after exposure to the 117 K (-250°F) temperature followed by simulated entry heating than was observed in the plasma heating tests or other radiant heating tests.

RECOMMENDATIONS

The work during this study leads to the following recommendations:

(a) The test results obtained during this contract have established: (1) the capability of an antenna window based on the design approach developed during the original contract to withstand the orbital cold and entry heating environments, and (2) the capability of off-the-shelf antennas to withstand the orbital cold and entry heating environments. Therefore, further development testing should be done on specific Orbiter Antenna System designs.

(b) Tests should be conducted to determine how to ensure that the carbonaceous deposit, attributed to the silicone waterproofing in the HRSI tiles, observed in the first S-band antenna system test does not occur during future high temperature tests. Preconditioning or elimination of the silicone in the HRSI tiles over the antennas are possible considerations. Preconditioning eliminates the need for special tiles. and may only be required for testing in a radiant heat facility. Elimination of the silicone requires special handling during processing of the HRSI tiles and preinspection during installation to ensure that the silicone impregnated and unimpregnated tiles are not interchanged.

INTRODUCTION

The purpose of this program was to evaluate the electrical performance of several candidate antenna types, which are suitable for Space Shuttle Orbiter application, after exposure to orbital cold soak followed by simulated entry heating. The antennas evaluated included the S-band antenna system built under the original contract effort and a group of selected off-the-shelf aircraft antennas. The primary objectives were to: (1) expose the S-band antenna system assembly to typical entry heating and pressure profiles in a radiant heat facility with provisions for cold soaking to temperatures of 172 K (-150°F) and 117 K (-250°F) to determine the effects of the applied environment on electrical performance and to define the skin-line temperature profiles for the off-the-shelf aircraft antenna tests; and (2) subject the selected off-the-shelf aircraft antennas to typical skin-line entry heating and pressure profiles in a radiant facility with provisions for cold soaking to temperatures of 172 K (-150°F) and 117 K (-250°F) and determine the effects of the applied environment on the electrical performance. Secondary objectives were to: (1) correlate radiant versus plasma heating for entry environment simulations; and (2) evaluate the effect of a simulated antenna window and TPS on the off-the-shelf aircraft antennas electrical performance.

The candidate antennas were tested in an MDC Mission Environment Simulator. This facility consists primarily of a radiant heat source, a cold box, a vacuum chamber, a controller, and data recording equipment. Test fixtures were designed and fabricated to permit moving the test article between the heat source and the cold box as required.

The effects of the simulated mission environments, orbital cold and entry heating, were evaluated by performing electrical tests, radiation pattern and impedance measurements, after each thermal environment exposure and comparing the results with data from preceding tests and/or reference data.

The test results demonstrate the validity and reuse capability of the basic design concept reported in Volume I of this report. Changes in electrical performance after both low and high temperature exposure were small and within acceptable limits. Physical examination shows the test articles to be in excellent shape after completion of testing, except where the maximum design temperatures were exceeded.

Mr. E. A. Kuhlman, Study Manager, was responsible for overall technical direction of this study. Other members of the McDonnell Douglas Astronautics Company - East (MDAC-E) engineering staff who contributed to this study are L. C. Baranowski, G. R. Gaumer, B. M. Kavanaugh, R. F. Sorensen, and T. Steinmeyer. Messrs. L. C. Baranowski and R. F. Sorensen conducted the thermal and electrical tests and evaluated the resulting data. The thermal test equipment was operated by J. H. Hill, and the antenna pattern range was operated by D. D. Russell, both of the McDonnell Aircraft Company.

Mr. J. S. Kelley of the Antenna System Section of the Telemetry and Communications System Division, Lyndon B. Johnson Space Center, Houston, Texas, was the NASA Technical Monitor for this study.

The units used for the physical quantities defined in this report are given in both the International System of Units (SI) and the U.S. customary units in the text. U.S. Customary units are used in the drawings and in some of the graphs and tables.

This report is designated as Volume II and is additional work related to the work reported in Volume I.

The task numbers used in the text correspond to the tasks given in the Statement of Work, Exhibit B, of Contract NAS9-13004 modification No. 1S.

S-BAND ANTENNA SYSTEM TESTS

The objective of this task (Task 2.3) was to determine the capability of the S-band antenna system to perform electrically after being subjected to orbital cold temperatures of 172 K (-150°F) and 117 K (-250°F) followed by entry heating simulated by a radiant heat source. This also involved part of Task 2.1, which defined the requirements for the test fixture design and instrumentation. Secondary objectives were: (1) to define skin temperature histories for use in the off-the-shelf antenna tests; and (2) to provide data for establishing a correlation between radiant and plasma heating for entry environment simulations. The test article was cooled to the desired initial temperature by radiation to a cold wall and then subjected to a radiant heat source which was controlled to simulate a surface temperature response to a typical Orbiter entry environment. The thermal tests were conducted in a vacuum chamber with the pressure controlled to represent orbital, entry, and arc tunnel conditions. Temperature histories were measured at selected points on the test article. The results of electrical tests, radiation pattern and impedance measurements, and physical examination were used to evaluate the effects of the applied environment.

The initial tests to checkout the test facility and provide data for comparing the radiant and plasma heating technique were run using the breadboard S-band antenna system. No electrical measurements were taken on the breadboard unit.

Prototype No. 2 S-band antenna system was used for tests P2-1 and P2-2. This unit was not used in the thermal tests conducted during the first part of this contract (ref. 1). However, following test P2-1 a carbonaceous deposit was found which resulted in a severe degradation of electrical performance. Therefore, Prototype No. 1 S-band antenna system, which was used for the tests in the NASA-JSC arc tunnel facility, was used for the tests P1-11 through P1-15 required by this contract. (Note: Tests P1-1 through P1-10 were identified as P-1 through P-10 and reported in reference 1). Initial temperatures for tests P2-1 and P2-2 were 327 K (130°F). Initial temperatures for the Prototype No. 1 tests are given in table I. The results of the electrical and thermal tests are given in separate subsections below.

Electrical Testing

The effects of orbital coldsoak and entry heating environments on the electrical performance of the prototype S-band antenna system were determined from radiation pattern and impedance measurements. Measurements were made prior to the start of the thermal tests to establish reference parameters and were repeated after the test. Changes in electrical performance were determined by comparing pre and posttest data. Comparison of data from several tests was used to determine if performance trends developed.

TABLE I
INITIAL TEMPERATURES
FOR
S-BAND ANTENNA SYSTEM TESTS

TEST NO.	INITIAL TEMPERATURE K (°F)
P1-11	172 (-150)
P1-12	172 (-150)
P1-13	294 (+70)
P1-14	327 (+130)
P1-15	117 (-250)

Test configuration. - The S-band antenna system, mounted in the test container assembly, was installed on a rotator unit as shown in figure 1. The radiation patterns were measured with the test article inside a small anechoic chamber with a transmission distance of approximately 2.74 m (9.0 ft).

The impedance measurements were made with the antenna system mounted in the test container assembly and placed above the test equipment as shown in figure 2.

Test techniques. - Standard radiation pattern and impedance measurement techniques were used to obtain the data given in this report. Figure 3 shows a block diagram of a typical test setup used for measuring the radiation patterns. Figure 4 shows a photo of the recording and control console. Impedance measurements were taken with a Hewlett Packard Model 8410A Network Analyzer System as shown in figure 2. Figure 5 shows a block diagram of a typical test setup for swept frequency impedance measurements.

Radiation patterns were measured using both rotating linear and circular polarizations. Rotating linear polarization provides a continuous axial ratio measurement. The linear field was obtained using a Scientific Atlanta SGH-1.7 horn. A helix (constructed for these tests) was used as a transmitting antenna to obtain the circularly polarized patterns. The axial ratio of the helix antenna ranged from 1.5 to 2.0 dB over the test frequency range. The axial orientation of the helix was held constant in order to eliminate the effects of axial ratio when comparing patterns from successive tests.

The radiation patterns were recorded on standard 40 dB polar graph paper. The linear isotropic gain level was measured using a standard gain horn and recorded on each pattern. The linear isotropic reference (LIR) level was

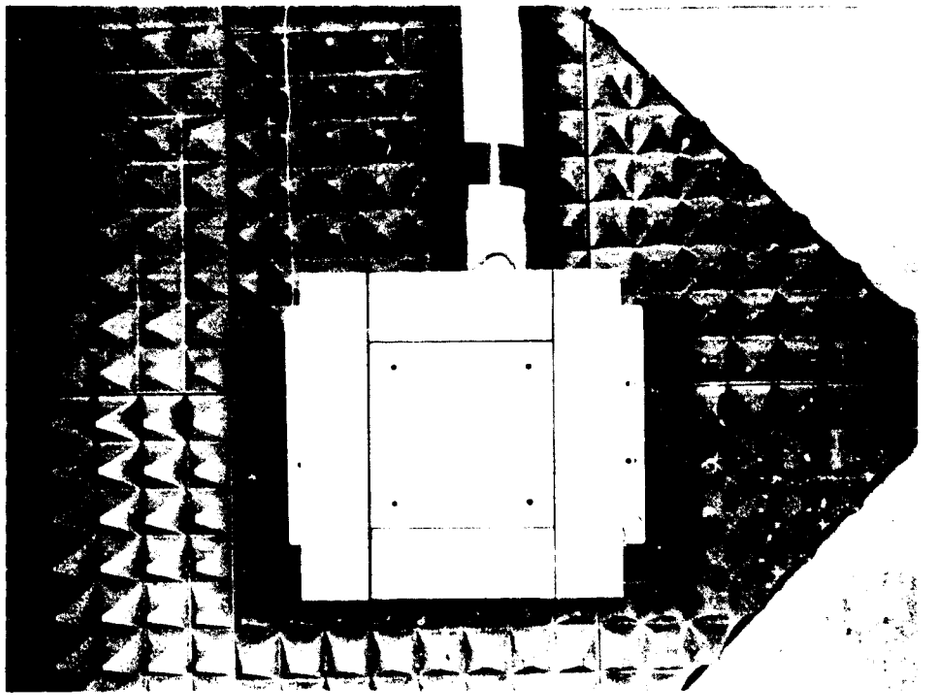

Front View

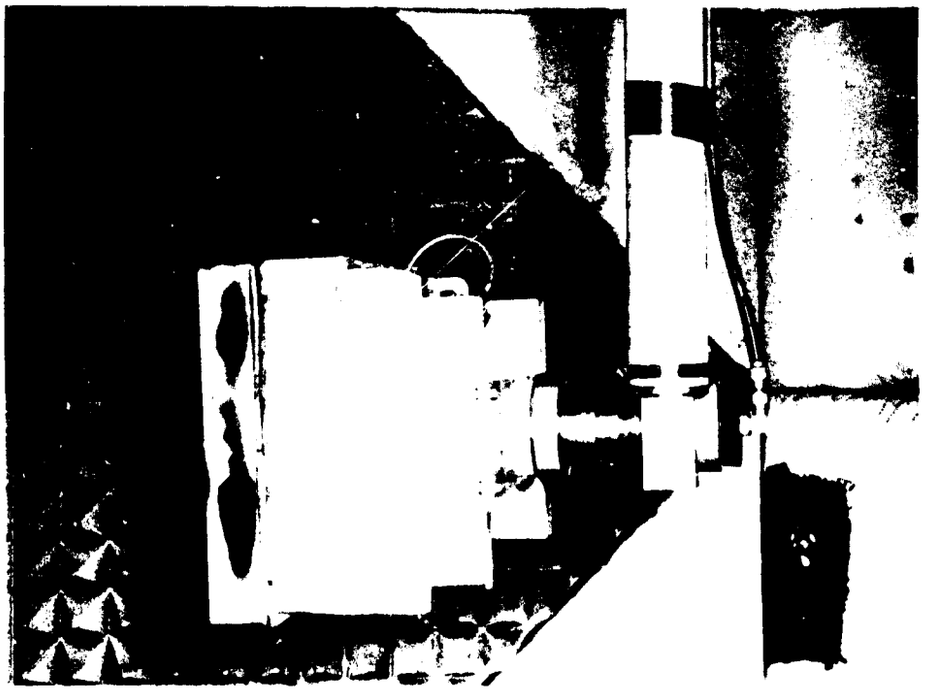

Side View

FIGURE 1 RADIATION PATTERN MEASUREMENT TEST CONFIGURATION FOR S-BAND ANTENNA SYSTEM

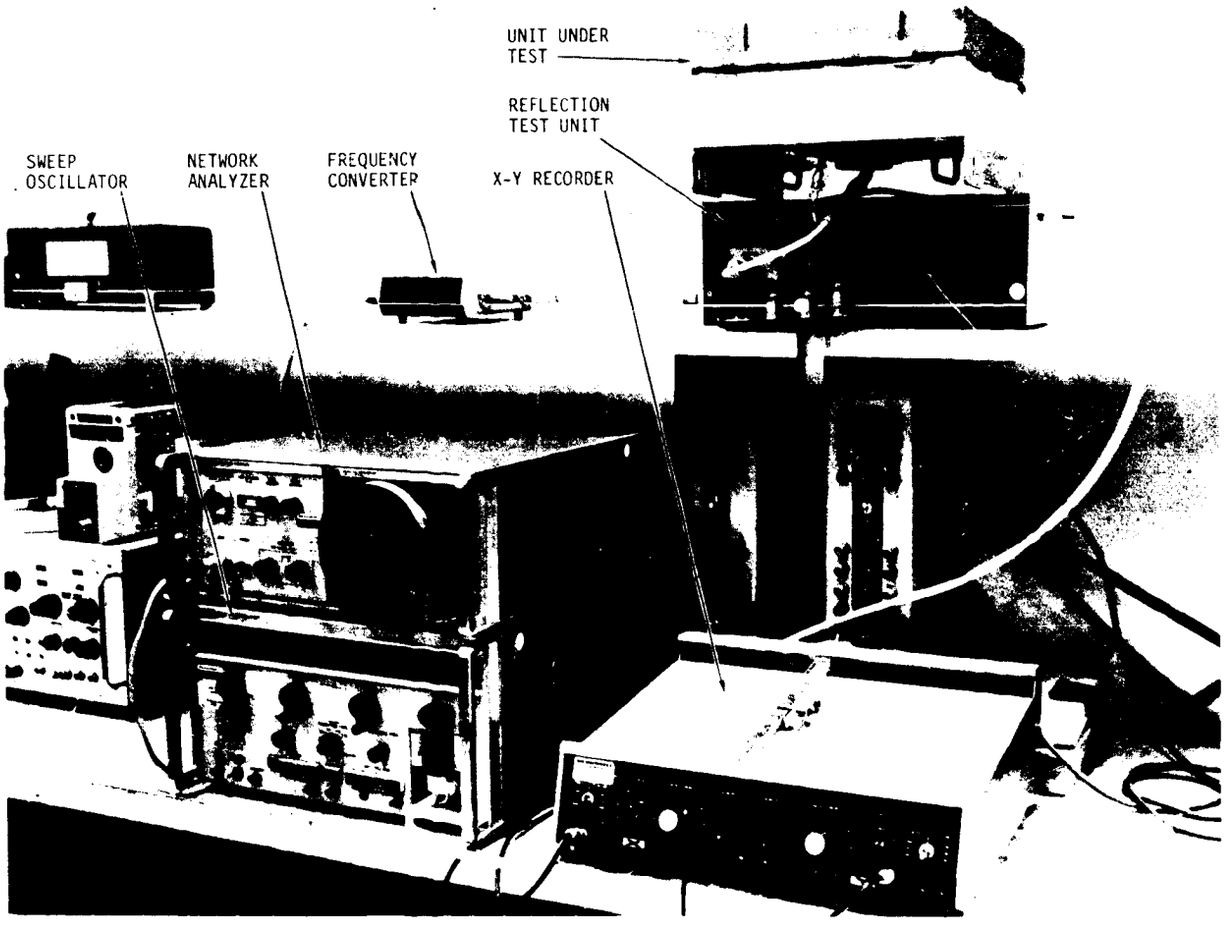

FIGURE 2 IMPEDANCE MEASUREMENT TEST CONFIGURATION FOR S-BAND ANTENNA SYSTEM

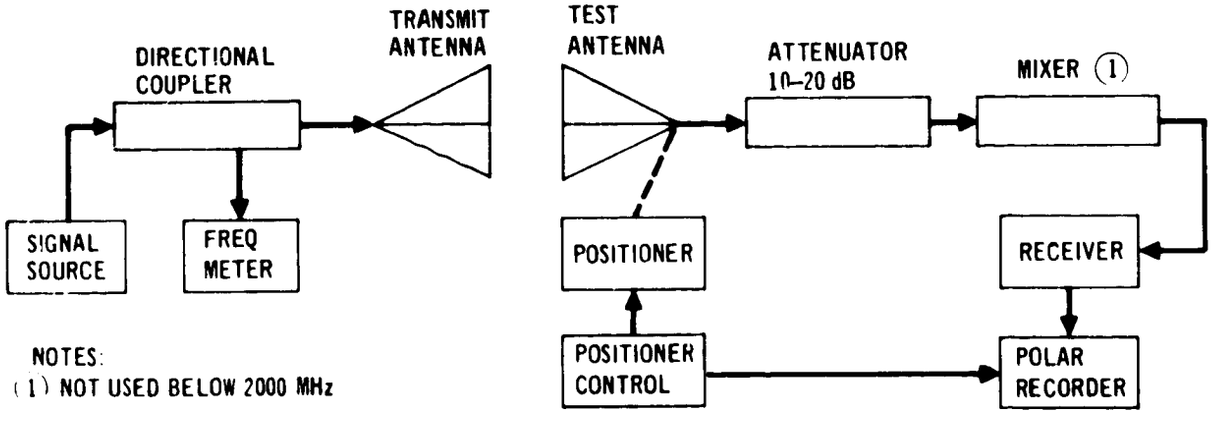

FIGURE 3 RADIATION PATTERN MEASUREMENT TEST SETUP BLOCK DIAGRAM

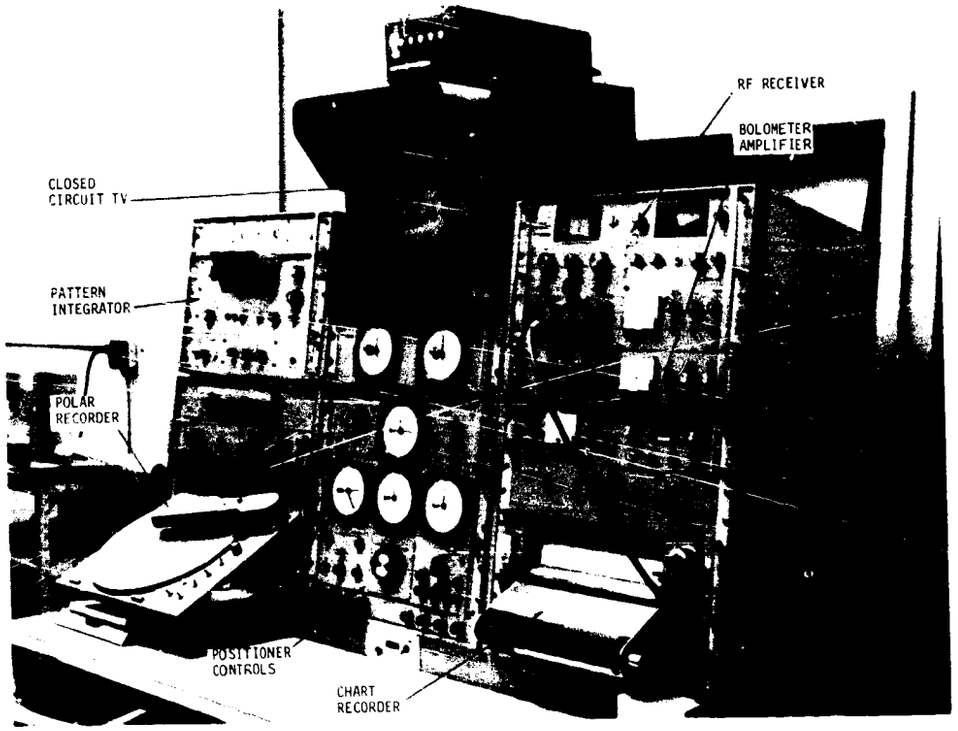

FIGURE 4 RADIATION PATTERN RECORDING AND CONTROL CONSOLE

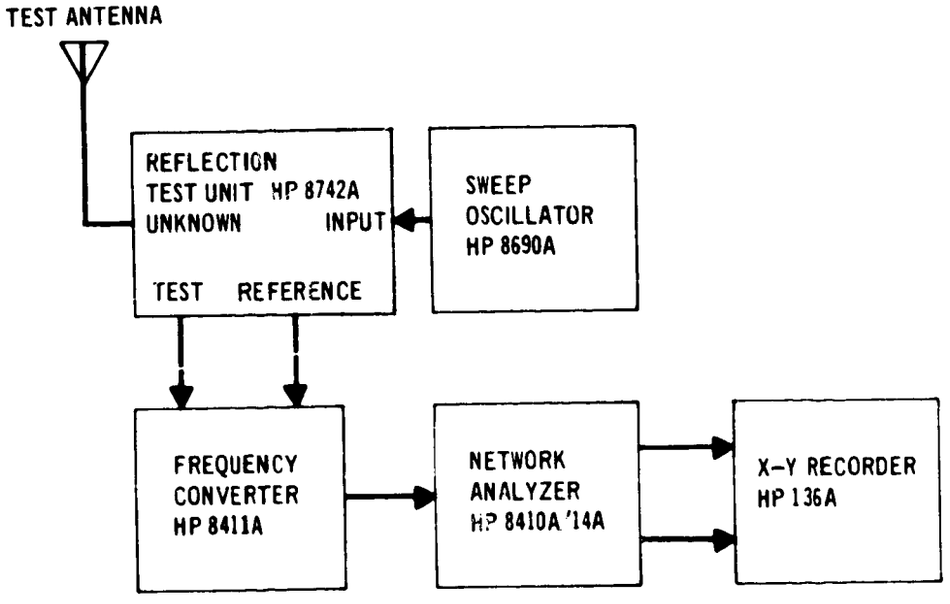

FIGURE 5 SWEPT FREQUENCY IMPEDANCE MEASUREMENT TEST SETUP BLOCK DIAGRAM

-10 dB for all patterns measured with rotating linear polarization (RLP). For right and left hand circularly polarized (RHC and LHC) patterns, the LIR was -10 dB for tests P2-1 and P2-2, and -13 dB for tests P1-11 through P1-15. After test P1-12 a bolometer detector was used for the remaining pattern measurements due to a receiver failure.

The coordinate system used for the radiation patterns is shown in figure 6. Unless otherwise identified, all radiation patterns presented for the S-band antenna system are oriented with $\vartheta = 0°$ toward the top of the page. For convenience, the principal plane patterns, which are in orthogonal planes, are referred to as X-plane ($\phi = 0°$ on pattern left) and Y-plane ($\phi = 90°$ on pattern right).

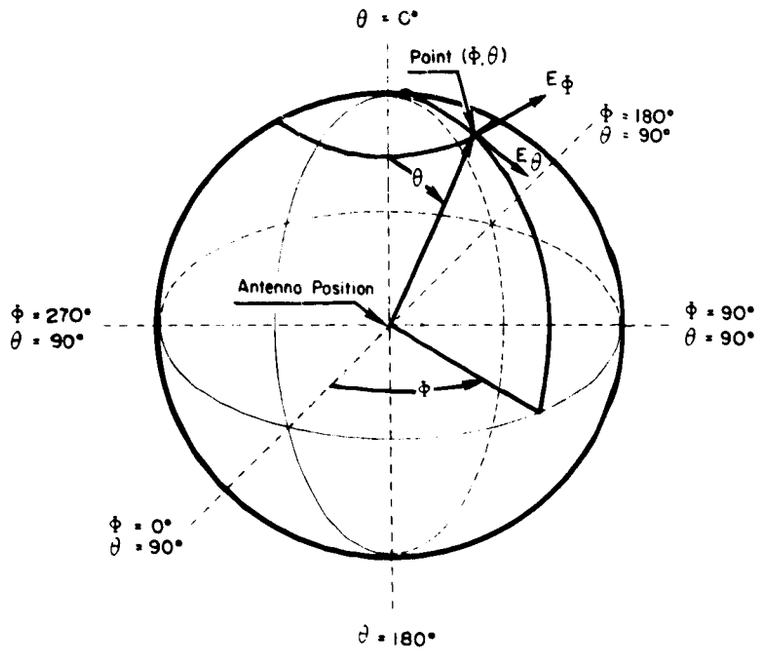

FIGURE 6 ANTENNA COORDINATE SYSTEM

The circular gain may be derived from the rotating linear patterns by adding the conversion gain factor (figure 7), which is a function of the voltage axial ratio, to the peak linear gain. Both axial ratio and peak linear gain are taken at a particular angle. The derivation of this function is discussed in reference 1, Appendix C.

Test results. - Electrical performance measurements were taken prior to thermal testing to establish reference data for comparison with results obtained after subjecting the antenna system to preentry and entry thermal environments.

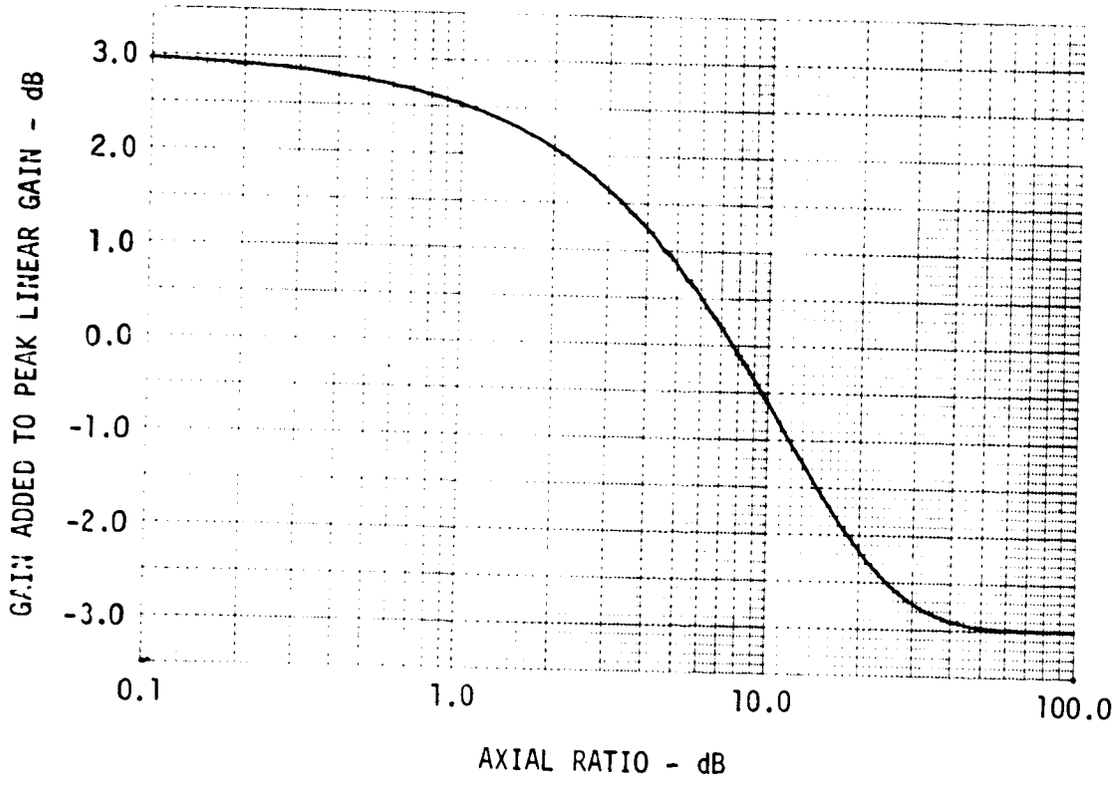

FIGURE 7 CONVERSION FROM PEAK LINEAR TO CIRCULAR GAIN

Prototype No. 2: The results of reference radiation pattern measurements for Prototype No. 2 are shown in figure 8. The results of reference impedance measurements (figure 9) are essentially identical to those reported in reference 1, Appendix F.

Measurements taken after the first thermal test (P2-1) show considerable change. The radiation patterns (figure 10) show a significant degradation in gain, axial ratio, and shape. The circular gain decreased 8 to 10 dB, depending on the particular direction angle considered. The axial ratio increased from 7 to 14 dB throughout the operating frequency range and over the entire pattern. Nulls appeared in the pattern at $\theta = 39°$, which is approximately the look angle that intersects the gap between the antenna window and the surrounding TPS. Other pattern distortions are also apparent when comparing figure 10 with figure 8. The results of impedance measurements are shown in figure 11. Comparison of these results with those of the reference condition (figure 9) shows a considerable spread in the positions of the noted frequencies. The maximum VSWR is 2:1 between 2.1 and 2.2 GHz and 2.4:1 between 2.2 and 2.3 GHz. At 2.1 GHz the VSWR improved from 1.26:1 to 1.15:1. Subsequent tests of only the S-band antenna (S/N 105) showed no change in the antenna performance.

The degraded performance was attributed to a carbonaceous deposit that developed on the LI-1500 tiles during the entry heating simulation. A detailed discussion of the caused of this deposit is given in the subsection of Thermal Testing which follows.

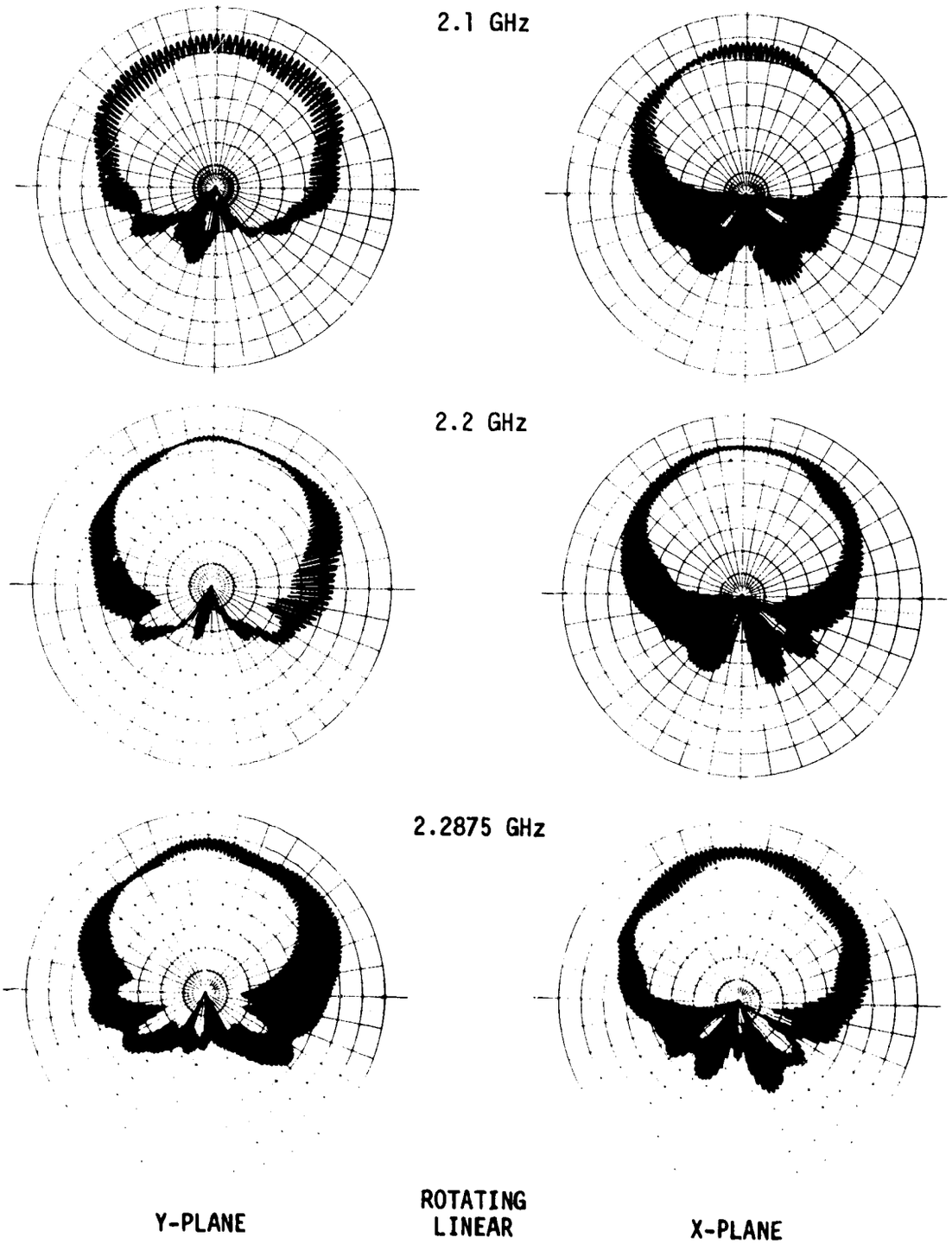

FIGURE 8 PROTOTYPE NO. 2 REFERENCE RADIATION PATTERNS

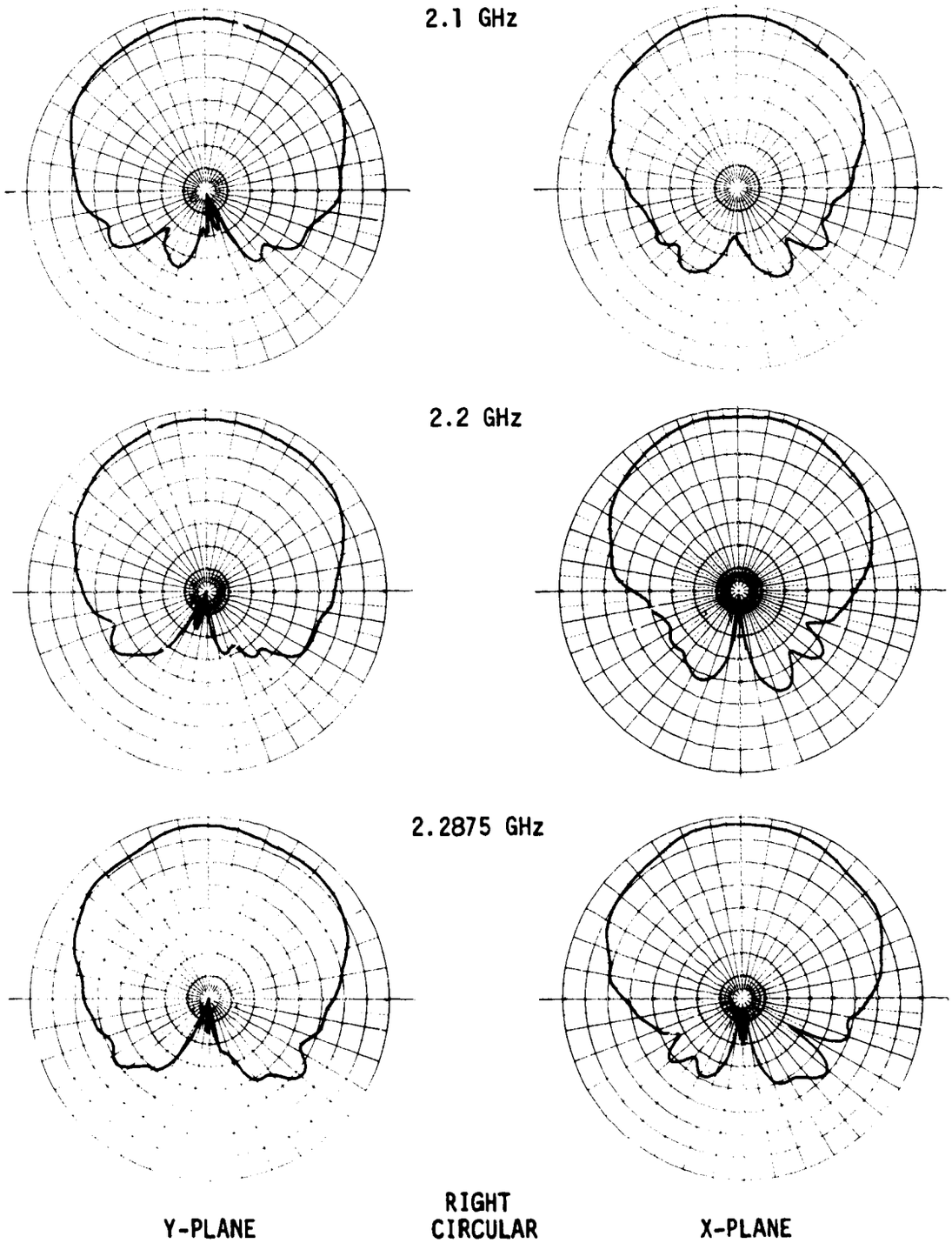

FIGURE 8 PROTOTYPE NO. 2 REFERENCE RADIATION PATTERNS (Continued)

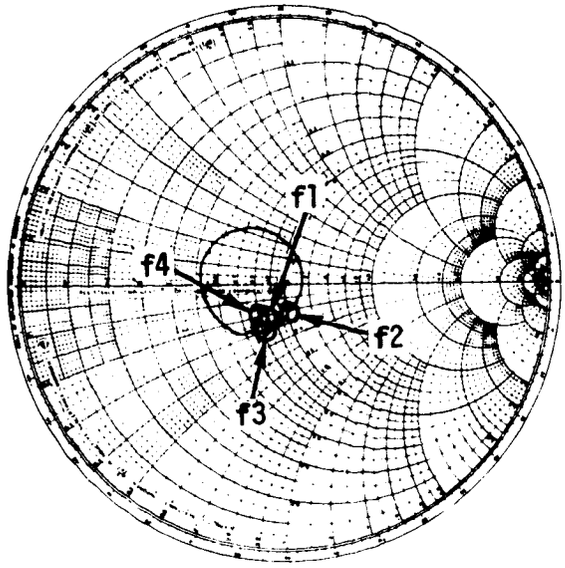

Z_o = 50 OHMS
f1 = 2.0 GHz
f2 = 2.1 GHz
f3 = 2.2 GHz
f4 = 2.3 GHz

FIGURE 9 PROTOTYPE NO. 2 REFERENCE IMPEDANCE

The electrical performance measurements were repeated after test P2-2 to determine if a repetition of the entry heating would remove the carbonaceous deposit. The RLP radiation patterns (figure 12) show very little change from those of figure 10 taken after test P2-1. The RHC patterns of figure 12 show further deterioration in gain and pattern shape when compared to the patterns in figure 10.

Because of the degraded electrical performance of Prototype No. 2, Prototype No. 1, which was used for the thermal tests conducted in the NASA-JSC arc tunnel facility, was used for the S-band antenna system test series. This substitution was considered acceptable because the breadboard unit, which was also used for preliminary thermal tests conducted in the NASA-JSC arc tunnel facility, did not show signs of a carbonaceous deposit during preliminary radiant heater testing.

Prototype No. 1: The results of reference radiation pattern measurements for Prototype No. 1 are shown in figure 13. The results of reference impedance measurements are shown in figure 14.

The results of radiation pattern measurements after the first thermal test (P1-11) are shown in figure 15. Although some changes in axial ratio may be noted, they are not sufficiently consistent to indicate a definite trend. The axial ratio increased at some angles while at others there is a decrease. The greatest change occurred at 2.1 GHz, $\theta = 60°$, the low end of the operating frequency range. This was a 3.0 dB increase in an axial ratio that was 20 dB

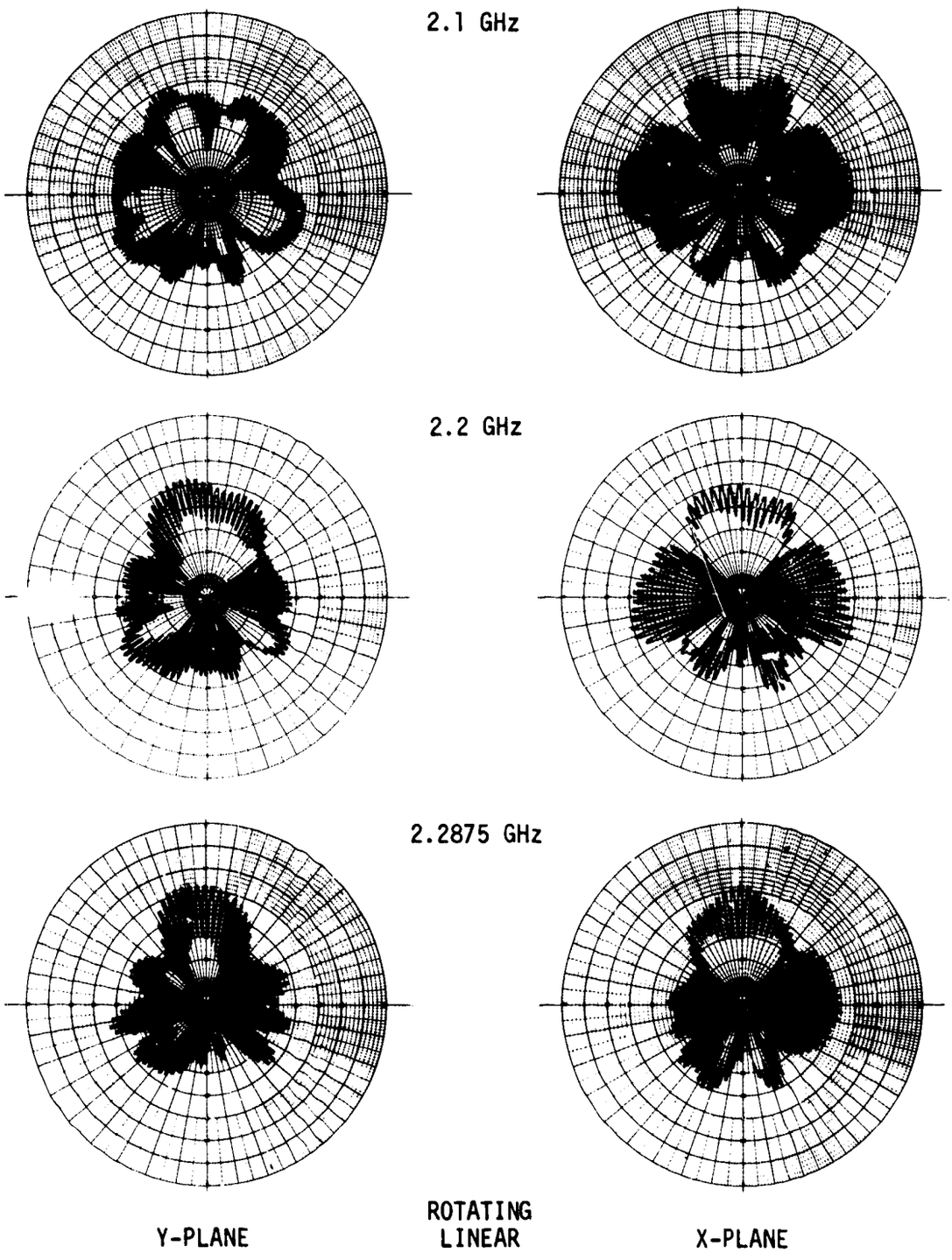

FIGURE 10 EFFECTS OF ENTRY ENVIRONMENT – TEST P2–1 RADIATION PATTERNS

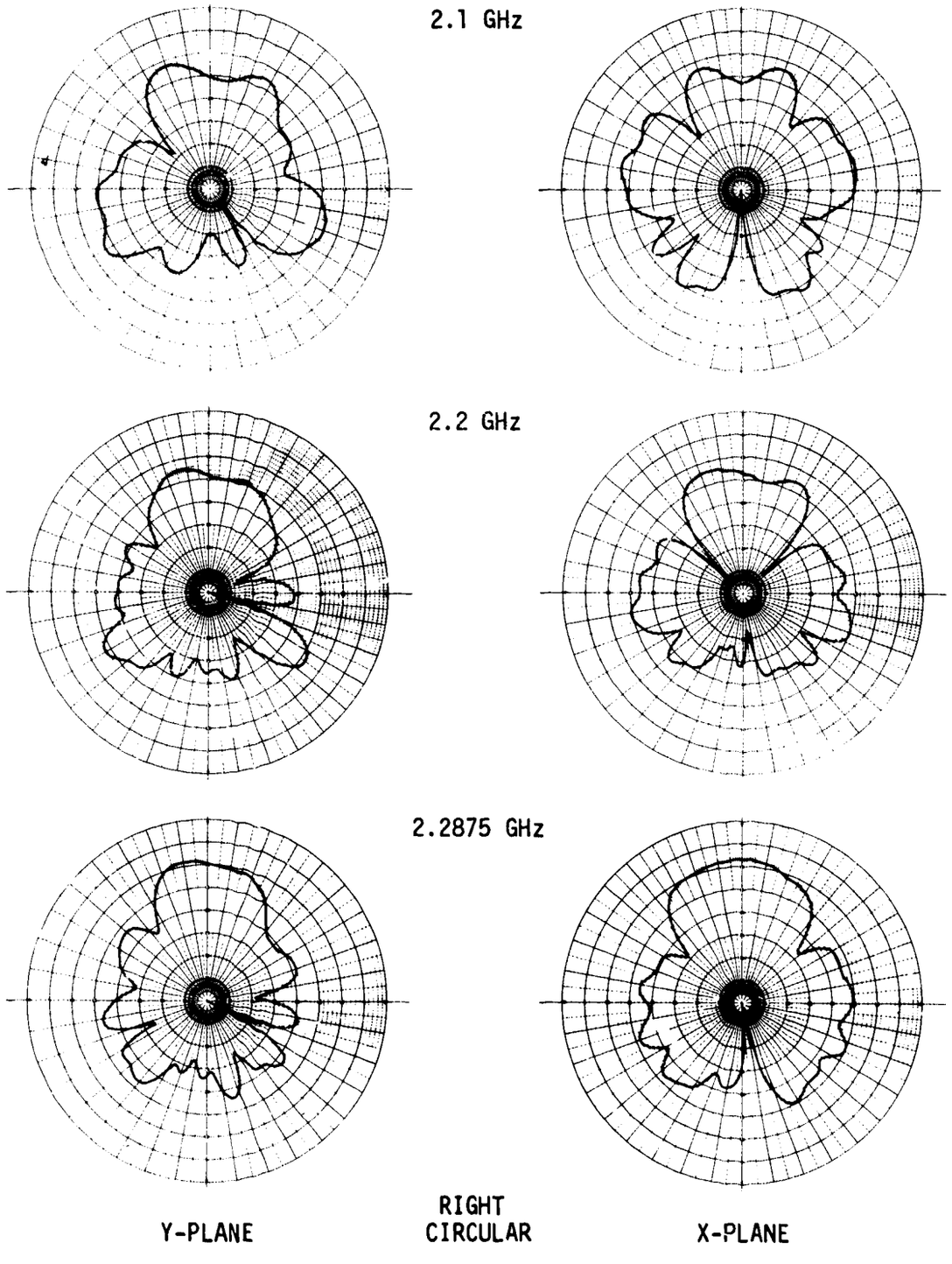

FIGURE 10 EFFECTS OF ENTRY ENVIRONMENT – TEST P2–1 RADIATION PATTERNS (Continued)

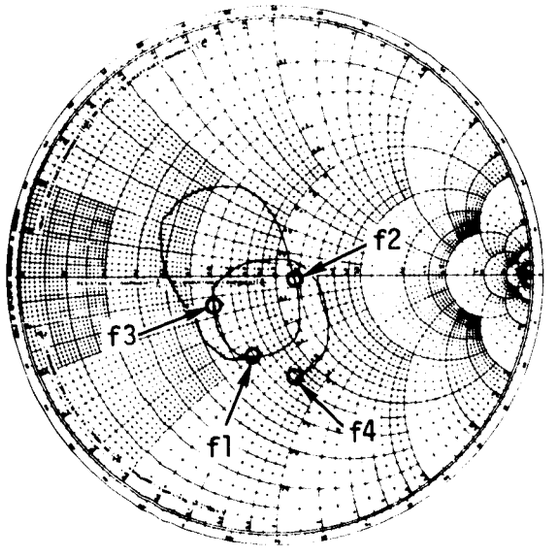

Z_o = 50 OHMS
f1 = 2.0 GHz
f2 = 2.1 GHz
f3 = 2.2 GHz
f4 = 2.3 GHz

FIGURE 11 EFFECTS OF ENTRY ENVIRONMENT – TEST P2-1 IMPEDANCE

in the reference measurement. Comparing the RHC patterns (figure 15) with the reference patterns (figure 13) shows minor changes in circular gain. For example, the maximum change was 0.4 dB at 2.1 GHz (θ = 0°). The results of the impedance measurements (figure 16) show the antenna VSWR was unchanged.

A change in measurement technique was required after test P1-12 due to a failure in the receiver used for radiation pattern measurements. Suitable replacement receivers were not available and the delay for repair was not acceptable. Therefore, a bolometer detector was used in place of the receiver.

The results of radiation pattern measurements after test P1-12 are shown in figure 17. These results show more change than was observed after test P1-11. For example, the circular gain (θ = 0°) obtained from the RHC patterns increased 1.3 dB at 2.1 GHz, decreased 1.0 dB at 2.2 GHz, and remained unchanged at 2.2875 GHz. The small changes observed in the gain at 2.1 and 2.2 GHz were attributed, in part, to differences in characteristics of the detector bolometer compared to the super-hetrodyne receiver. At 2.2875 GHz the changes were within measurement error tolerances. A comparison of these patterns (figure 17) with those of figure 13 shows that the overall pattern characteristics were unchanged. Likewise the impedance measurements (figure 18) show no change in the antenna system VSWR.

Electrical performance measurements were not made after the third thermal test (P1-13) since there were no significant changes observed in the data obtained after test P1-12 and test P1-13 did not represent a severe thermal condition. Therefore, tests P1-13 and P1-14, with initial temperatures of 244 K (70°F) and 327 K (130°F), were run consecutively in one day.

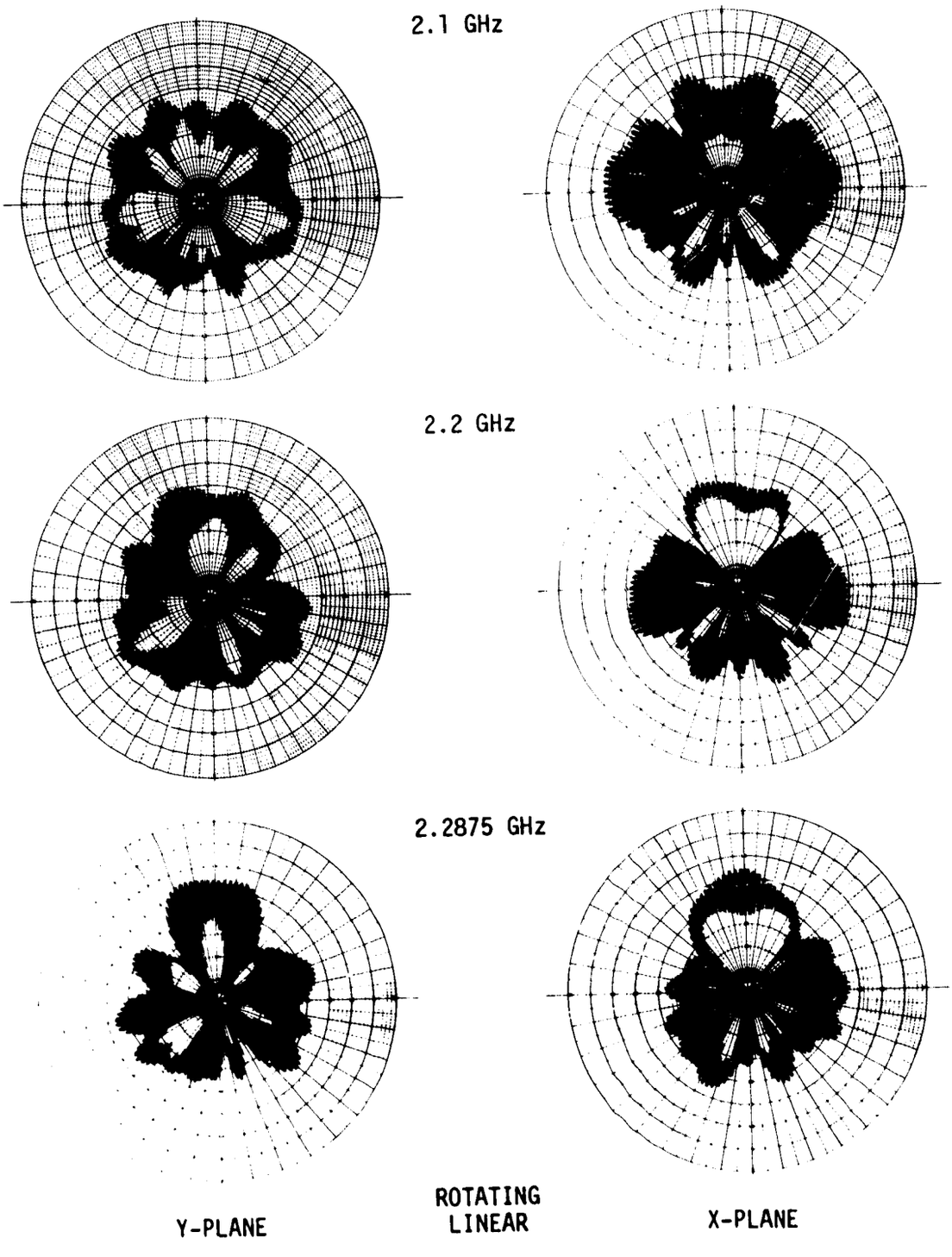

FIGURE 12 EFFECTS OF ENTRY ENVIRONMENT – TEST P2–2 RADIATION PATTERNS

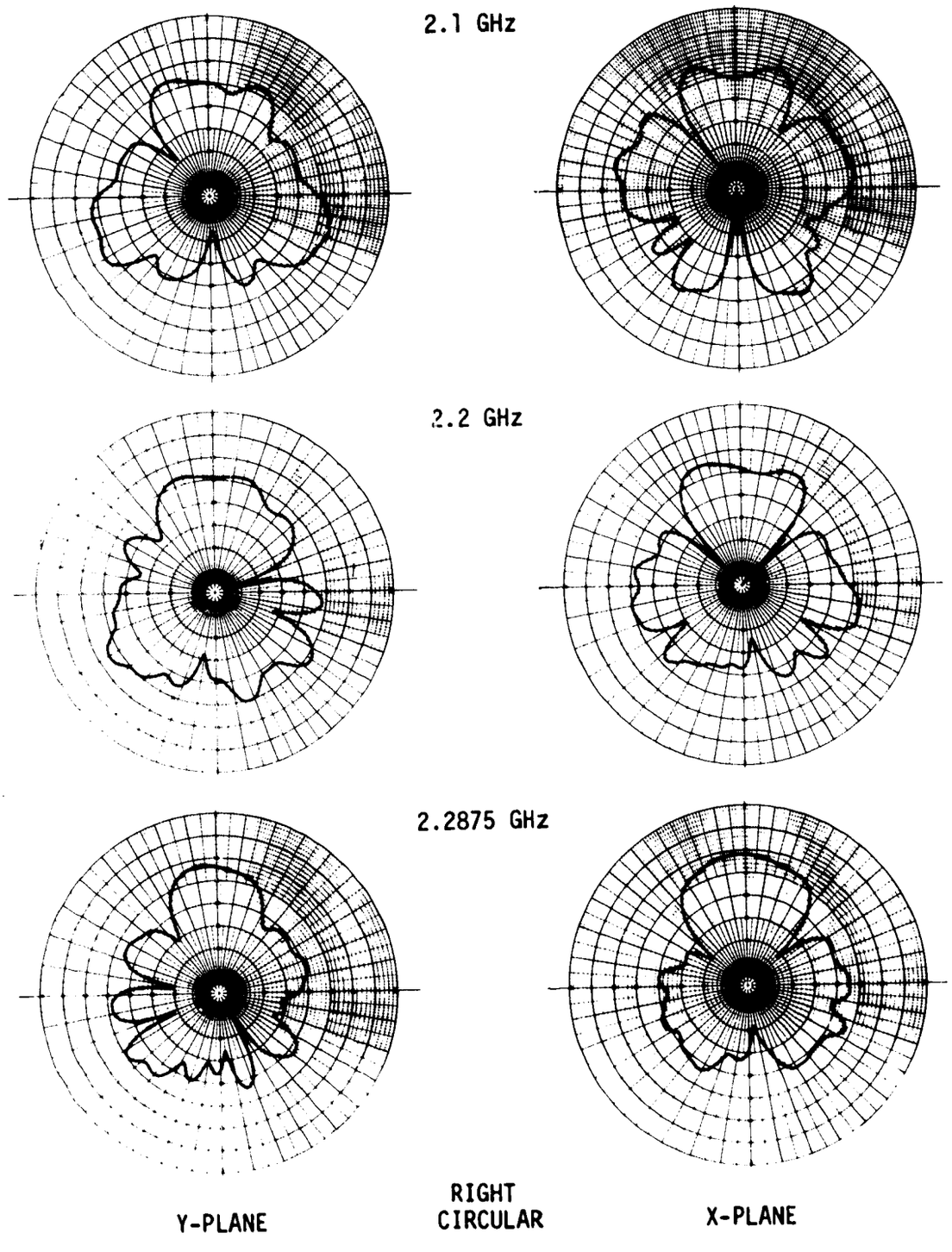

FIGURE 12 EFFECTS OF ENTRY ENVIRONMENT – TEST P2–2 RADIATION PATTERNS (Continued)

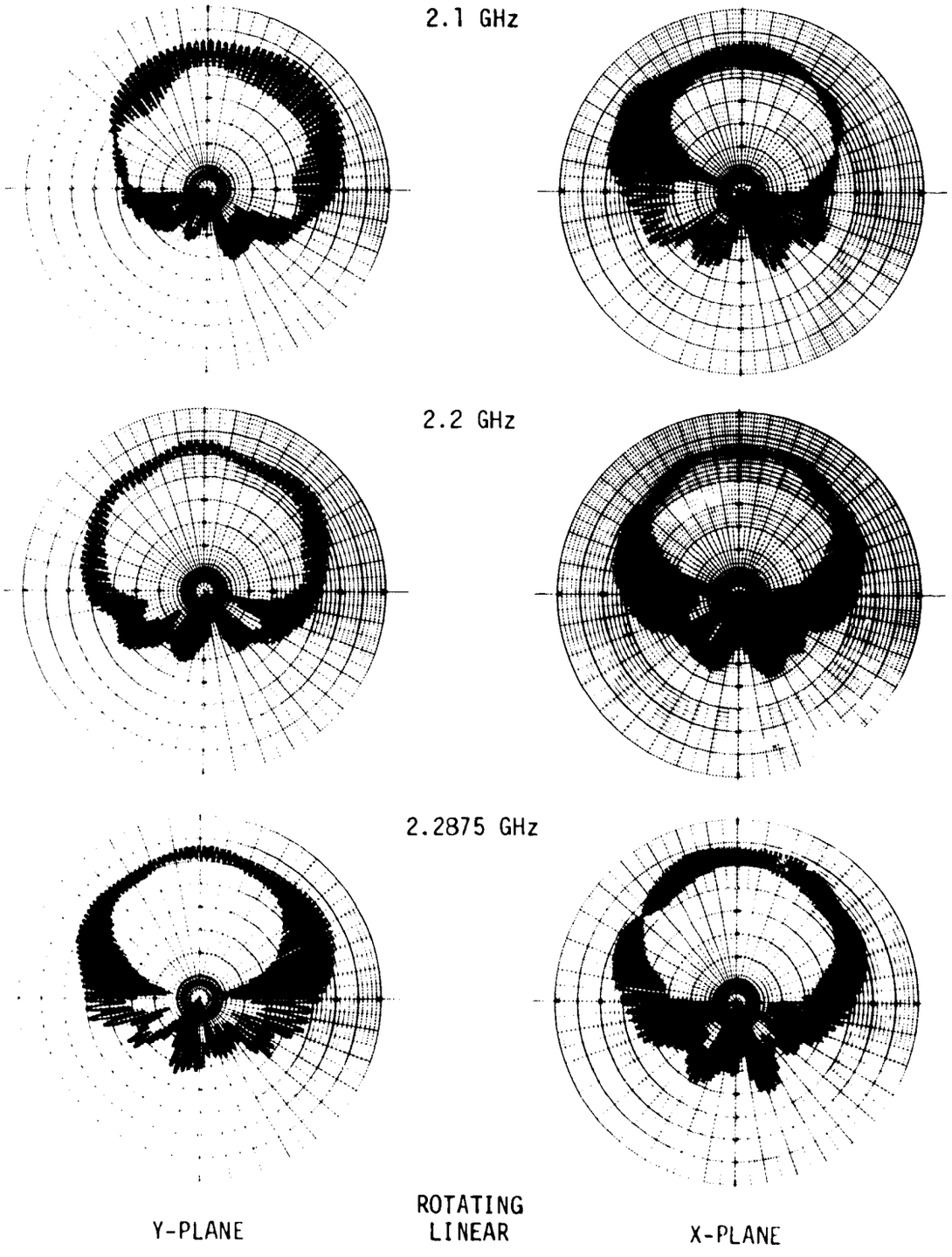

FIGURE 13 PROTOTYPE NO. 1 REFERENCE RADIATION PATTERNS

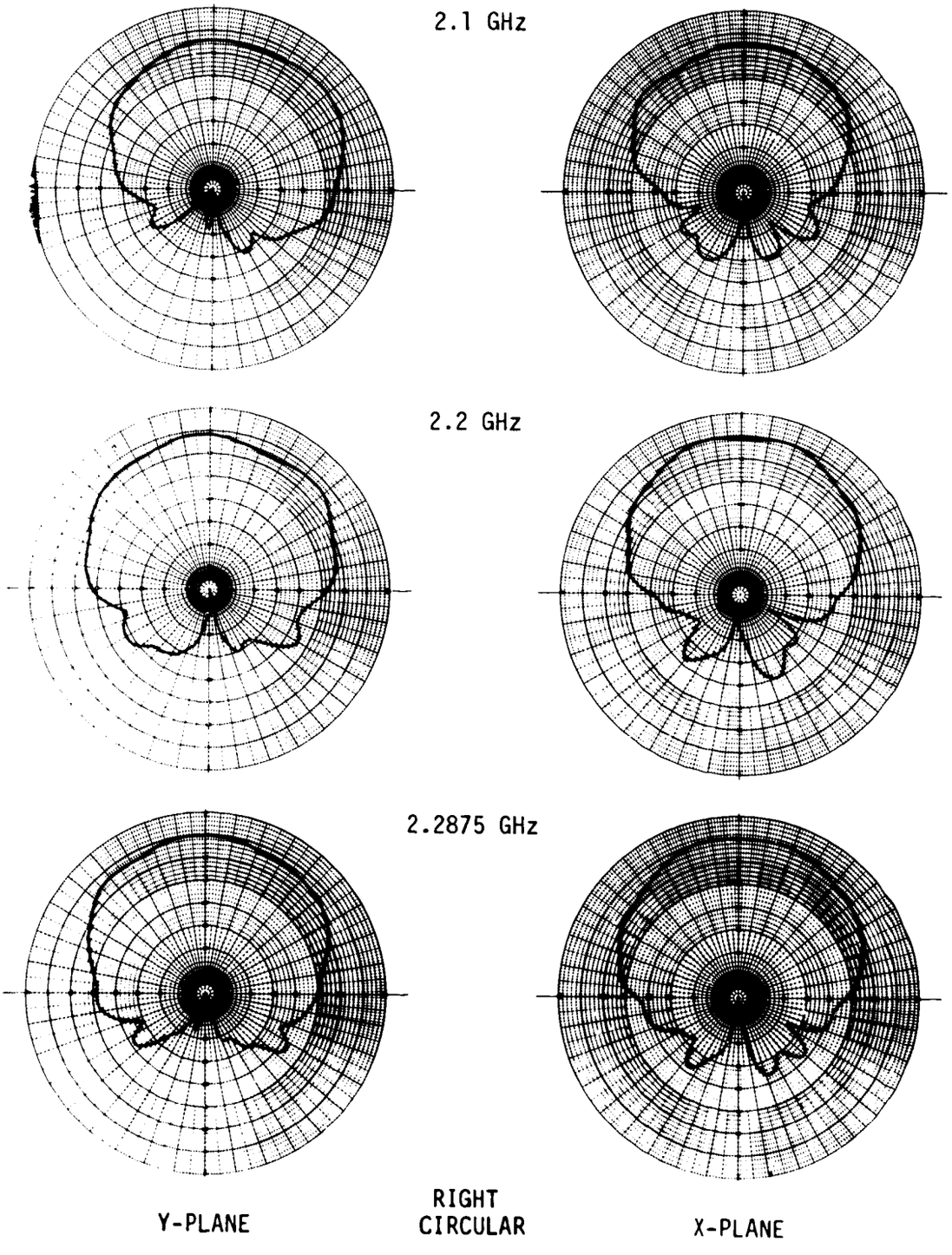

FIGURE 13 PROTOTYPE NO. 1 REFERENCE RADIATION PATTERNS (Continued)

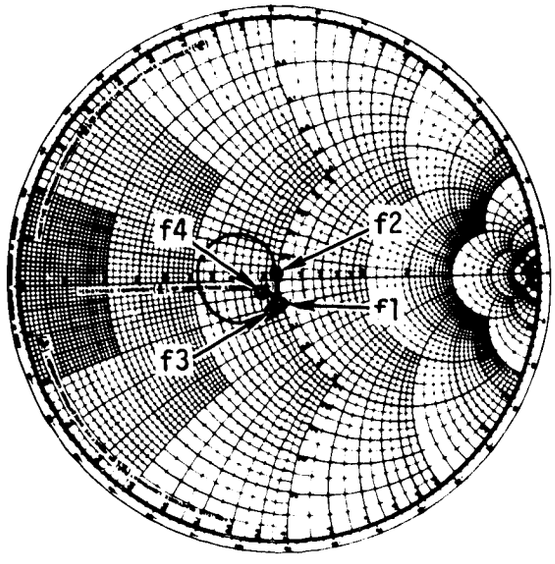

Z_o = 50 OHMS
f1 = 2.0 GHz
f2 = 2.1 GHz
f3 = 2.2 GHz
f4 = 2.3 GHz

FIGURE 14 PROTOTYPE NO. 1 REFERENCE IMPEDANCE

Electrical performance measurements after thermal tests P1-14 and P1-15 completed the S-band antenna system tests. The results for P1-14 are shown in figures 19 and 20; those for P1-15 are shown in figures 21 and 22. These test results show that no major change in antenna electrical performance had occurred throughout the test sequence.

Thermal Testing

The Thermal Testing consisted of subjecting the S-band antenna system (built under the original contract) to cold soak and entry heating simulations, and measuring the temperature responses at selected points. Thermal performance was verified by correlating surface temperature histories to profiles representing exposure to theoretical entry and experimental plasma environments. Instrumentation of the test articles was the same as for the original contract.

The S-band antenna system testing was conducted in two phases: one with the breadboard unit and the other with prototype units. An overview of all tests conducted under this study and the original contract is illustrated in table II. The breadboard tests were used for validating the capabilities of the test facility and the integrity of the test article assembly, and for

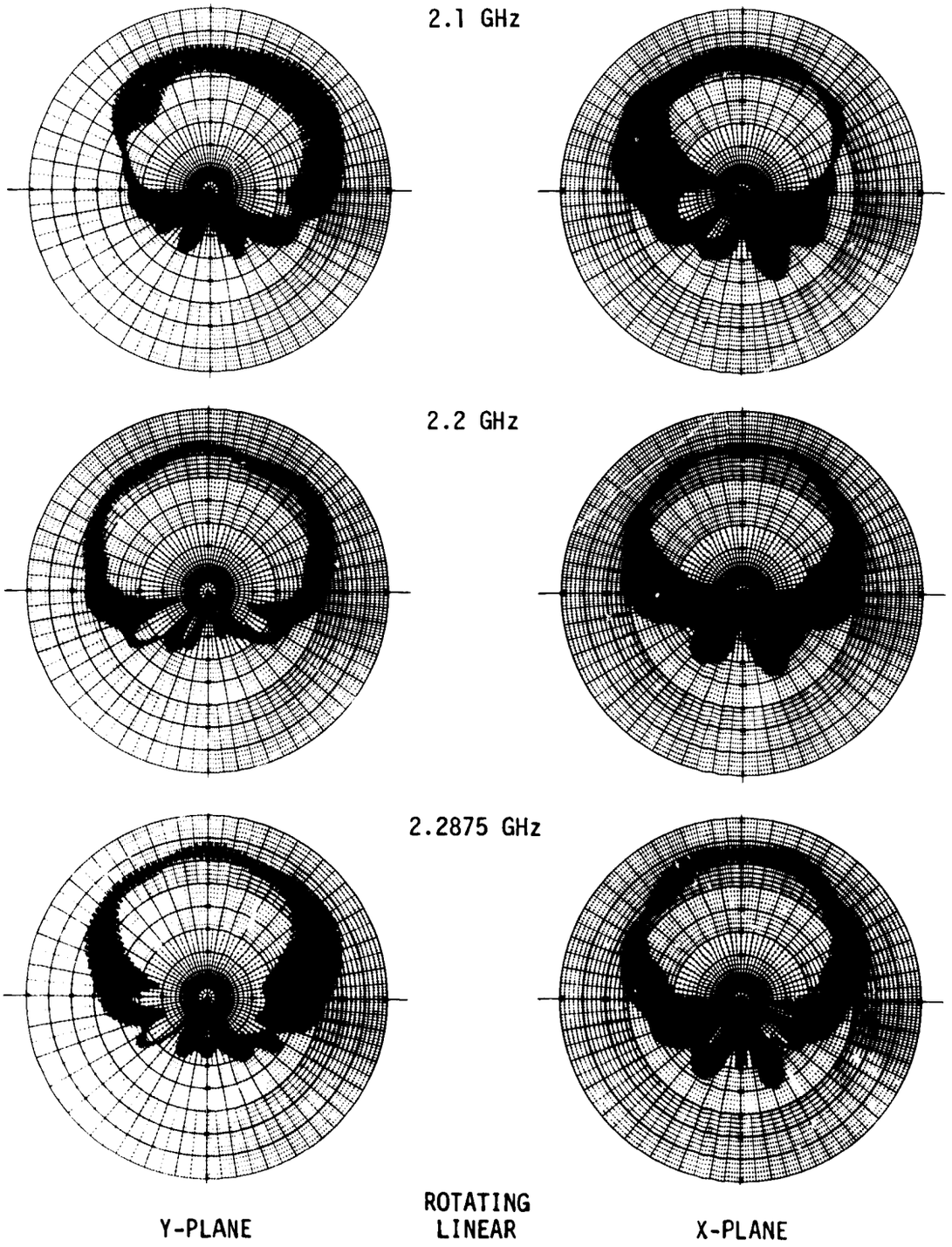

FIGURE 15 EFFECTS OF ENTRY ENVIRONMENT – TEST P1-11 RADIATION PATTERNS (T_0 = 172 K (-150°F))

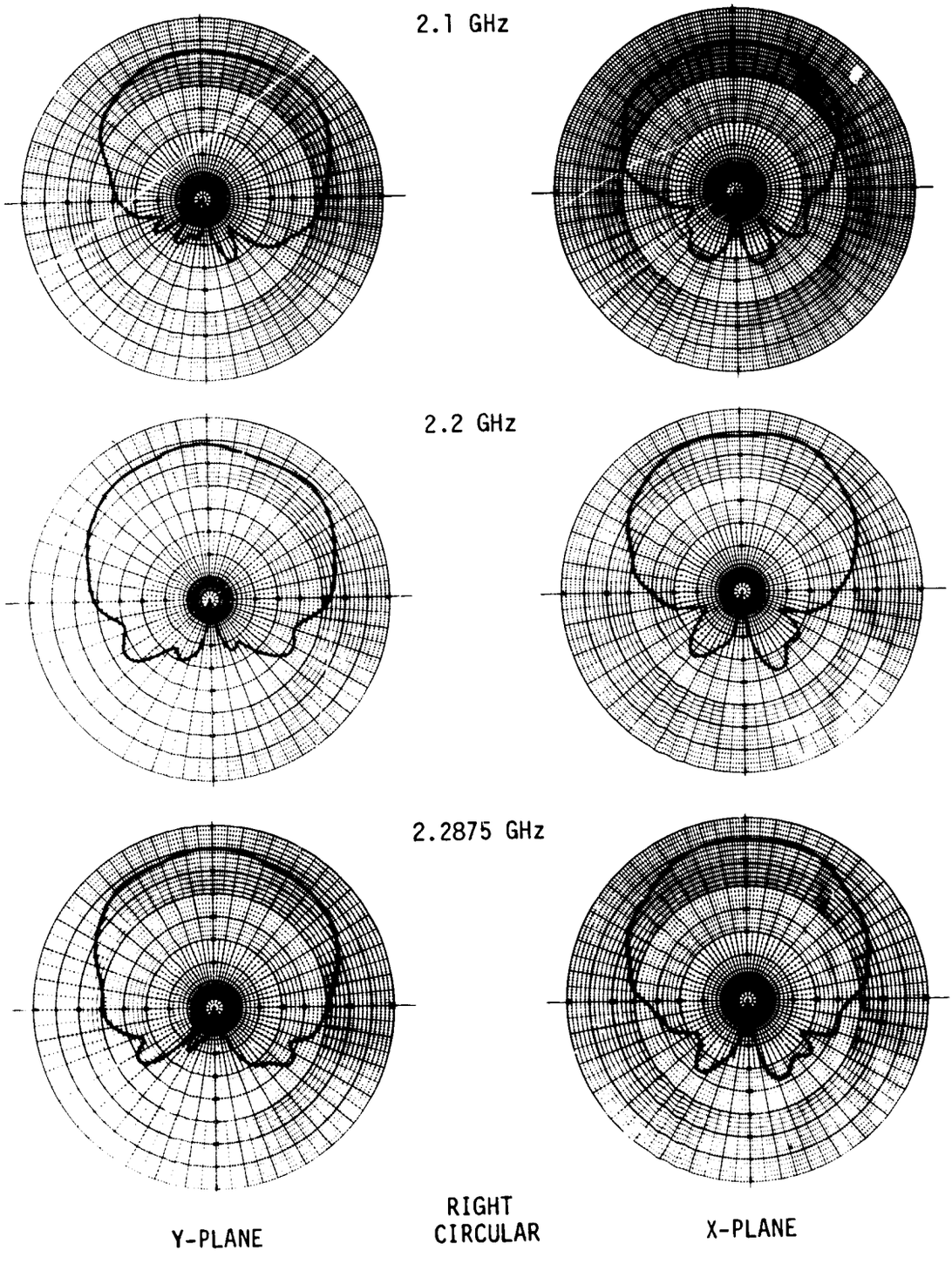

FIGURE 15 EFFECTS OF ENTRY ENVIRONMENT – TEST P1–11 RADIATION PATTERNS (T_0 = 172 K (–150°F)) (Continued)

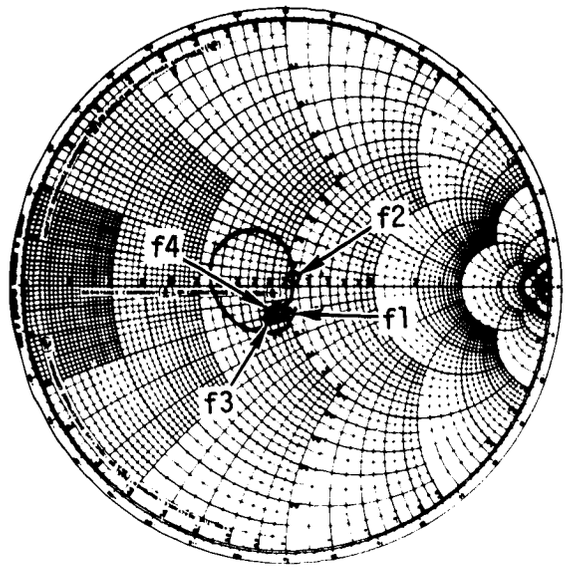

Z_0 = 50 OHMS
f1 = 2.0 GHz
f2 = 2.1 GHz
f3 = 2.2 GHz
f4 = 2.3 GHz

FIGURE 16 EFFECTS OF ENTRY ENVIRONMENT – TEST P1-11 IMPEDANCE (T_0 = 172 K (-150°F))

acquiring data to compare radiant and plasma heating test results. More breadboard tests were run than originally intended because of changes to the test setup prompted by test results. The prototype tests were conducted to: (1) verify the capability of the antenna system to withstand and function after exposure to orbital temperature environments of 117 K (-250°F) to 328 K (130°F) and subsequent entry heating; and (2) provide skin-line temperature histories off-the-shelf antenna testing.

Facility description. - All thermal tests were conducted in an MDC Mission Environment Simulator. This facility consists of six functional parts: (1) a graphic heater; (2) a 1.68 m (5.5 ft) diameter vacuum chamber, (3) a cold box; (4) a mechanism for moving the specimen; (5) a data acquisition system; and (6) associated control equipment. These main parts are shown schematically in figure 23.

The graphic heater assembly (figure 24) provides a controllable radiant heat source capable of attaining maximum temperatures of 1644 K (2500°F). The heater can be controlled to the desired temperature history manually or automatically through a Data Trak and an ignitron power controller (figure 25). The heater, consisting of 12 two pass (hair pin type) graphite elements, is operated in a nitrogen purged enclosure to prevent oxidation. The susceptor plate forms part of the enclosure and provides a test area of approximately 53 x 53 cm (21 x 21 in.).

The vacuum chamber provides controllable pressures from sea level to 1.3×10^{-6} N/m^2 (10^{-8} torr). The atmosphere in the chamber can be air or nitrogen. Electrical power, instrumentation leads, and coolants (water and gas) are introduced into the chamber through vacuum pass-through on the chamber door.

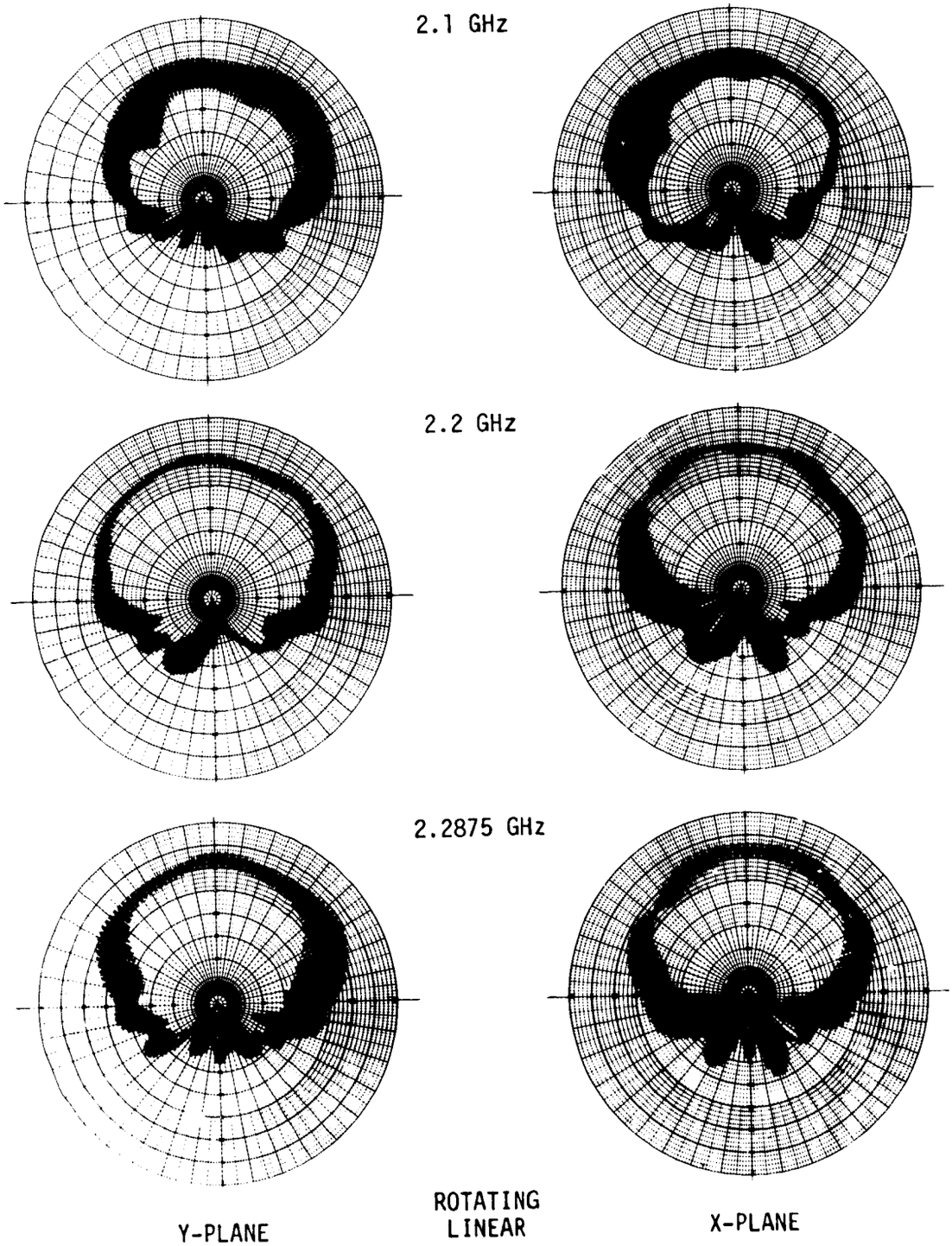

FIGURE 17 EFFECTS OF ENTRY ENVIRONMENT – TEST P1–12 RADIATION PATTERNS
(T_0 = 172 K (–150°F))

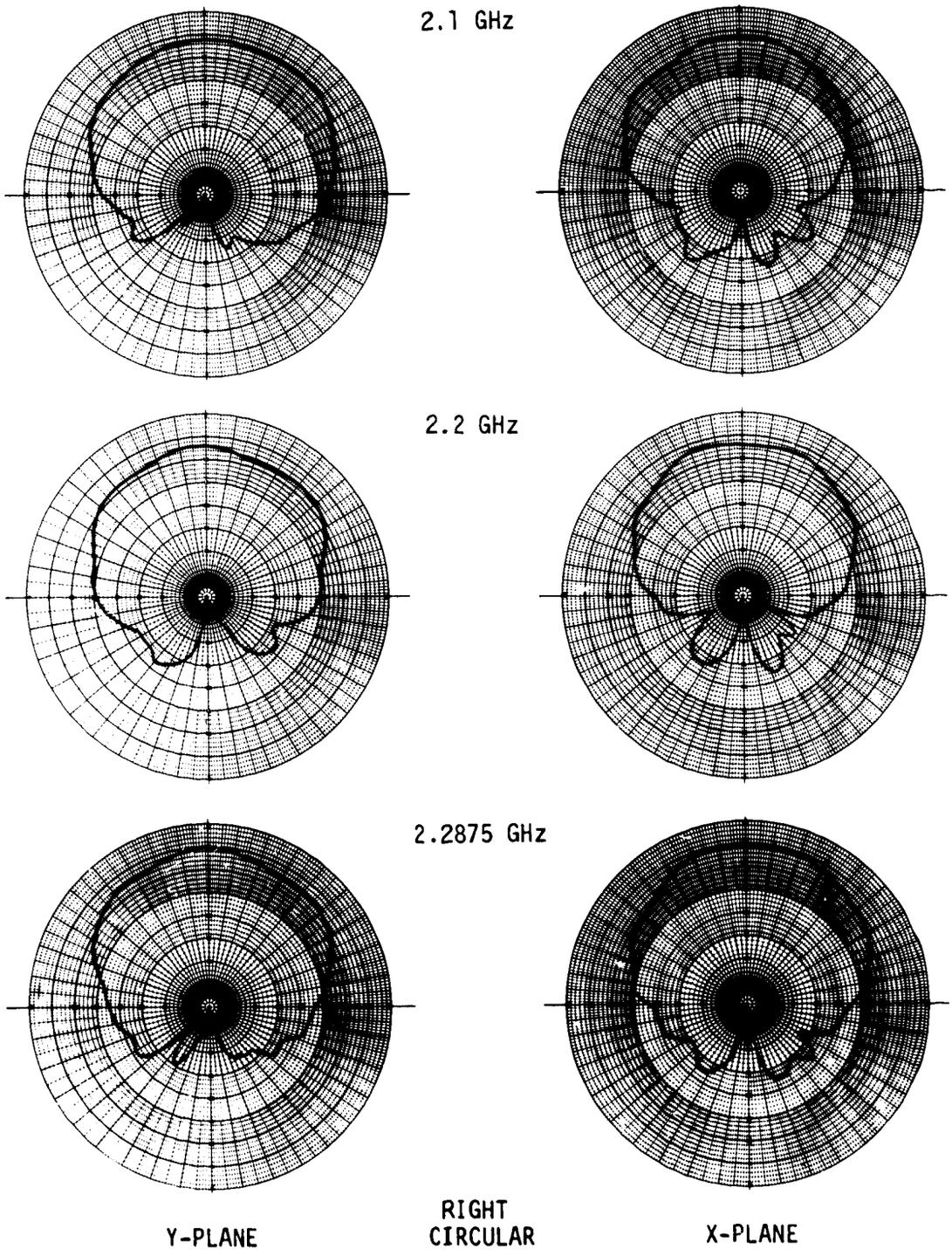

FIGURE 17 EFFECTS OF ENTRY ENVIRONMENT – TEST P1-12 RADIATION PATTERNS (T_0 = 172 K (-150°F)) (Continued)

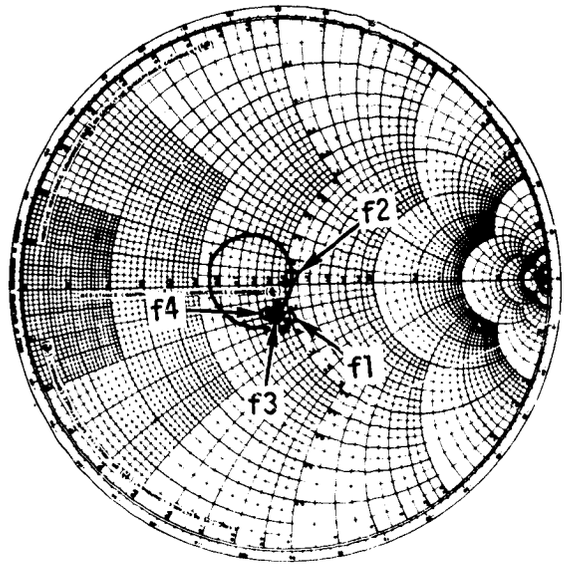

Z_o = 50 OHMS
f1 = 2.0 GHz
f2 = 2.1 GHz
f3 = 2.2 GHz
f4 = 2.3 GHz

FIGURE 18 EFFECTS OF ENTRY ENVIRONMENT – TEST P1–12 IMPEDANCE (T_0 = 172 K (–150°F))

The cold box is a five sided aluminum structure with nitrogen coolant lines brazed to the exterior (figure 26). The temperature of the nitrogen was controlled to provide the desired cold soak temperature.

A motorized mechanism (figure 26) was provided to transport the specimen between the cold box and the heater. The transport system consists of a rack and pinion gear driven by an electrical motor.

The data acquisition system (figure 25) consisted of a two functional real-time plotter, a Dymec fifty channel scanner and a tape recorder. A print out of the thermocouple outputs is made at selected intervals (e.g., 20 sec). After the tests the data may be tabulated in engineering units (e.g., °F) and/or plotted as a function of time.

Test installation. - The S-band antenna system test articles were installed in the test container assembly (figure 77 in ref. 1) used in the NASA-JSC arc tunnel testing reported in reference 1. The test container assembly was attached to the trusses of the transport mechanism (figure 26). Instead of the water cooled cover assembly (figure 78 in ref. 1) used in reference 1 arc tunnel tests, the specimen was thermally guarded around the periphery with a 5.1 cm (2.0 in.) wide by 6.0 cm (2.4 in.) thick ring of HCF (hardened compacted fibers) insulation. The HCF was bonded to an aluminum ring which was supported from the back side of the test container assembly as shown in figure 26.

Test environment. - Two thermal environments were employed, one to simulate an orbiter entry and the other the NASA-JSC arc tunnel tests conducted during the original contract. The basis for the orbiter entry environment is

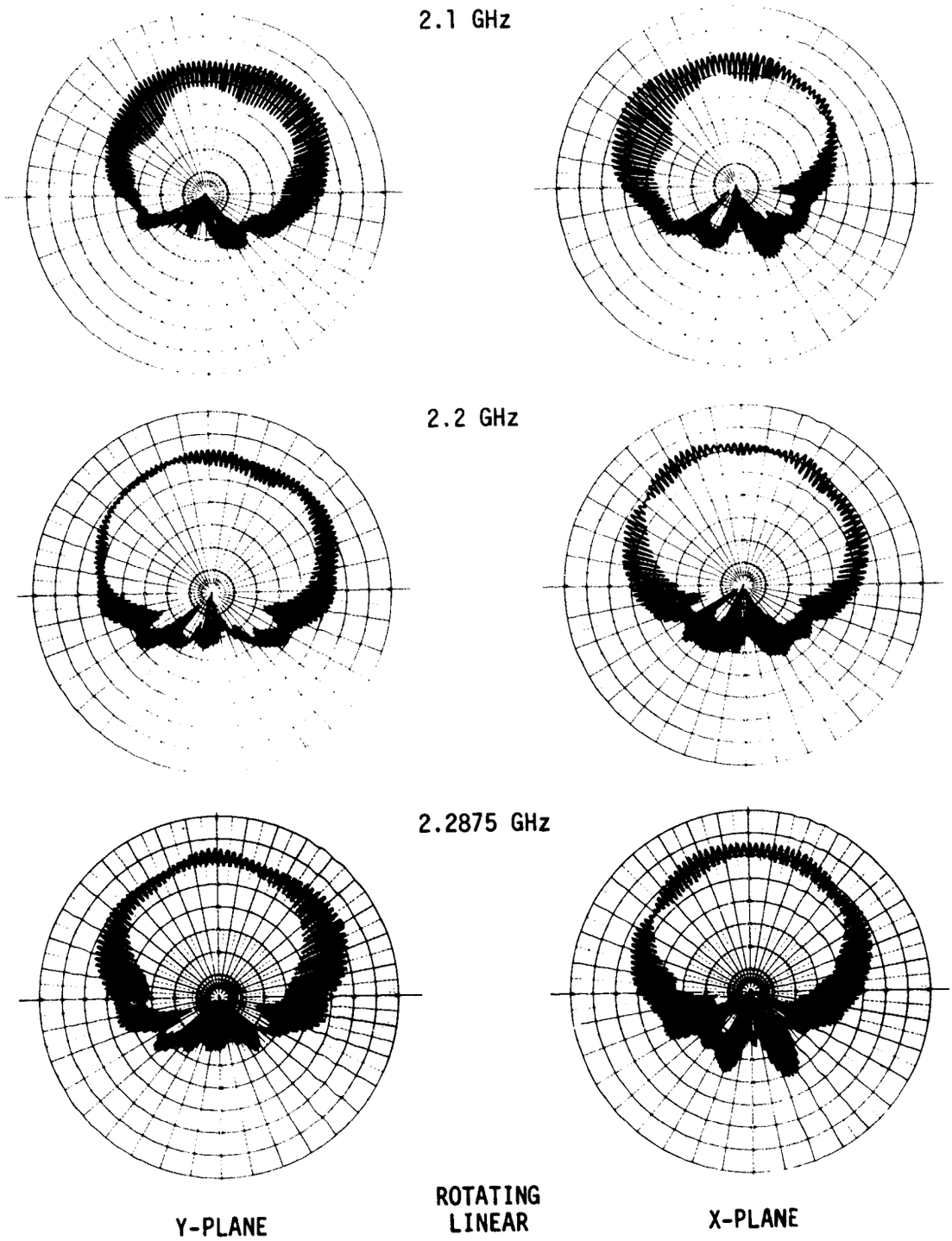

FIGURE 19 EFFECTS OF ENTRY ENVIRONMENT – TEST P1–14 RADIATION PATTERNS (T_0 = 172 K (130°F))

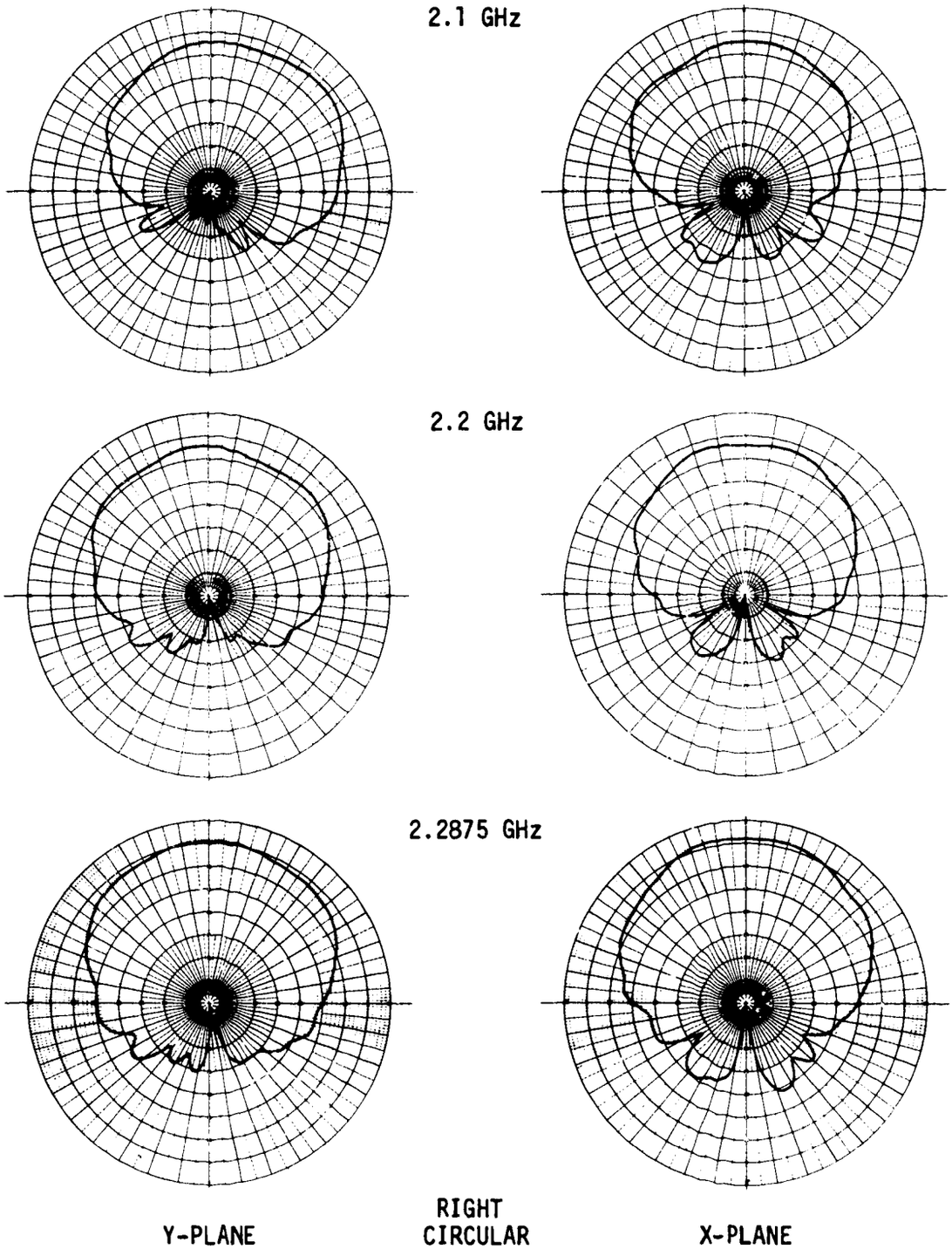

FIGURE 19 EFFECTS OF ENTRY ENVIRONMENT – TEST P1-14 RADIATION PATTERNS (T_0 = 172 K (130°F)) (Continued)

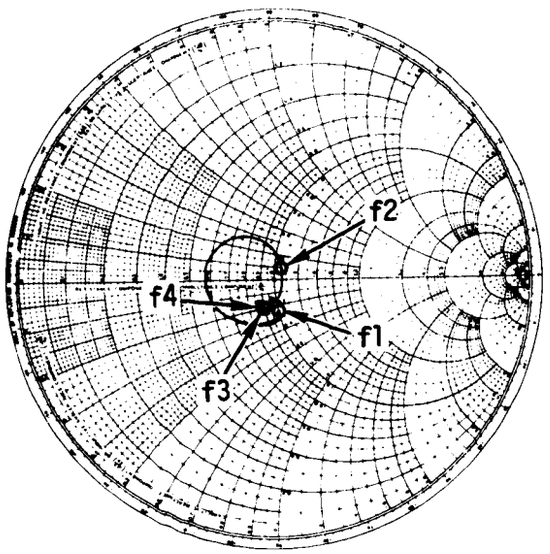

Z_o = 50 OHMS
f1 = 2.0 GHz
f2 = 2.1 GHz
f3 = 2.2 GHz
f4 = 2.3 GHz

FIGURE 20 EFFECTS OF ENTRY ENVIRONMENT – TEST P1-14 IMPEDANCE (T_0 = 327 K (130°F))

discussed in reference 1. Simulation consisted of reproducing surface temperature and pressure histories. These are defined in figures 27 and 28. One run was conducted with a truncated orbited thermal environment where the maximum temperature was limited to 1366 K (2000°F) (figure 27). The initial temperatures, 117, 172 and 328 K (-250, -150 and +130°F), were obtained by a cool down or heating period followed by a soak at that temperature. Usually, this preconditioning was accomplished in a 12 hour time period. A pressure of 1.3 N/m^2 (10^{-2} torr) was also maintained during this period. The temperature history was generated by a combination of automatic (Data Trak) and manual control.

Breadboard tests. - Breadboard unit tests were conducted from 28 October to 27 November 1973. The purposes of these tests were the definition of test procedures, refinement of the test installation, and acquisition of data for the correlation of radiant versus plasma heating. The breadboard unit (figure 29) was also used for the preliminary plasma heating tests reported in reference 1.

Three tests (B-5 through B-7) were run for the same environment until control tolerances, procedures, and the installation were considered acceptable. Most notable among the findings from these runs were:

(a) Due to the sensitivity of the radiant graphite heater, it was usually necessary to manually override the Data Trak to correlate the surface temperature with the desired profile.

(b) Surface temperature correlation could be enhanced during cool down by moving the test article from over the heater into the cold soak box, and spraying gaseous nitrogen over the HRSI surface.

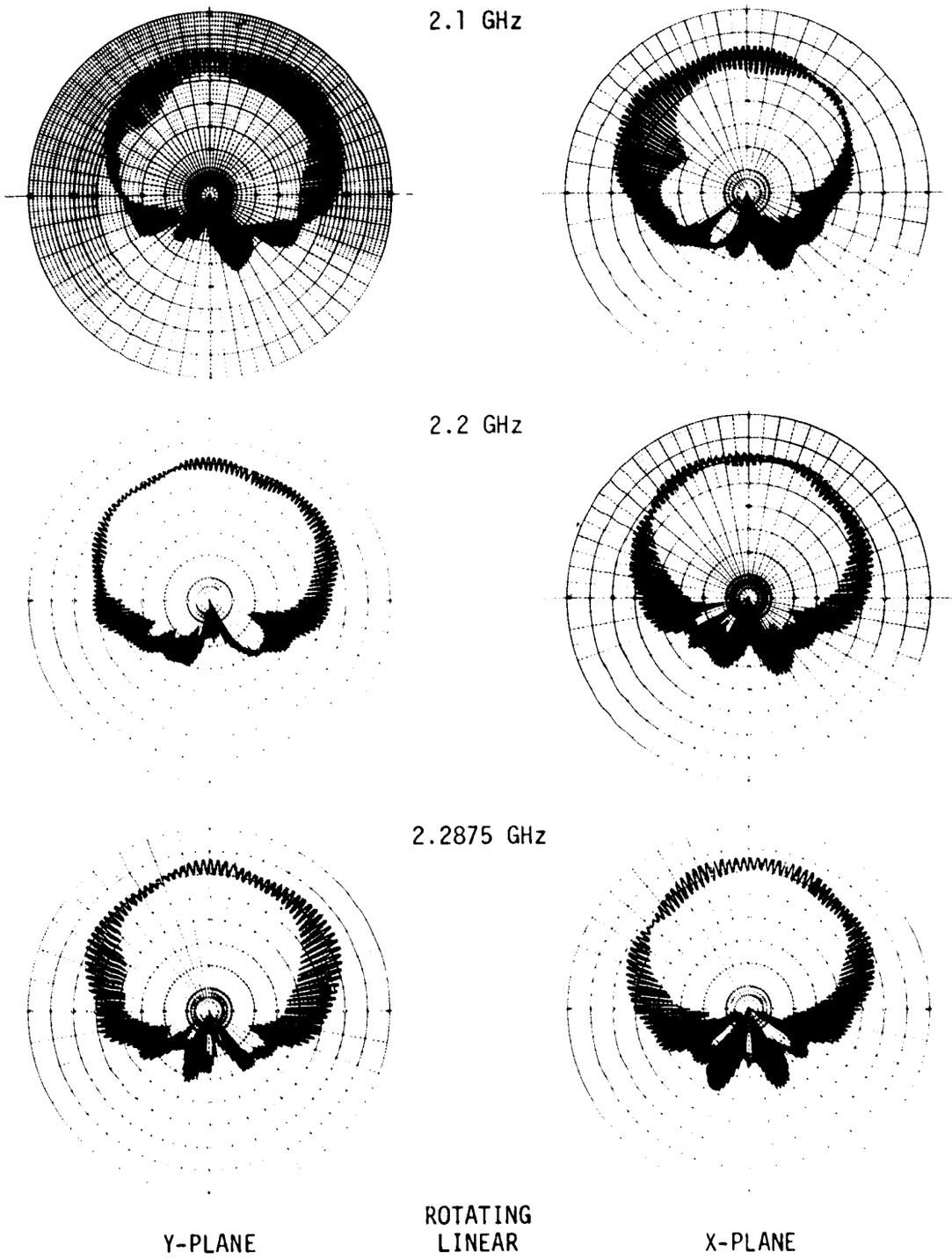

FIGURE 21 EFFECTS OF ENTRY ENVIRONMENT – TEST P1-15 RADIATION PATTERNS (T_0 = 327 K (-250°F))

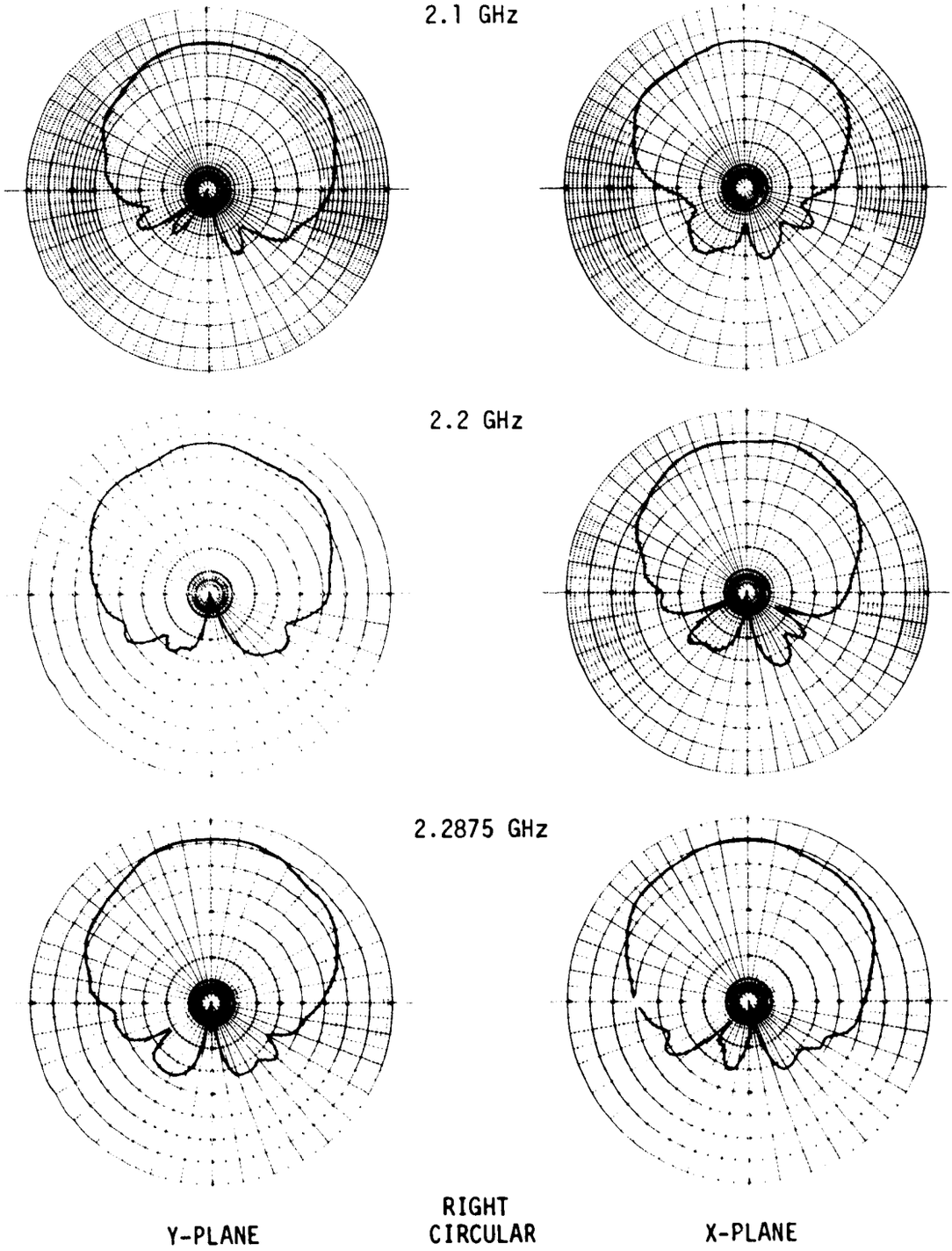

FIGURE 21 EFFECTS OF ENTRY ENVIRONMENT – TEST P1-15 RADIATION PATTERNS (T_0 = 327 K (-250°F)) (Continued)

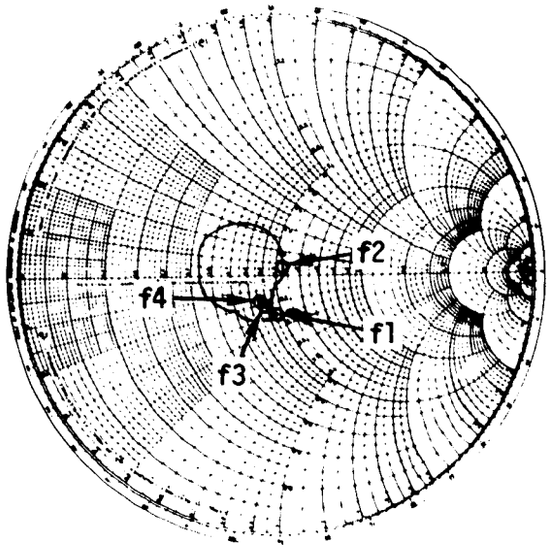

Z_0 = 50 OHMS
f1 = 2.0 GHz
f2 = 2.1 GHz
f3 = 2.2 GHz
f4 = 2.3 GHz

FIGURE 22 EFFECTS OF ENTRY ENVIRONMENT – TEST P1-15 IMPEDANCE (T_0 = 117 K (-250°F))

(c) Due to significant interfacing between the test article and facility, an insulation box (figure 30) around the test article was required to minimize backside heat transfer and the associated uncertainties in the data.

Tests B-8 through B-12 were run to ascertain the effects of deviations in simulated environments. For the first four of these tests (B-8 through B-11) the surface temperature and pressure histories were correlated with the entry environment for initial conditions ranging from room temperature to 172 K (-150°F). During the first attempt to cold soak the test article to 172 K (-150°F) (test B-10), it was discovered that heat leaks through the test article support structure limited the cold soak temperature to 211 K (-80°F). The desired temperature was achieved after modification of the test installation. Test B-12, with an initial temperature of 291 K (65°F), was made to obtain data for correlation with the corresponding data from testing (Test B-4) in the NASA-JSC ARMSEF 10 Megawatt Arc Tunnel.

Instrumentation: The breadboard unit instrumentation consisted of the same 30 thermocouple installations used during the original contract. The thermocouples (figure 31) were located on the surface of the HRSI, in depth in the HRSI, on the backside aluminum skin adjacent to window attachment holes, on the bondline and in back of the honeycomb support panel over the antenna, on the antenna backcap, and on the bottom and end of a tile joint gap. Plane and side view X-rays (figures 127 and 128 in ref. 1) show further details of the thermocouple installations. Platinum - 10% rhodium (+)/platinum (-) thermocouples (ISA type S, 30 gage wire) were used for the surface temperature measurements. Chrome (+)/Alumel (-) thermocouples (ISA type K, 30 gage wire) were used for the indepth, bondline, and backside temperature measurements.

TABLE II
S-BAND ANTENNA SYSTEM THERMAL TESTS
(In Chronological Order)

TEST				SURFACE ENVIRONMENT			
No.	Unit	Time[a] Sec.	Init. Temp.[b] K (°F)	Correlation	Max. Temp.[c] K (°F)	Facility Test No.	Elec. Test Schedule
Facility: NASA-JSC ARMSEF 10 Megawatt Arc Tunnel							
B-1	Breadboard	1695	294 (70)	N/A	1205 (1710)	S404	
B-2	↓	1215	302 (84)	↓	1394 (2050)	S405	
B-3		1391	299 (78)		1339 (1950)	S406	
B-4	↓	1504	298 (77)	↓	1333 (1940)	S407	X
P-1	Prototype #1	2352	295 (71)	N/A	1239 (1770)	S442	X
P-2	↓ ↓	2966	295 (71)	↓	1289 (1860)	S443	X
P-3		3927	299 (78)		1289 (1860)	S444	
P-4		3947	303 (86)		1272 (1830)	S445	
P-5		3961	304 (88)		1261 (1810)	S446	X
P-6		3950	295 (71)		1316 (1910)	S447	
P-7		3946	314 (106)		1311 (1900)	S448	
P-8		3946	310 (98)		1316 (1910)	S449	
P-9		3945	325 (126)		1311 (1900)	S450	
P-10	↓ ↓	3946	296 (74)	↓	1300 (1880)	S451	X
Facility: MDC Mission Environment Simulator (Radiant Heater)							
B-5	Breadboard	1310	291 (65)	Arc Tunnel	1294 (1870)	1	
B-6	↓	1340	291 (65)	↓ ↓	1277 (1840)	2	
B-7		1200	291 (65)		1277 (1840)	3	
B-8		1160	287 (58)	Orbiter Entry	1372 (2010)	4	
B-9		A/R	292 (66)		1539 (2310)	5	
B-10		↓	211 (-80)	↓ ↓	1516 (2270)	6	
B-11			172(-150)		1533 (2300)	7	
B-12	↓	1380	291 (65)	Arc Tunnel	1266 (1820)	8	
P2-1	Prototype #2	A/R	327 (130)	Orbiter Entry	1544 (2320)	9	X
P2-2	↓ ↓	↓	322 (120)		(d)	10	X
P1-11	Prototype #1	A/R	177(-140)	Orbiter Entry	1505 (2250)	11	X
P1-12			177(-140)		1516 (2270)	12	X
P1-13			292 (67)		1516 (2270)	13	
P1-14			330 (135)		1516 (2270)	14	X
P1-15	↓ ↓	↓	119(-245)	↓ ↓	1505 (2250)	15	X

NOTES: (a) Arc or Heater Run Time
(b) Nominal Value
(c) T/C 30
(d) Surface T/C's Lost During Preceding Test
A/R As Required to Correlate Environment

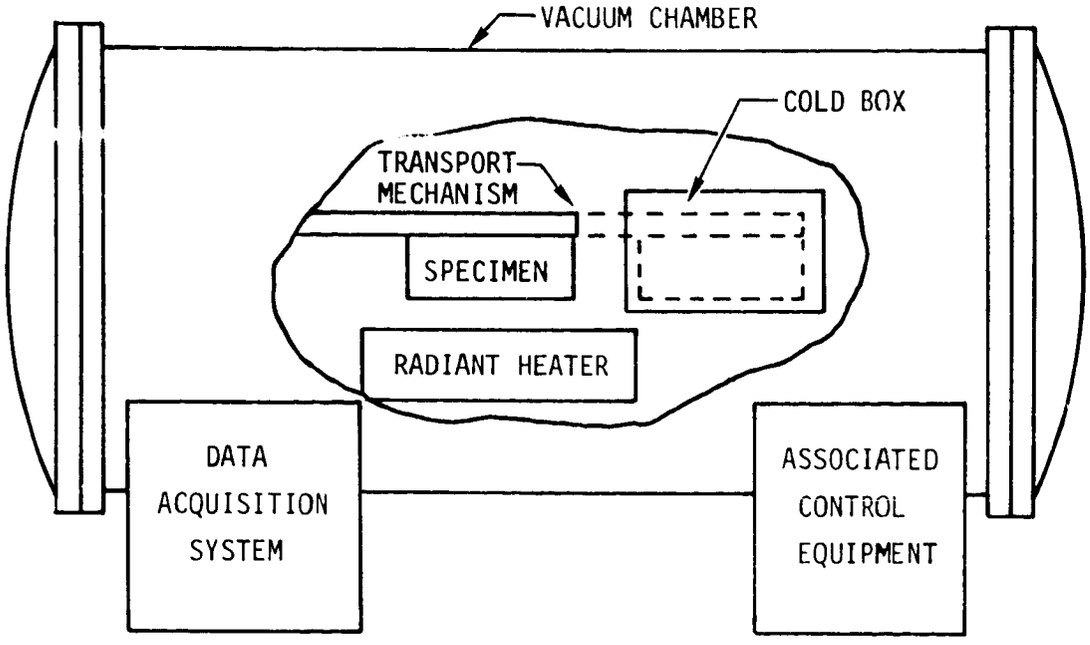

FIGURE 23 MDC MISSION ENVIRONMENT SIMULATOR SCHEMATIC

Thermocouples (ISA type K) were also installed on an inner surface of an HCF guard tile, and on the foil bonded to the inside of backside insulation box. Additional thermocouples were installed on structures, such as the test article support truss, and the cold box. Data from these thermocouples were used to monitor support equipment temperatures in order to determine its effect on the test article.

Test results: Test B-5 was conducted to check out instrumentation and the environmental simulation capability of the facility. Heater power and chamber pressure were regulated attempting to follow profiles representative of an arc tunnel environment with the HRSI surface temperature peaking at about 1294 K (1870°F). Using the Data Trak alone, it was very difficult to follow the desired surface temperature profile. Problems were encountered primarily at abrupt changes corresponding to tunnel startup and shutdown. Surface temperature response tended to overshoot the profile in these regions. However, it was felt that simulation of tunnel startup and shutdown was inconsequential relative to the tolerances required in duplicating the surface temperature profile. Therefore, simulation of the arc tunnel environment would be considered acceptable as long as the average, or overall, change in temperature with respect to time was about the same.

Difficulties were also encountered in trying to maintain the relatively constant surface temperature corresponding to the constant flow and heat transfer conditions in the arc tunnel. First, as discussed above, the temperature tended to overshoot the desired level. Data points were taken every twenty seconds, during which temperature fluctuations as high as 55 K (100°F) were measured. That is, the surface temperature response appeared very sensi-

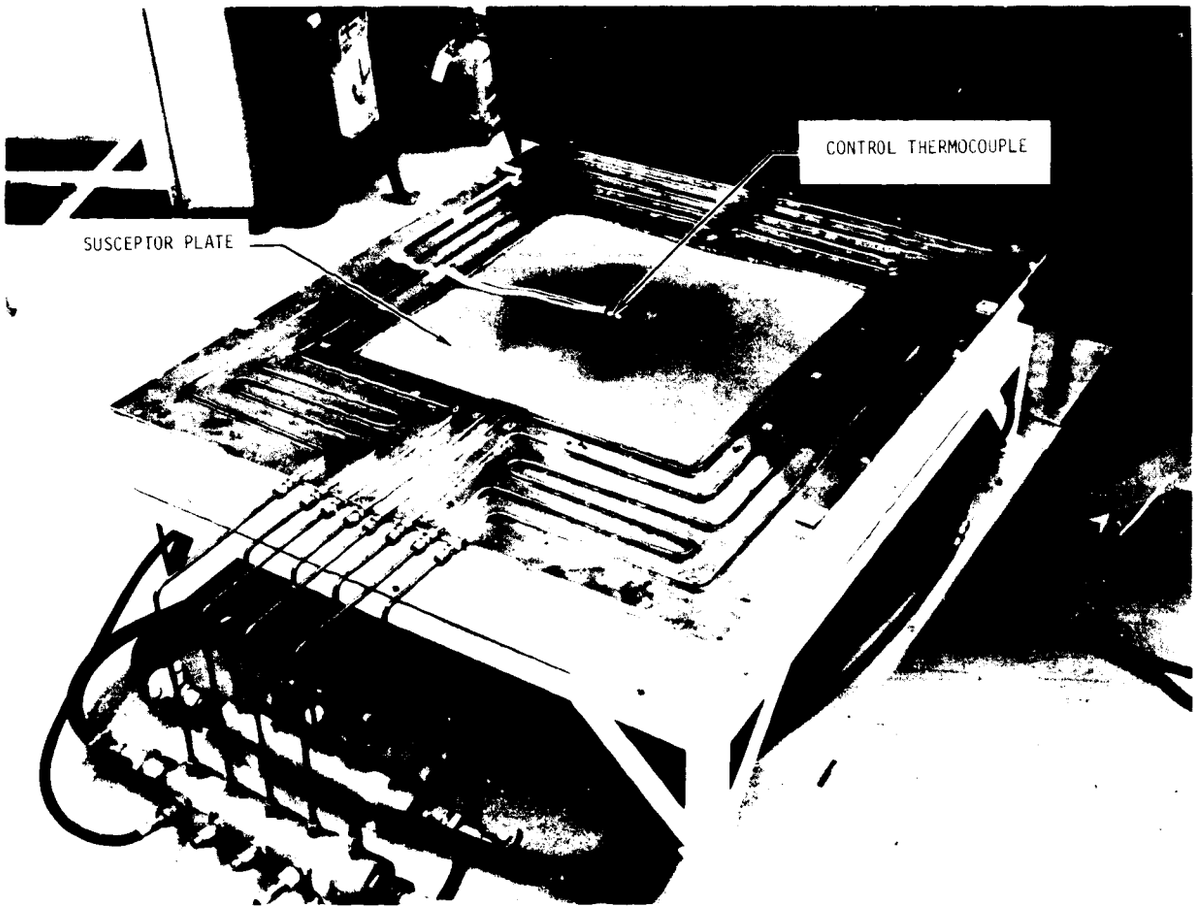

FIGURE 24 RADIANT HEATER ASSEMBLY

tive to heater power requirements as regulated by the Data Trak. Therefore, it was decided that in future tests the surface temperature should be monitored more closely and the Data Trak manually overridden when necessary.

The second test (B-6) was run as a repeat of the first, except that the Data Trak trace was replaced with a smoother profile, and manually overridden as considered necessary for correlation. The resulting correlation and measurements obtained were considered satisfactory.

Some anomalies in the responses of pertinent thermocouples indicated the occurrence of backside heating. To minimize this heat transfer, a box was constructed of Rigidized Dynaflex insulation with aluminum foil bonded on the inside (figure 31). Thermocouples were also installed on the foil in order to establish the thermal environment seen by the back side of the test article.

The third test (B-7) was run as a final check of procedures and modifications to the installation, and to obtain data for direct correlation with arc tunnel data. The comparison of the measured surface temperature with the

FIGURE 25 MDC MISSION ENVIRONMENT SIMULATOR CONTROL AND DATA ACQUISITION SYSTEMS

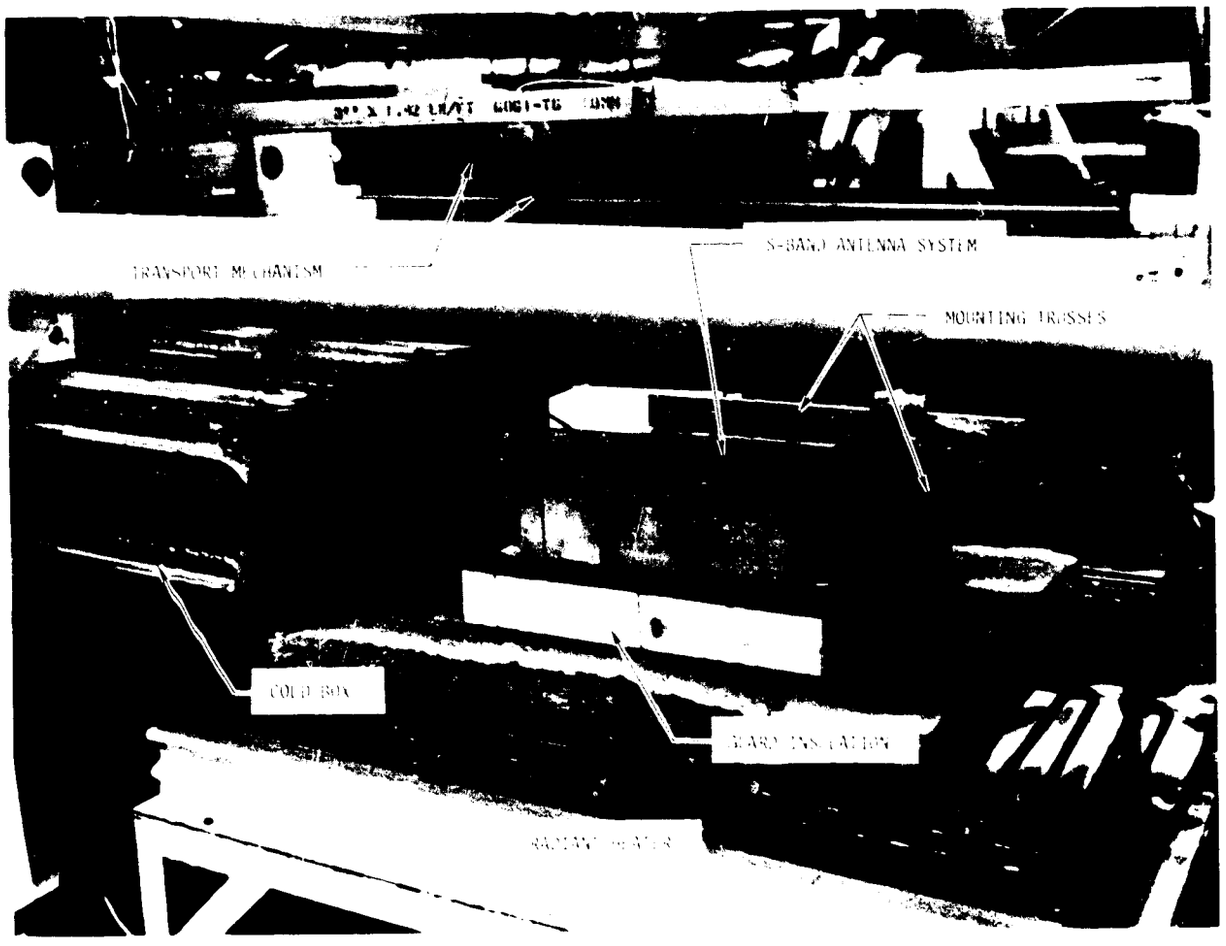

FIGURE 26 S-BAND ANTENNA SYSTEM THERMAL TEST INSTALLATION

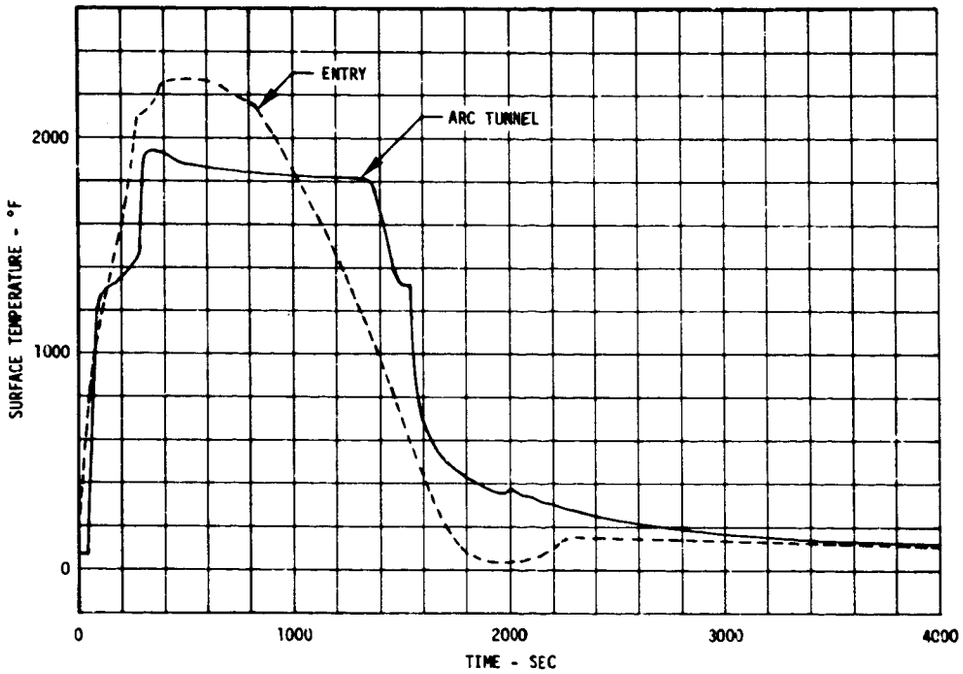

FIGURE 27 PREDICTED ENTRY AND ARC TUNNEL TEST HEATING HISTORIES

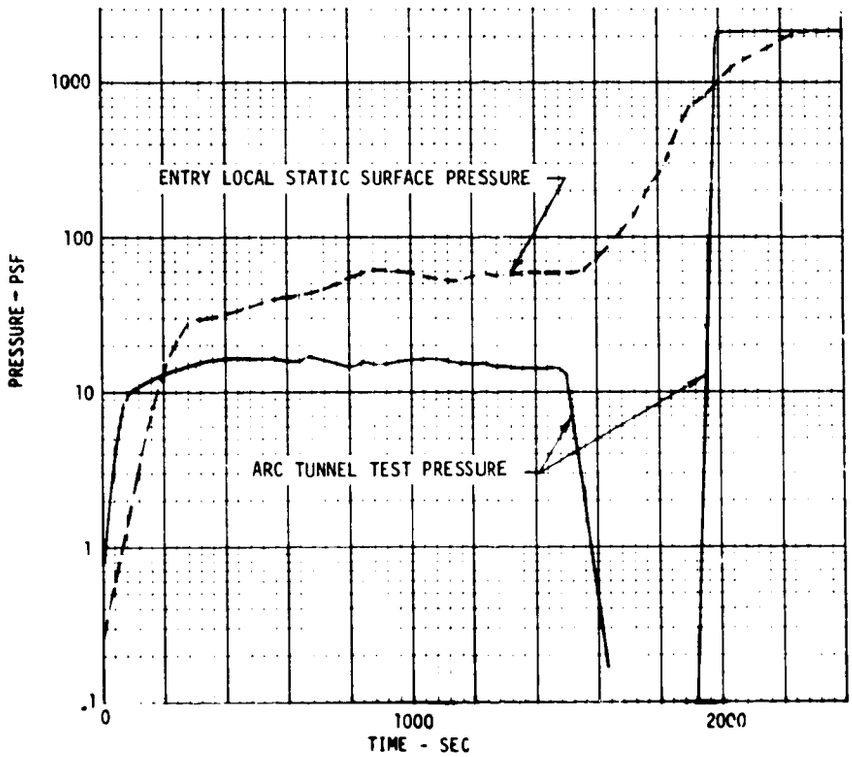

FIGURE 28 ENTRY AND ARC TUNNEL TEST PRESSURE HISTORIES

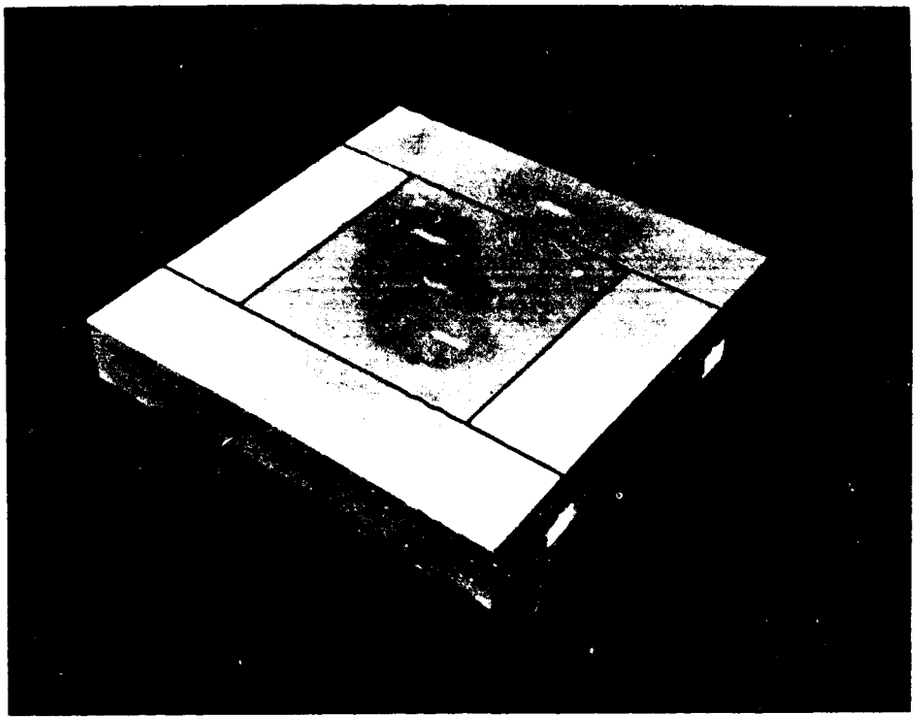

Top View

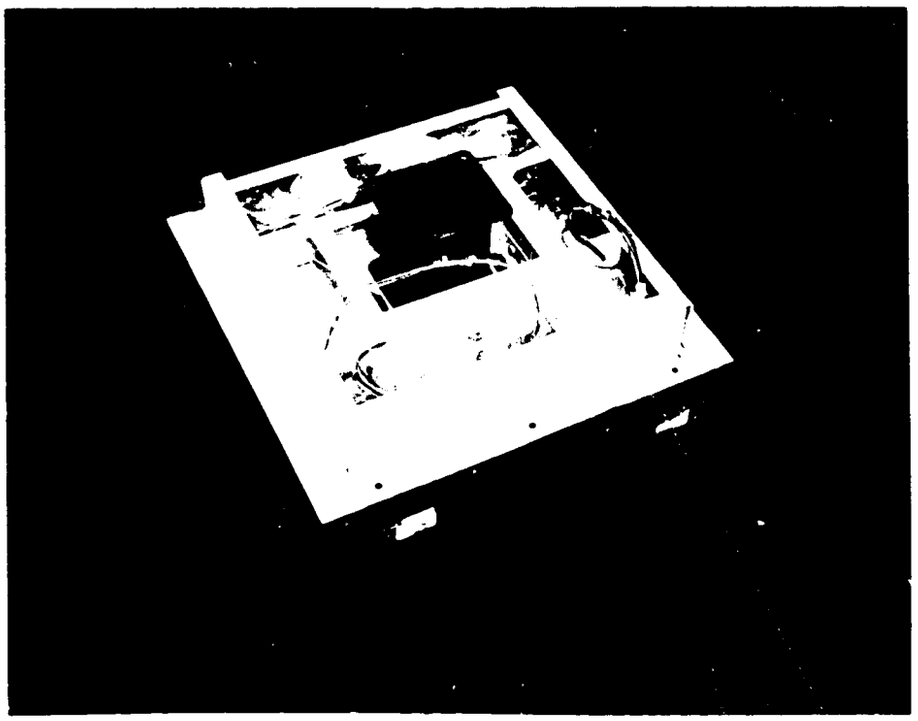

Bottom View

FIGURE 29 BREADBOARD S-BAND ANTENNA SYSTEM ASSEMBLY

FIGURE 30 BACKSIDE THERMAL INSULATION BOX FOR S-BAND ANTENNA SYSTEM TESTS

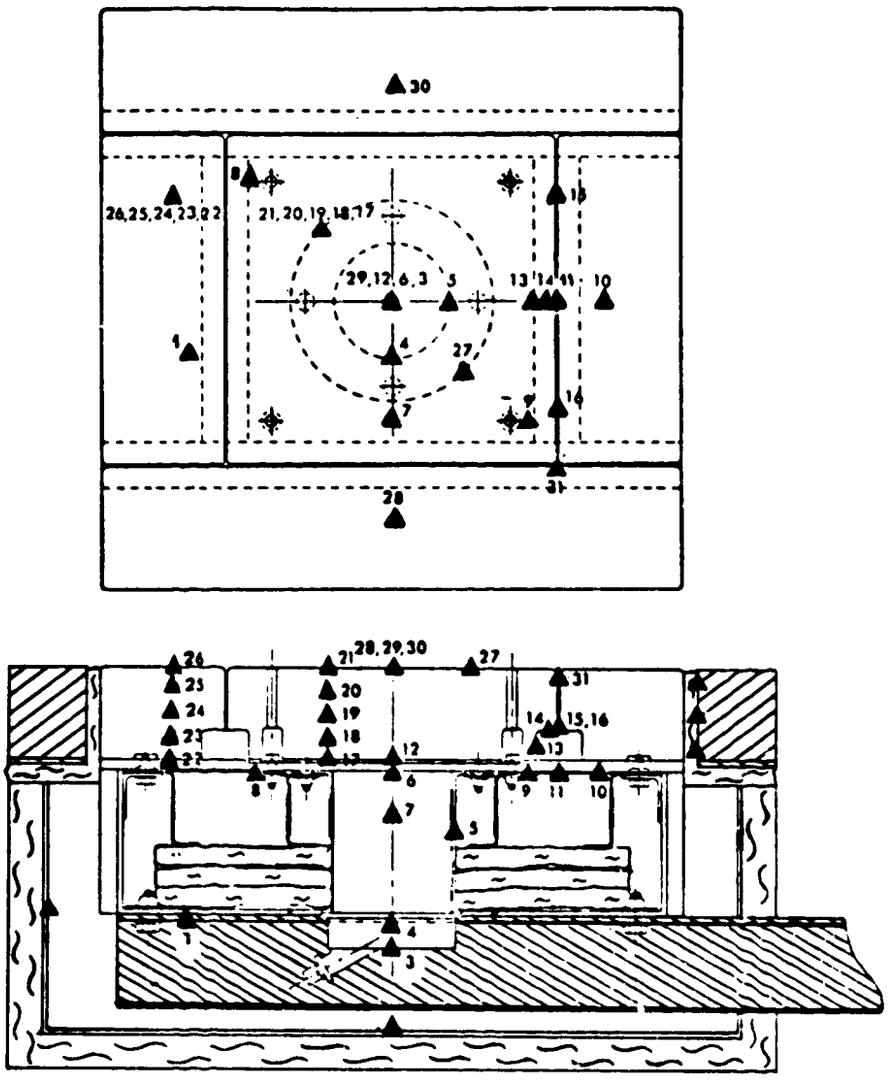

FIGURE 31 THERMOCOUPLE LOCATIONS FOR BREADBOARD TESTS

desired temperature is shown in figure 32. Since the period of high temperature was shorter than desired and the cool down too slow, this data was not considered satisfactory for correlation with the arc tunnel data. The measured and desired temperature during initial cool down compared satisfactorily; however, at about 540-430 K (100-800°F) the temperature tended to plateau out and remain relatively high for almost 1000 seconds. This phenomenon was attributed to heat stored in the heater susceptor plate. The slow cool down results in an increase in total heat load which biases or adds uncertainty to the backside structural temperatures. Therefore, in order to obtain improved cool down rate for subsequent testing the test article was moved into the cold box at an appropriate time.

The fourth test (B-8) simulating an entry environment with maximum surface temperature truncated to 1366 K (2000°F) was conducted to check the test article and instrumentation at a more severe condition than the plasma environment and yet less severe than the entry environment. Posttest inspection of the unit did not reveal any adverse or detrimental effects. The surface temperature response (figure 33) followed the desired temperature satisfactorily. Therefore, it was felt that exposure to the more severe orbiter entry environment could be tolerated. In test B-8, the test article was transported from the heater to the cold box to improve the surface temperature cool down rate. This was done when a real-time plot of temperature began to level off at about 866 K (1100°F). The surface temperature (figure 33) did respond to the movement of the test article but not to the extent desired. Temperature dropped only slightly, and then resumed leveling out. At the time the test article was moved, chamber pressure was still relatively low and radiation was the primary mode of heat transfer. Therefore, to improve the cool down response, the cold box was coated inside with a high emittance paint and a surface spary bar installed to permit blowing nitrogen over the surface of the test article.

The fifth test (B-9) was the first exposure of the breadboard unit to a full simulation of the orbiter entry environment (figure 34). The desired cool down rate was achieved by coating the inside of the cold box and using nitrogen cooling. The test was initiated at room temperature to avoid excessive thermal shocking of the unit and still ascertain capability with this more severe environment. No degradation was noted afterwards and the thermal data obtained was satisfactory.

Typical temperature responses measured by thermocouples (T/C's) at the HRSI tile/strain isolator bondline (T/C 12, 17, & 22), backside surface of the structural skin (T/C 8), and the antenna (T/C 3, 5, & 6) are shown in figure 35. All measurements of the structural skin temperatures are shown in figure 36. Structural skin temperatures were relatively uniform. In general, all substrate temperatures were higher than measured during the arc tunnel testing, but were about 16 K (28°F) lower than the design values. The lower temperatures are attributed to the heat sink provided by the test container assembly in which the antenna assembly was mounted.

Test B-10 was intended to check out the coldsoak capability of the antenna system. However, with the test article suspended on the truss structure in the

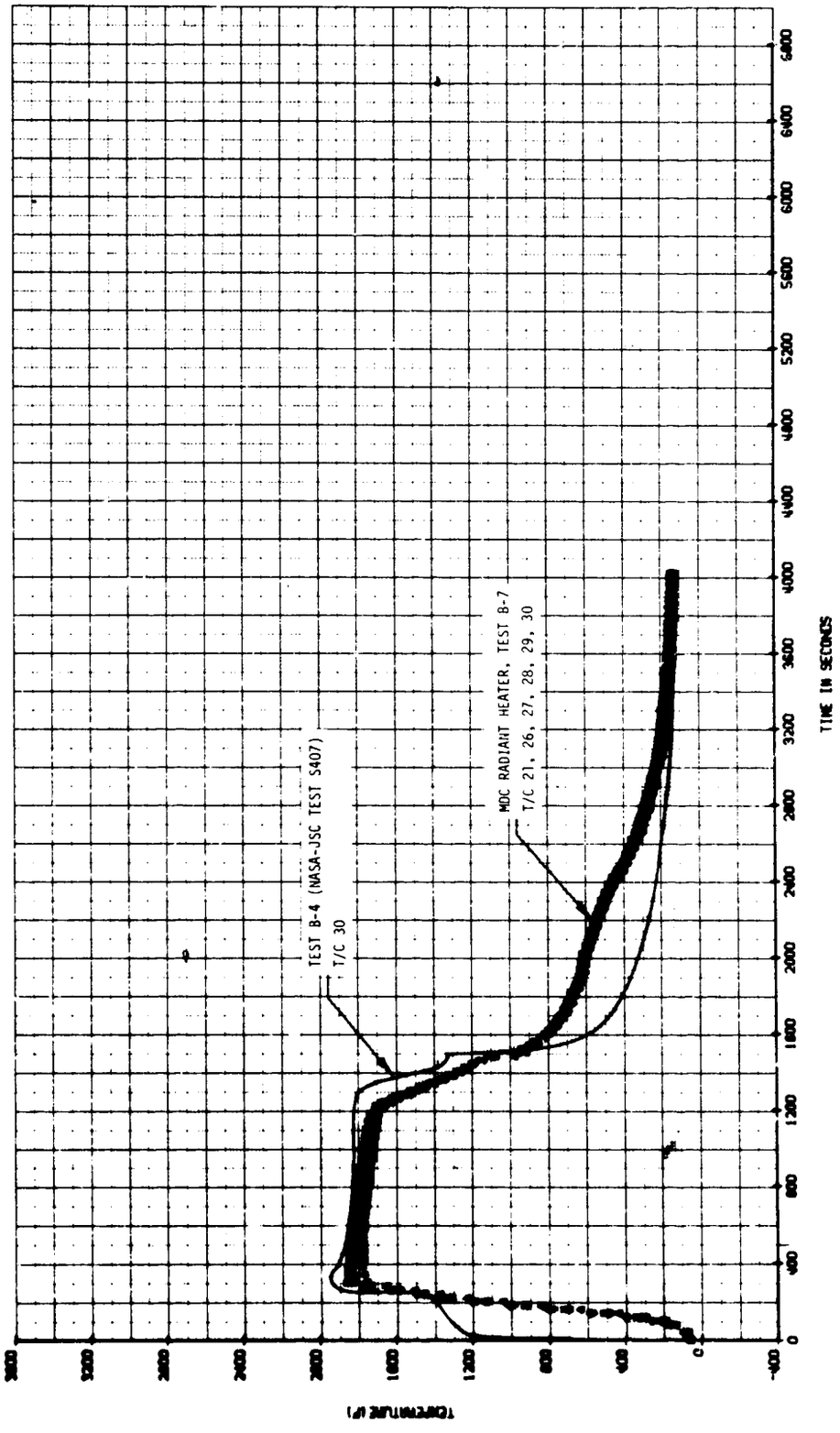

FIGURE 32 HRSI SURFACE TEMPERATURE HISTORY COMPARISON FOR PLASMA AND RADIANT HEATING

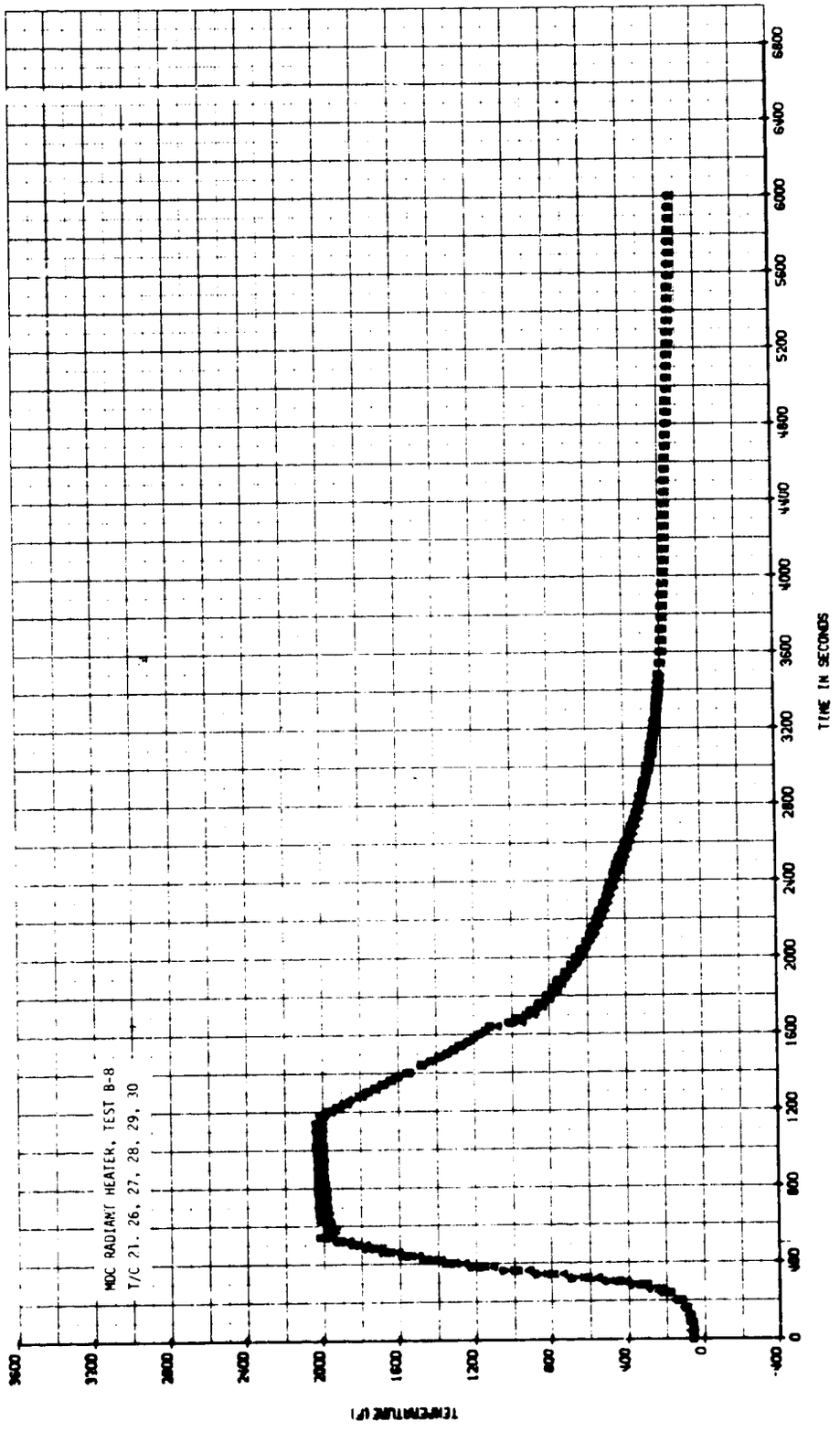

FIGURE 33 HRSI SURFACE TEMPERATURE HISTORY – TEST ARTICLE AND INSTRUMENTATION VERIFICATION (TEST B-8)

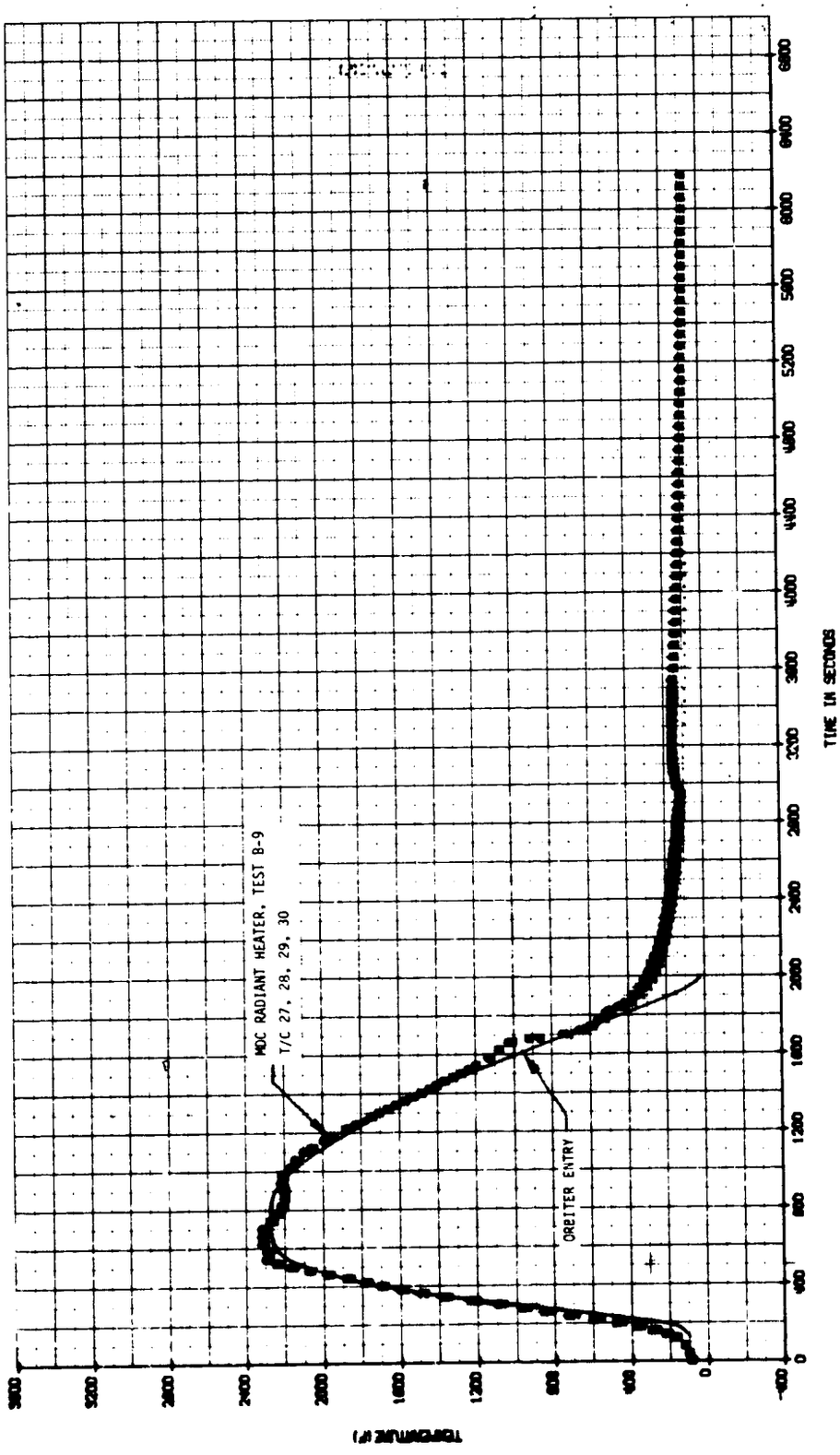

FIGURE 34 HRSI SURFACE TEMPERATURE HISTORIES – ORBITER ENTRY ENVIRONMENT (TEST B-9)

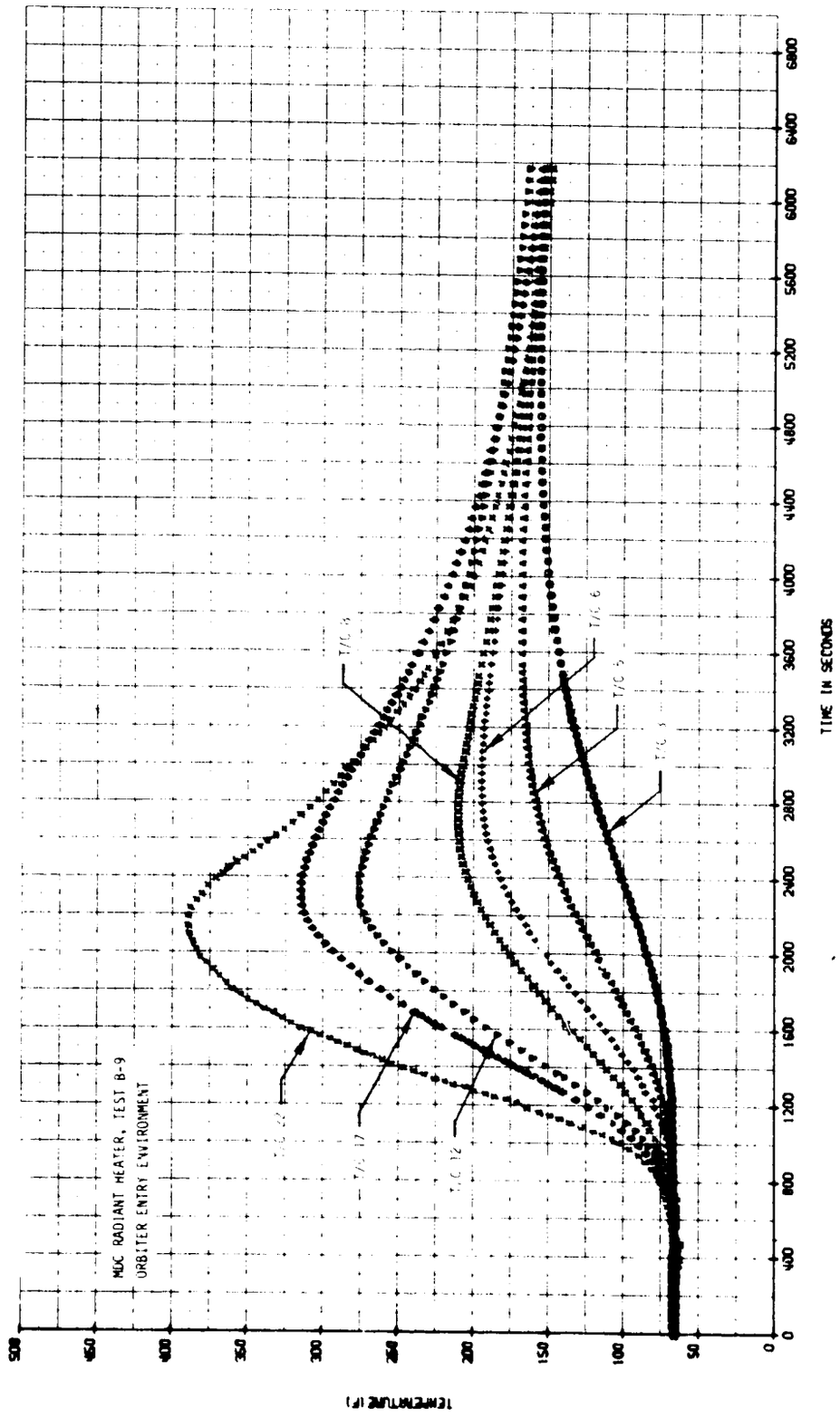

FIGURE 35 BONDLINE STRUCTURAL SKIN AND ANTENNA TEMPERATURE HISTORIES – ORBITER ENTRY ENVIRONMENT (TEST B-9)

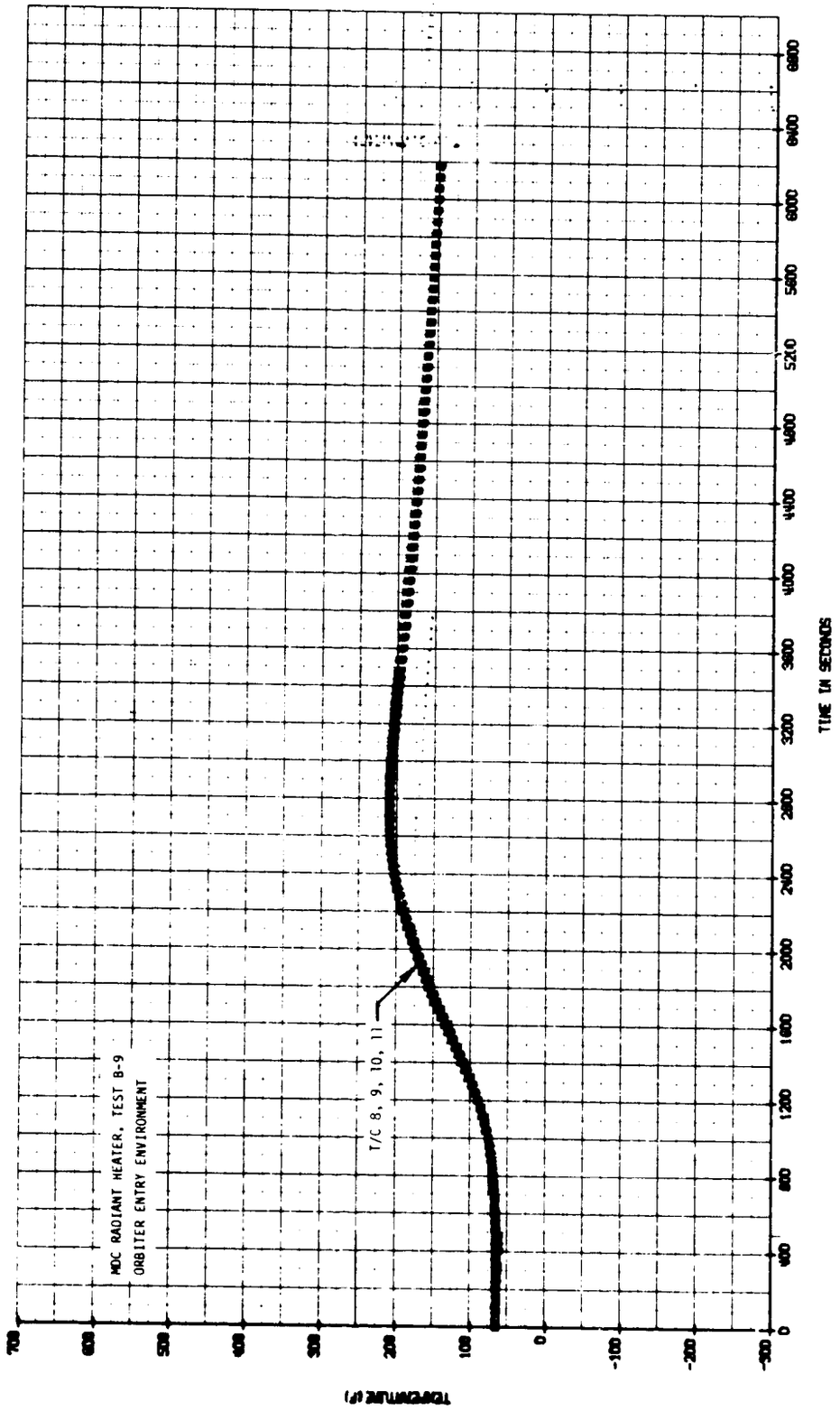

FIGURE 36 STRUCTURAL SKIN TEMPERATURE HISTORIES – ORBITER ENTRY ENVIRONMENT (TEST B-9)

cold box for about 24 hours, substructural and antenna temperatures of 172 K (-150°F) could not be achieved. With the cold box wall temperatures at about 160 K (-280°F) test article temperatures stabilized to about 211 to 216 K (-80 to -70°F). Therefore, a test was made to obtain an intermediate data point. Some typical surface and substrate temperature responses are shown in figures 37 and 38. Note the initial values. During the time required to transport the test article from the cold box to the heater and start the thermal cycle, the surface temperatures rose to about 255 K (0°F).

The inability to achieve the desired temperature was attributed primarily to heat conduction into the test article along the truss support structure, which was 1/4 inch thick aluminum L-angle. Outside the cold soak box this structure was exposed to chamber environment of about 272 K (30°F). Another contributing factor was that the cold soak box itself was open to the chamber environment. The rear plate had about a 2.5 cm (1.0 in.) cut out for the spray bar, and the front was completely open to permit model transport.

A check was performed to verify the basic adequacy of the cold box by isolating the heat path of the support truss. The test unit assembly, including backside insulation box, was removed from the truss structure and placed inside the cold box. In this condition the cold soak was repeated, and no difficulties in reaching the desired temperature level of 172 K (-150°F) were encountered.

The test facility was modified to minimize this interface with the chamber environment during cold soak. One arm of the truss support structure was shortened to reduce the number of attachment points and improve the test article installation access. Teflon washers were installed between the test container assembly and truss structure at the three remaining attachment points. Liquid nitrogen cooling lines were also added to the truss structure to provide a heat flow barrier.

For test B-11, the test assembly was cold soaked to 172 K (-150°F) and the surface temperature of the HRSI tile correlated with the temperature history representative of a typical Orbiter entry. The correlation of surface temperature, representative of simulating the orbiter entry environment is shown in figure 39. Temperature responses measured at the HRSI bondline (T/C 12, 17 & 22), on the backside of the structural skin (T/C 8 & 10) and on the antenna case and support (T/C 3 & 5) are shown in figure 40. As in preceeding tests, the HRSI surface temperatures rose considerably from the cold soak level during the time when the test article was moved over the heater and the heating was initiated. Because of the low initial value, temperatures of deeper components (skin and antenna) do not even achieve room temperature during the test. Even after 2600 seconds, representative of the end of entry and the orbiter having landed, the antenna was still relatively cold.

The last breadboard test (B-12) was intended to provide data for comparison with similar results from testing in NASA-JSC arc tunnel. The test was initiated at room temperature and a pressure profile corresponding to arc tunnel startup. The surface temperature correlation is shown in figure 41. The rise to "constant" temperature did not occur as rapidly as desired. To

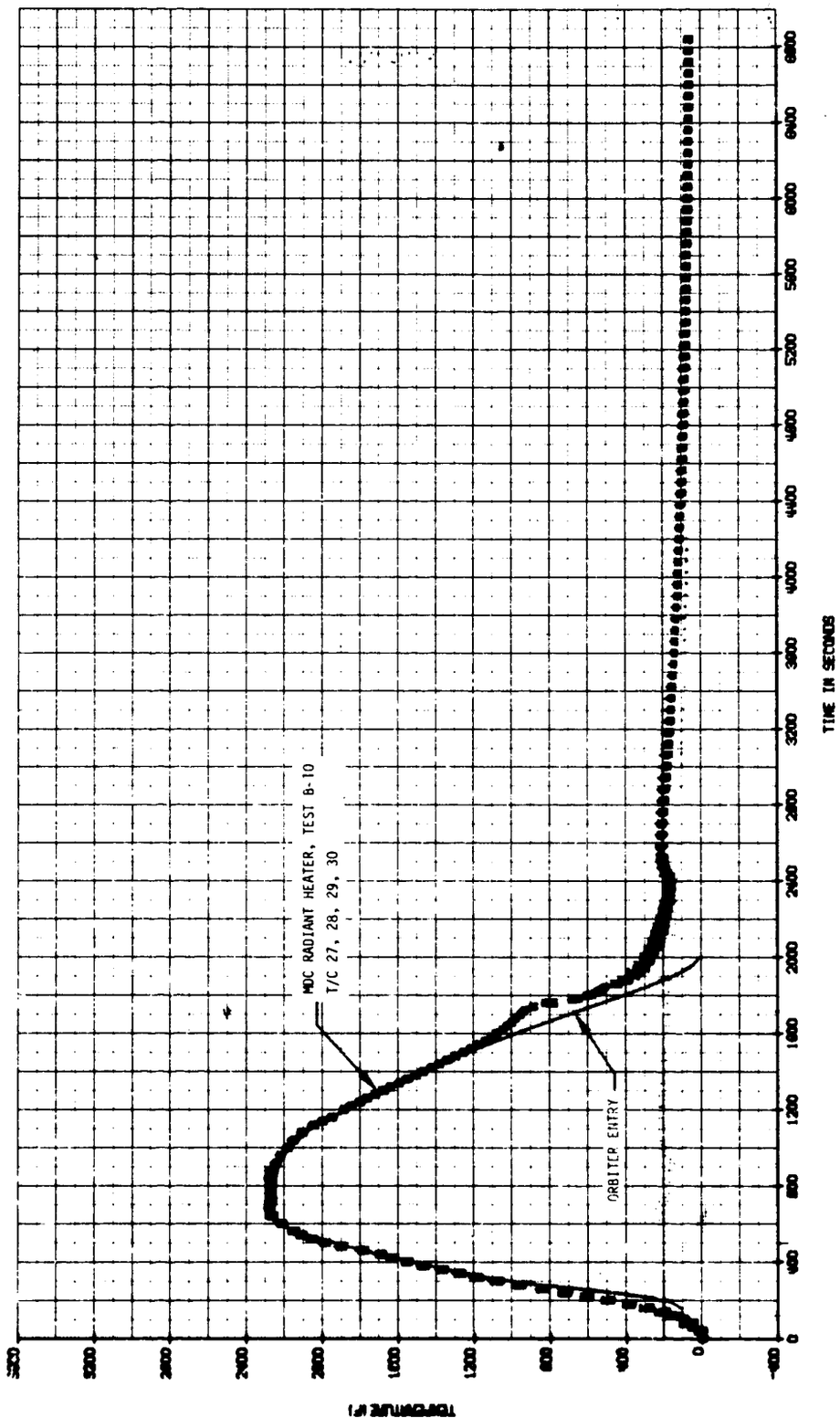

FIGURE 37 HRSI SURFACE TEMPERATURE HISTORIES – ORBITER ENTRY ENVIRONMENT
(TEST B-10, T_o = 216 K (-70°F))

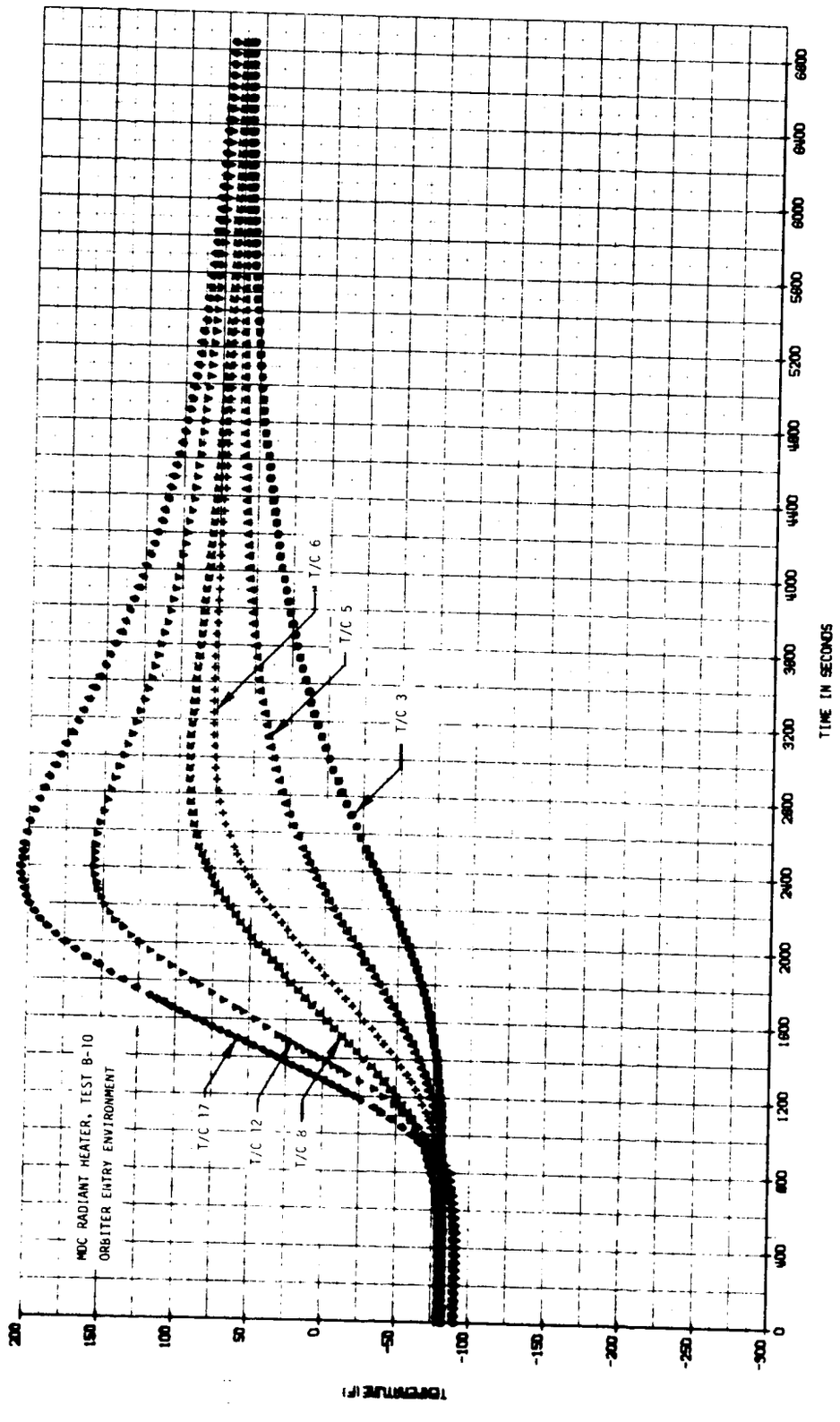

FIGURE 38 BONDLINE, STRUCTURAL SKIN AND ANTENNA TEMPERATURE HISTORIES – ORBITER ENTRY ENVIRONMENT (TEST B-10, T_o = 216 K (-70°F))

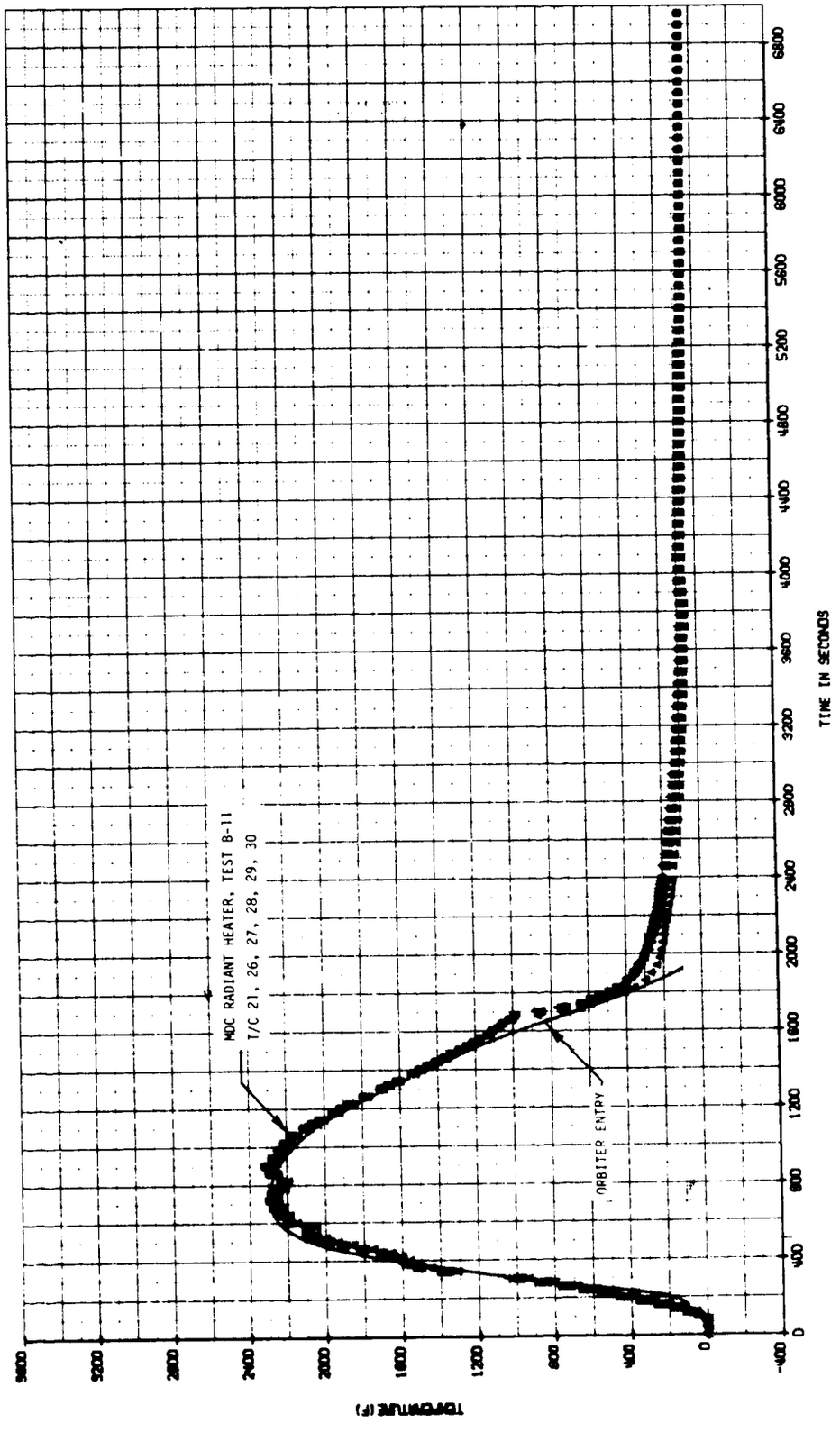

FIGURE 39 HRSI SURFACE TEMPERATURE HISTORIES – ORBITER ENTRY ENVIRONMENT
(TEST B-11, T_O = 172 K (-150°F))

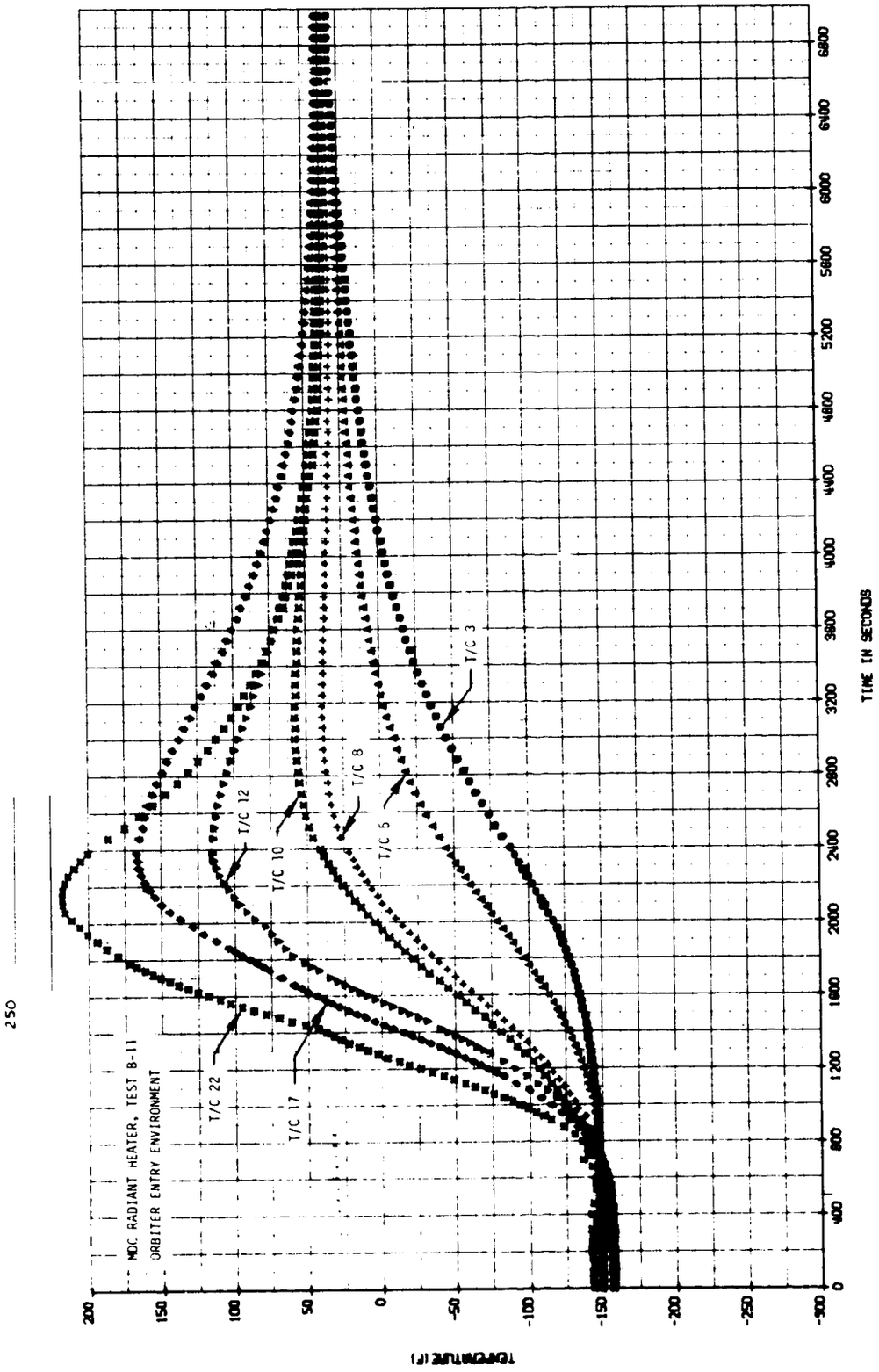

FIGURE 40 BONDLINE, STRUCTURAL SKIN AND ANTENNA TEMPERATURE HISTORIES – ORBITER ENTRY ENVIRONMENT (TEST B-11, T_0 = 172 K (–150°F))

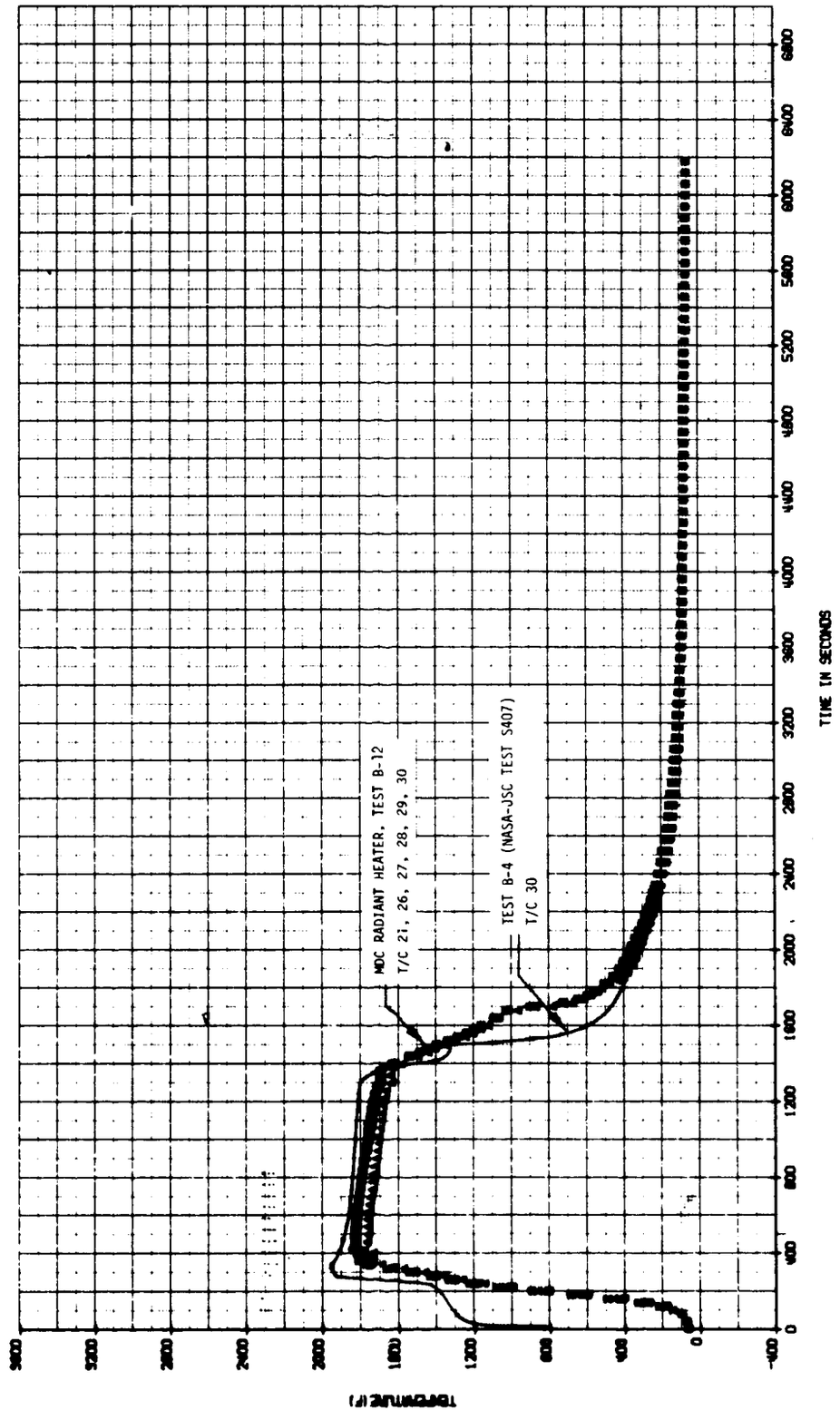

FIGURE 41 HRSI SURFACE TEMPERATURE HISTORIES – SIMULATED ARC TUNNEL ENVIRONMENT (TEST B-12)

compensate for this, the correlation profile was essentially shifted by extending the cool down portion slightly beyond the desired trace. Typical corresponding responses measured in the substructure are presented in figure 42. The rise to a second peak in the responses for bondline thermocouples (T/C 12, 17 & 22) occurred during vacuum chamber repressurization which simulated back-fill of the arc tunnel chamber.

Prototype tests. - These were conducted on the prototype units between 3 December 1973 and 22 January 1974. The purpose of these tests was: (1) to determine the effect of cold soak on the S-band antenna system; and (2) to obtain skin line temperature histories for the subsequent testing of the off-the-shelf antennas. This testing was initiated with Prototype No. 2 because this specimen had not been used in the plasma testing of the original contract. However, due to degradation on Prototype No. 2 resulting from the first thermal test, Prototype No. 1 was used to obtain the desired data.

The test installation included all the modifications, such as the addition of the backside insulation box, as discussed in the section on breadboard testing. An additional installation modification was made to thermally isolate the test container assembly from the antenna assembly. This modification consisted of the removal of the support flanges from the test container assembly. Insulation was placed between the container and the antenna assembly and long bolts with insulating washers secured the antenna system to the container assembly (figure 43).

Instrumentation: The instrumentation on the prototype article was essentially the same as on the breadboard article except that there was no thermocouple on the antenna window or in the LI-1500 HRSI around the window. Twenty-one thermocouples (figure 44) were used to monitor temperatures. Plane view X-rays (figure 151 in ref. 1) show further detail of thermocouple installation.

Test results: The first test (P2-1) used an initial temperature of 328 K (130°F) and the heating was simulated to represent the Orbiter entry environment. The initial temperature of 328 K (130°F) was achieved by utilizing the cold box as an oven by pumping hot gaseous nitrogen through the cooling coils. Bondline, structural skin, and antenna temperatures from this test are shown in figures 45 and 46. These temperatures were about 55 K (100°F) higher than expected, thus, the model was removed from the test facility and examined. Deposits of a black carbonaceous substance were found on the surfaces of the HRSI tiles and extended into the gaps (figure 47). These deposits are attributed to an exothermic reaction associated with the silicone resin used for water proofing. This reaction would account for the higher than expected temperatures. A checking of Lockheed (LMSC) records indicated that the percent silicon resin in the tiles supplied to MDC was somewhat high, running about 4.1 to 5.2 percent of the base fiber weight (normal about 3%).

A second test (P2-2) using the same initial conditions and thermal environment was conducted to determine if further burning of the silicone resin in the LI-1500 would occur and if the carbonaceous deposit would burn

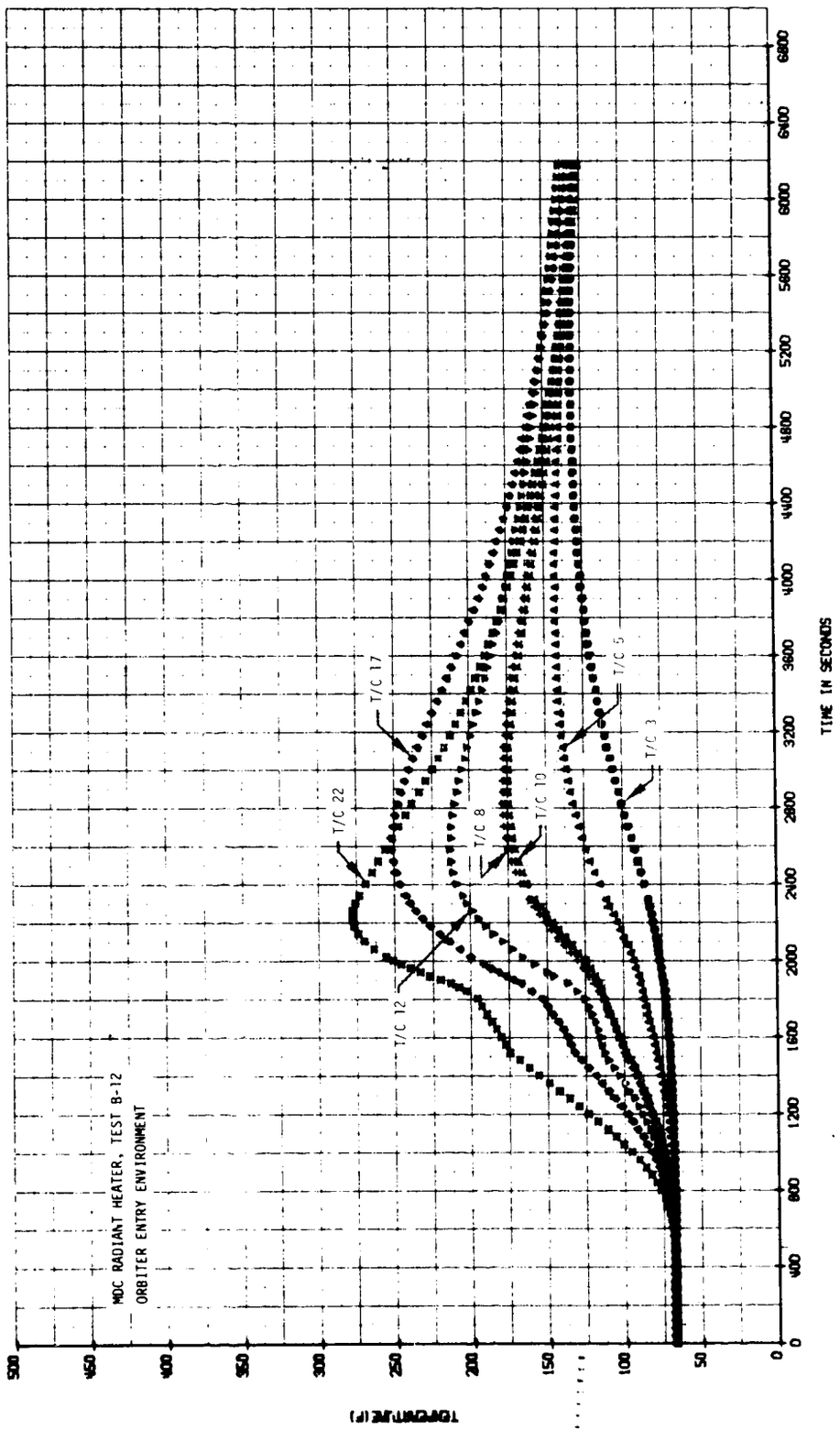

FIGURE 42 BONDLINE, STRUCTURAL SKIN AND ANTENNA TEMPERATURE HISTORIES – SIMULATED ARC TUNNEL ENVIRONMENT (TEST B-12)

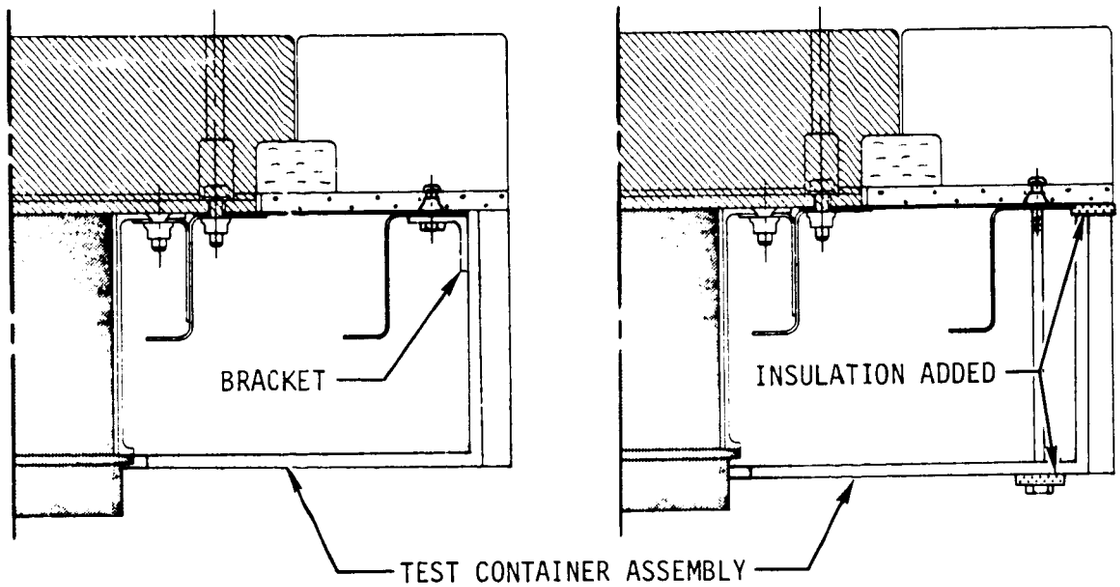

(a) BEFORE MODIFICATION (b) AFTER MODIFICATION

FIGURE 43 MOUNTING MODIFICATIONS FOR INSULATING S-BAND ANTENNA SYSTEM FROM TEST CONTAINER ASSEMBLY

off. The maximum measured temperatures of both tests are summarized in table III. The temperatures from test (P2-2) were still substantially higher than obtained from the breadboard tests performed in the NASA-JSC arc tunnel facility but lower and more realistic (i.e., of the magnitude anticipated based on initial conditions, thermal environment, and improved isolation of the model from the test container) than those from the first test. The results of the second test essentially verify that the high backside temperature during the first test were caused by the silicone combustion. The surface color was also somewhat lighter after the second test, but apparently no significant change in the deposit occurred as indicated by the electrical test results discussed in the preceeding subsections on Electrical Testing.

Since the electrical testing of Prototype No. 2 showed significant degradation in performance due to the carbonaceous deposits, it was decided, with NASA-JSC approval, to discontinue all testing on Prototype No. 2 and use Prototype No. 1 for the remaining S-band tests. Five tests simulating the Orbiter entry environment were conducted using Prototype No. 1. The initial temperatures used for these tests are given in table I.

Initial and maximum temperatures measured during those tests are summarized in table IV. The maximum temperatures are in the range expected, based on previous testing with breadboard and Prototype No. 2 units. Typical

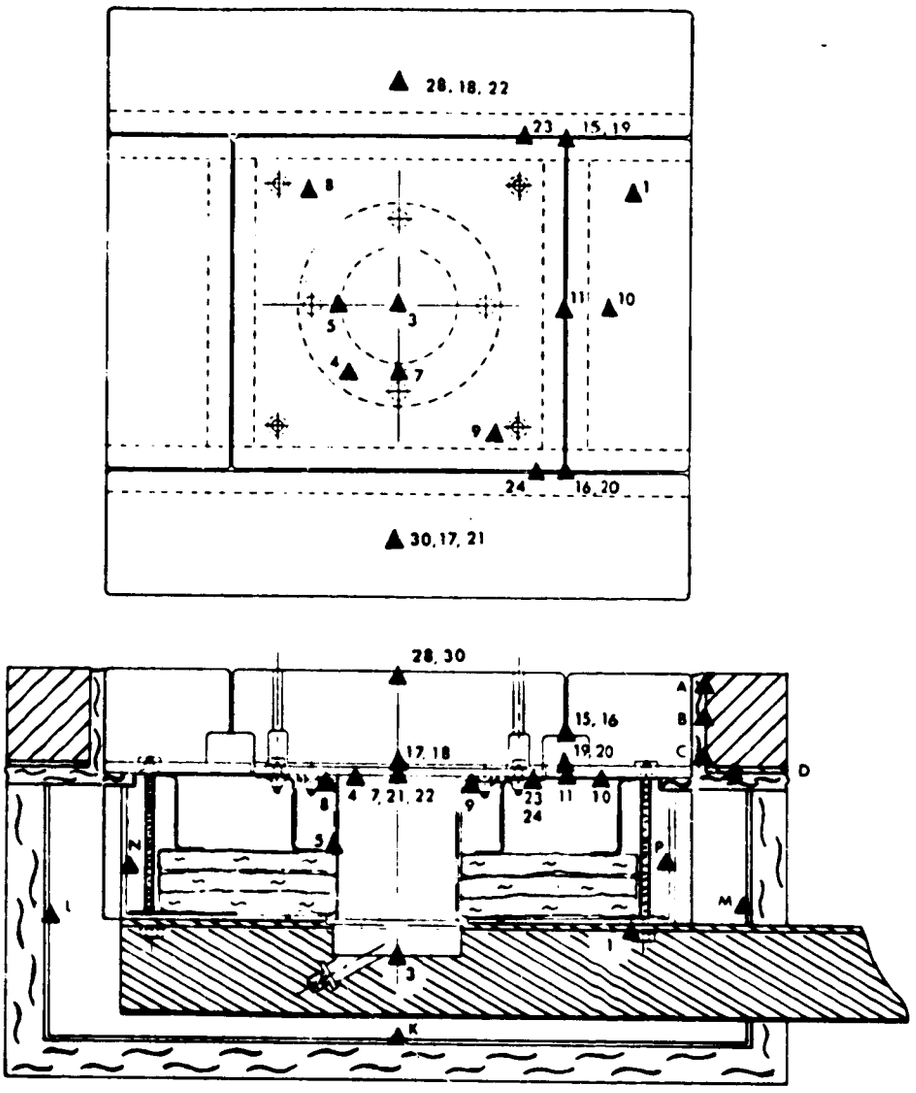

FIGURE 44 THERMOCOUPLE LOCATIONS FOR PROTOTYPE TESTS

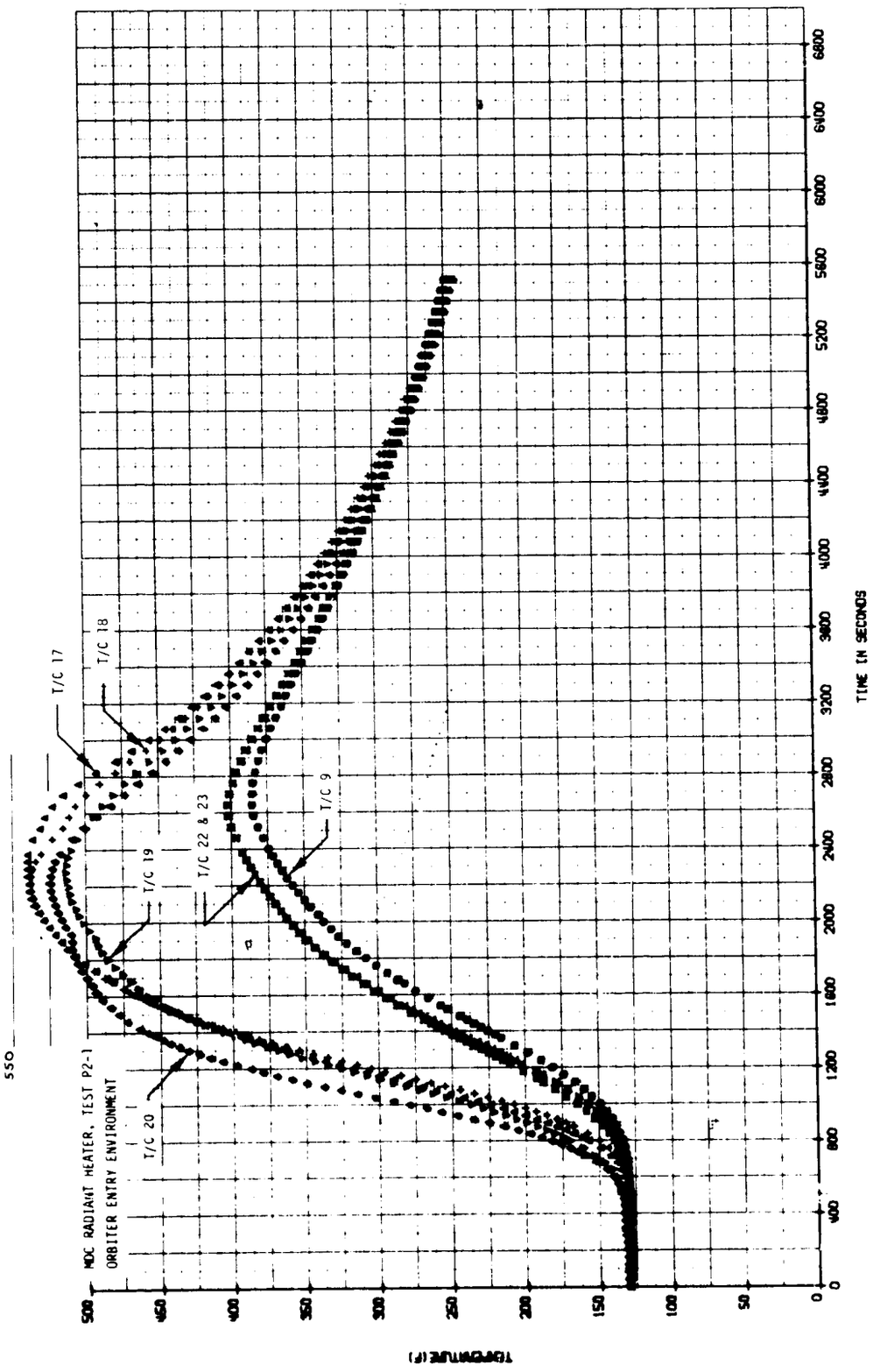

FIGURE 45 BONDLINE AND STRUCTURAL SKIN TEMPERATURE HISTORIES – ORBITER ENTRY ENVIRONMENT (TEST P2-1, T_0 = 328 K (130°F))

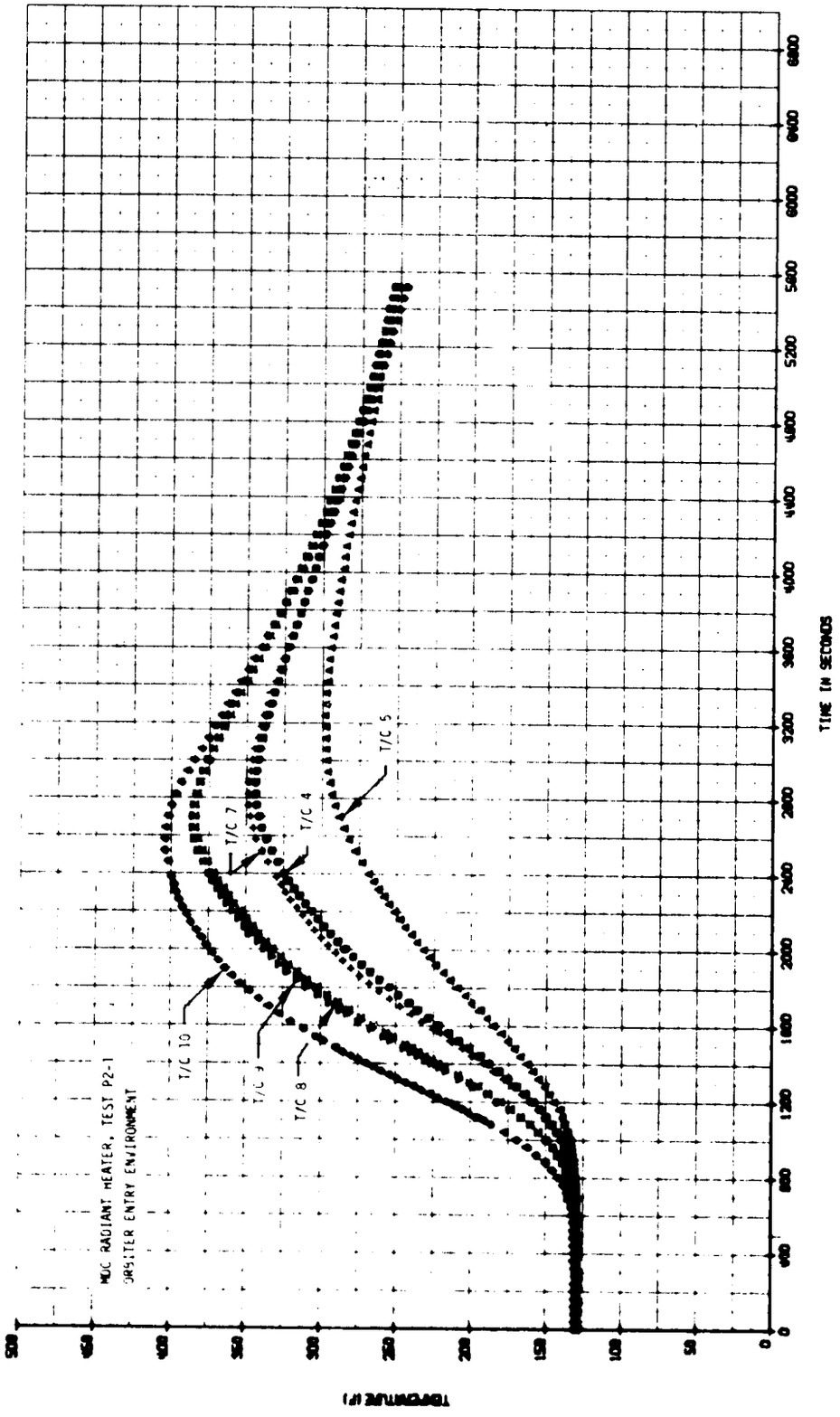

FIGURE 46 STRUCTURAL SKIN AND ANTENNA TEMPERATURE HISTORIES – ORBITER ENTRY ENVIRONMENT (TEST P2-1, T_0 = 328 K (130°F))

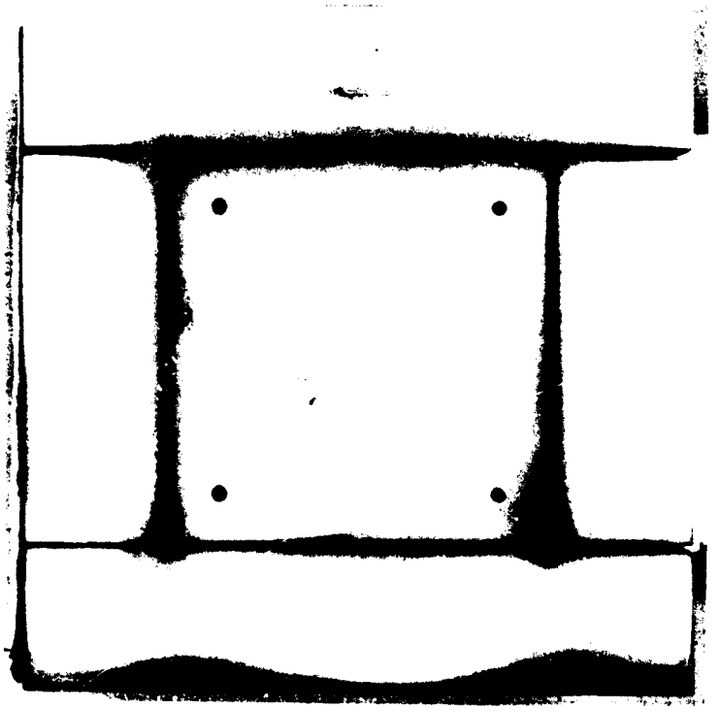

Top View

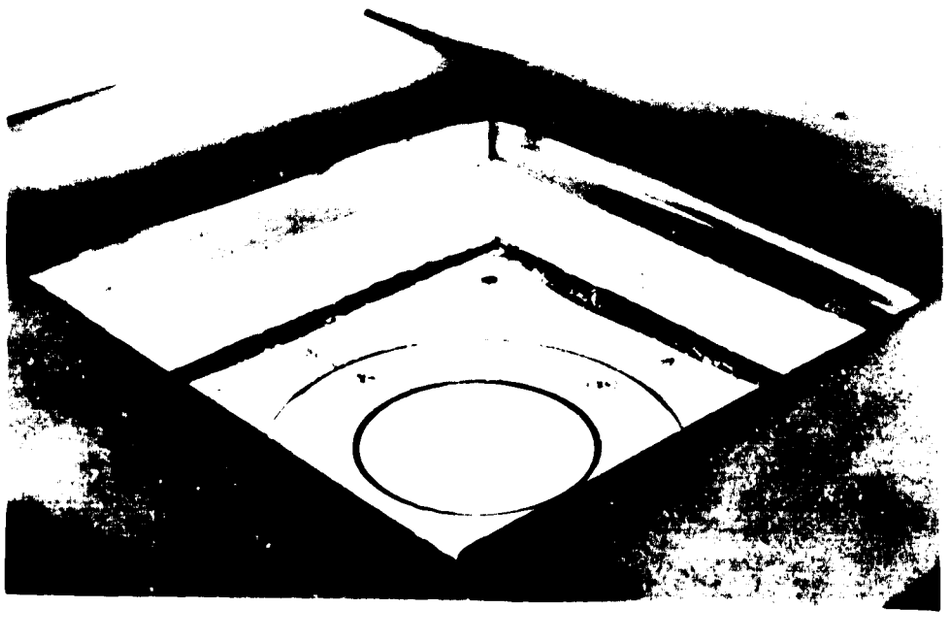

With Antenna Window Removed

FIGURE 47 PHOTOS OF PROTOTYPE NO. 2 SHOWING CARBONACEOUS DEPOSIT ON HRSI SURFACE OBSERVED AFTER FIRST THERMAL TEST

TABLE III
MAXIMUM TEMPERATURES FROM PROTOTYPE NO. 2 TESTS

THERMOCOUPLE		MAX. TEMP. (°F)	
LOCATION	NO.	TEST P2-1	TEST P2-2
SURFACE - LI-1500 TILE	28 30	2320 2320	(a) (a)
SURFACE - FILLER STRIP	15 16	1130 1435	970 1330
BONDLINE - LI-1500 TILE	17 18	540 540	385 410
BONDLINE - FILLER STRIP	19 20	515 525	370 400
SKIN - UNDER LI-1500 TILE	10 21 22	405 400 405	290 280 290
SKIN - UNDER FILLER STRIP	11 23 24	390 400 400	280 285 290
SKIN - STRINGER	8 9	385 385	275 280
ANTENNA - SUPPORT FLANGE - FLANGE BOLT - SIDE - BACK CAP	4 7 5 3	345 350 300 (b)	250 255 215 190
TEST CONTAINER ASSY - BACK - SIDE - SIDE	1 N P	(b) (c) 250	125 160 175
GUARD TILE - SIDE	A B C	2060 1695 825	1865 1020 535
GUARD TILE COLLAR	D	560	370
INSULATION BOX - BACK - SIDE - SIDE	K L M	(c) 170 175	150 120 110
RADIANT HEATER SUSCEPTOR PLATE	50	2360	2320

NOTES: (a) SURFACE T/C LOST DURING OR AFTER TEST
(b) T/C WAS NOT TAPED DOWN
(c) T/C LEAD PIN LOOSE IN CONNECTOR
(d) INITIAL TEMPERATURE WAS 130°F FOR BOTH TESTS

TABLE IV
MAXIMUM TEMPERATURES FROM PROTOTYPE NO. 1 TESTS

THERMOCOUPLE		TEST P1-11		TEST P1-12		TEST P1-13		TEST P1-14		TEST P1-15	
LOCATION	NO.	T_o	T_{max}	T_o	T_{max}	T_o	T_{max}	T_o	T_{max}	T_o	T_{max}
SURFACE - LI-1500 TILE	28	-2	2250	-2	2260	55	2260	186	2260	-2	2240
	30	-2	2250	-2	2270	55	2270	191	2270	-2	2250
SURFACE - FILLER STRIP	15	-164	894	-177	858	64	978	188	1045	-256	817
	16	-162	1049	-175	1027	64	1103	185	1172	-254	978
BONDLINE - LI-1500 TILE	17	-144	218	-144	173	67	379	141	430	-247	127
	18	-141	223	-142	185	67	356	140	413	-246	161
BONDLINE - FILLER STRIP	19	-141	197	-140	170	67	343	138	398	-246	116
	20	-140	211	-140	189	66	342	137	398	-247	151
SKIN - UNDER LI-1500 TILE	10	-136	123	-136	105	67	258	134	312	-245	51
	21	-140	119	-140	95	67	266	136	324	-244	32
	22	-136	126	-138	105	67	261	135	319	-243	52
SKIN - UNDER FILLER STRIP	11	-138	111	-138	92	66	249	134	305	-247	35
	23	-139	117	-138	95	67	260	135	316	-245	34
	24	-138	123	-138	104	67	258	134	314	-244	52
SKIN STRINGER	8	-141	107	-140	85	67	252	135	311	-245	22
	9	-139	113	-138	94	67	250	134	307	-244	38
ANTENNA - SUPPORT FLANGE	4	-140	78	-140	60	67	219	133	281	-246	3
- FLANGE BOLT	7	-139	86	-138	67	67	225	133	282	-244	9
- SUPPORT SIDE	5	-140	66	-140	48	67	192	132	249	-246	1
- BACK CAP	3	-139	(61)	-139	(45)	67	174	130	225	-246	(2)

NOTES: ALL TEMPERATURES IN °F
T_o INDICATES INITIAL TEMPERATURE
T_{max} INDICATES MAXIMUM TEMPERATURE
(XX) INDICATES T_{max} OCCURRED AT END OF DATA RECORD

temperature histories of the structural skin and antenna mounting flange, obtained from tests P1-11 through P1-15, are shown in figures 48 and 49. The temperature histories shown in figure 48 were selected as the thermal control standard for the off-the-shelf antenna tests. The effects of the initial temperature on the maximum skin temperature is shown in figure 50. These data, from comparable thermocouples on the breadboard and Prototype No. 1 tests, also show that isolating the test article from the test container assembly increased the structural skin temperatures.

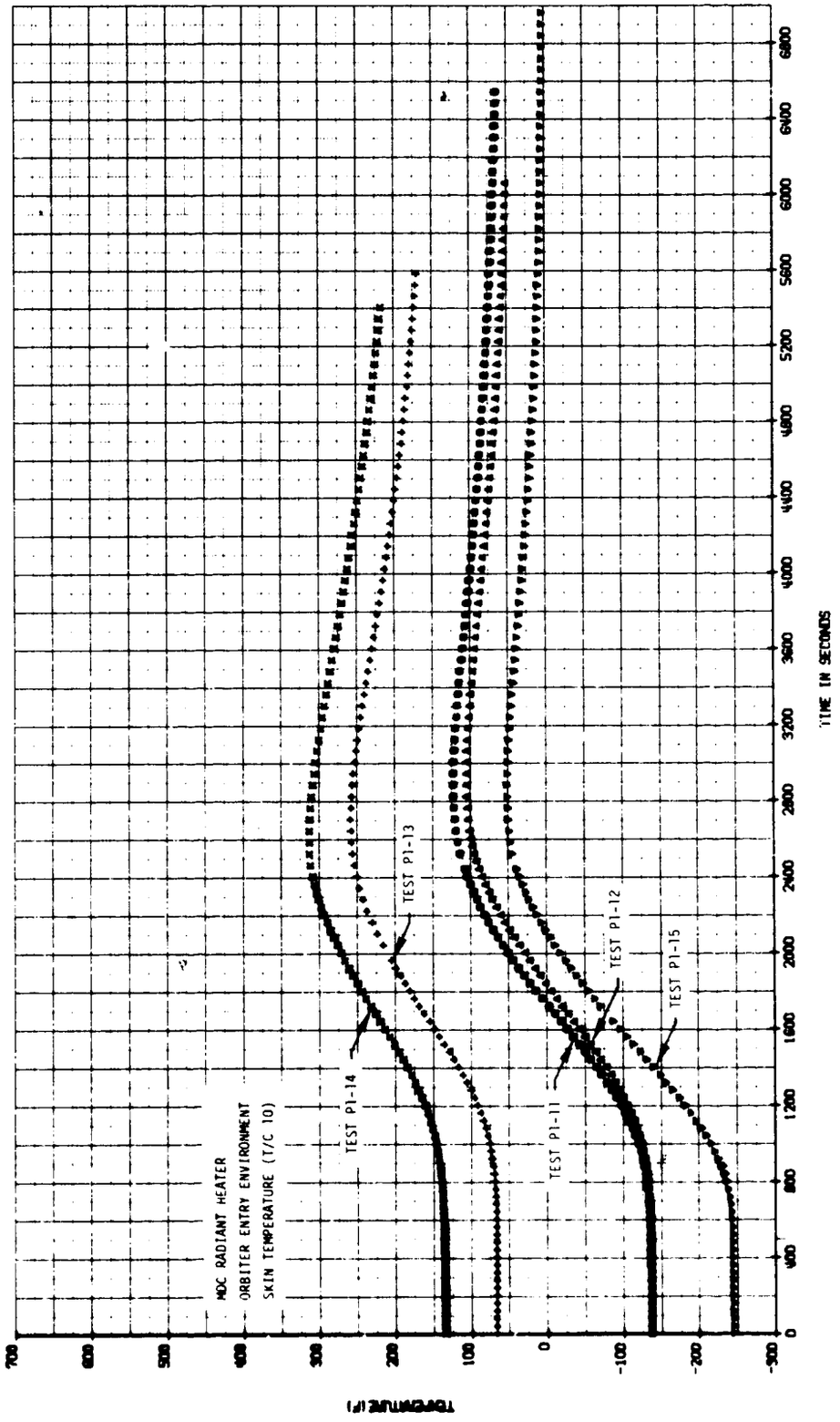

FIGURE 48 TYPICAL STRUCTURAL SKIN TEMPERATURE HISTORIES – TESTS P1-11 THROUGH P1-15

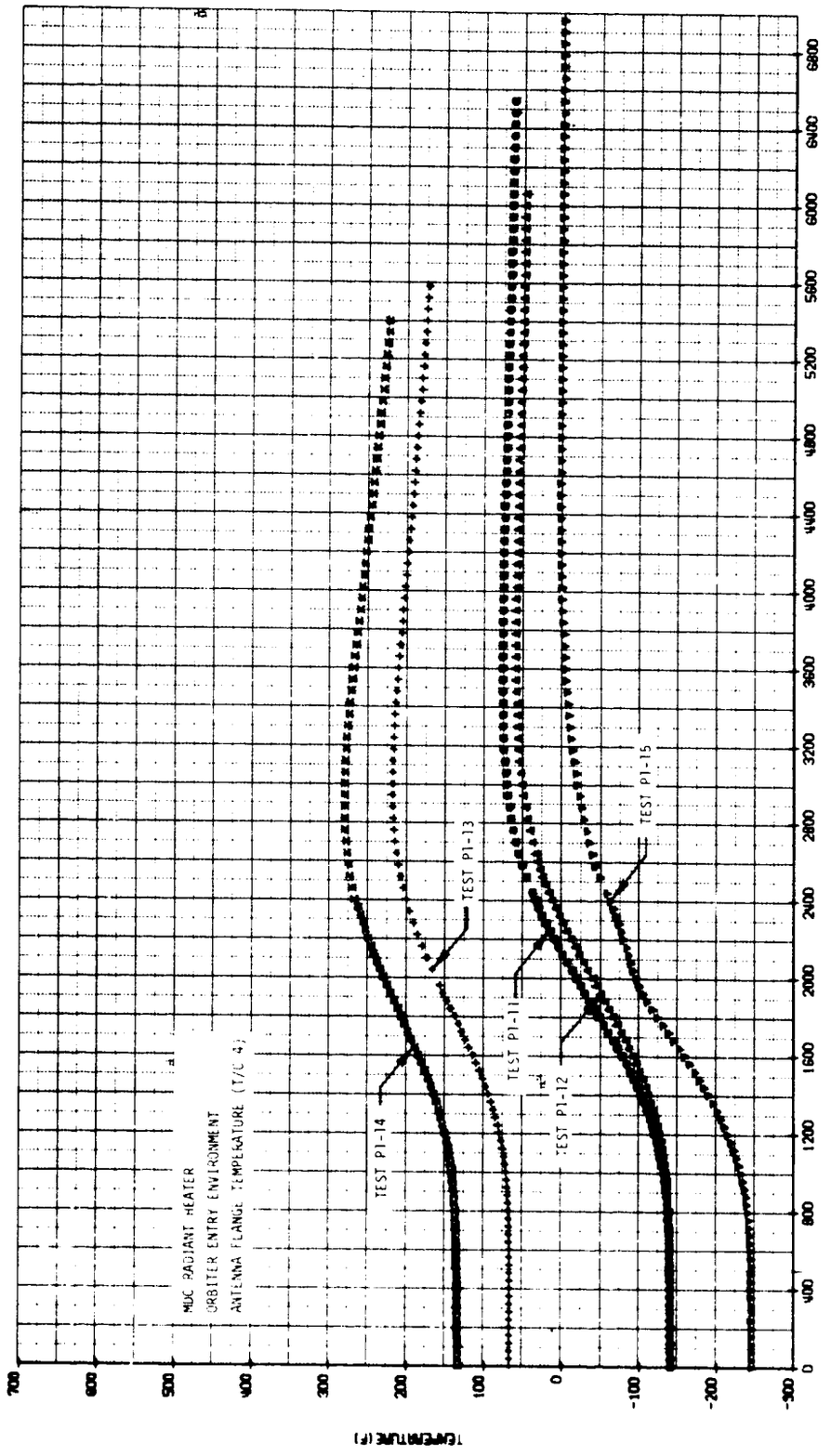

FIGURE 49 TYPICAL ANTENNA SUPPORT FLANGE TEMPERATURE HISTORIES – TESTS P1-11 THROUGH P1-15

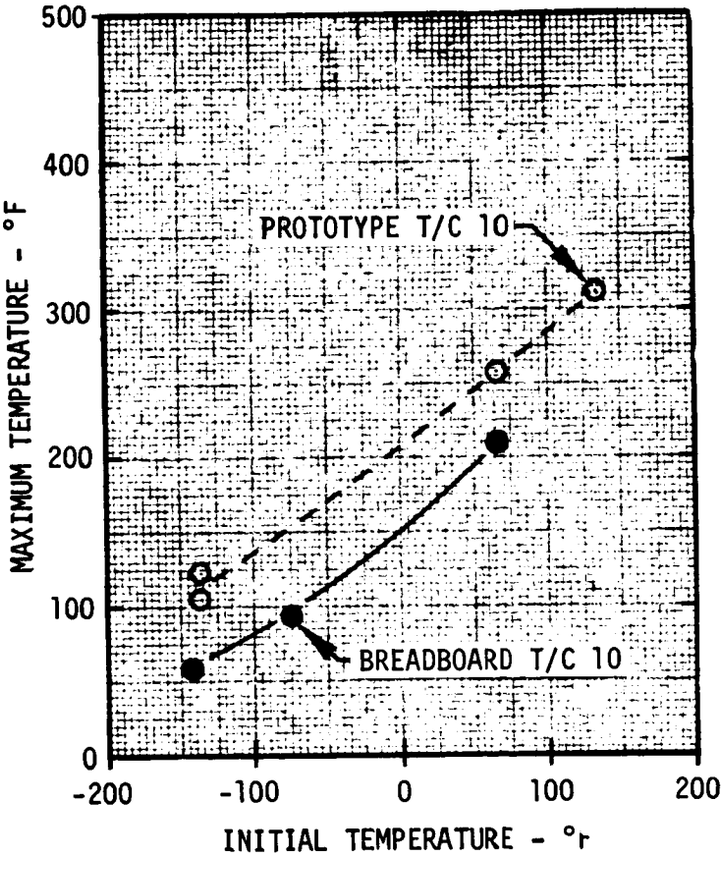

FIGURE 50 EFFECT ON INITIAL TEMPERATURE ON MAXIMUM STRUCTURAL SKIN TEMPERATURE

OFF-THE-SHELF ANTENNA TESTS

The objective of this task (Task 2.4) was to determine the capability of a group of selected off-the-shelf (OTS) antenna to meet the Shuttle Orbiter electrical and thermal requirements. This task also involved part of Task 2.1 which defined the requirements for the test fixture design and instrumentation.

The OTS antenna tests included two test phases. Phase 1 consisted of electrical tests to determine the effects of an antenna window and surrounding TPS (thermal protection system). The antennas were mounted in a ground plane and covered with simulated antenna windows and TPS. Phase 2 consisted of thermal and electrical tests to determine the effects of the Shuttle orbital and entry environments on physical integrity due to the thermal environment and electrical performance. The antennas were mounted in a structure designed to provide a realistic thermo-structural environment. The test articles were cooled to the desired initial temperature (e.g., 172 K (-150°F) or 117 K (-250°F)) simulating orbital cold soak and then subjected to simulated entry heating. The heat source was controlled to follow the structural skin temperature histories (figure 48) measured during the S-band antenna system test. The thermal tests were conducted in a vacuum chamber and the pressure controlled to simulate orbital and entry conditions. Temperature histories were measured at selected points on the test articles. The initial temperatures for each test are given in table V. The results of electrical tests, radiation pattern and impedance measurements, and physical examination were used to evaluate the effects of the applied environment. The results of the electrical and thermal tests are given in separate subsections which follow.

Test Article Selection

The OTS antennas were selected from those described in the antenna equipment survey discussed in reference 1 and a brief review of other possible candidates. Candidate antennas were selected with the concurrence of NASA-JSC for functions of TACAN (L-band), radar altimeter (C-band), and communication (S-band). In the latter case, antennas were considered which could readily be scaled to operate from 1.75 to 2.30 GHz. The maximum operating temperature of the candidate OTS antennas was a primary consideration in the selection process.

The OTS antennas selected and obtained for testing are given in table VI. A Transco C-band horn antenna was also tested because it was available and resulted in no impact on testing. The selected antennas were designed and qualified for use on commercial and military aircraft. For these applications maximum operating temperatures vary from 394 to 478 K (250 to 400°F) and minimum operating temperatures vary from 208 to 219 K (-85 to -65°F).

TABLE V
INITIAL TEMPERATURES FOR OTS ANTENNA TESTS

TEST NO.	INITIAL TEMPERATURE K (°F)	APPLIED TEMPERATURE HISTORY
1	172 (-150)	NOMINAL*
2	172 (-150)	NOMINAL
3	294 (+70)	NOMINAL (300°F MAX)
4	117 (-250)	NOMINAL
5	172 (-150)	EXCURSION** OFF NOMINAL
6	294 (+70)	NOMINAL HEATING RATE TO 350°F MAX

NOTES: *THE "NOMINAL" TEMPERATURE IS DEFINED AS THE SKIN TEMPERATURE HISTORY MEASURED DURING AN S-BAND ANTENNA SYSTEM TEST WITH AN EQUIVALENT INITIAL TEMPERATURE.

**NOMINAL HEAT RATE INCREASED TO PRODUCE SAME PEAK IN 25% (±5%) SHORTER TIME.

TABLE VI
CTS ANTENNAS SELECTED FOR TESTING

FUNCTION	ANTENNA TYPE	PART NO.	MANUFACTURER
TACAN	L-BAND ANNULAR SLOT	22630	TRANSCO PRODUCTS, INC.
		DMR29-2*	DORNE & MARGOLIN, INC.
RADAR ALTIMETER	C-BAND HORN	AK-112-4	RANTEC
		DM PN3-3E*	DORNE & MARGOLIN, INC.
COMMUNICATIONS	S-BAND SPIRAL	AS-39	SANDERS ASSOCIATES, INC.
		ASN 112A	AMERICAN ELECTRONICS LABORATORIES, INC.

NOTES: * MODIFIED FOR OPERATION TO 300°F.

Electrical Testing

The electrical testing consisted of radiation pattern and impedance measurements for both Phase 1 and 2 tests. The test configurations, techniques, and results are given in this section.

Test configurations. - The radiation pattern and impedance measurements for the Phase 1 tests were made with the OTS antennas mounted in the center of a 91.4 cm (36.0 in.) square ground plane. Figure 51 shows a sketch of a typical configuration used for the antenna window and TPS simulation and gives the materials used. The individual TPS tiles were not duplicated. Previous testing at L-band frequencies (ref. 2) indicate the tile gaps do not affect antenna performance. At S-band C-band frequencies the design concepts (refs. 1 and 2) utilized a single tile centered over the antenna. The simulated antenna window and TPS (figure 52) which covered a 76.2 cm (30.0 in.) square area were constructed to provide for easy attachment and removal. Two window sizes were used; the smaller 15.88 cm (6.25 in.) square, and the larger 26.04 cm (10.25 in.) square. The small window was used with the Rantec C-band, the Transco C-band, and the Sanders Associates (SA) S-band antennas. The large window was used with the Transco L-band, the Dorne and Margolin (D&M) L-band and C-band, and the American Electronics Laboratories (AEL) S-band antennas. Pattern measurements were made in a large anechoic chamber with a transmission distance of approximately 21.3 m (70 ft).

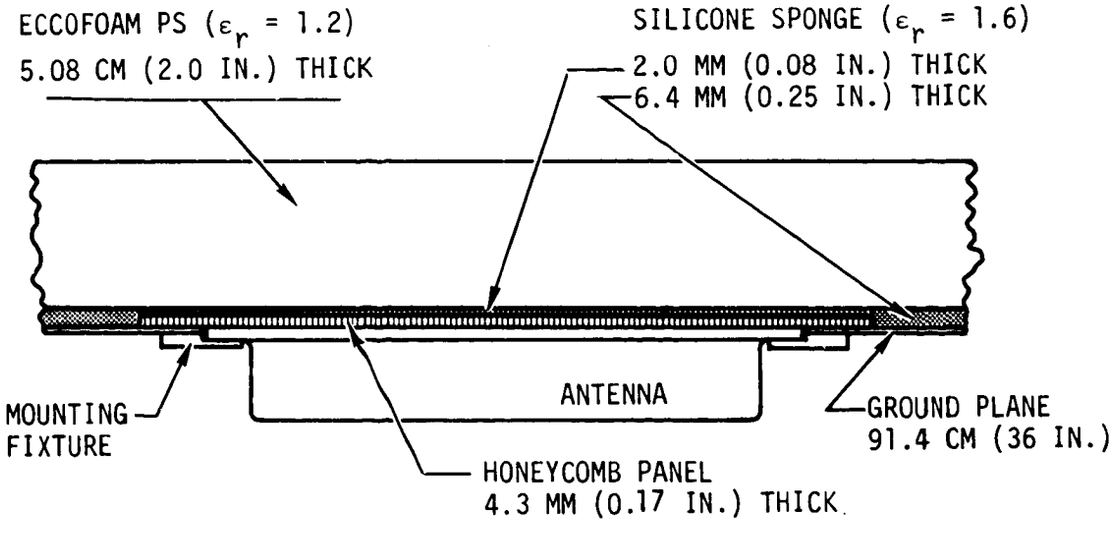

FIGURE 51 SIMULATED ANTENNA WINDOW AND TPS – CROSS-SECTIONAL VIEW

The radiation pattern and impedance measurements for the Phase 2 tests were made with the OTS antennas mounted in the center of a 91.4 cm (36.0 in.)

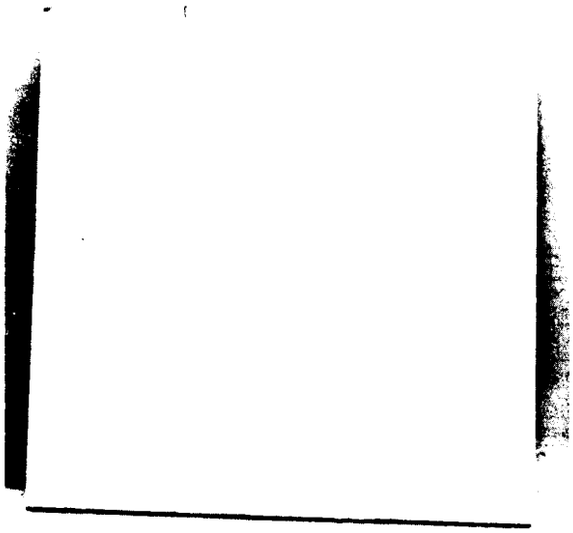

Simulated Antenna Window and TPS

26.04 CM (10.25 In.) Window

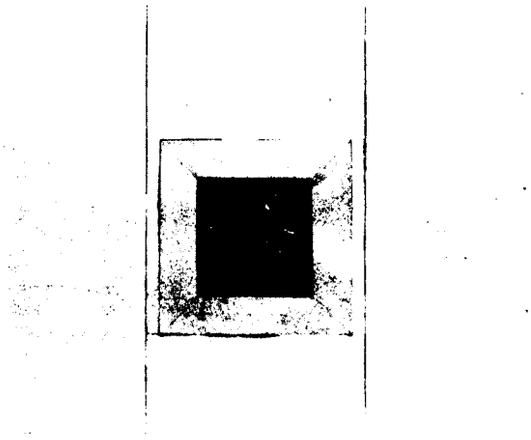

15.88 CM (6.25 IN.) Window

FIGURE 52 SIMULATED ANTENNA WINDOW AND TPS TEST CONFIGURATION

square ground plane. The pattern measurements were made in a small anechoic chamber with a transmission distance of approximately 27 m (9 ft). A comparison of patterns taken in the small anechoic chamber with those taken in the large anechoic chamber, particularly at L-band, showed that the patterns measured in the small chamber were satisfactory for the Phase 2 test objective. The orientation of each antenna was indexed in the ground plane to maintain an accurate physical relationship from test to test. Reference antennas were attached to the structure supporting the ground plane to ensure a constant transmitted signal level for each test. The ground plane support structure remained attached to the positioner throughout the Phase 2 tests.

Test techniques. - The test techniques used for the OTS antenna tests are essentially the same as those described in the section on S-BAND ANTENNA SYSTEM TESTS, under Electrical Testing. The patterns at each frequency are referenced either to linear isotropic gain level or a secondary antenna gain level. This enables direct comparison of data obtained from the different tests.

A single wide band horn was used as the transmitting antenna at all test frequencies. This antenna could be rotated to obtain rotating linear polarization or held fixed for a particular linear polarization. Helix antennas were used to obtain the circularly polarized radiation field for the Phase 1 tests. The axial ratios of these transmitting antennas were measured and found to range from 0.5 to 2.5 dB.

Test results - simulated antenna window and TPS effects. - Radiation pattern and impedance measurements were made with and without a simulated antenna window and surrounding TPS. Typical results of the measurements are given to illustrate the effects. The test antennas included L-band annular slots, C-band horns, and S-band spirals as outlined in table VI.

L-Band antennas: The results of the L-band annular slot antenna radiation pattern measurements (figures 53 and 54) show similar effects for both the Transco and the D&M antennas. The effects of the antenna window and TPS are relatively small. The gain decreased about 1.0 dB at the peak of the main lobe but increased 0.5 to 1.0 dB in the plane of the ground plane ($\theta = 90°$). The dissymmetry of the Transco L-band antenna pattern at 1090 Mhz is attributed to reflection from the anechoic chamber walls. Subsequent patterns in the small anechoic chamber for the same configuration showed a significant improvement in symmetry and improved null depth at $\theta = 0°$ (see figure 53). The results of impedance measurements are shown in figures 55 and 56. The Transco antenna impedance plot rotates and the VSWR decreased at the low frequencies but increased to about 3:1 at 1220 MHz. The D&M antenna impedance rotates slightly and the VSWR generally increases a small amount at all frequences.

S-band antennas: The results of the S-band spiral antenna radiation pattern measurements (figures 57 and 58) show similar effects for both the AEL and SA antennas. The effects of the antenna window and TPS are small. The linear gain of the AEL antenna was essentially unchanged. The linear gain of the SA antenna was essentially unchanged at the two low test frequencies but decreased about 2.0 dB at 5.2 GHz. The axial ratio of both

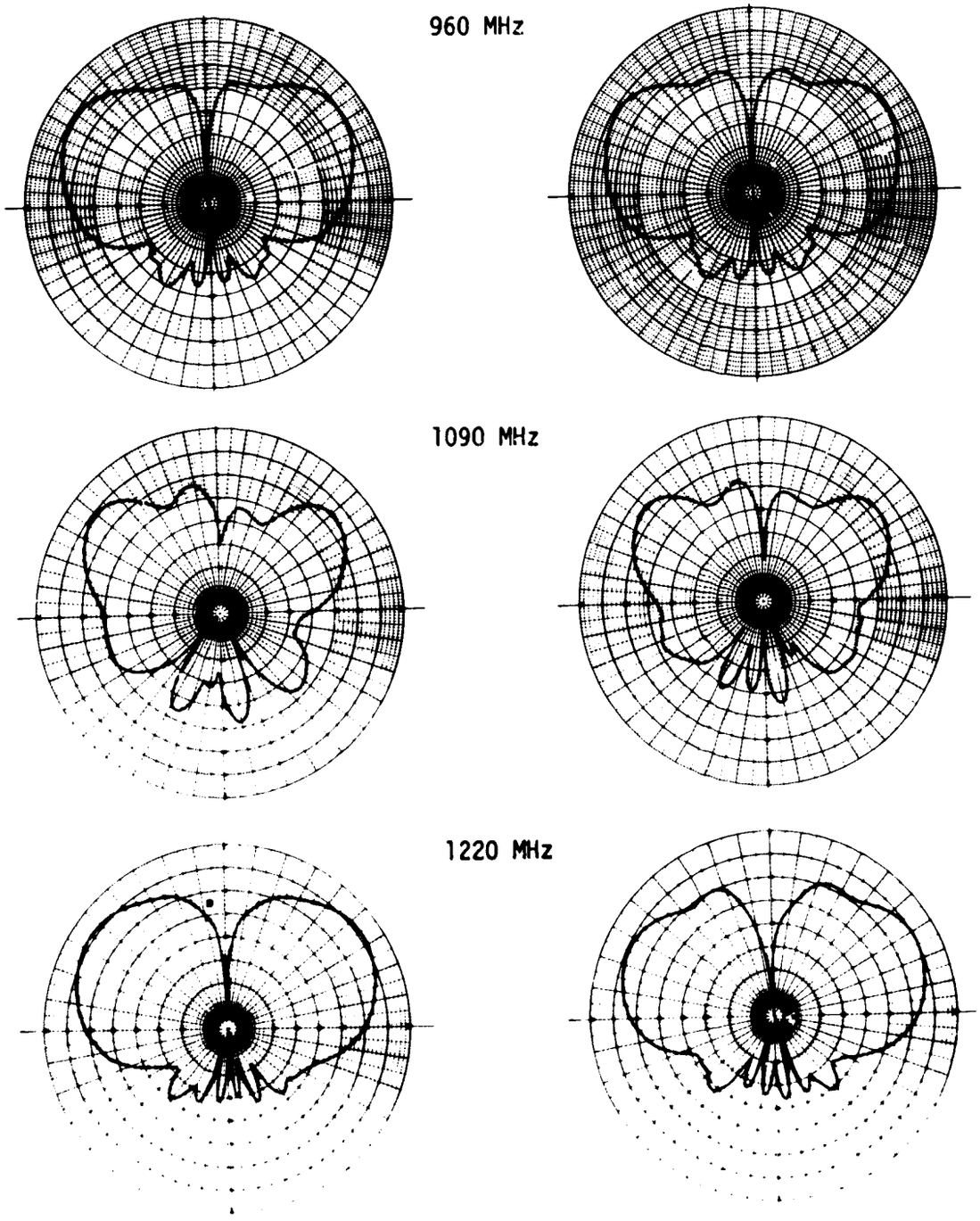

FIGURE 53 EFFECTS OF SIMULATED ANTENNA WINDOW AND TPS – TRANSCO L-BAND ANTENNA RADIATION PATTERNS

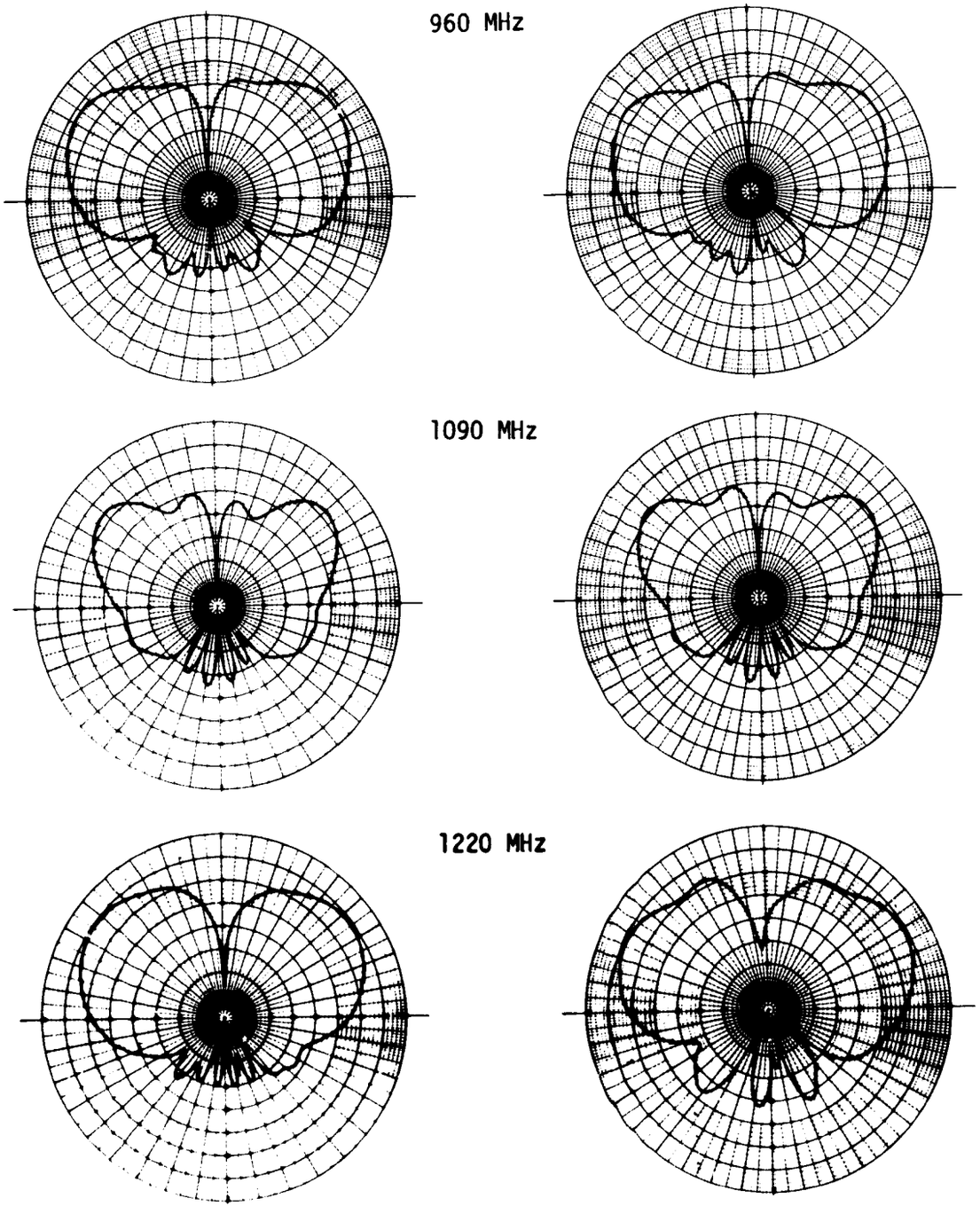

FIGURE 54 EFFECTS OF SIMULATED ANTENNA WINDOW AND TPS - D&M L-BAND ANTENNA RADIATION PATTERNS

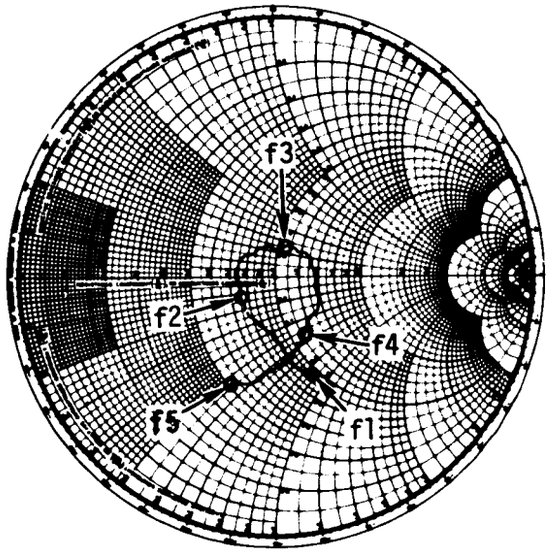

REFERENCE

Z_o = 50 OHMS
f1 = 900 MHz
f2 = 960 MHz
f3 = 1090 MHz
f4 = 1220 MHz
f5 = 1300 MHz

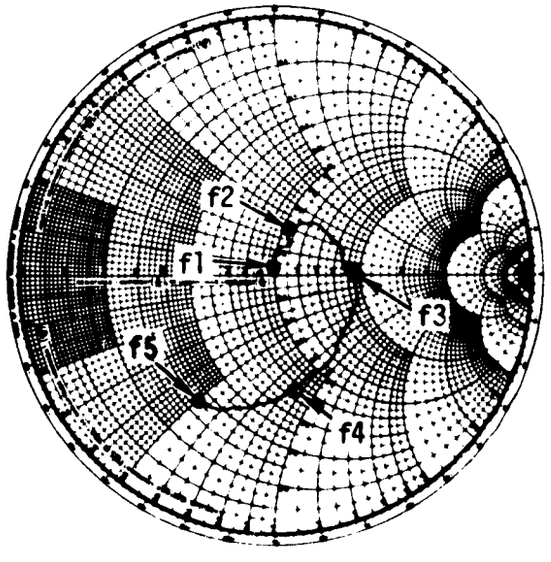

ANTENNA WINDOW AND TPS

FIGURE 55 EFFECTS OF SIMULATED ANTENNA WINDOW AND TPS – TRANSCO L-BAND ANTENNA IMPEDANCE

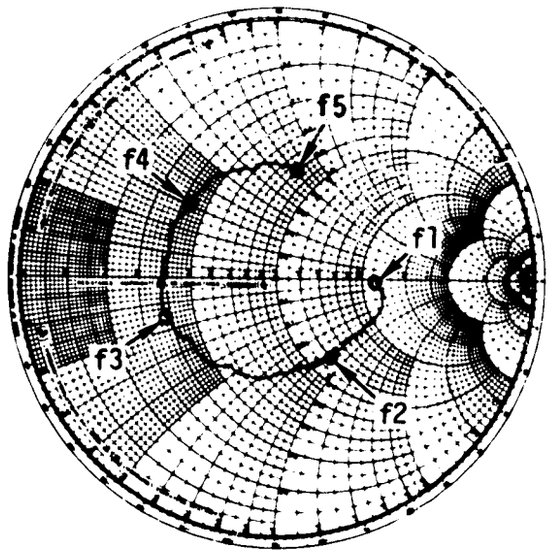

REFERENCE

Z_o = 50 OHMS
f1 = 900 MHz
f2 = 960 MHz
f3 = 1090 MHz
f4 = 1220 MHz
f5 = 1300 MHz

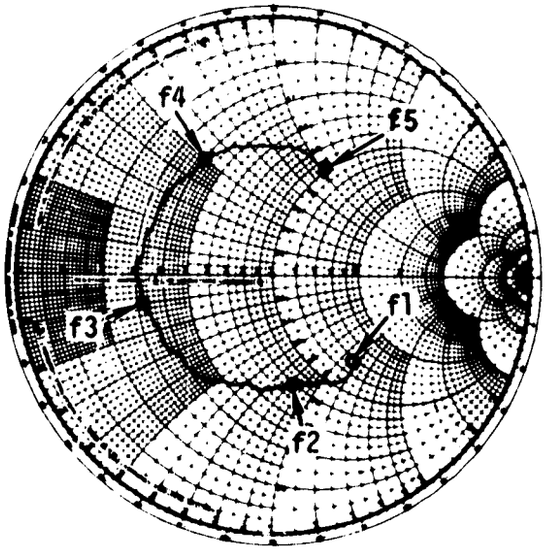

ANTENNA WINDOW AND TPS

FIGURE 56 EFFECTS OF SIMULATED ANTENNA WINDOW AND TPS – D&M L-BAND ANTENNA IMPEDANCE

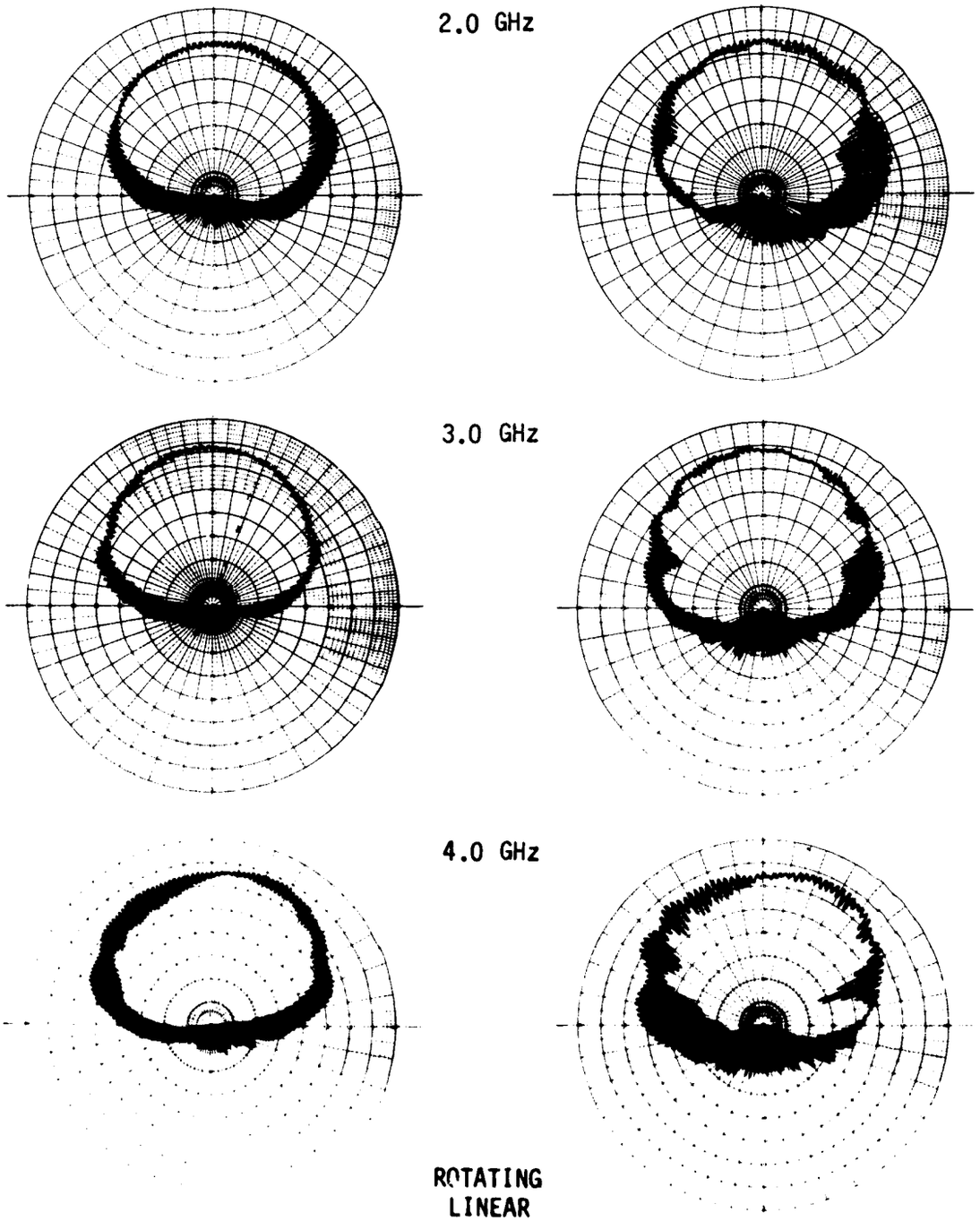

FIGURE 57 EFFECTS OF SIMULATED ANTENNA WINDOW AND TPS – AEL S-BAND ANTENNA RADIATION PATTERNS

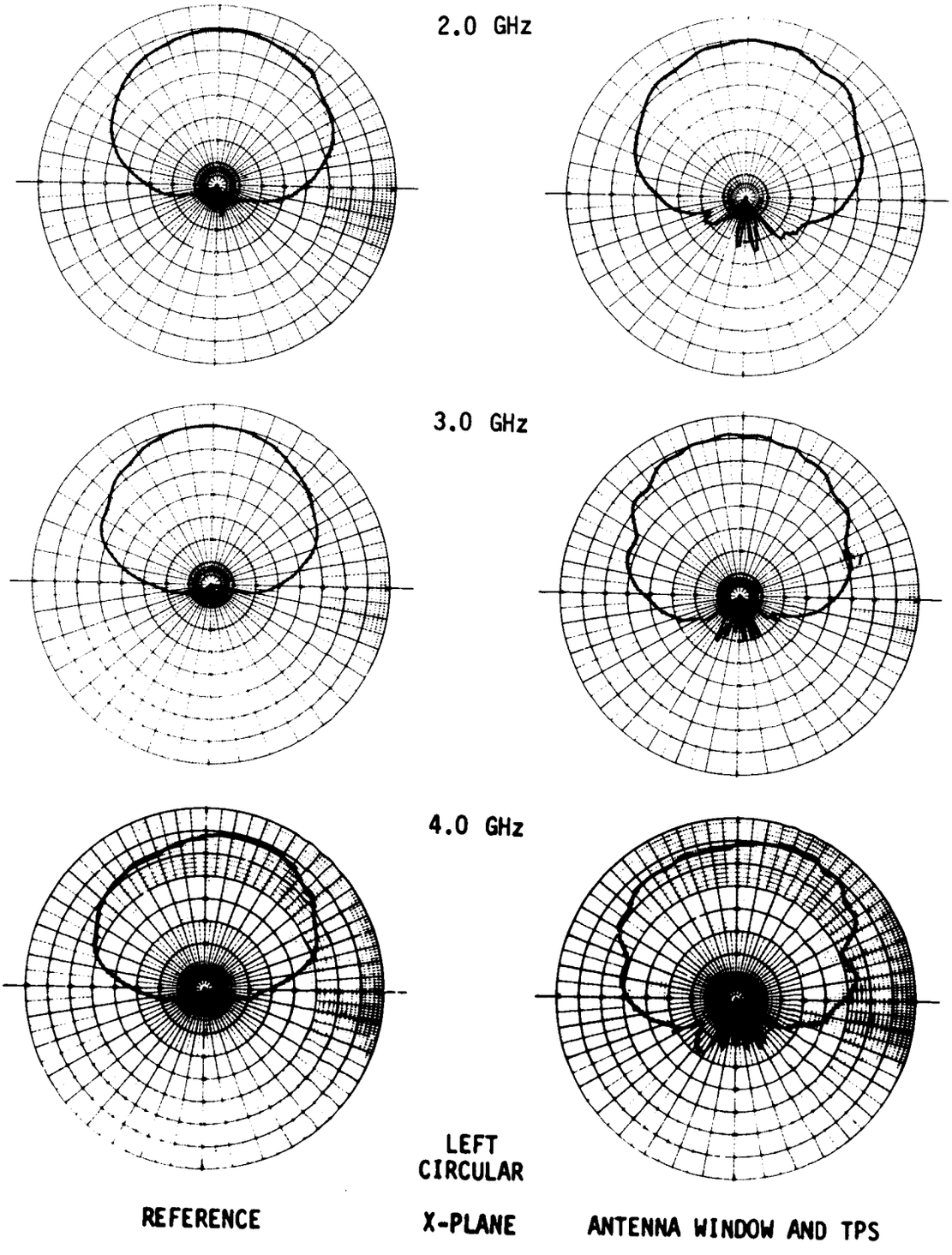

FIGURE 57 EFFECTS OF SIMULATED ANTENNA WINDOW AND TPS – AEL S-BAND ANTENNA RADIATION PATTERNS (Continued)

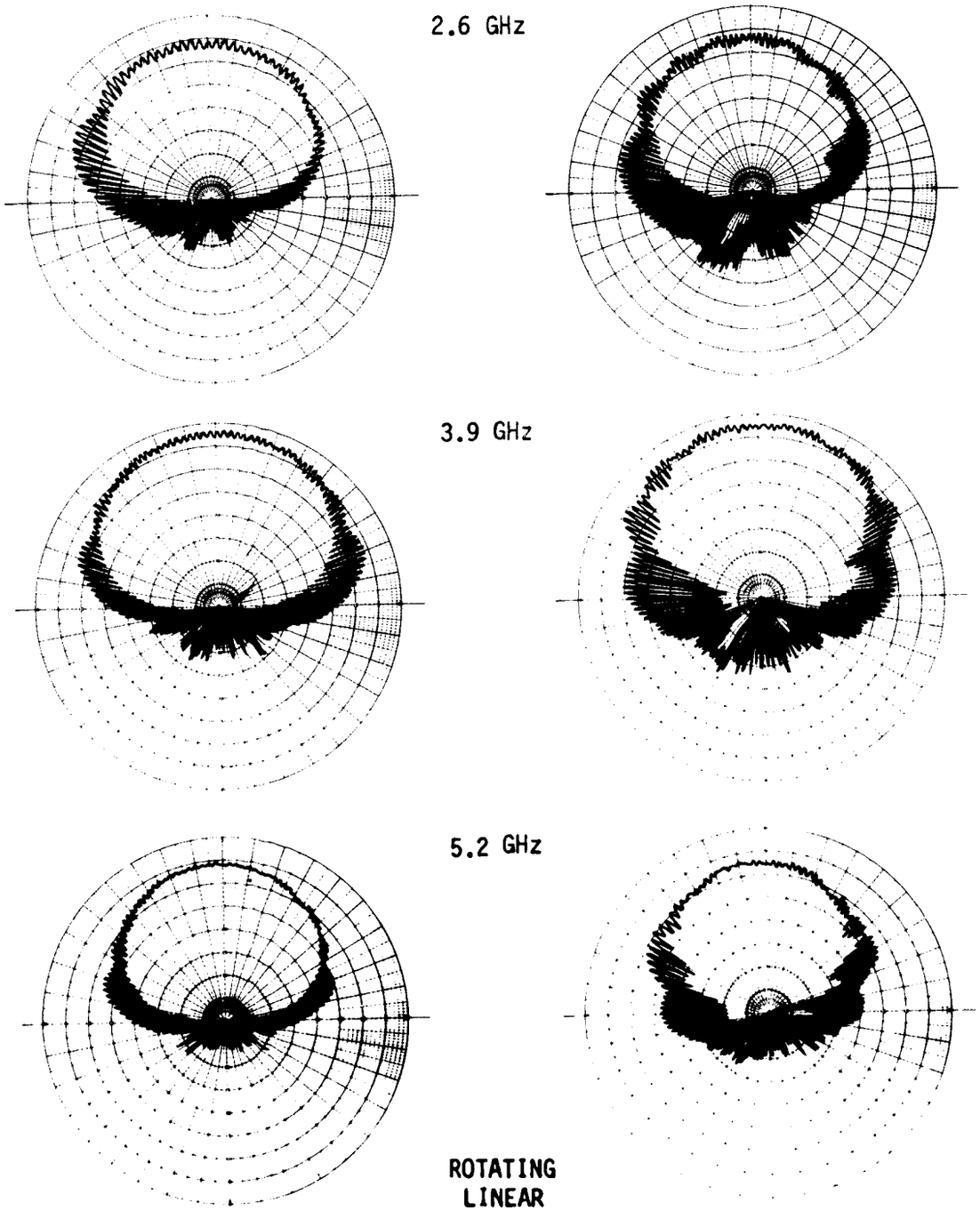

FIGURE 58 EFFECTS OF SIMULATED ANTENNA WINDOW AND TPS – SA S-BAND ANTENNA RADIATION PATTERNS

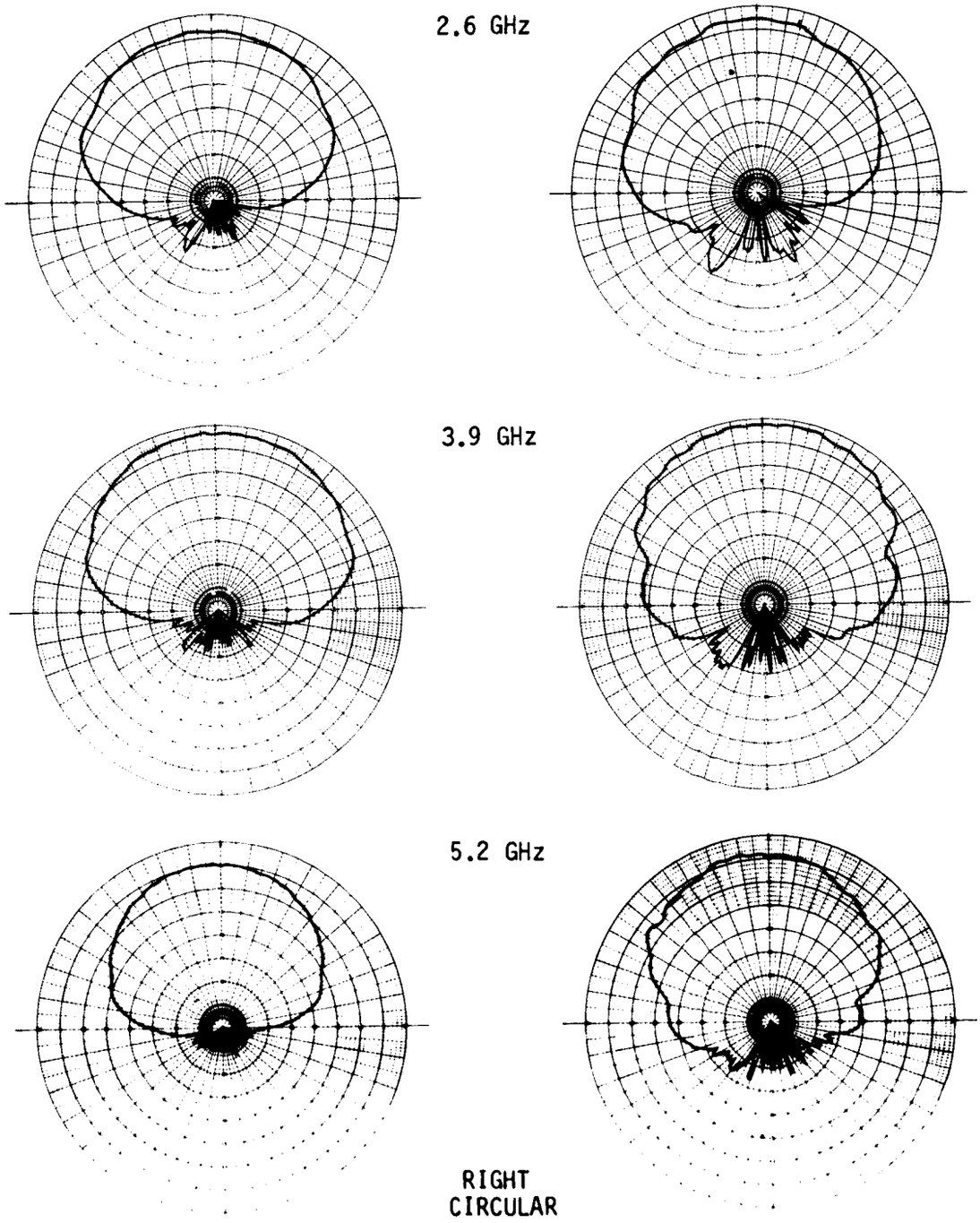

FIGURE 58 EFFECTS OF SIMULATED ANTENNA WINDOW AND TPS – SA S-BAND ANTENNA RADIATION PATTERNS (Continued)

antennas remained low over a bean width of 120° ($\theta = \pm 60°$) but increased, as expected, at angles greater than $\theta = 60°$. The results of impedance measurements (figures 59 and 60) show no significant change in input impedance for either antenna.

C-band antennas: The results of the C-band horn antenna radiation pattern measurements (figures 61, 62 and 63) show similar effects for the D&M, Rantec, and Transco antennas. The effects of the antenna window and TPS are most prominent in the E-plane pattern where -15 dB sidelobes develop at $\theta = 90°$. In the H-plane the 3.0 dB beamwidth increased slightly. The peak gain also decreased about 1 dB. The results of the impedance measurements (figures 64, 65 and 66) show a general shift in the impedance. The most significant change was noted in the Transco antenna where the VSWR increased from 1.35:1 to 2.1:1 at 4.4 GHz.

Test results - thermal environment effects. - Radiation pattern and impedance measurements were taken before the initial thermal test (reference condition) and repeated after each test. The initial temperature for each test is given in table V. Reference patterns for the thermal tests were taken with the same ground plane configuration used for the antenna window and TPS investigation, but were measured in a small anechoic chamber. Because of the large amount of repetitive patterns, only test results which best characterize the performance variations throughout the test sequence are given. These results include the reference data and data obtained after thermal tests 1, 2, and 6. In general, the pattern shape was essentially constant for all the OTS antennas. The primary change observed was in the pattern gain. The effect on impedance of the OTS antennas was minor in all cases.

L-band antennas: Radiation patterns of the Transco annular slot antenna (figure 67) show the most significant change at 1090 MHz. The peak gain decreased to about 3.0 dB below the reference level after tests 1 and 2 and remained at that level throughout the succeeding tests. At 1220 MHz, the gain decreased by 1.5 dB through test 3 but increased until after test 6 it was 0.8 dB greater than the reference. At 960 MHz, the gain was essentially unchanged. The results of the impedance measurements (figure 68) show the thermal test environment has negligible effect on the Transco antenna input impedance.

Radiation patterns of the D&M annular slot antenna (figure 69) show a decrease in peak gain at all three test frequencies after the first thermal test. The gain at 960 and 1090 MHz decreased 1.5 dB and remained at that magnitude throughout the succeeding tests. During the succeeding tests, however, the gain at 1220 MHz increased until it was 0.8 dB above the reference after test 6. The results of the impedance measurements (figure 70) do not show any significant effects of the thermal test environment.

During the radiation pattern measurements after test 6, it was found that one of the elements used in the test setup was particularly gain sensitive at 1220 MHz. For example, a 3.0 dB gain decreased could be observed for a 5 MHz increase in frequency. Although the frequency was set using a frequency meter, the gain changes obtained at 1220 MHz should be considered with some degree of caution.

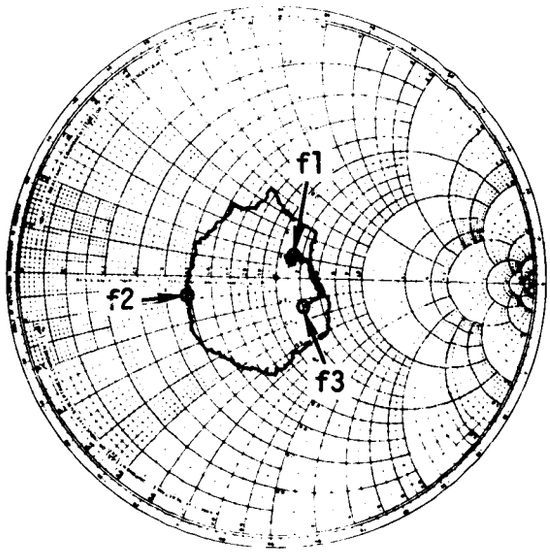

REFERENCE

Z_o = 50 OHMS
f1 = 2.0 GHz
f2 = 3.0 GHz
f3 = 4.0 GHz

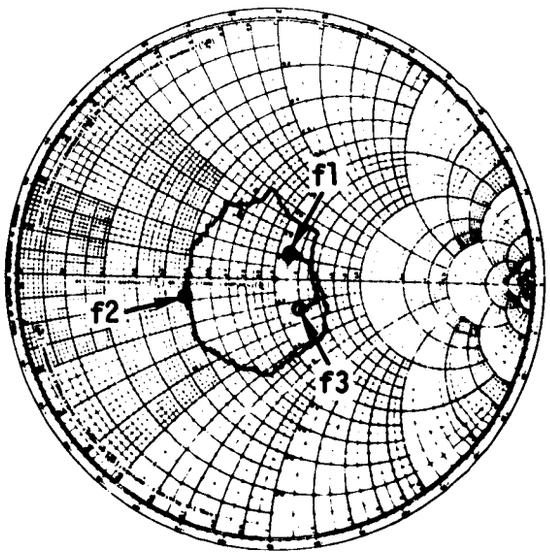

ANTENNA WINDOW AND TPS

FIGURE 59 EFFECTS OF SIMULATED ANTENNA WINDOW AND TPS – AEL S-BAND ANTENNA IMPEDANCE

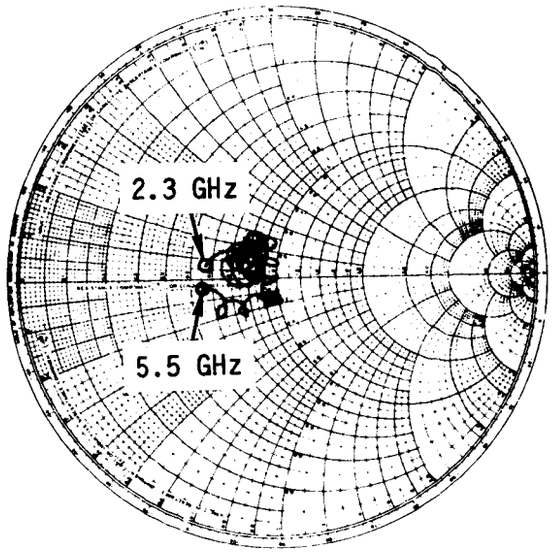

REFERENCE

Z_o = 50 OHMS
SWEEP RANGE
2.3 GHz to 5.5 GHz

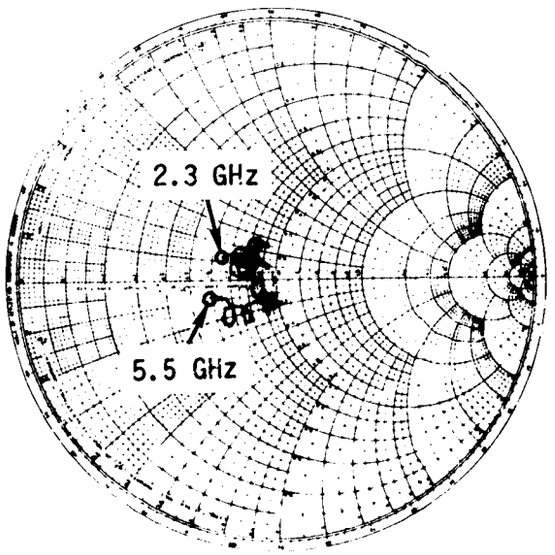

ANTENNA WINDOW AND TPS

FIGURE 60 EFFECTS OF SIMULATED ANTENNA WINDOW AND TPS – SA S-BAND ANTENNA IMPEDANCE

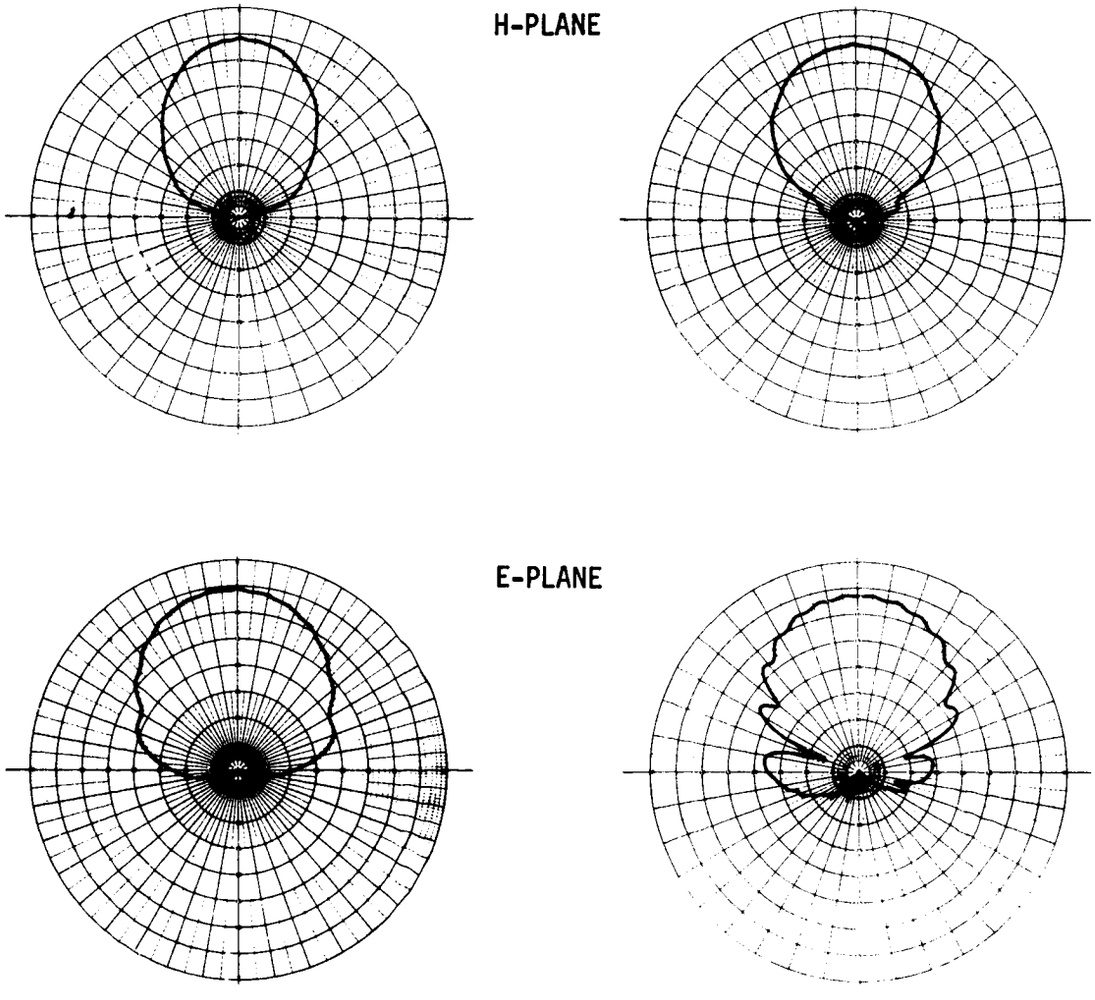

FIGURE 61 EFFECTS OF SIMULATED ANTENNA WINDOW AND TPS – D&M C-BAND ANTENNA RADIATION PATTERNS

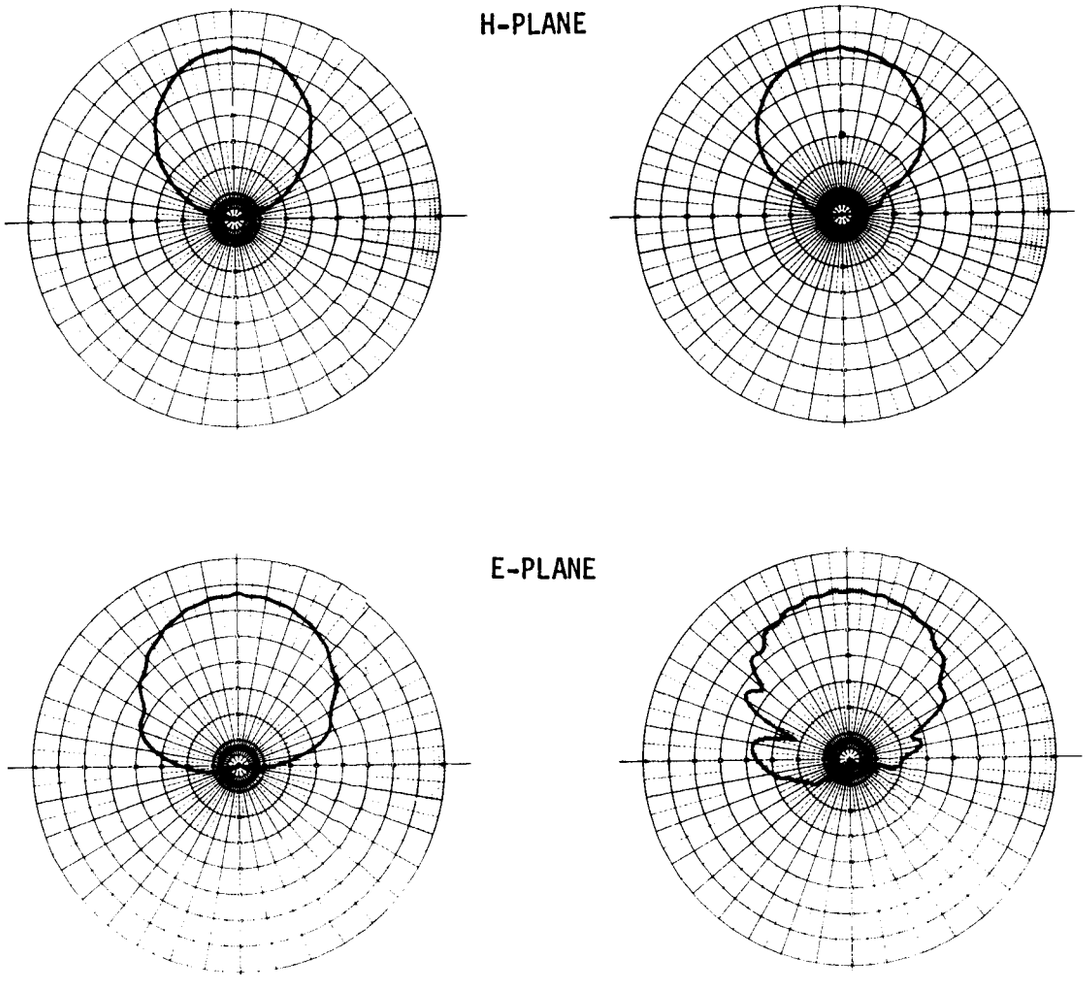

FIGURE 62 EFFECTS OF SIMULATED ANTENNA WINDOW AND TPS – RANTEC C-BAND ANTENNA RADIATION PATTERNS

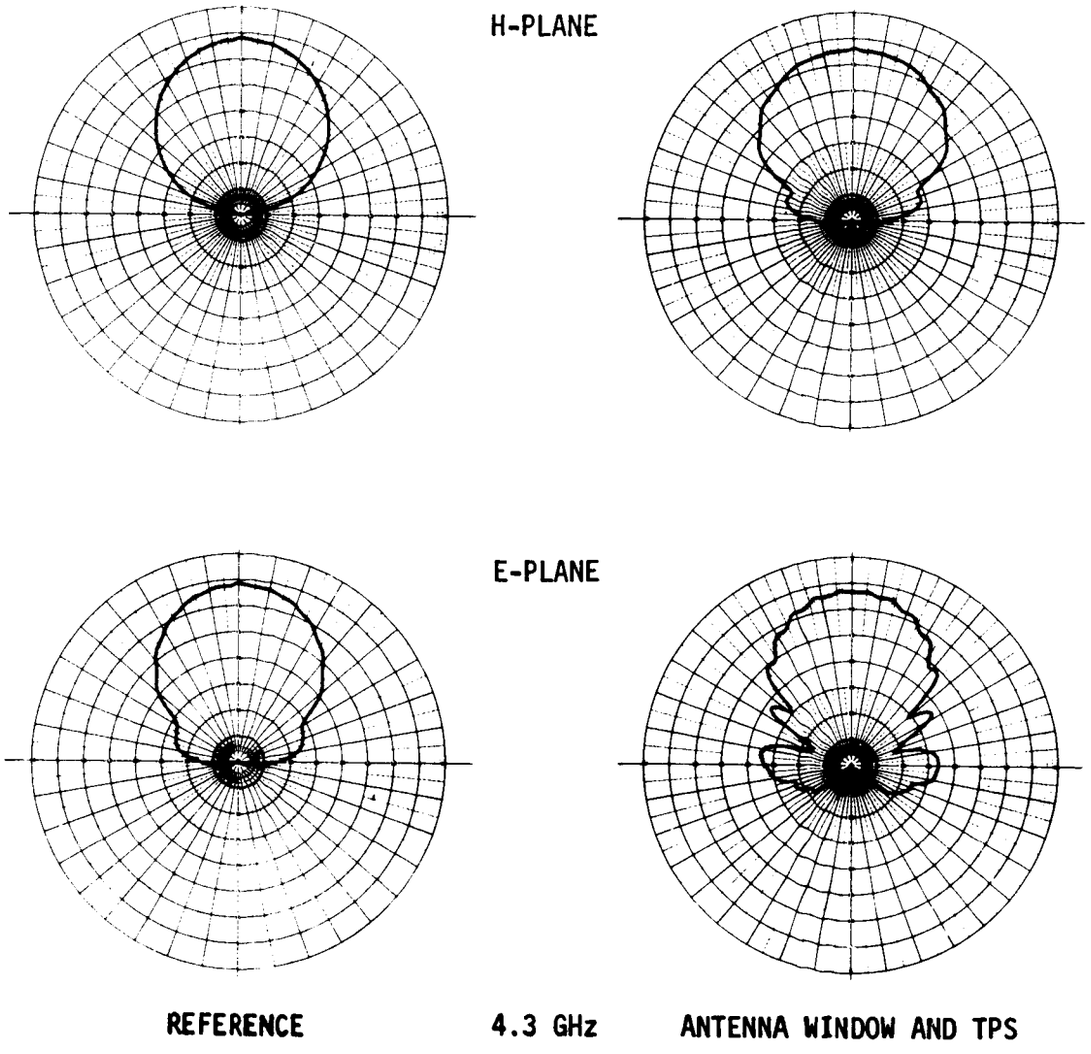

FIGURE 63 EFFECTS OF SIMULATED ANTENNA WINDOW AND TPS – TRANSCO C-BAND ANTENNA RADIATION PATTERNS

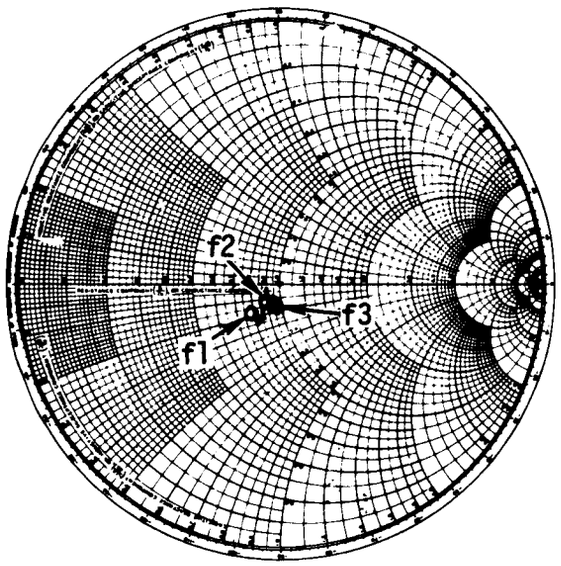

REFERENCE

Z_o = 50 OHMS
f1 = 4.2 GHz
f2 = 4.3 GHz
f3 = 4.4 GHz

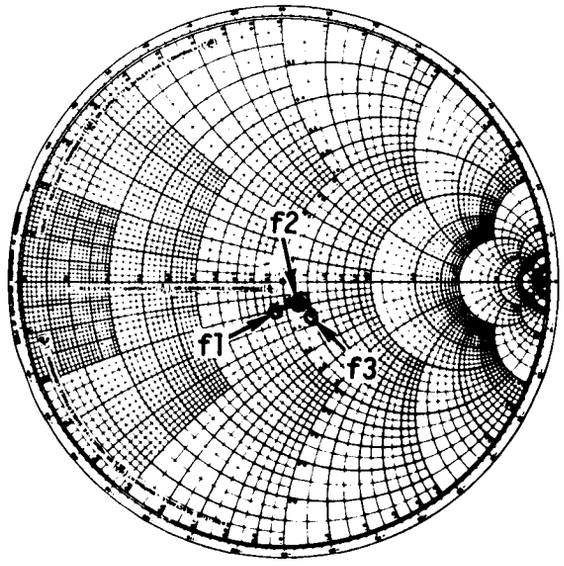

ANTENNA WINDOW AND TPS

FIGURE 64 EFFECTS OF SIMULATED ANTENNA WINDOW AND TPS – D&M C-BAND ANTENNA IMPEDANCE

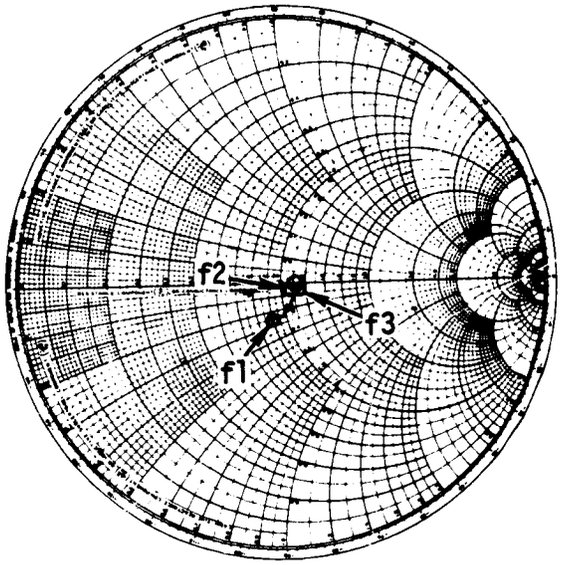

REFERENCE

Z_0 = 50 OHMS
f1 = 4.2 GHz
f2 = 4.3 GHz
f3 = 4.4 GHz

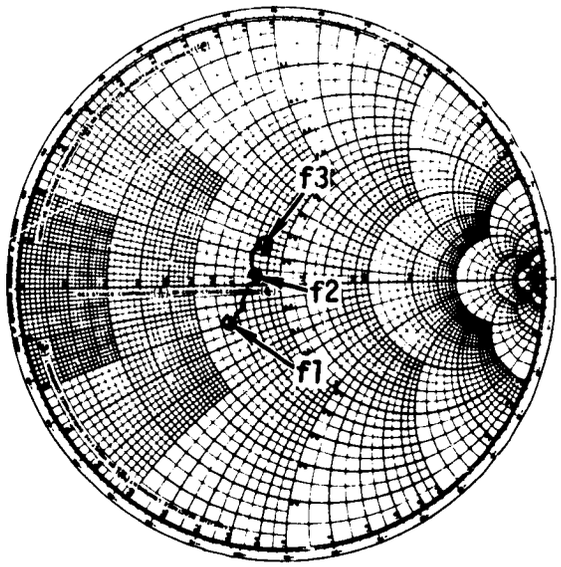

ANTENNA WINDOW AND TPS

FIGURE 65 EFFECTS OF SIMULATED ANTENNA WINDOW AND TPS – RANTEC C-BAND ANTENNA IMPEDANCE

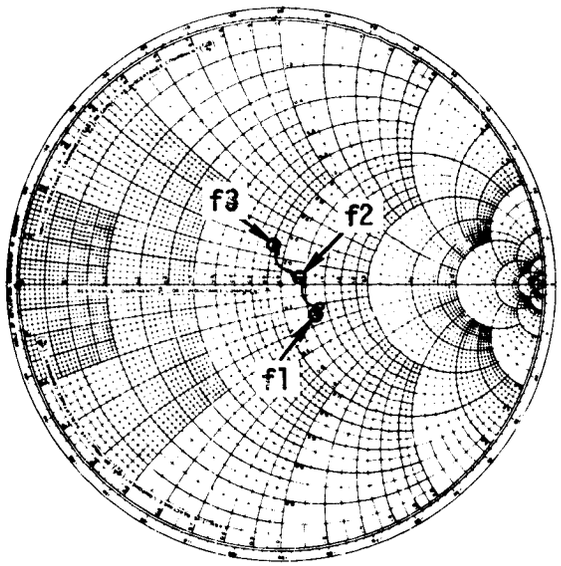

REFERENCE

Z_o = 50 OHMS
f1 = 4.2 GHz
f2 = 4.3 GHz
f3 = 4.4 GHz

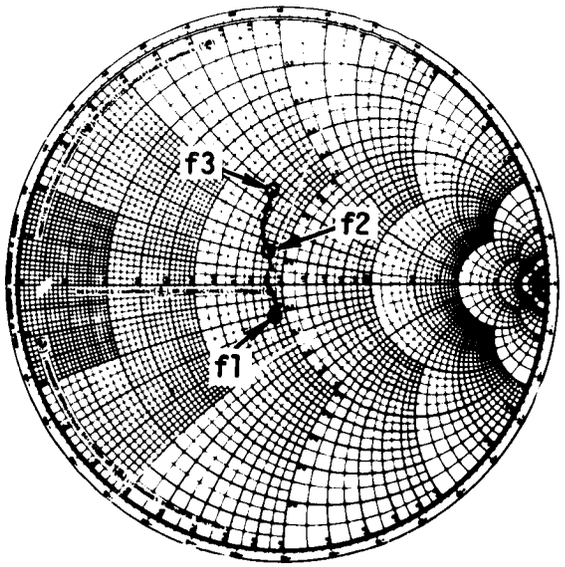

ANTENNA WINDOW AND TPS

FIGURE 66 EFFECTS OF SIMULATED ANTENNA WINDOW AND TPS - TRANSCO C-BAND ANTENNA IMPEDANCE

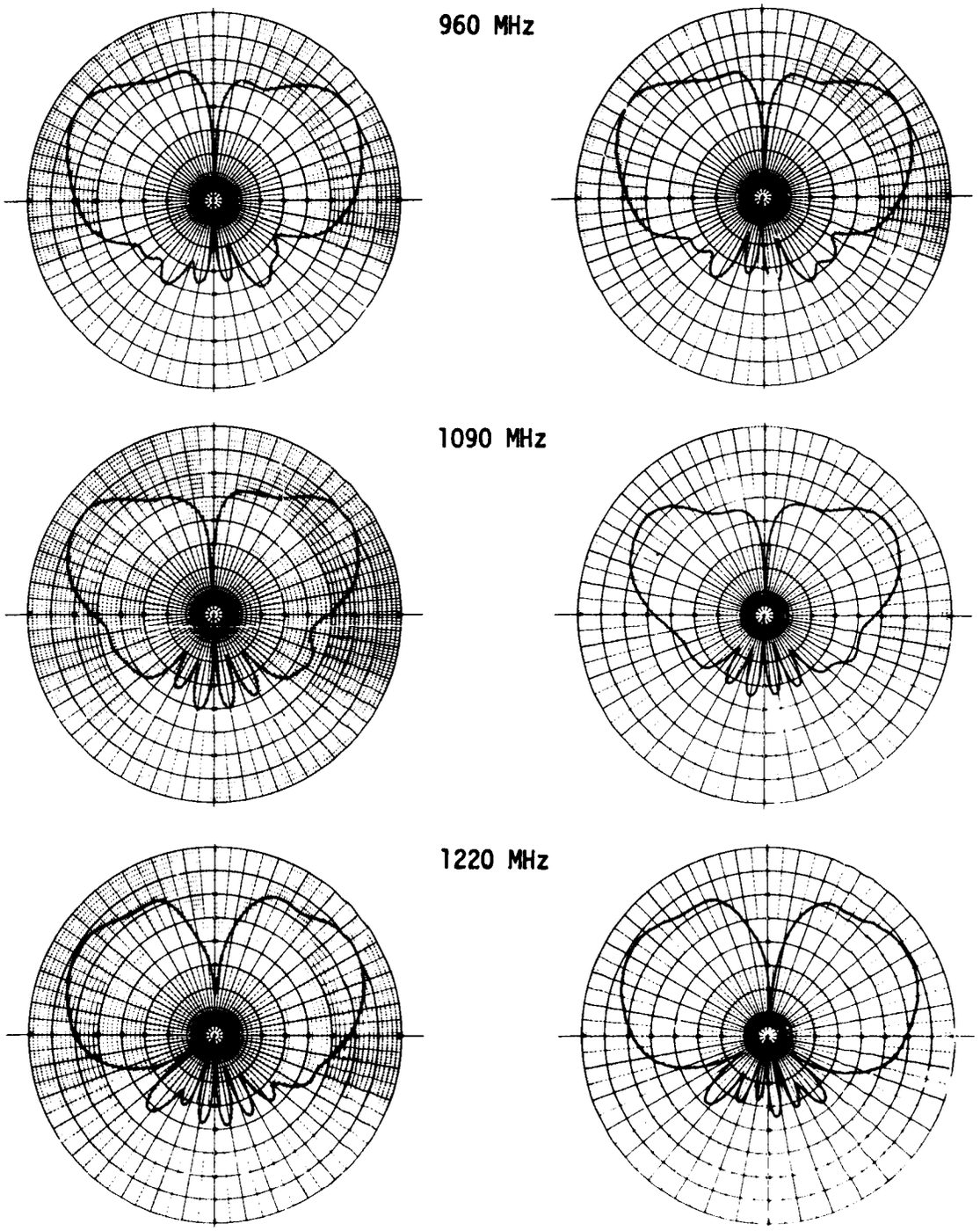

FIGURE 67 EFFECTS OF THERMAL ENVIRONMENT – TRANSCO L-BAND ANTENNA RADIATION PATTERNS

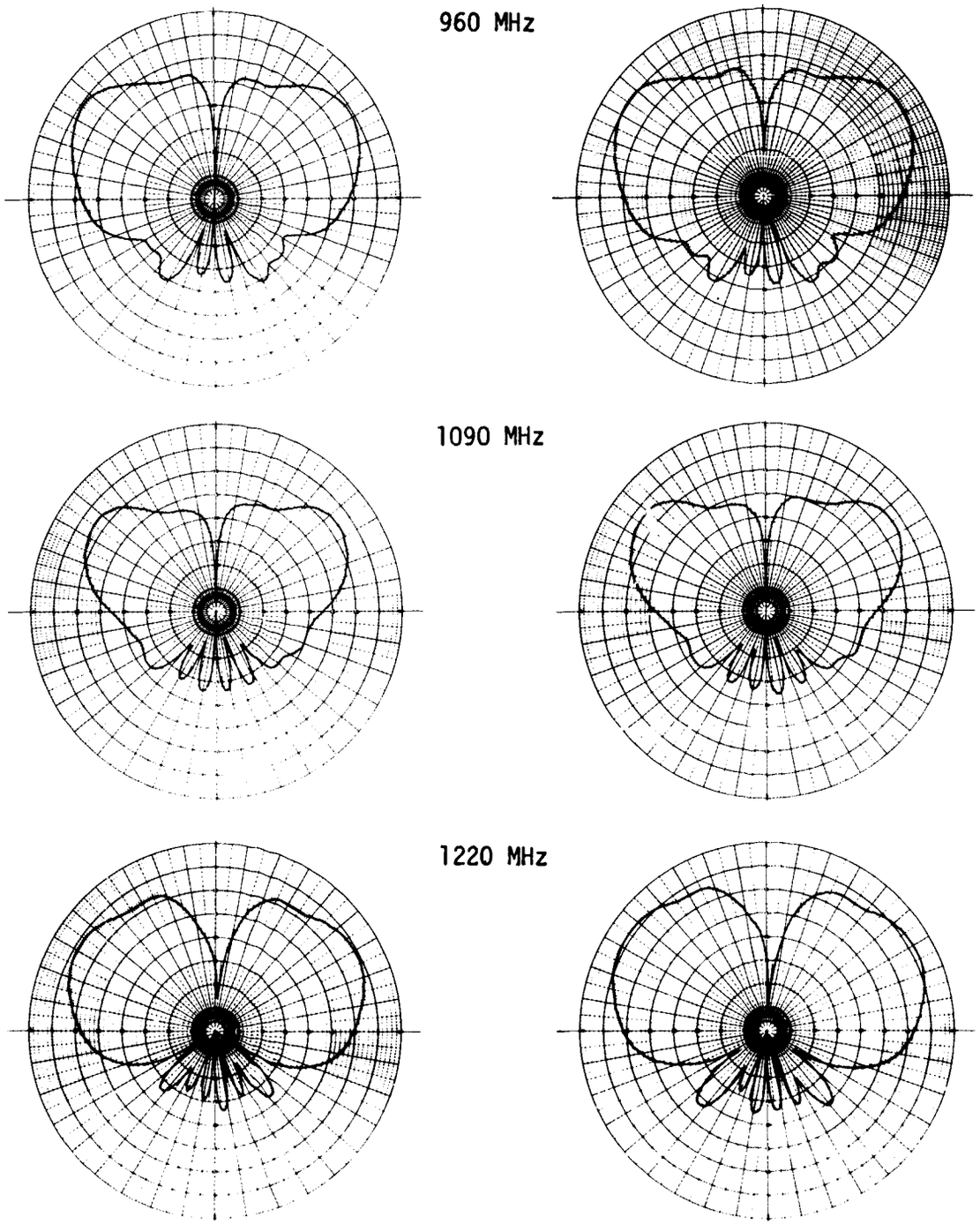

FIGURE 67 EFFECTS OF THERMAL ENVIRONMENT – TRANSCO L-BAND ANTENNA RADIATION PATTERNS (Continued)

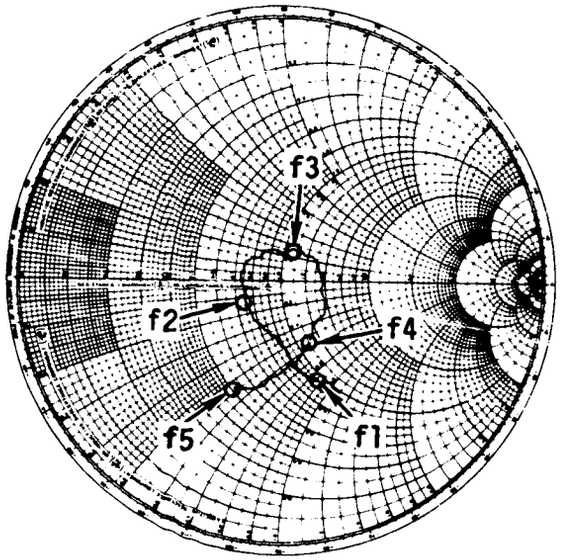

REFERENCE

Z_o = 50 OHMS
f1 = 900 MHz
f2 = 960 MHz
f3 = 1090 MHz
f4 = 1220 MHz
f5 = 1300 MHz

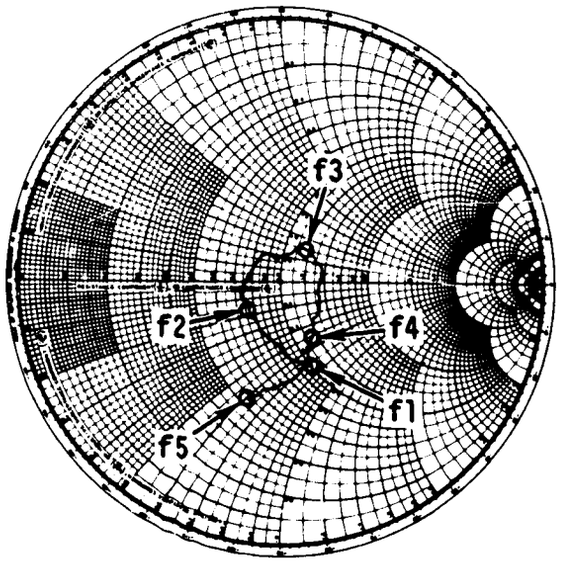

SIXTH

FIGURE 68 EFFECTS OF THERMAL ENVIRONMENT – TRANSCO L-BAND ANTENNA IMPEDANCE

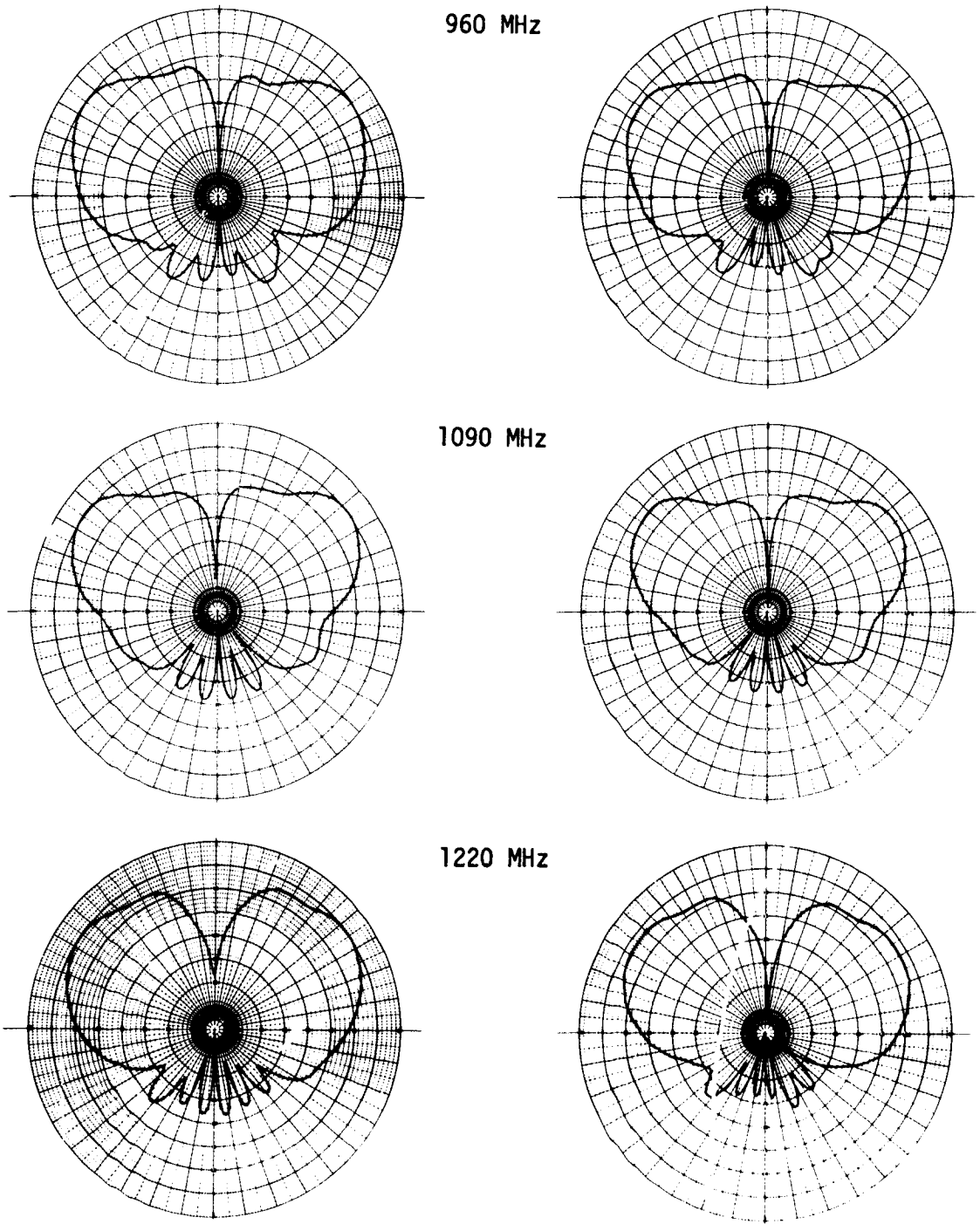

FIGURE 69 EFFECTS OF THERMAL ENVIRONMENT – D&M L-BAND ANTENNA RADIATION PATTERNS

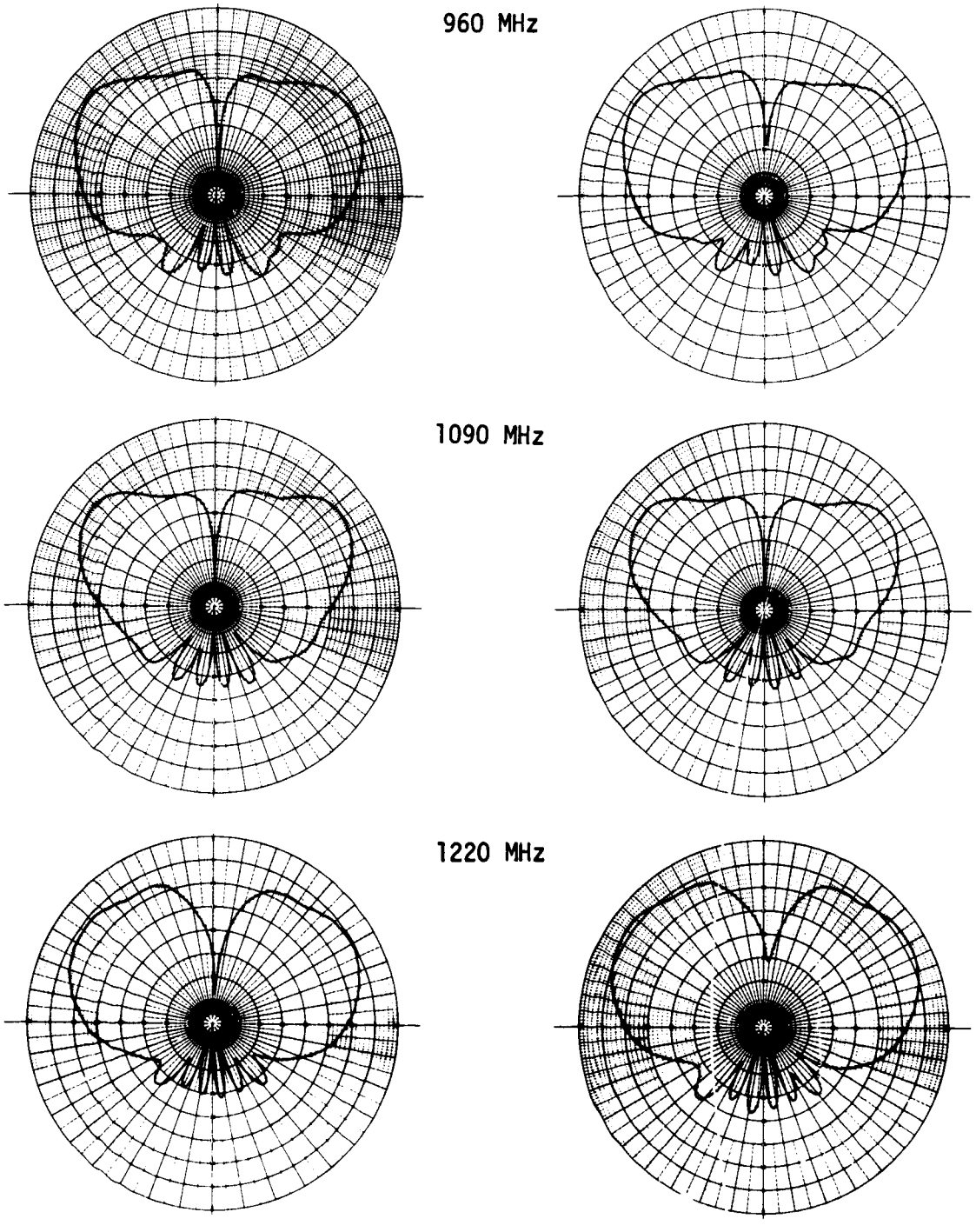

FIGURE 69 EFFECTS OF THERMAL ENVIRONMENT – D&M L-BAND ANTENNA RADIATION PATTERNS (Continued)

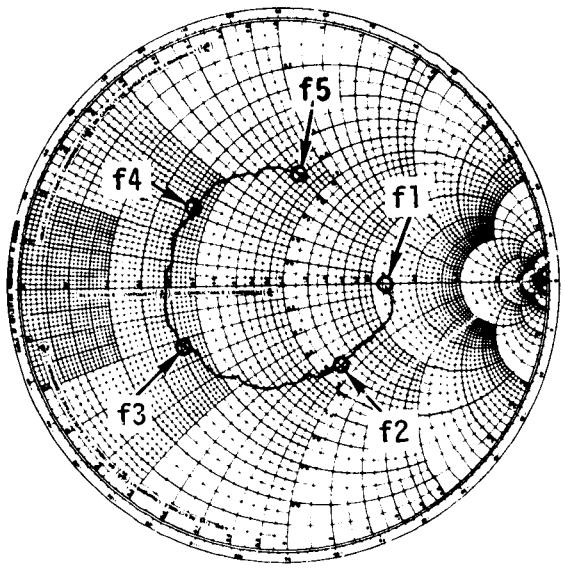

REFERENCE

Z_o = 50 OHMS
f1 = 900 MHz
f2 = 960 MHz
f3 = 1090 MHz
f4 = 1220 MHz
f5 = 1300 MHz

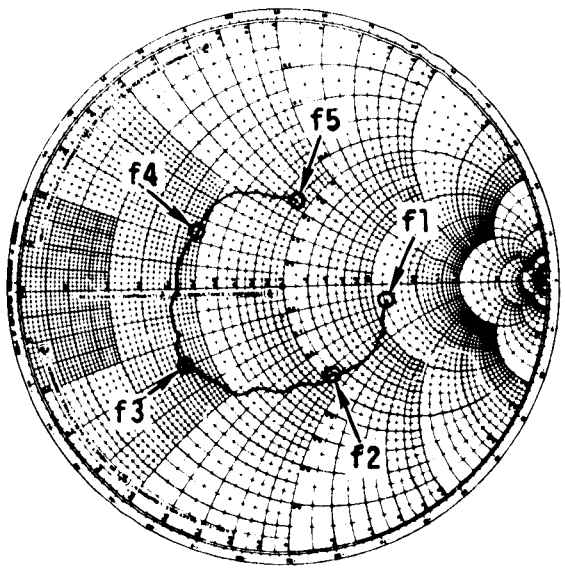

SIXTH

FIGURE 70 EFFECTS OF THERMAL ENVIRONMENT – D&M
L-BAND ANTENNA IMPEDANCE

S-band antennas: Radiation patterns and impedance plots of the AEL and SA spiral antennas (figures 71 and 72) show the various thermal test environments had little effect on the performance of these antennas. The shape, gain, and axial ratio of the radiation patterns show only minor variations after the applied thermal environments. Some variations can be observed in the impedance plots (figures 73 and 74) but the maximum VSWR did not exceed the reference value. In general, the variation observed in the patterns and impedance of the S-band antennas were within the measurement accuracy of the test equipment.

C-band antennas: The results of the radiation pattern and impedance measurements are similar for all three C-band horn antennas.

Radiation patterns of the D&M antenna (figure 75) show a gain increase of 1.5 dB at all three test frequencies after the initial test. After the initial gain change, further changes (both increases and decreases) were observed at the two low test frequencies. A typical result of the impedance measurements (figure 76) shows no significant change from the reference. The results after some of the thermal tests show small differences in the impedance plot but no significant change in VSWR.

Radiation patterns of the Rantec antenna (figure 77) show a general decrease in gain after the initial test followed by a compensating increase after test 2. Further increases and decreases were observed after subsequent thermal tests with a net increase in gain averaging about 2.0 dB measured after test 6. The results of the impedance measurements showed no significant change in the impedance plot or the VSWR. Figure 78 shows typical impedance measurement results.

Radiation patterns of the Transco antenna (figure 79) show a gain increase of 1.0 dB at 4.3 GHz after the initial test. After this initial change, the gain decreased about 1.0 dB after test 4 and then increased about 1.0 dB after test 5. A typical result of the impedance measurements is shown in figure 80. Similar differences, compared to the reference impedance, were observed after other thermal tests. However, there was no significant difference in VSWR noted after any particular thermal test environment.

Thermal Testing

Thermal tests were conducted on the OTS antennas between 4 and 29 March 1974. The purpose of these tests was to expose the antennas to a cold soak followed by a simulated entry heat pulse. In all tests, the antennas were soaked overnight at the desired initial temperature (table V) and pressure (260 N/m^2 (2 torr) or less).

Since the test configuration did not include TPS, the applied heating pulse simulated the heat that passed through the TPS and impinged on the antenna and Orbiter structure. The heating pulses were defined from the S-band antenna system testing results for each initial temperature condition.

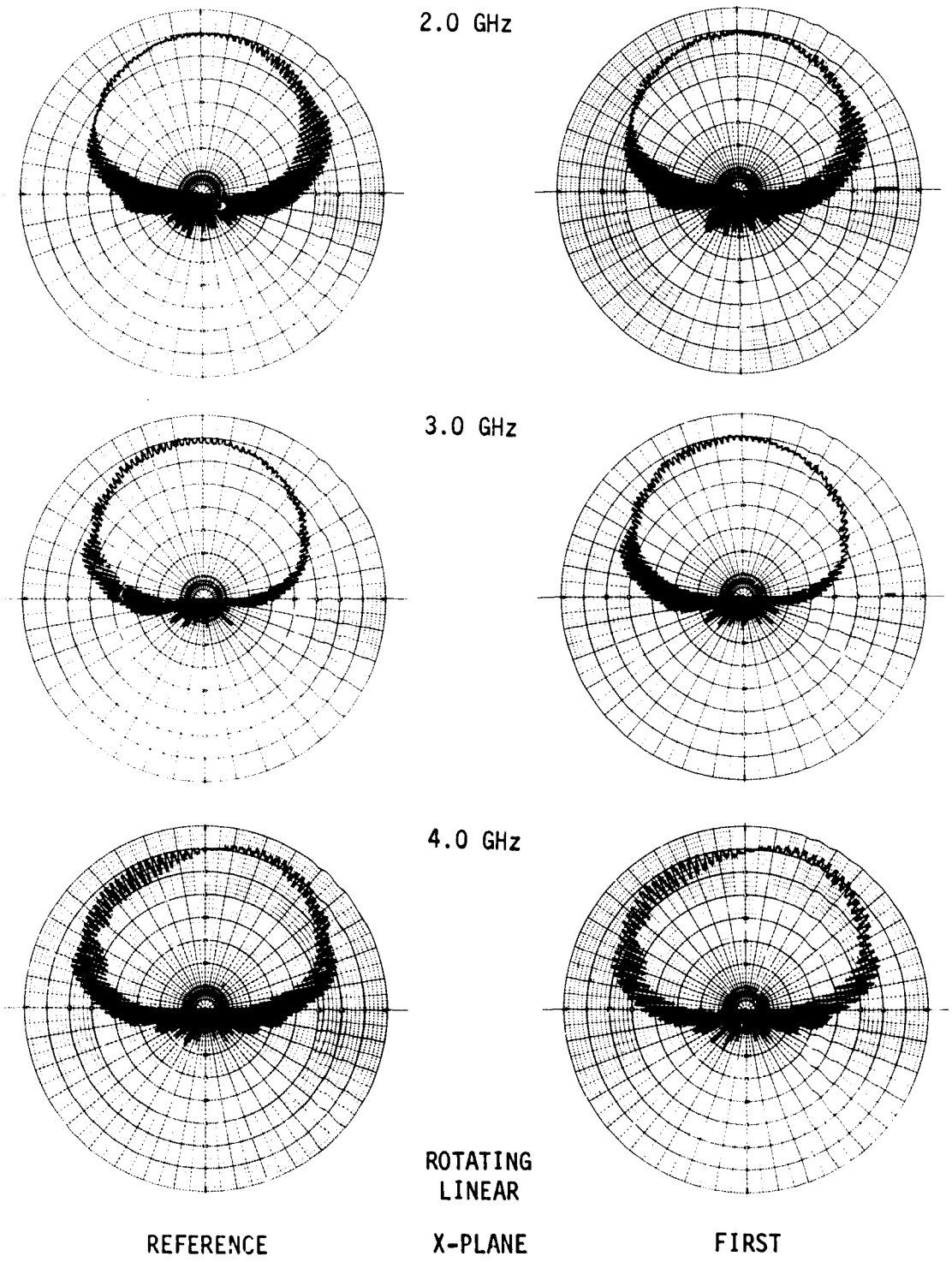

FIGURE 71 EFFECTS OF THERMAL ENVIRONMENT – AEL S-BAND ANTENNA RADIATION PATTERNS

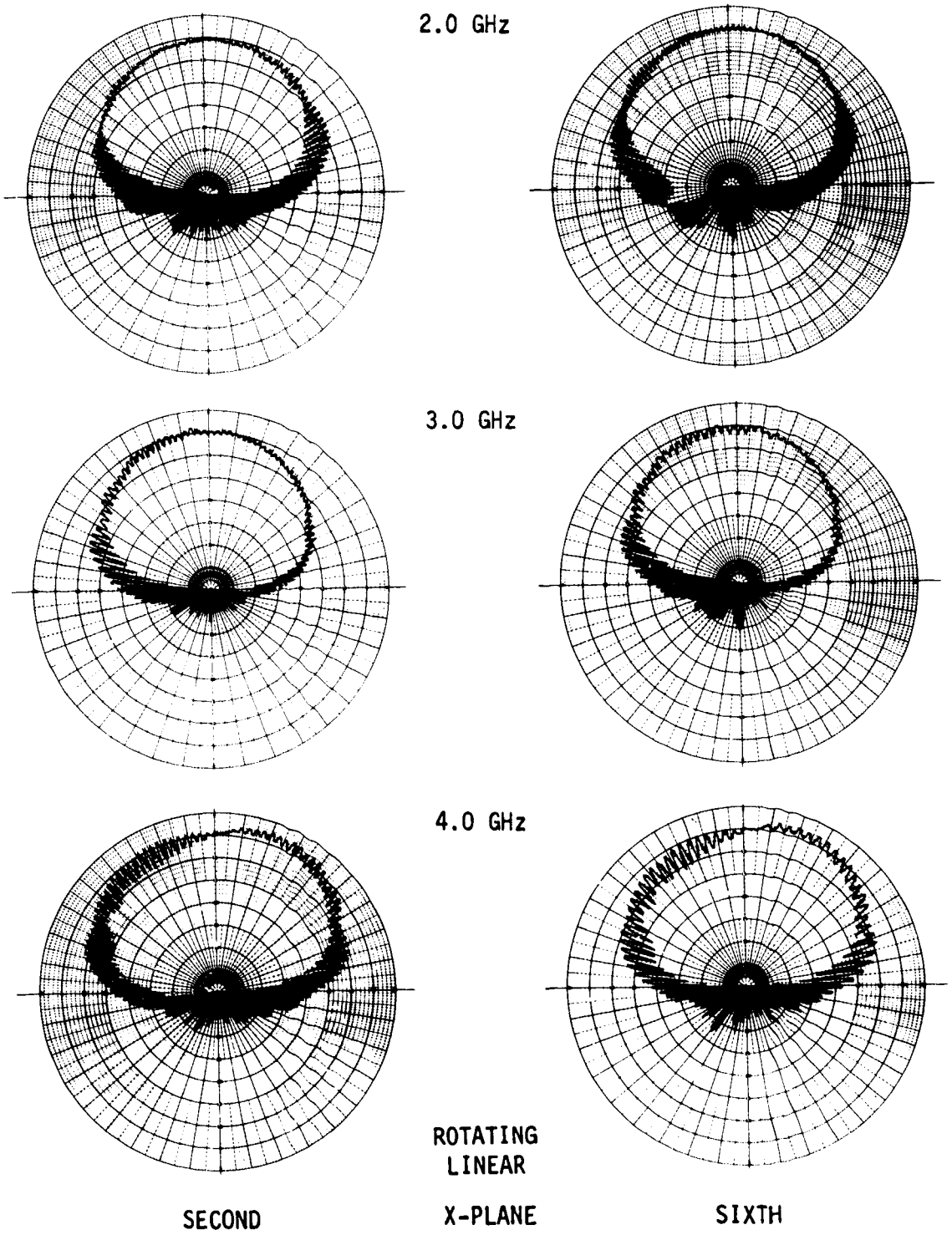

FIGURE 71 EFFECTS OF THERMAL ENVIRONMENT – AEL S-BAND ANTENNA RADIATION PATTERNS (Continued)

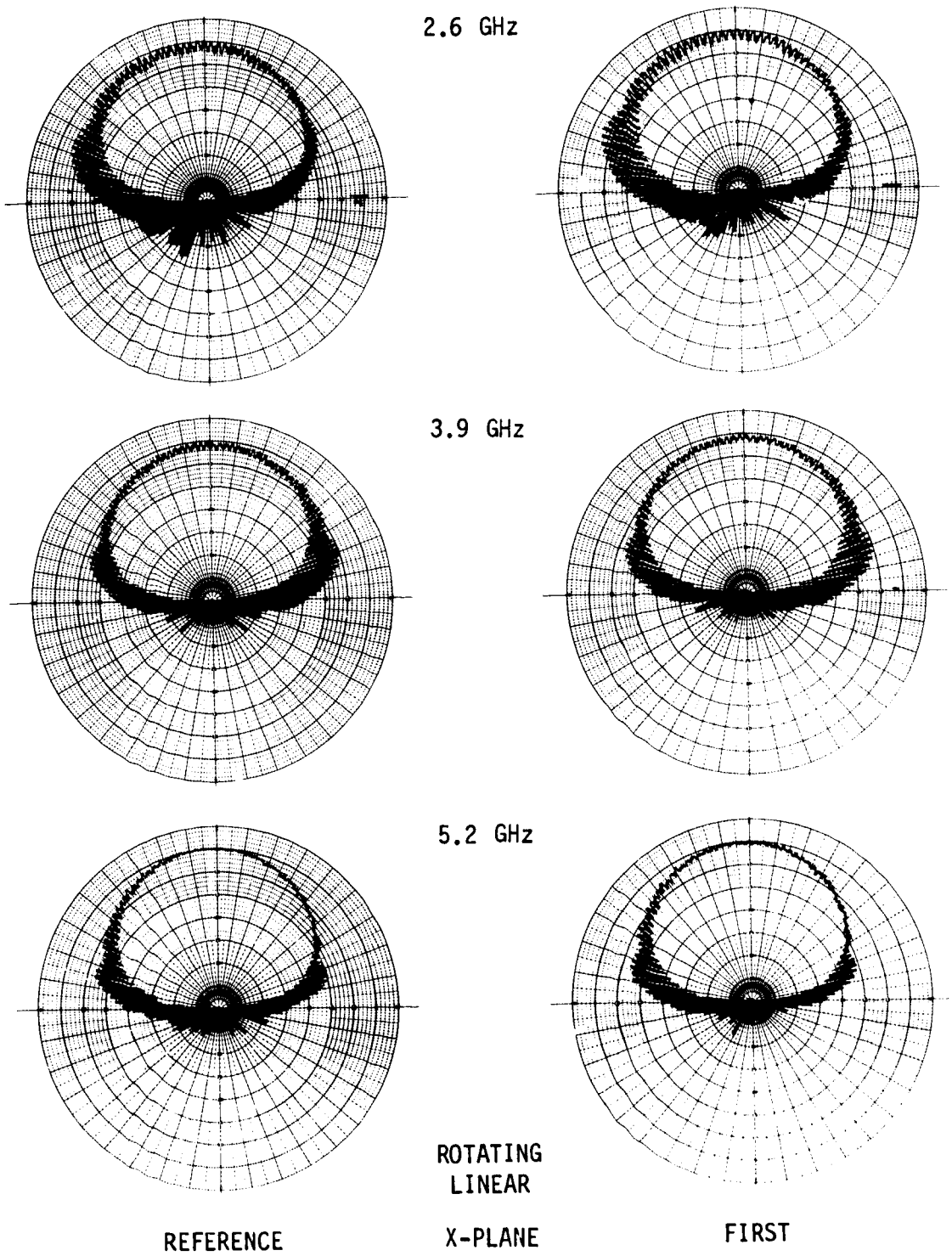

FIGURE 72 EFFECTS OF THERMAL ENVIRONMENT – SA S-BAND ANTENNA RADIATION PATTERNS

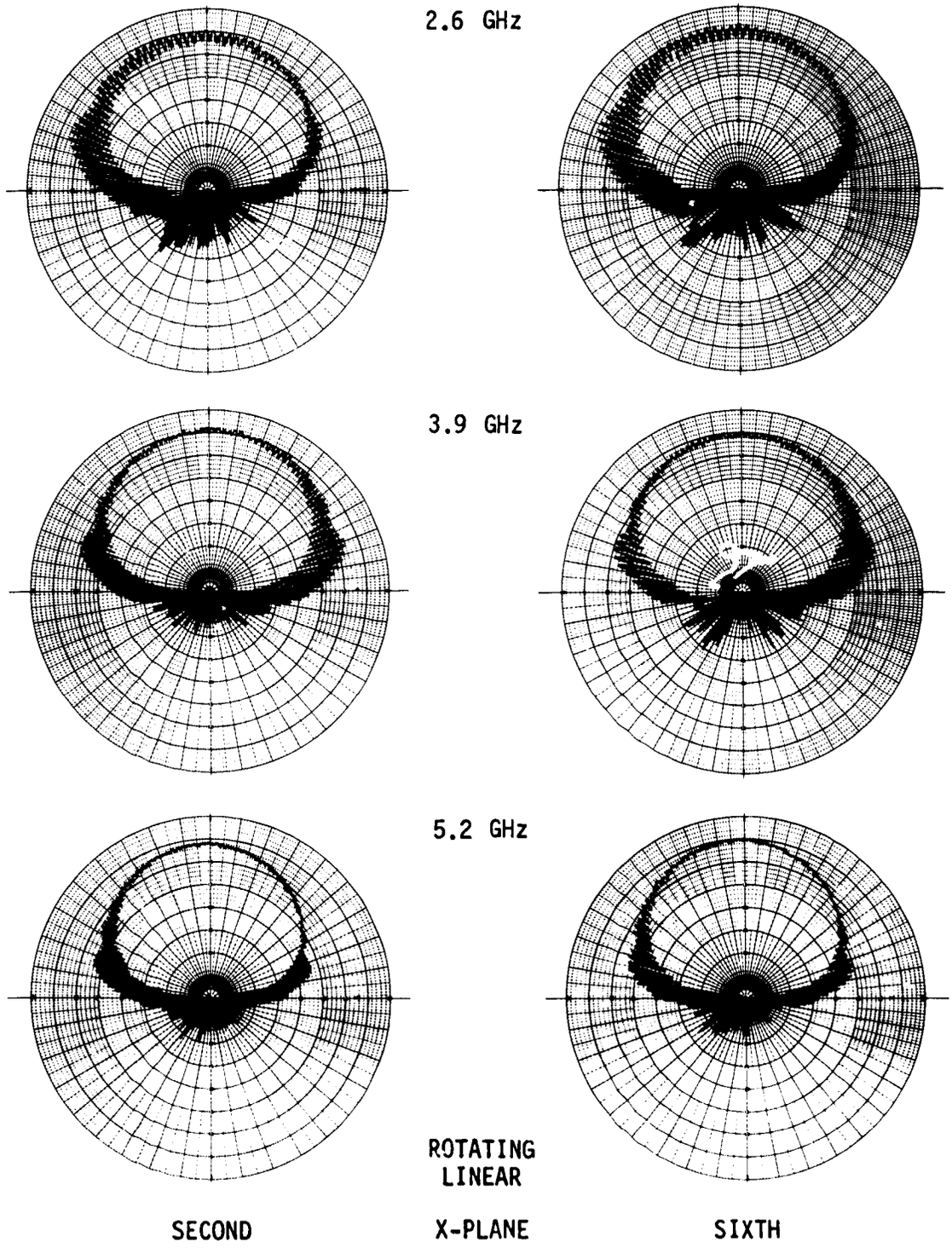

FIGURE 72 EFFECTS OF THERMAL ENVIRONMENT – SA S-BAND ANTENNA RADIATION PATTERNS (Continued)

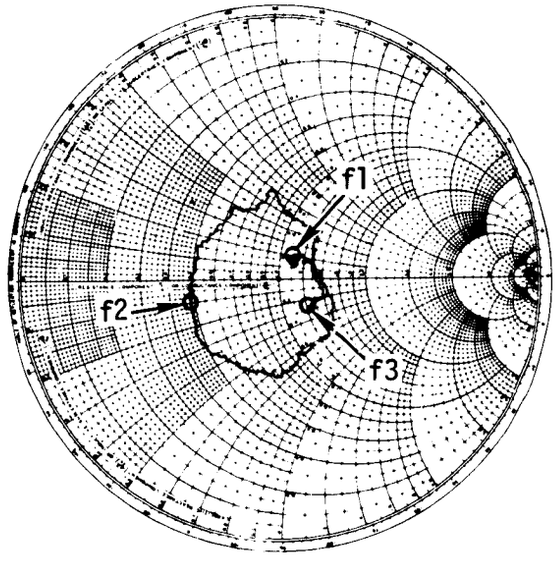

REFERENCE

Z_o = 50 OHMS
f1 = 2.0 GHz
f2 = 3.0 GHz
f3 = 4.0 GHz

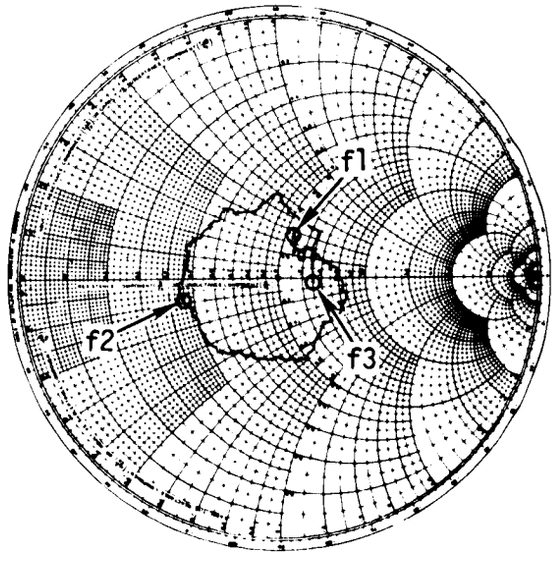

SIXTH

FIGURE 73 EFFECTS OF THERMAL ENVIRONMENT – AEL S-BAND ANTENNA IMPEDANCE

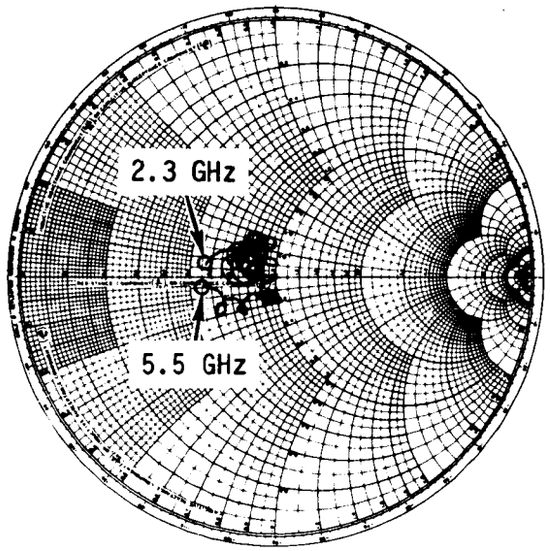

REFERENCE

Z_o = 50 OHMS
SWEEP RANGE
2.3 GHz to 5.5 GHz

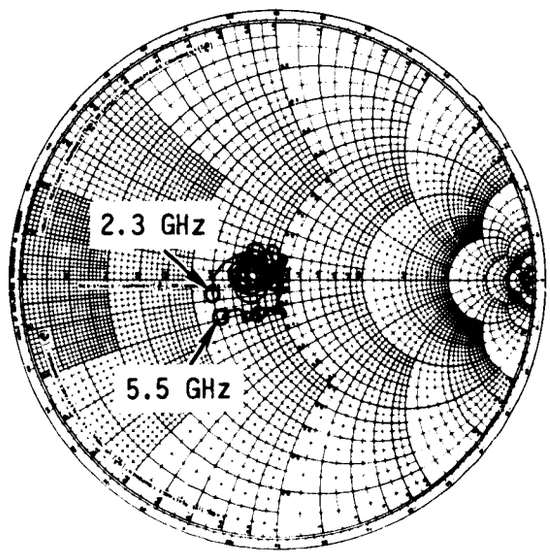

SIXTH

FIGURE 74 EFFECTS OF THERMAL ENVIRONMENT – SA S-BAND ANTENNA IMPEDANCE

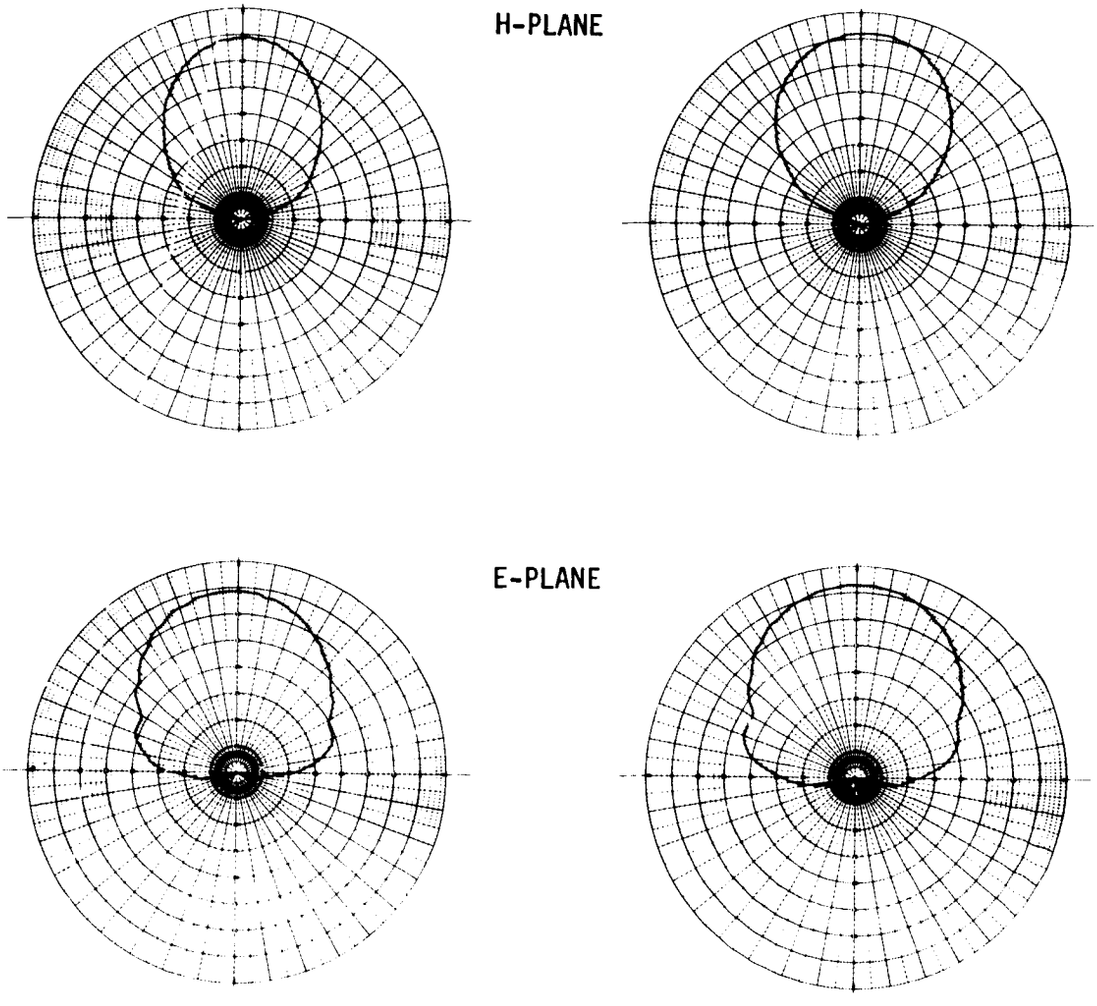

FIGURE 75 EFFECTS OF THERMAL ENVIRONMENT – D&M C-BAND ANTENNA RADIATION PATTERNS

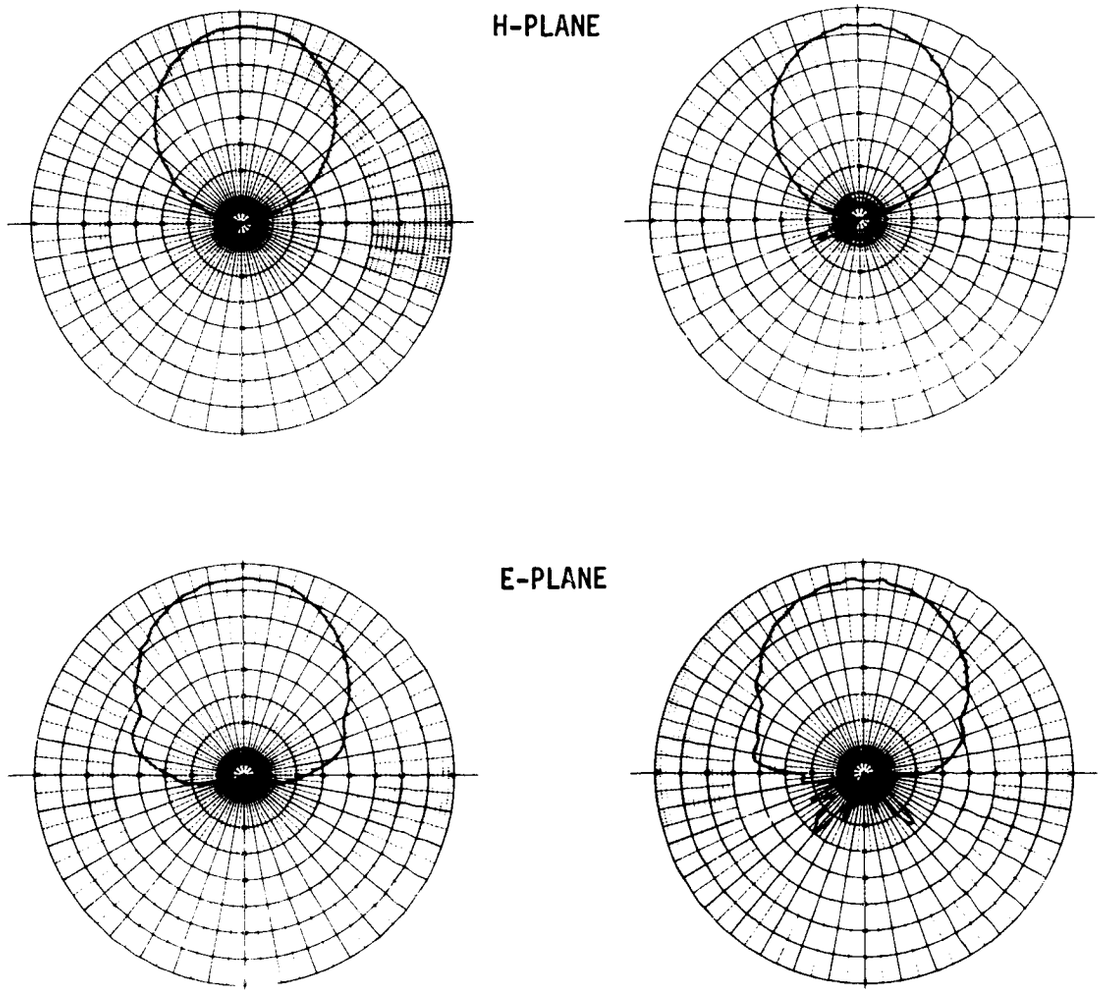

FIGURE 75 EFFECTS OF THERMAL ENVIRONMENT – D&M C-BAND ANTENNA RADIATION PATTERNS (Continued)

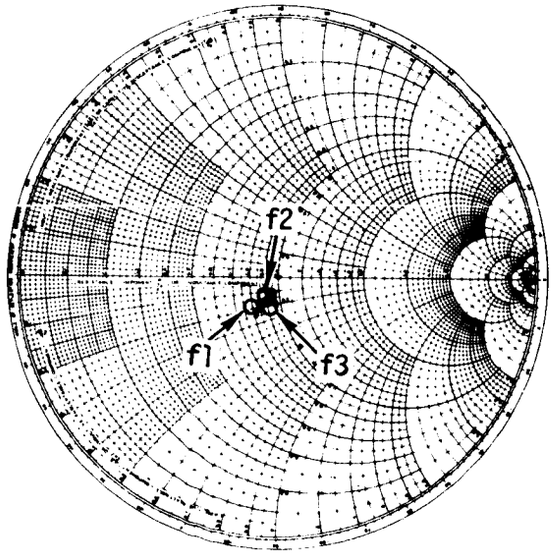

REFERENCE

Z_o = 50 OHMS
f1 = 4.2 GHz
f2 = 4.3 GHz
f3 = 4.4 GHz

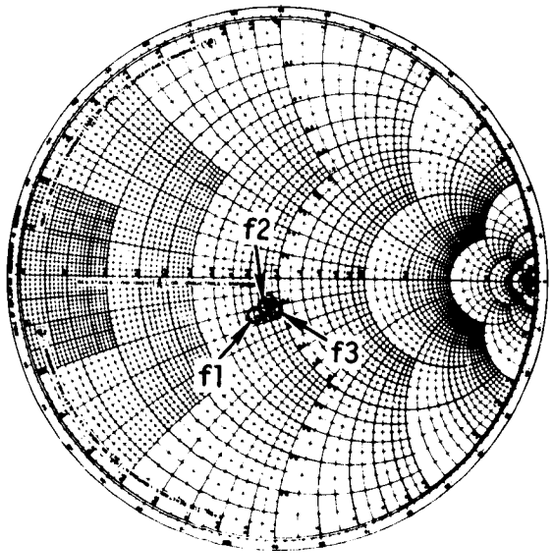

SIXTH

FIGURE 76 EFFECTS OF THERMAL ENVIRONMENT – D&M C-BAND ANTENNA IMPEDANCE

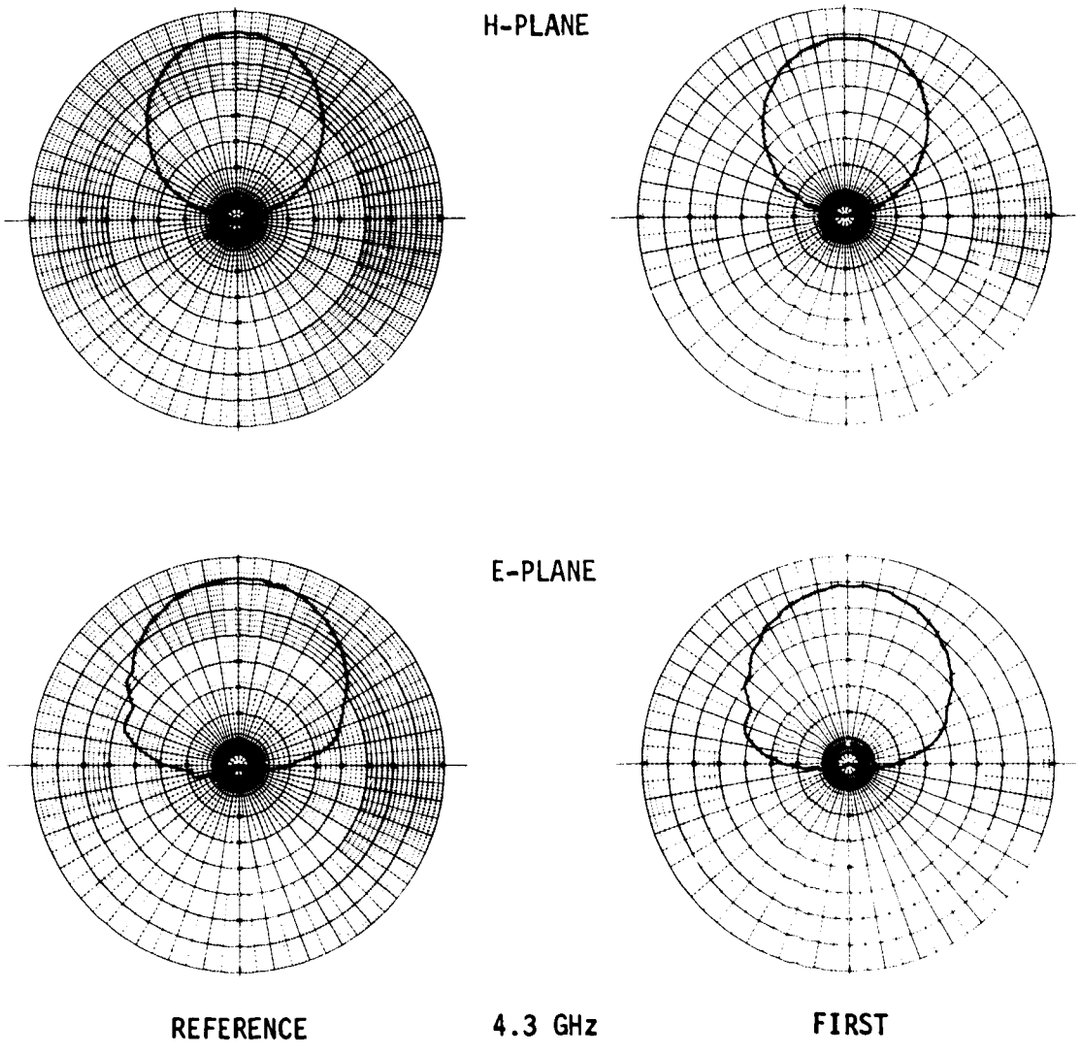

FIGURE 77 EFFECTS OF THERMAL ENVIRONMENT – RANTEC C-BAND ANTENNA RADIATION PATTERNS

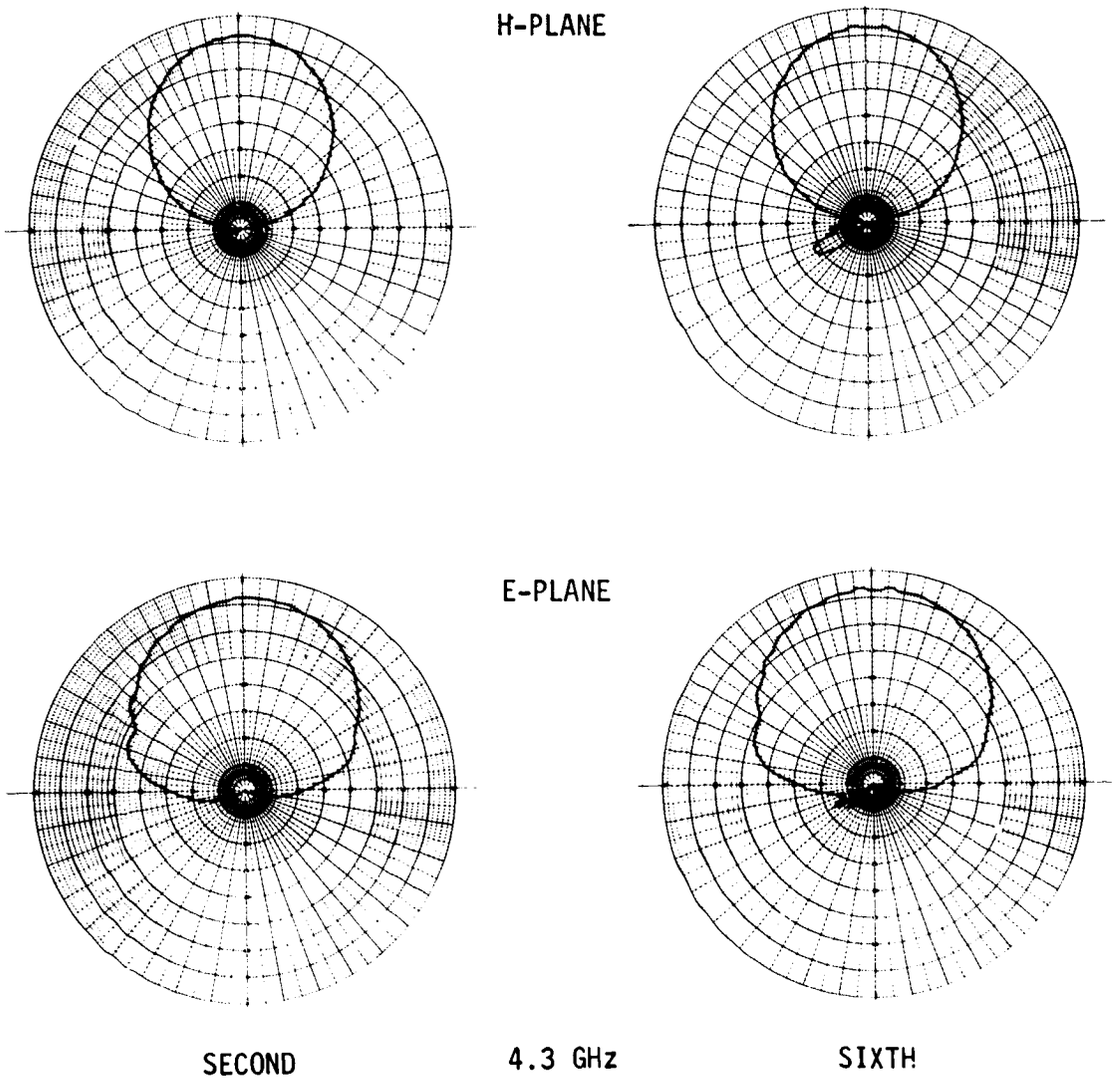

FIGURE 77 EFFECTS OF THERMAL ENVIRONMENT – RANTEC C-BAND ANTENNA RADIATION PATTERNS (Continued)

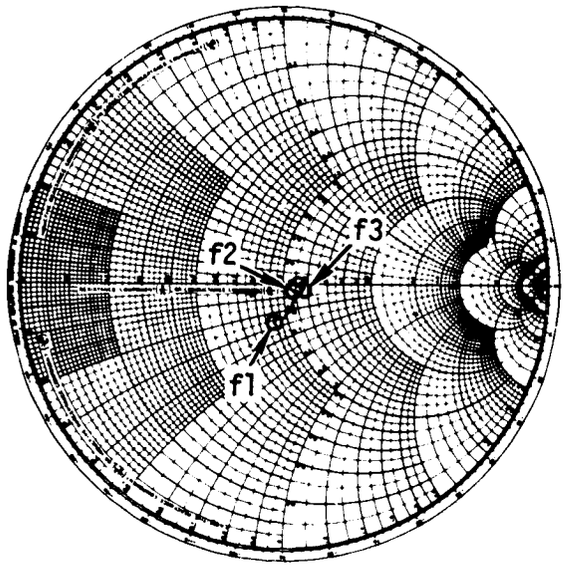

REFERENCE

Z_o = 50 OHMS
f1 = 4.2 GHz
f2 = 4.3 GHz
f3 = 4.4 GHz

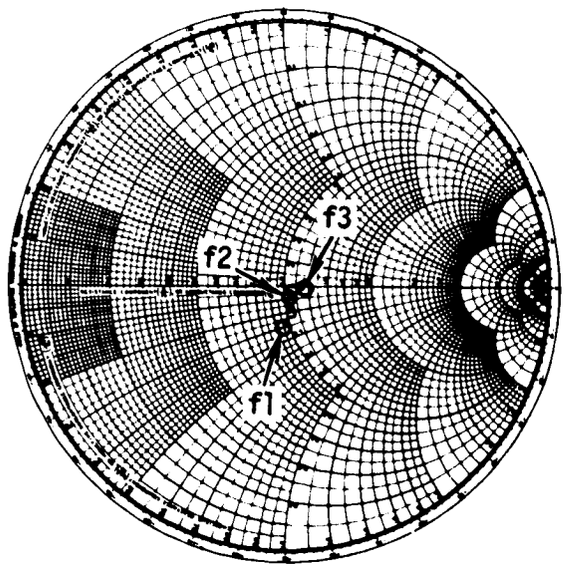

SIXTH

FIGURE 78 EFFECTS OF THERMAL ENVIRONMENT – RANTEC C-BAND ANTENNA PATTERNS

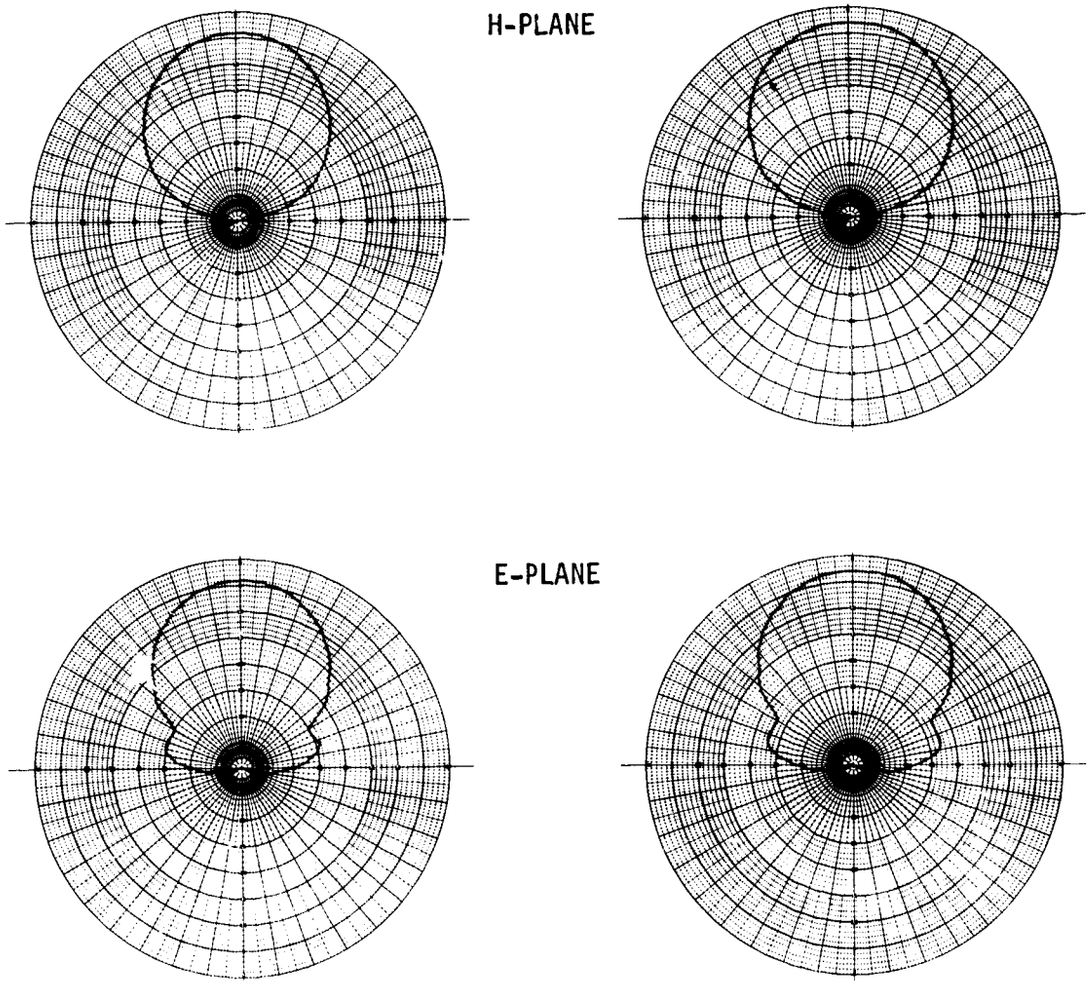

FIGURE 79 EFFECTS OF THERMAL ENVIRONMENT – TRANSCO C-BAND ANTENNA RADIATION PATTERNS

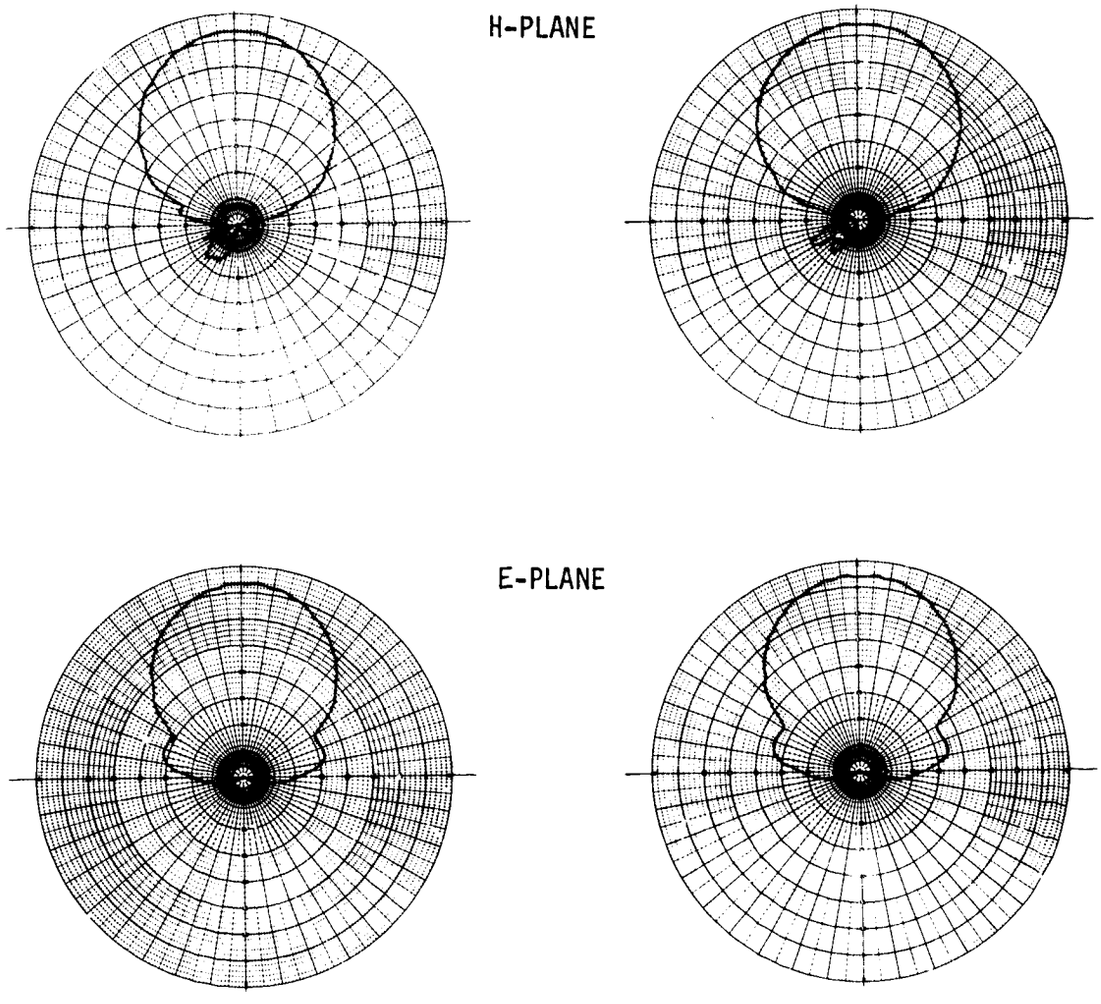

FIGURE 79 EFFECTS OF THERMAL ENVIRONMENT – TRANSCO C-BAND ANTENNA RADIATION PATTERNS (Continued)

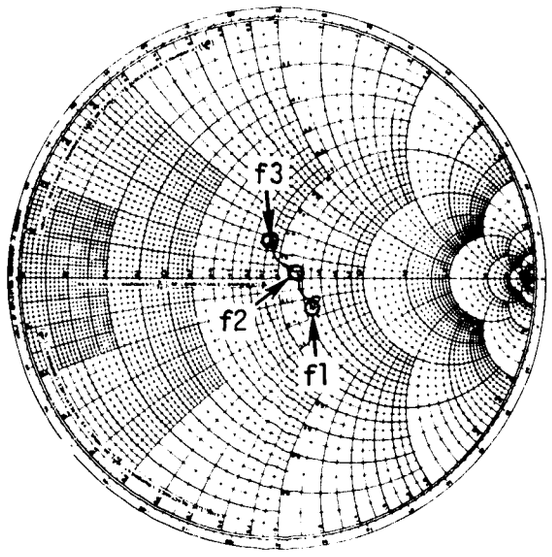

REFERENCE

Z_o = 50 OHMS
f1 = 4.2 GHz
f2 = 4.3 GHz
f3 = 4.4 GHz

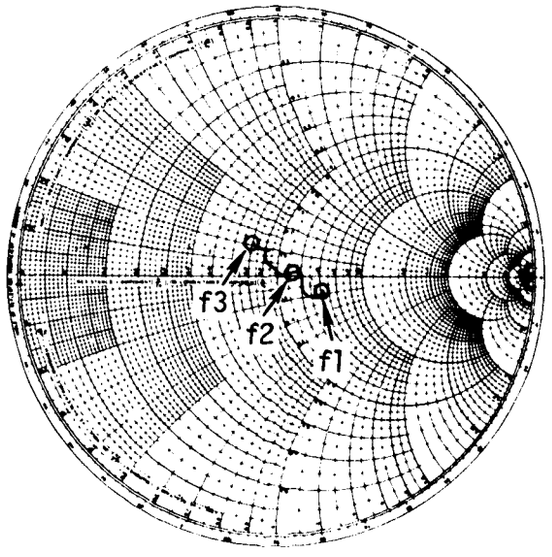

SIXTH

FIGURE 80 EFFECTS OF THERMAL ENVIRONMENT – RANTEC C-BAND ANTENNA IMPEDANCE

Each of the seven OTS antennas were subjected to six environments (table V). The antennas were tested in three groups. An overview of the OTS antenna tests is given in table VII.

TABLE VII
SUMMARY OF CONTROL TEMPERATURES FOR OTS ANTENNA THERMAL TESTS

TEST	PANEL	INITIAL TEMPERATURE K (°F)	MAXIMUM TEMPERATURE K (°F)
OTS-A1	A	170 (-154)	321 (118)
OTS-A2	A	169 (-155)	325 (125)
OTS-A3	A	292 (67)	407 (274)
OTS-A4	A	113 (-256)	286 (56)
OTS-A5	A	166 (-161)	327 (129)
OTS-A6	A	289 (60)	447 (345)
OTS-B1	B	173 (-148)	327 (129)
OTS-B2	B	169 (-156)	324 (124)
OTS-B3	B	295 (71)	409 (277)
OTS-B4	B	110 (-261)	297 (76)
OTS-B5	B	167 (-158)	326 (126)
OTS-B6	B	292 (67)	450 (350)
OTS-C1	C	171 (-152)	331 (137)
OTS-C2	C	168 (-158)	326 (127)
OTS-C3	C	293 (68)	404 (268)
OTS-C4	C	113 (-256)	294 (69)
OTS-C5	C	169 (-156)	327 (129)
OTS-C6	C	292 (66)	450 (350)

NOTES: PANEL A - CONTAINED TRANSCO L-BAND AND RANTEC C-BAND ANTENNAS
PANEL B - CONTAINED D&M C-BAND AND L-BAND ANTENNAS
PANEL C - CONTAINED SA S-BAND, TRANSCO C-BAND AND AEL S-BAND ANTENNAS

Facility description. - All tests were conducted in the MDC Mission Environment Simulator. This facility is described in the section on S-BAND ANTENNA SYSTEM TESTS under Thermal Testing.

Test installation. - The installation of the seven antennas on the three panels is shown in figures 81, 82 and 83. The Orbiter structure around each antenna was simulated to provide realistic heat conduction into or out of the antenna. Each antenna installation was thermally isolated on the test panel so that the heat sink effect of one did not affect the thermal environment of another on the same panel. The heat flux to the respective antenna installations was controlled to produce the desired temperature history on an aluminum control plate located on each panel.

Each antenna was attached to two annular rings (figure 84). The "S" shape ring simulated typical attachment structure and the flat ring simulated the Orbiter skin and stringers. The annular rings were attached to a 51.0 cm x 53.5 cm (20.0 in. x 21.0 in.) fiberglass panel 0.31 cm (0.125 in.) thick as shown in figures 81, 82 and 83. The 10.1 cm (4.0 in.) square aluminum control plate 0.15 cm (0.060 in.) thick was also attached to the fiberglass panel. The aluminum rings and control plate were coated with Krylon #12 ultra flat black enamel (0.9 emittance) to match the antenna surface emittances of 0.88 to 0.92 (table VIII) to provide uniform heating over the surface of the assembly.

The fiberglass panel was supported by aluminum frame around its perimeter. To simulate the insulation on the interior of the shuttle skin, 48 kg/m^3 (3 lb/ft^3) density CERAFELT insulation 7.62 cm (3.0 in.) thick was placed on the backside of the antennas and fiberglass plate. The support frame was attached to the transport mechanism as shown in figure 85.

Test environment. - Since TPS was not used in these tests, the applied heating simulated the heat flux at the TPS structural bondline rather than at the TPS surface as was the case for the preceding S-band antenna system tests. The heat input to the OTS antennas was controlled to the nominal structural temperature histories (T/C 10) of tests P1-11, P1-13, and P1-15 with initial temperatures of 172 K (-150°F), 294 K (70°F), and 117 K (-250°F), respectively. To evaluate the case for antennas located on the Orbiter leeward side, where the TPS thickness is relatively thin, tests were made where excursions from the nominals (tests P1-11 and P1-13) were used.

Figure 86 defines the five control temperature histories employed and identifies the OTS antenna tests associated with each. Due to the large time lag between TPS surface temperature and structural temperatures, time zero for the OTS antenna tests corresponded to time 800 seconds of the S-band antenna system tests. For the 172 K (-150°F) conditions of tests 1 and 2, trial runs were made to define the temperature control procedure. It was learned that for peak temperatures of 450 K (350°F) or less the time lag between the radiative thermal coupling of the heater and the antenna test article was so large that automatic control was not feasible. Thus, a manual control procedure was developed to obtain the desired heat flux.

For tests 1 and 2, the pressure was varied to simulate that of entry (figure 87). During these tests, however, it was discovered that the temperature control was affected by the increasing pressure. Therefore, since pressure simulation was not considered mandatory to meet test objectives, with NASA-JSC approval, the pressure was held constant at 1820 N/m^2 (14 torr) for the remaining tests.

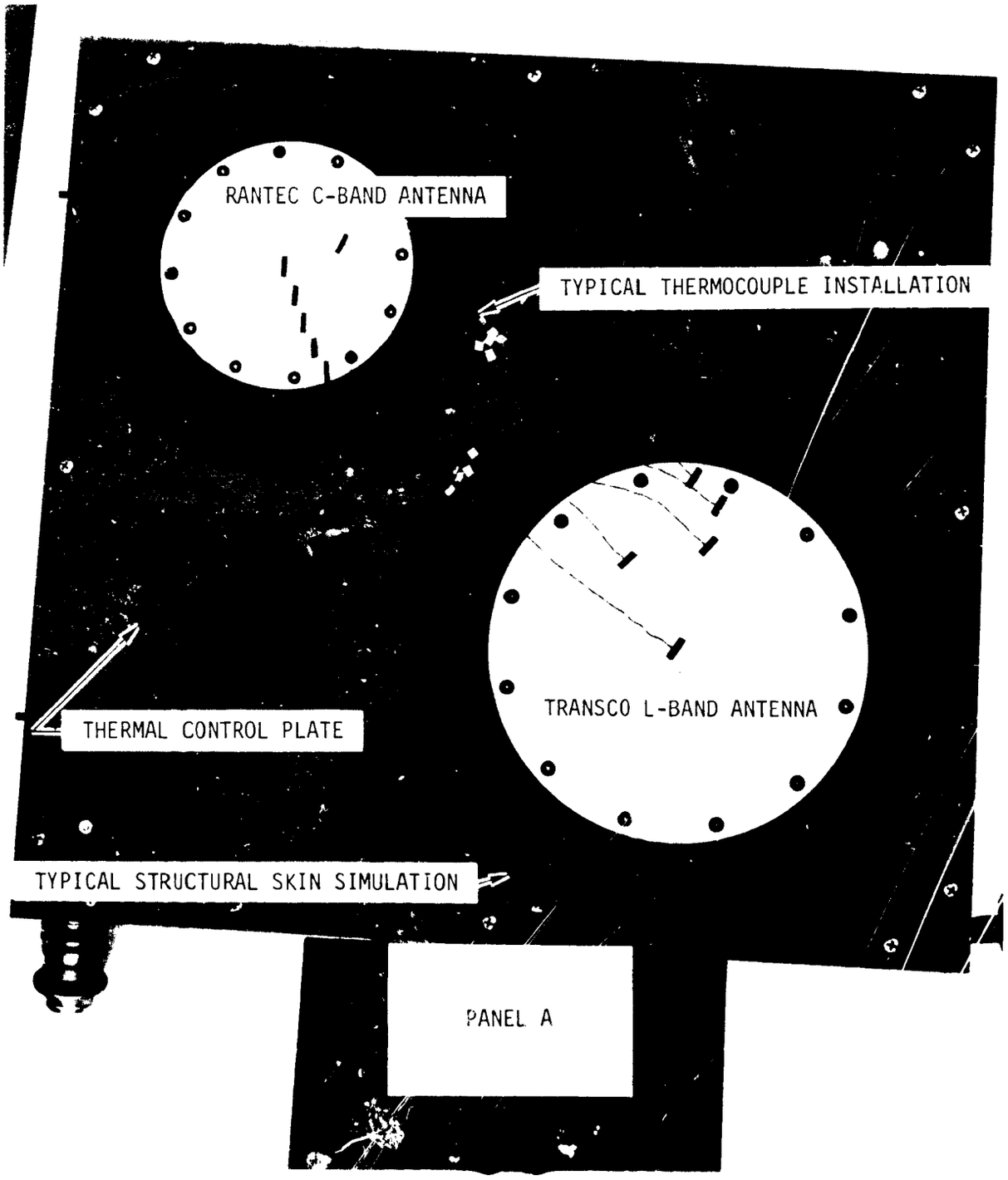

FIGURE 8: OTS ANTENNA THERMAL TEST PANEL A

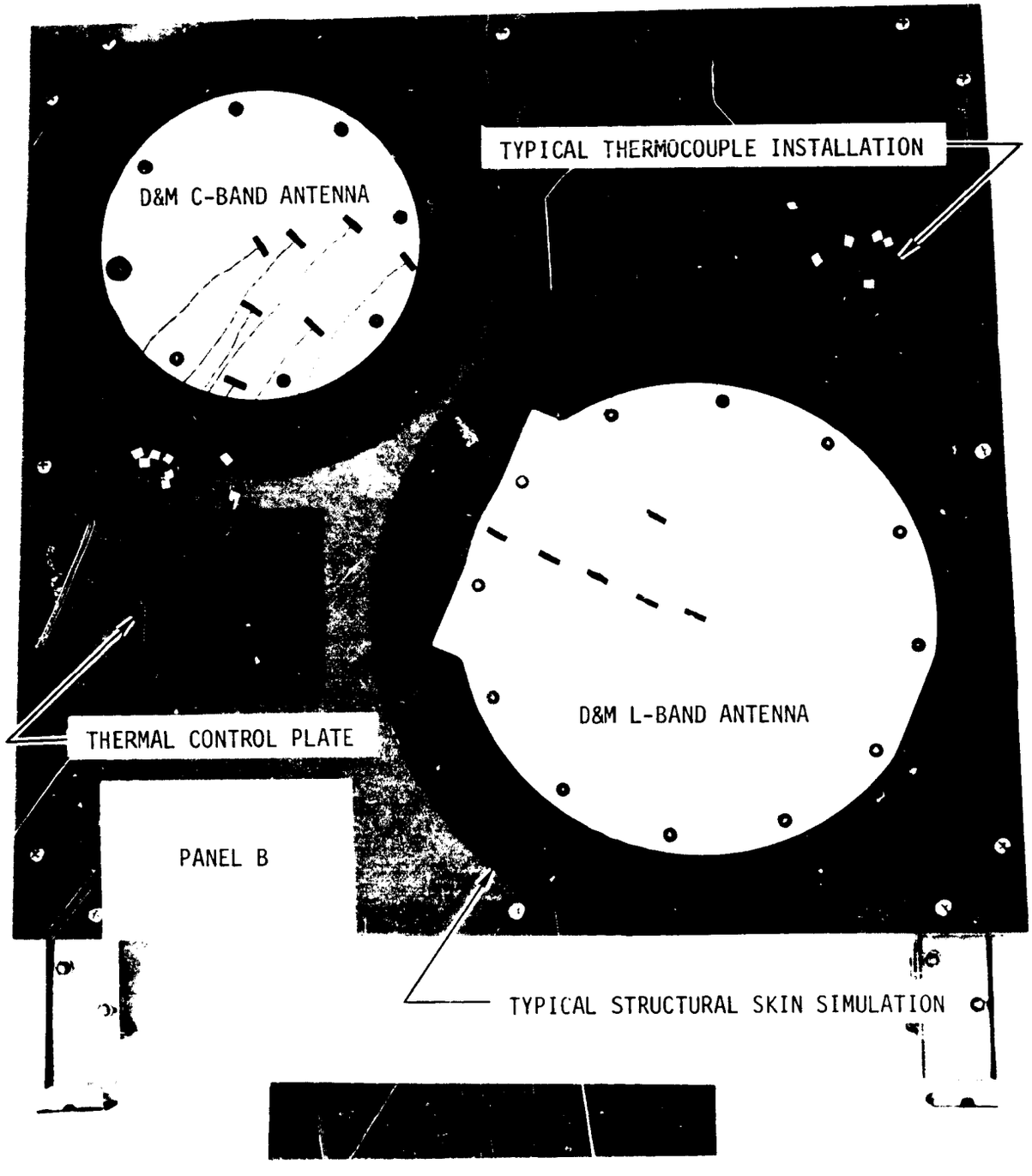

FIGURE 82 OTS ANTENNA THERMAL TEST PANEL B

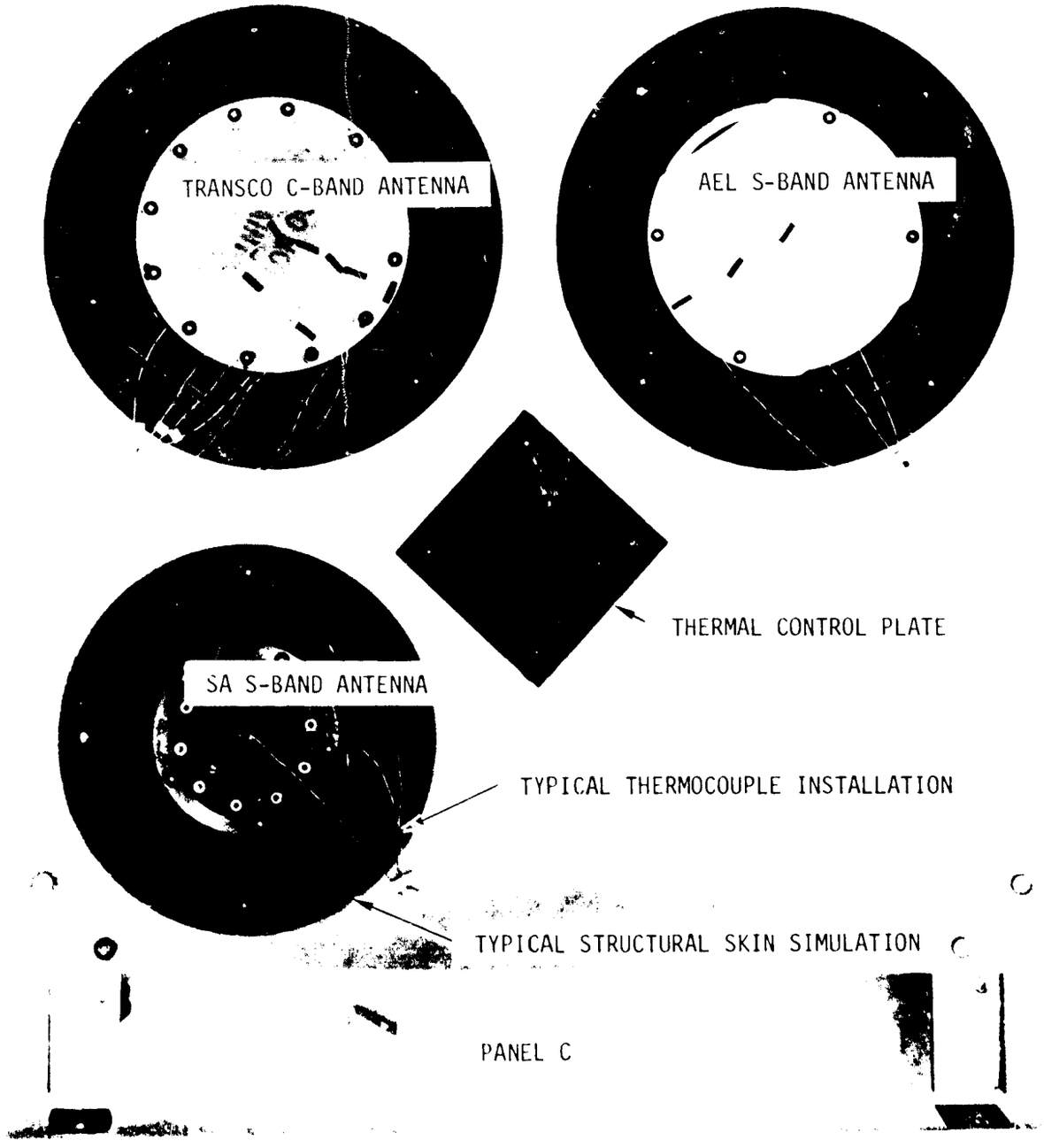

FIGURE 83 OTS ANTENNA THERMAL TEST PANEL C

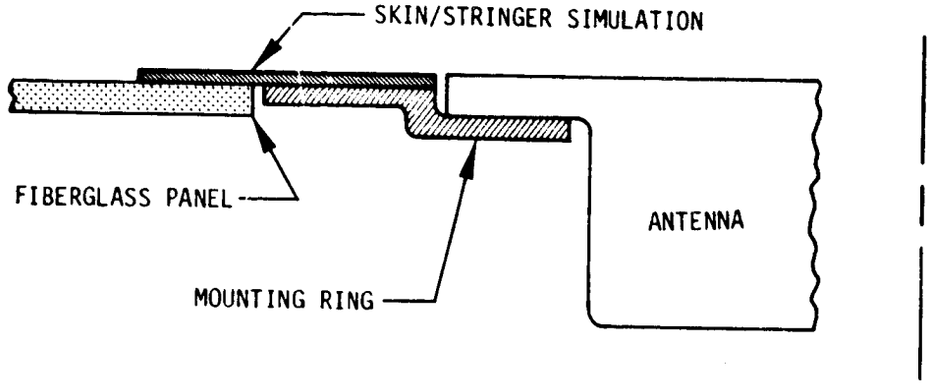

FIGURE 84 MOUNTING STRUCTURE SIMULATION FOR OTS ANTENNA THERMAL TESTS

TABLE VIII
SURFACE EMITTANCE OF OTS ANTENNAS

ANTENNA	EMITTANCE
TRANSCO L-BAND	0.90
RANTEC C-BAND	0.90
D&M C-BAND	0.88
D&M L-BAND	0.92
SA S-BAND	0.91
TRANSCO C-BAND	0.91
AEL S-BAND	0188

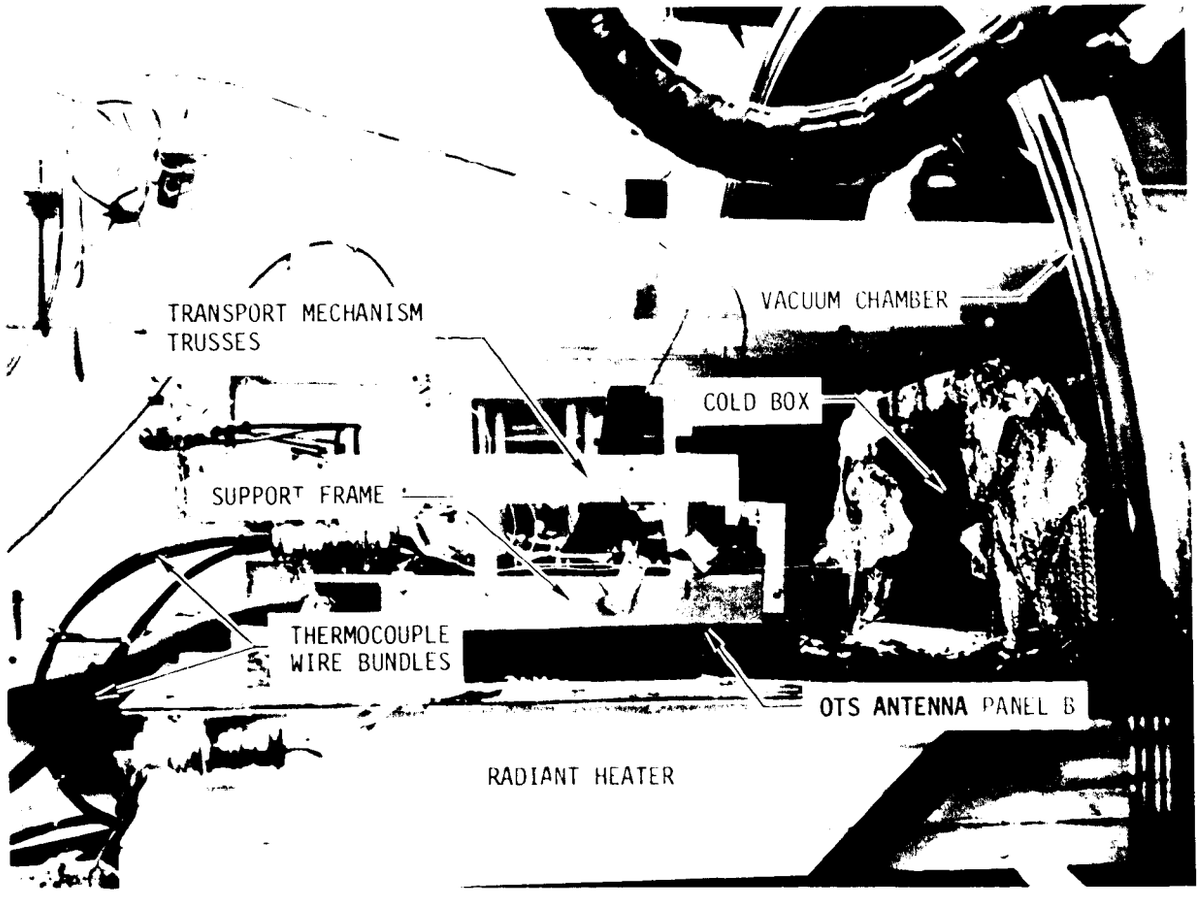

FIGURE 85 THERMAL TEST SETUP FOR OTS ANTENNAS

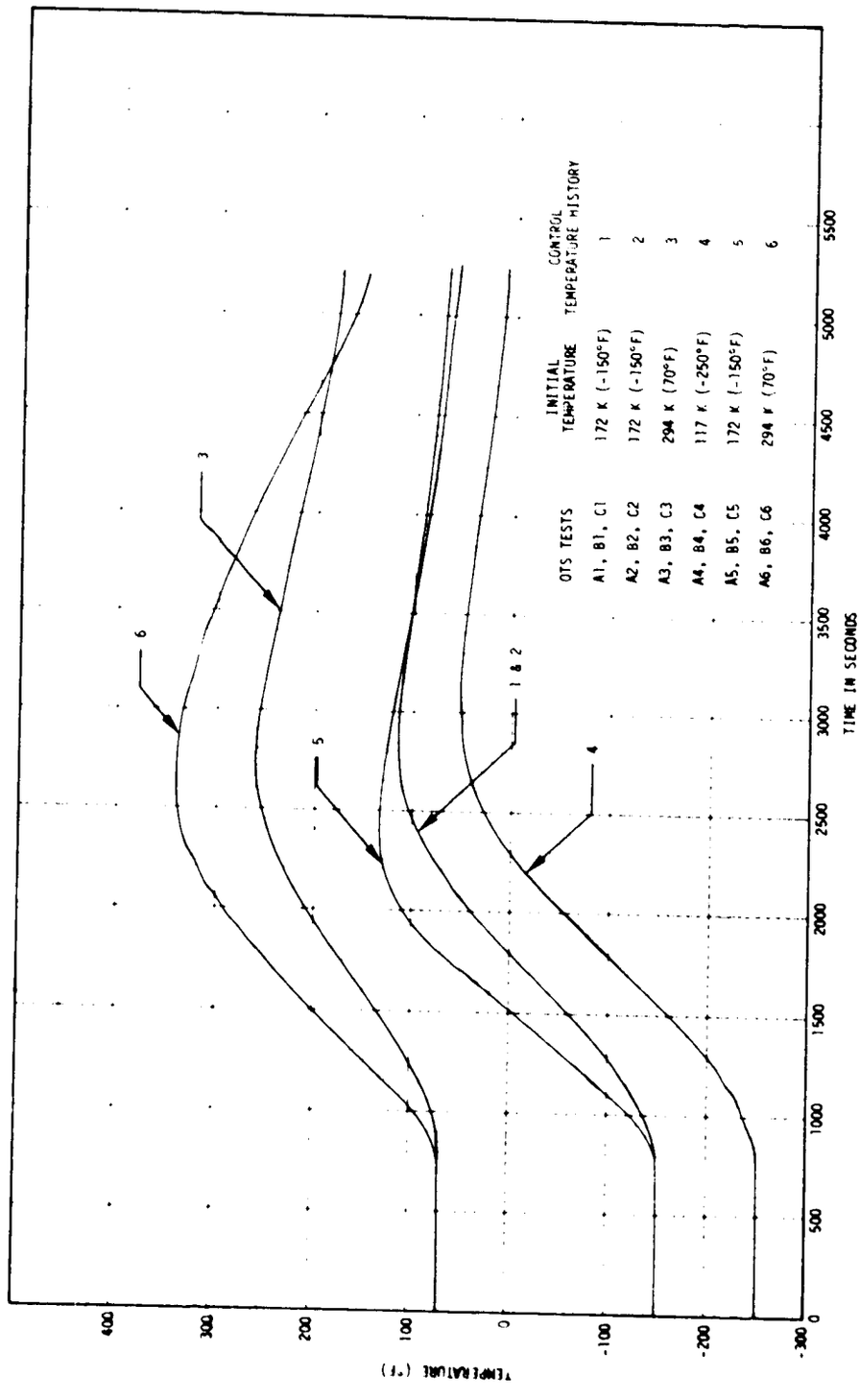

FIGURE 86 CONTROL TEMPERATURE HISTORIES FOR OTS ANTENNA THERMAL TESTS

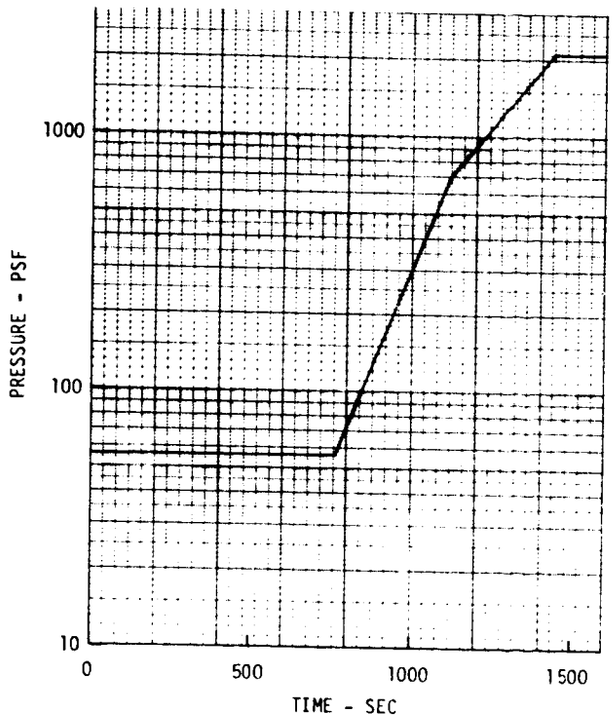

FIGURE 87 PRESSURE HISTORY FOR OTS ANTENNA THERMAL TESTS

Instrumentation. - Each antenna panel assembly was instrumented with 37 Chromel (+)/Alumel (-) thermocouples (ISA type K 30 gauge wire). One thermocouple was attached to the control plate on each panel. The general distribution of instrumentation on each antenna is shown in table IX. The thermocouples were attached to external surfaces of the antennas and mounting rings. No attempt was made to measure internal temperatures. The thermocouples on the antenna faces were attached by tape to permit removal for electrical tests. The thermocouples on the antenna cases away from the radiating apertures were bonded to the test article.

The internal configuration of the antenna was considered when locating the thermocouples. To measure maximum surface temperature differences, the thermocouples on the face were located at points that had both good and poor thermal communication with the internal parts. The location of thermocouples on each antenna is shown in figures 88, 89 and 90.

Test results. - The results of the temperature measurements (initial and maximum temperatures) for all antennas and each test condition are summarized in tables X through XVI. The measured temperature histories for each of the antennas for test 2 are shown in figures 91 through 97. The measured temperature histories on the Transco C-band antenna for all test conditions are shown in figures 97 through 101.

TABLE IX
THERMOCOUPLE DISTRIBUTION FOR OTS ANTENNA THERMAL TESTS

PANEL	ANTENNA	ANTENNA FACE	STRUCTURE RING	ANTENNA FLANGE	ANTENNA CASE	TOTAL
A	TRANSCO L-BAND	5	4	4	4	17
	RANTEC C-BAND	6	4	4	5	19
B	D&M C-BAND	7	3	3	5	18
	D&M L-BAND	6	3	3	6	18
C	SA S-BAND	3	2	2	3	10
	AEL S-BAND	3	2	2	3	10
	TRANSCO C-BAND	7	2	2	5	16

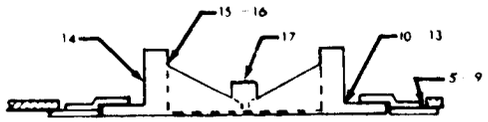

TRANSCO L-BAND ANTENNA

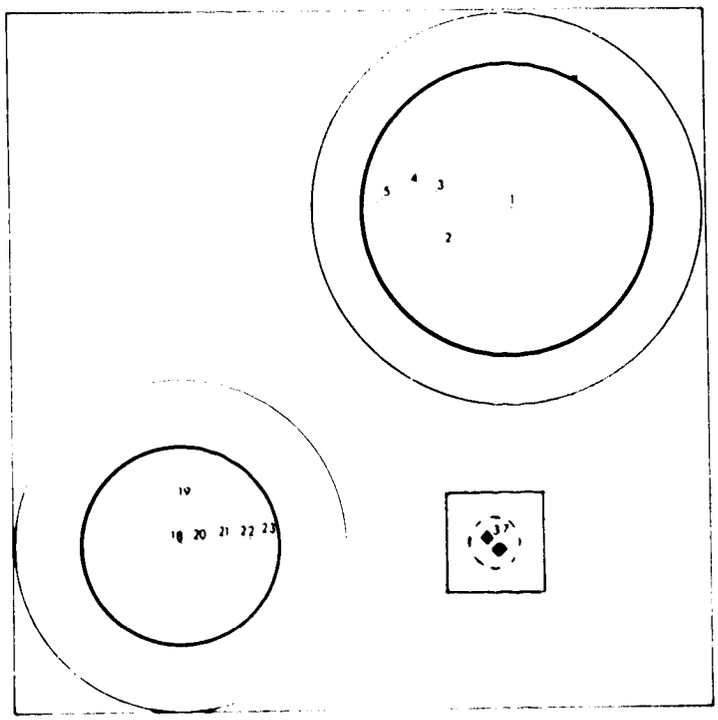

RANTEC C-BAND ANTENNA

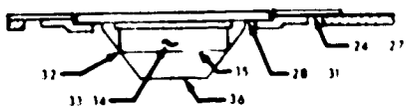

FIGURE 88 THERMOCOUPLE LOCATION FOR OTS ANTENNA PANEL A

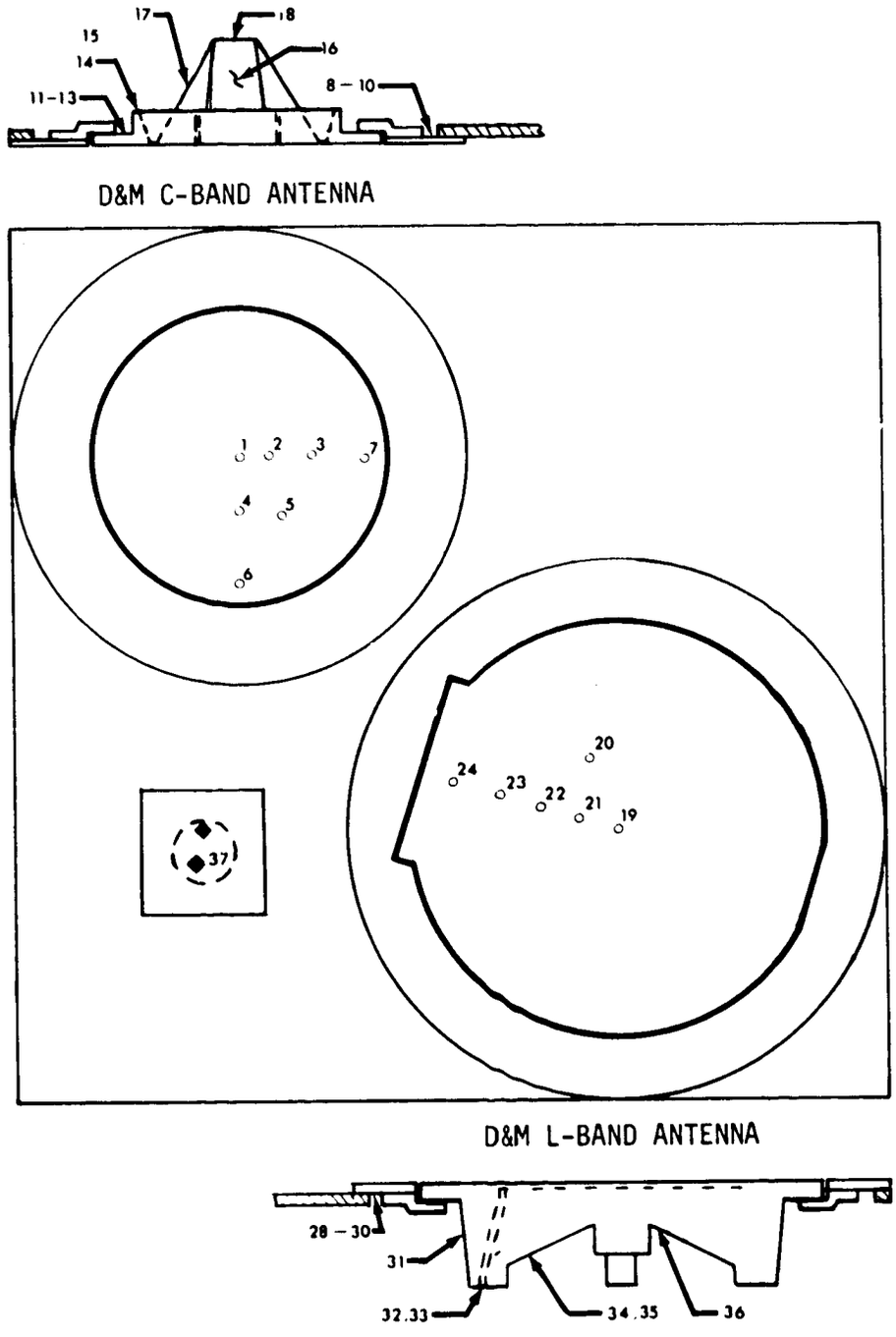

FIGURE 89 THERMOCOUPLE LOCATION FOR OTS ANTENNA PANEL B

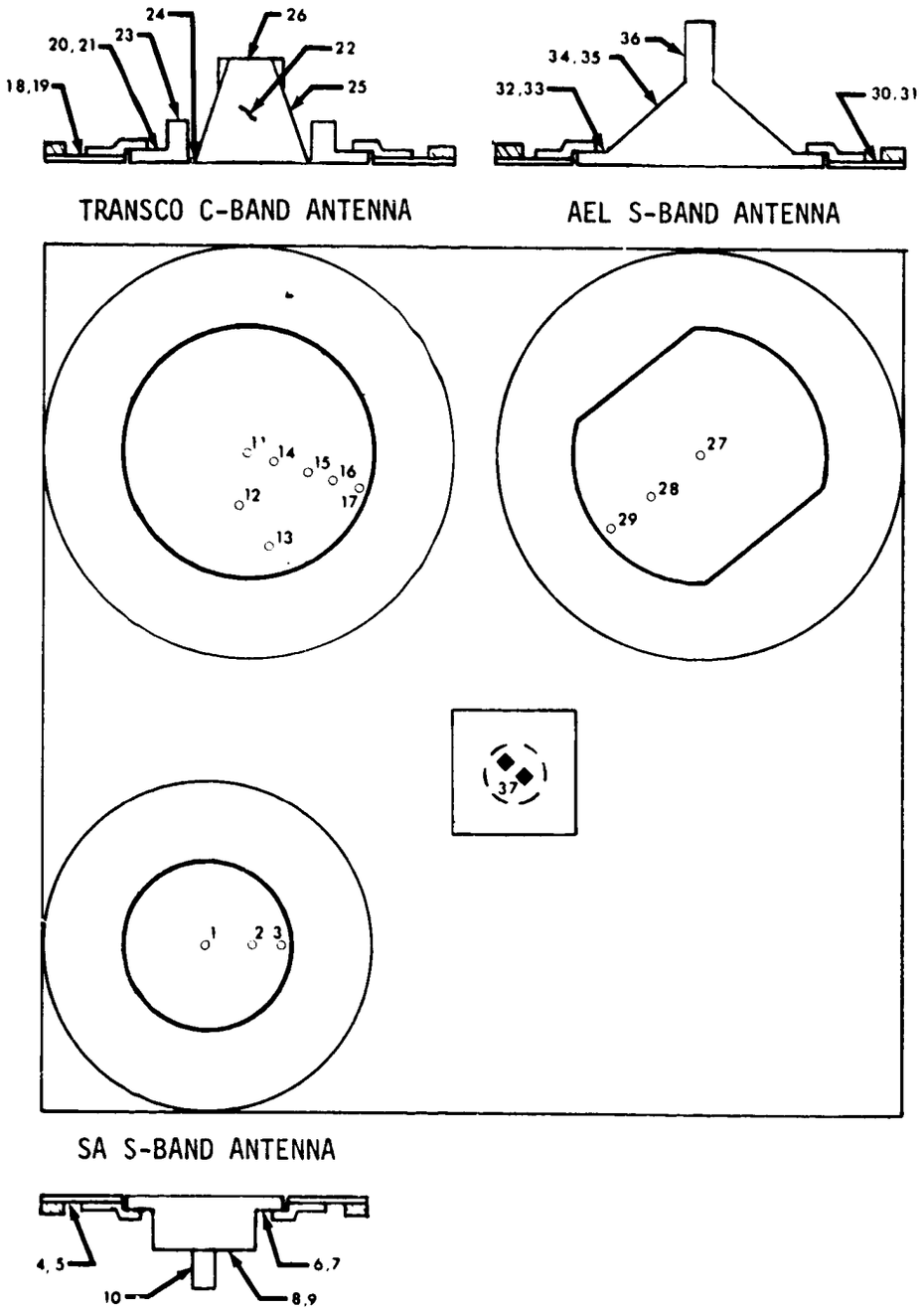

FIGURE 90 THERMOCOUPLE LOCATION FOR OTS ANTENNA PANEL C

TABLE X
THERMAL TEST RESULTS – TRANSCO L-BAND ANTENNA (PANEL A)

T/C No.	TEST NUMBER											
	OTS-A1		OTS-A2		OTS-A3		OTS-A4		OTS-A5		OTS-A6	
	T_o[b] K (°F)	T_{max} K (°F)	T_o[b] K (°F)	T_{max} K (°F)	T_o K (°F)	T_{max} K (°F)	T_o[b] K (°F)	T_{max} K (°F)	T_o[b] K (°F)	T_{max} K (°F)	T_o K (°F)	T_{max} K (°F)
Front Surface												
1	174 (-146)	311 (100)	172 (-149)	316 (109)[a]	294 (69)	441 (334)	122 (-240)	273 (32)[c]	170 (-153)	310 (98)	289 (60)	469 (384)
2	173 (-148)	319 (114)	172 (-150)	325 (125)[a]	296 (73)	414 (285)	120 (-244)	285 (54)	166 (-161)	321 (118)	290 (62)	441 (334)
3	173 (-148)	317 (112)	172 (-150)	322 (120)[a]	295 (72)	411 (281)	120 (-244)	283 (50)	166 (-160)	319 (114)	289 (61)	441 (334)
4	173 (-148)	310 (98)	172 (-149)	313 (104)[a]	295 (71)	406 (271)	121 (-241)	274 (33)	169 (-156)	319 (114)	289 (61)	441 (335)
5	174 (-146)	304 (88)	172 (-149)	309 (96)	293 (68)	397 (256)	122 (-239)	272 (30)[c]	170 (-153)	306 (91)	289 (60)	435 (324)
Skin Plate												
6	174 (-146)	305 (89)	172 (-149)	310 (98)	292 (66)	394 (250)	122 (-240)	272 (30)[c]	171 (-152)	304 (88)	287 (58)	431 (317)
7	175 (-144)	304 (87)	173 (-148)	308 (95)	292 (66)	392 (247)	122 (-240)	272 (30)[c]	170 (-153)	303 (86)	287 (58)	430 (314)
8	178 (-139)	303 (86)	176 (-143)	306 (92)	291 (65)	377 (219)	125 (-235)	272 (31)[c]	173 (-148)	296 (73)	287 (58)	407 (274)
9	180 (-135)	304 (87)	176 (-143)	307 (94)	291 (65)	377 (220)	126 (-233)	272 (31)[c]	174 (-146)	296 (74)	287 (58)	407 (274)
Flange												
10	175 (-145)	304 (88)	172 (-149)	309 (97)	291 (65)	392 (246)	121 (-241)	272 (30)[c]	170 (-153)	303 (86)	287 (58)	428 (311)
11	175 (-144)	304 (87)	173 (-148)	307 (94)	291 (65)	390 (243)	122 (-239)	272 (30)[c]	171 (-152)	302 (84)	287 (58)	426 (308)
12	177 (-140)	303 (86)	175 (-145)	306 (92)	291 (65)	379 (223)	124 (-236)	272 (31)[c]	172 (-150)	297 (75)	287 (58)	410 (279)
13	177 (-140)	304 (88)	175 (-145)	307 (94)	291 (65)	380 (225)	124 (-237)	272 (31)[c]	172 (-150)	297 (76)	287 (58)	411 (281)
Case												
14	175 (-144)	303 (86)	173 (-148)	307 (94)	291 (65)	387 (238)	122 (-239)	272 (30)[c]	171 (-152)	301 (82)	237 (58)	423 (302)
15	175 (-144)	304 (88)	174 (-147)	308 (95)	291 (64)	387 (238)	122 (-239)	272 (30)[c]	171 (-152)	301 (82)	287 (58)	422 (301)
16	175 (-144)	304 (87)	173 (-148)	308 (95)	291 (64)	387 (237)	123 (-238)	272 (31)[c]	172 (-150)	301 (82)	287 (58)	422 (301)
17	176 (-142)	303 (86)	174 (-146)	307 (93)	291 (64)	384 (232)	123 (-238)	272 (31)[c]	171 (-151)	299 (79)	287 (58)	417 (292)
Control Sample												
37	170 (-154)	321 (118)	169 (-155)	325 (125)	292 (67)	407 (274)	113 (-256)	286 (56)	166 (-161)	327 (129)	289 (60)	447 (345)

TABLE XI
THERMAL TEST RESULTS – RANTEC C-BAND ANTENNA (PANEL A)

T/C No.	TEST NUMBER											
	OTS-A1		OTS-A2		OTS-A3		OTS-A4		OTS-A5		OTS-A6	
	T_o[b] K (°F)	T_{max} K (°F)	T_o[b] K (°F)	T_{max} K (°F)	T_o K (°F)	T_{max} K (°F)	T_o[b] K (°F)	T_{max} K (°F)	T_o[b] K (°F)	T_{max} K (°F)	T_o K (°F)	T_{max} K (°F)
Front Surface												
18	165 (-162)	334 (142)[a]	165 (-162)	341 (155)[a]	296 (74)	441 (335)	107 (-267)	313 (104)	160 (-172)	370 (206)	290 (62)	476 (398)
19	165 (-162)	332 (138)[a]	166 (-161)	336 (145)[a]	296 (74)	434 (322)	106 (-269)	310 (98)	160 (-172)	362 (192)	290 (63)	469 (385)
20	166 (-160)	324 (123)[a]	166 (-160)	332 (139)[a]	296 (74)	434 (321)	109 (-264)	299 (78)	163 (-166)	356 (182)	290 (62)	470 (386)
21	169 (-156)	299 (79)	169 (-156)	302 (84)	292 (67)	399 (258)	112 (-257)	267 (21)[c]	167 (-158)	308 (95)	289 (60)	445 (342)
22	169 (-155)	299 (79)	169 (-156)	302 (84)	294 (70)	411 (281)	112 (-257)	267 (21)[c]	167 (-158)	308 (95)	289 (61)	445 (342)
23	169 (-155)	299 (79)	169 (-156)	302 (84)	295 (71)	401 (262)	112 (-257)	267 (21)[c]	167 (-159)	310 (98)	289 (60)	446 (343)
Skin Plate												
24	169 (-155)	299 (79)	169 (-156)	302 (84)	292 (67)	397 (256)	112 (-257)	266 (20)[c]	169 (-156)	307 (94)	288 (59)	442 (337)
25	169 (-155)	299 (78)	169 (-156)	302 (84)	292 (66)	396 (254)	112 (-258)	266 (20)[c]	168 (-157)	307 (93)	288 (59)	441 (334)
26	169 (-155)	296 (74)	169 (-155)	299 (79)	291 (65)	389 (240)	113 (-256)	266 (19)[c]	169 (-156)	301 (83)	288 (59)	430 (315)
27	170 (-153)	296 (74)	170 (-153)	299 (79)	292 (66)	389 (241)	114 (-254)	266 (20)[c]	169 (-155)	303 (86)	288 (59)	430 (315)
Flange												
28	169 (-156)	298 (77)	169 (-156)	301 (83)	292 (66)	395 (252)	112 (-257)	266 (19)[c]	167 (-158)	306 (92)	287 (58)	440 (332)
29	169 (-155)	299 (78)	169 (-156)	302 (84)	292 (66)	396 (254)	112 (-257)	266 (20)[c]	168 (-157)	307 (93)	288 (59)	441 (334)
30	169 (-155)	297 (75)	169 (-156)	300 (81)	291 (65)	392 (247)	112 (-257)	266 (19)[c]	169 (-156)	304 (88)	287 (58)	435 (324)
31	169 (-155)	297 (75)	169 (-155)	300 (81)	291 (65)	392 (246)	113 (-256)	266 (20)[c]	168 (-157)	304 (88)	288 (59)	434 (322)
Case												
32	169 (-155)	297 (76)	169 (-156)	301 (82)	291 (65)	394 (249)	(d)	(d)	168 (-157)	305 (90)	(d)	(d)
33	169 (-155)	297 (76)	169 (-155)	301 (82)	291 (65)	392 (247)	112 (-257)	266 (19)[c]	168 (-157)	305 (89)	288 (59)	435 (324)
34	169 (-155)	299 (78)	169 (-156)	302 (84)	292 (66)	396 (254)	112 (-257)	266 (20)[c]	168 (-157)	307 (93)	287 (58)	440 (333)
35	169 (-155)	298 (77)	169 (-156)	301 (83)	292 (66)	395 (251)	112 (-257)	266 (20)[c]	168 (-157)	306 (91)	288 (59)	439 (330)
36	169 (-155)	297 (76)	169 (-155)	301 (82)	291 (65)	392 (247)	113 (-256)	266 (20)[c]	168 (-157)	305 (90)	287 (58)	436 (325)
Control Sample												
37	170 (-154)	321 (118)	169 (-155)	325 (125)	292 (67)	407 (274)	113 (-256)	286 (56)	166 (-161)	327 (129)	289 (60)	447 (345)

TABLE XII
THERMAL TEST RESULTS – D&M C-BAND ANTENNA (PANEL B)

T/C No.	TEST NUMBER											
	OTS-B1		OTS-B2		OTS-B3		OTS-B4		OTS-B5		OTS-B6	
	T_o[b] K (°F)	T_{max} K (°F)	T_o[b] K (°F)	T_{max} K (°F)	T_o K (°F)	T_{max} K (°F)	T_o[b] K (°F)	T_{max} K (°F)	T_o[b] K (°F)	T_{max} K (°F)	T_o K (°F)	T_{max} K (°F)
Front Surface												
1	170 (-153)	326 (128)[a]	166 (-161)	335 (143)[a]	297 (75)	420 (296)	108 (-265)	315 (108)	166 (-161)	347 (166)	292 (67)	469 (385)
2	175 (-145)	294 (69)	168 (-157)	294 (70)[a]	295 (72)	391 (244)	112 (-258)	265 (17)[c]	169 (-155)	292 (67)	292 (67)	432 (318)
3	176 (-142)	287 (57)	169 (-155)	283 (50)	295 (71)	377 (219)	113 (-256)	261 (11)[c]	172 (-150)	280 (45)	292 (67)	417 (292)
4	172 (-150)	323 (122)[a]	167 (-159)	320 (117)[a]	297 (75)	415 (288)	110 (-262)	309 (96)	167 (-159)	342 (156)	292 (67)	464 (376)
5	176 (-143)	289 (60)	169 (-156)	289 (60)	295 (72)	382 (229)	112 (-257)	262 (13)[c]	171 (-152)	281 (47)	292 (67)	427 (310)
6	176 (-142)	287 (58)	170 (-154)	283 (50)	294 (70)	377 (220)	113 (-256)	261 (11)[c]	172 (-150)	280 (45)	292 (67)	419 (295)
7	176 (-143)	287 (58)	169 (-156)	283 (50)	295 (71)	377 (220)	112 (-257)	262 (12)[c]	171 (-151)	281 (46)	292 (67)	423 (301)
Skin Plate												
8	176 (-143)	287 (58)	169 (-155)	284 (51)	294 (70)	379 (223)	113 (-256)	261 (11)[c]	171 (-151)	281 (47)	292 (67)	421 (298)
9	176 (-142)	287 (58)	169 (-155)	284 (51)	294 (70)	378 (221)	112 (-257)	261 (11)[c]	171 (-152)	281 (46)	292 (67)	419 (294)
10	176 (-142)	286 (56)	170 (-154)	282 (49)	294 (69)	370 (206)	115 (-252)	264 (15)[c]	172 (-150)	279 (42)	292 (67)	406 (272)
Flange												
11	176 (-142)	287 (57)	170 (-154)	283 (50)	294 (69)	376 (218)	113 (-256)	260 (9)[c]	172 (-150)	280 (45)	292 (67)	417 (291)
12	176 (-142)	287 (57)	170 (-154)	283 (50)	294 (69)	376 (217)	113 (-256)	261 (10)[c]	172 (-150)	280 (45)	292 (67)	416 (289)
13	176 (-142)	287 (57)	170 (-154)	283 (50)	294 (69)	374 (213)	113 (-256)	261 (10)[c]	172 (-150)	279 (43)	293 (68)	413 (284)
Case:												
14	176 (-142)	287 (57)	169 (-155)	283 (50)	294 (69)	375 (216)	113 (-256)	260 (9)[c]	172 (-150)	280 (45)	292 (67)	415 (288)
15	176 (-142)	287 (57)	170 (-154)	283 (50)	294 (69)	375 (216)	113 (-256)	260 (9)[c]	172 (-150)	280 (45)	292 (67)	415 (288)
16	177 (-141)	287 (57)	170 (-154)	283 (50)	294 (69)	374 (213)	113 (-256)	260 (8)[c]	172 (-149)	279 (43)	293 (68)	413 (284)
17	176 (-142)	287 (57)	169 (-155)	283 (50)	294 (69)	374 (214)	112 (-257)	260 (8)[c]	172 (-150)	280 (44)	293 (68)	414 (285)
18	177 (-141)	286 (56)	170 (-154)	283 (50)	294 (69)	373 (212)	113 (-256)	260 (8)[c]	172 (-150)	279 (43)	293 (68)	412 (282)
Control Sample												
37	173 (-148)	327 (129)	169 (-156)	324 (124)	295 (71)	409 (277)	110 (-261)	297 (76)	167 (-158)	326 (127)	292 (67)	450 (350)

TABLE XIII
THERMAL TEST RESULTS – D&M L-BAND ANTENNA (PANEL B)

T/C No.	TEST NUMBER											
	OTS-B1		OTS-B2		OTS-B3		OTS-B4		OTS-B5		OTS-B6	
	T_o[b] K (°F)	T_{max} K (°F)	T_o[b] K (°F)	T_{max} K (°F)	T_o K (°F)	T_{max} K (°F)	T_o[b] K (°F)	T_{max} K (°F)	T_o[b] K (°F)	T_{max} K (°F)	T_o K (°F)	T_{max} K (°F)
Front Surface												
19	181 (-134)	305 (90)	172 (-149)	306 (92)	295 (72)	391 (244)	119 (-245)	273 (32)	174 (-147)	300 (81)	292 (67)	442 (337)
20	171 (-151)	(d)	168 (-157)	330 (135)[a]	297 (76)	406 (272)	114 (-255)	315 (108)	169 (-156)	338 (149)	292 (66)	458 (365)
21	181 (-134)	305 (90)	173 (-148)	306 (92)	295 (72)	390 (242)	119 (-245)	273 (32)	174 (-146)	300 (81)	292 (67)	500 (440)[a]
22	181 (-134)	306 (91)	172 (-149)	307 (93)	295 (72)	390 (243)	118 (-247)	274 (34)	174 (-146)	299 (79)	292 (67)	445 (341)
23	171 (-151)	335 (143)[a]	168 (-157)	342 (156)[a]	298 (77)	406 (272)	115 (-253)	329 (133)	169 (-156)	341 (155)	292 (66)	457 (364)
24	184 (-128)	297 (76)	174 (-147)	300 (81)[a]	295 (72)	380 (224)	121 (-242)	267 (22)[c]	176 (-142)	288 (59)	292 (67)	422 (300)[a]
Skin Plate												
25	191 (-115)	297 (76)	180 (-136)	296 (73)	294 (69)	359 (187)	128 (-229)	267 (22)[c]	182 (-132)	282 (49)	292 (67)	409 (248)
26	183 (-130)	295 (71)	175 (-144)	294 (70)	294 (70)	376 (217)	118 (-247)	267 (21)[c]	176 (-143)	287 (57)	292 (67)	415 (287)
27	184 (-129)	295 (72)	175 (-144)	295 (71)	294 (70)	377 (220)	120 (-244)	266 (20)[c]	176 (-143)	287 (57)	292 (67)	417 (291)
Flange												
28	184 (-128)	295 (72)	176 (-143)	294 (70)	294 (69)	372 (210)	121 (-241)	266 (19)[c]	177 (-140)	285 (53)	292 (67)	410 (278)
29	184 (-129)	294 (70)	175 (-144)	294 (69)	294 (69)	373 (212)	122 (-240)	266 (19)[c]	177 (-140)	285 (54)	292 (67)	411 (280)
30	204 (-121)	295 (72)	177 (-140)	294 (69)	294 (69)	359 (186)	122 (-240)	266 (20)[c]	179 (-137)	282 (48)	292 (67)	393 (248)
Case												
31	184 (-128)	294 (70)	175 (-144)	294 (69)	294 (69)	369 (205)	121 (-242)	265 (18)[c]	177 (-140)	284 (51)	292 (67)	422 (271)
32	184 (-128)	293 (69)	176 (-143)	293 (68)	293 (68)	366 (200)	121 (-242)	265 (18)[c]	177 (-140)	283 (50)	292 (67)	402 (265)
33	184 (-128)	293 (68)	176 (-143)	292 (67)	294 (69)	366 (200)	122 (-240)	265 (18)[c]	178 (-139)	283 (50)	292 (67)	403 (266)
34	185 (-127)	293 (68)	176 (-143)	292 (67)	294 (69)	365 (197)	125 (-235)	265 (18)[c]	178 (-139)	282 (49)	292 (67)	400 (261)
35	185 (-127)	293 (68)	176 (-143)	292 (67)	293 (68)	364 (196)	121 (-241)	265 (18)[c]	178 (-139)	283 (50)	292 (67)	400 (261)
36	185 (-126)	293 (68)	176 (-142)	292 (67)	293 (68)	362 (193)	122 (-239)	265 (17)[c]	178 (-139)	282 (49)	292 (67)	397 (256)
Control Sample												
37	173 (-148)	327 (129)	169 (-156)	324 (124)	295 (71)	409 (277)	110 (-261)	297 (76)	167 (-158)	326 (127)	292 (67)	450 (350)

TABLE XIV
THERMAL TEST RESULTS – SA S-BAND ANTENNA (PANEL C)

T/C No.	TEST NUMBER											
	OTS-C1		OTS-C2		OTS-C3		OTS-C4		OTS-C5		OTS-C6	
	T_o [b] K (°F)	T_{max} K (°F)	T_o [b] K (°F)	T_{max} K (°F)	T_o K (°F)	T_{max} K (°F)	T_o [b] K (°F)	T_{max} K (°F)	T_o [b] K (°F)	T_{max} K (°F)	T_o K (°F)	T_{max} K (°F)
Front Surface												
1	131 (-133)	320 (116)	176 (-142)	319 (114)	294 (70)	385 (234)	125 (-235)	277 (39)	176 (-143)	302 (84)	292 (66)	433 (320)
2	131 (-133)	321 (118)	177 (-141)	318 (113)	294 (69)	385 (234)	125 (-235)	277 (39)	176 (-143)	302 (84)	292 (66)	429 (312)
3	132 (-131)	317 (111)	177 (-140)	317 (111)	293 (68)	382 (228)	126 (-232)	278 (38)	177 (-141)	300 (81)	291 (64)	426 (307)
Skin Plate												
4	132 (-132)	317 (111)	176 (-142)	317 (111)	292 (66)	381 (227)	125 (-235)	276 (37)	176 (-143)	300 (81)	291 (64)	424 (304)
5	133 (-130)	315 (108)	178 (-139)	316 (109)	292 (66)	379 (222)	127 (-231)	275 (35)	177 (-140)	299 (79)	291 (64)	420 (296)
Flange												
6	132 (-131)	316 (110)	177 (-140)	316 (110)	292 (66)	380 (225)	125 (-235)	275 (36)	176 (-142)	300 (80)	291 (64)	422 (301)
7	(d)	316 (109)	178 (-139)	316 (110)	292 (66)	380 (224)	126 (-233)	(d)	177 (-140)	300 (80)	291 (64)	422 (300)
Case												
8	133 (-130)	315 (108)	177 (-140)	316 (110)	292 (66)	380 (224)	126 (-233)	275 (36)	177 (-141)	299 (79)	290 (63)	421 (299)
9	133 (-130)	315 (108)	177 (-140)	316 (110)	292 (66)	380 (224)	127 (-231)	275 (36)	177 (-140)	299 (79)	291 (64)	422 (300)
10	133 (-130)	315 (108)	177 (-140)	316 (110)	291 (65)	380 (224)	126 (-232)	275 (36)	177 (-141)	300 (80)	291 (64)	422 (300)
Control Sample												
37	171 (-152)	331 (137)	168 (-158)	326 (127)	293 (68)	404 (268)	113 (-256)	294 (69)	169 (-156)	327 (129)	292 (66)	450 (350)

TABLE XV
THERMAL TEST RESULTS – AEL S-BAND ANTENNA (PANEL C)

T/C No.	TEST NUMBER											
	OTS-C1		OTS-C2		OTS-C3		OTS-C4		OTS-C5		OTS-C6	
	T_o[b] K (°F)	T_{max} K (°F)	T_o[b] K (°F)	T_{max} K (°F)	T_c K (°F)	T_{max} K (°F)	T_o[b] K (°F)	T_{max} K (°F)	T_o[b] K (°F)	T_{max} K (°F)	T_o K (°F)	T_{max} K (°F)
Front Surface												
27	169 (-155)	317 (111)[a]	167 (-159)	306 (91)[a]	295 (72)	399 (259)	110 (-261)	284 (52)	168 (-157)	328 (131)	292 (66)	445 (342)
28	167 (-158)	328 (131)[a]	167 (-160)	320 (116)[a]	298 (77)	415 (287)	100 (-279)[a]	330 (135)[a]	167 (-159)	357 (183)	292 (67)	462 (373)
29	171 (-151)	302 (82)	169 (-156)	291 (64)	292 (67)	378 (221)	113 (-256)	267 (22)[c]	171 (-152)	285 (53)	292 (67)	418 (293)
Skin Plate												
30	171 (-151)	302 (84)	169 (-156)	292 (66)	292 (67)	381 (227)	113 (-256)	267 (22)[c]	171 (-152)	286 (55)	291 (65)	421 (299)
31	175 (-145)	301 (83)	171 (-151)	296 (74)	292 (67)	379 (222)	119 (-245)	269 (25)[c]	174 (-147)	287 (57)	291 (65)	417 (291)
Flange												
32	171 (-151)	300 (81)	169 (-156)	291 (64)	292 (67)	377 (220)	113 (-256)	267 (21)[c]	170 (-153)	285 (54)	291 (65)	416 (290)
33	171 (-151)	299 (78)	169 (-155)	290 (63)	292 (67)	374 (214)	113 (-256)	267 (21)[c]	170 (-153)	284 (51)	291 (64)	412 (282)
Case												
34	171 (-151)	300 (80)	169 (-156)	291 (64)	292 (66)	376 (218)	113 (-256)	267 (21)[c]	170 (-153)	285 (53)	291 (64)	415 (287)
35	171 (-151)	299 (79)	169 (-156)	290 (63)	292 (67)	375 (216)	113 (-256)	267 (21)[c]	170 (-153)	284 (52)	291 (64)	413 (284)
36	170 (-152)	299 (79)	169 (-156)	290 (63)	292 (66)	375 (216)	114 (-255)	267 (21)[c]	170 (-153)	284 (52)	291 (64)	413 (284)
Control Sample												
37	171 (-152)	331 (137)	168 (-158)	326 (127)	293 (68)	404 (268)	113 (-256)	294 (69)	169 (-156)	327 (129)	292 (66)	450 (350)

TABLE XVI
THERMAL TEST RESULTS – TRANSCO C-BAND ANTENNA
(PANEL C)

T/C No.	TEST NUMBER											
	OTS-01		OTS-02		OTS-03		OTS-04		OTS-05		OTS-06	
	T_o[b] K (°F)	T_{max} K (°F)	T_o[b] K (°F)	T_{max} K (°F)	T_o K (°F)	T_{max} K (°F)	T_o[b] K (°F)	T_{max} K (°F)	T_o[b] K (°F)	T_{max} K (°F)	T_o K (°F)	T_{max} K (°F)
Front Surface												
11	169 (-156)	334 (141)[a]	166 (-160)	331 (137)[a]	295 (72)	425 (305)[a]	111 (-260)	308 (95)	166 (-161)	365 (198)	292 (67)	476 (397)
12	169 (-155)	332 (138)[a]	167 (-158)	333 (140)[a]	295 (72)	423 (302)[a]	112 (-257)	301 (82)	168 (-157)	362 (193)	292 (67)	475 (396)
13	174 (-146)	307 (93)	170 (-153)	300 (80)	294 (69)	390 (243)	117 (-249)	266 (19)	173 (-148)	294 (69)	292 (66)	431 (316)
14	170 (-154)	326 (127)[a]	167 (-158)	323 (122)[a]	295 (72)	418 (293)[a]	114 (-255)	296 (73)	169 (-156)	355 (180)	292 (67)	469 (384)
15	174 (-146)	306 (91)	170 (-153)	299 (79)	295 (71)	390 (243)	117 (-248)	268 (23)	173 (-148)	294 (69)	292 (67)	436 (325)
16	174 (-146)	317 (111)	170 (-154)	302 (84)	296 (73)	396 (254)	116 (-250)	272 (31)	172 (-150)	315 (108)	294 (69)	450 (351)
17	175 (-145)	305 (90)	170 (-153)	299 (78)	294 (69)	386 (235)	118 (-247)	266 (20)	174 (-147)	292 (66)	293 (68)	429 (312)
Skin Plate												
18	175 (-145)	305 (90)	171 (-152)	299 (79)	292 (67)	387 (237)	118 (-247)	269 (24)[c]	173 (-148)	292 (66)	292 (66)	429 (312)
19	171 (-151)	297 (76)	169 (-156)	290 (62)	292 (67)	374 (213)	115 (-253)	267 (22)[c]	170 (-153)	282 (49)	291 (65)	410 (278)
Flange												
20	174 (-146)	304 (88)	170 (-153)	299 (78)	292 (67)	385 (234)	117 (-248)	269 (24)[c]	173 (-148)	291 (64)	291 (65)	426 (308)
21	175 (-145)	303 (86)	170 (-153)	299 (78)	292 (67)	385 (233)	119 (-246)	269 (24)[c]	173 (-148)	290 (63)	291 (65)	425 (306)
Case												
22	175 (-145)	302 (85)	171 (-152)	297 (76)	292 (67)	382 (229)	118 (-247)	269 (24)[c]	173 (-148)	290 (62)	291 (65)	423 (302)
23	175 (-145)	303 (86)	171 (-152)	298 (77)	292 (67)	384 (231)	118 (-247)	269 (24)[c]	173 (-148)	290 (63)	291 (65)	425 (306)
24	175 (-145)	303 (86)	171 (-152)	298 (77)	292 (67)	384 (231)	119 (-246)	268 (23)[c]	173 (-148)	290 (63)	291 (65)	424 (304)
25	175 (-145)	302 (85)	171 (-152)	297 (76)	292 (67)	382 (228)	119 (-246)	269 (24)[c]	173 (-148)	290 (62)	291 (64)	423 (302)
26	175 (-145)	302 (84)	171 (-152)	297 (76)	292 (67)	381 (227)	119 (-246)	269 (24)[c]	173 (-148)	289 (61)	291 (65)	421 (299)
Control Sample												
37	171 (-152)	331 (137)	168 (-158)	326 (127)	293 (68)	404 (268)	113 (-256)	294 (69)	169 (-156)	327 (129)	292 (65)	450 (350)

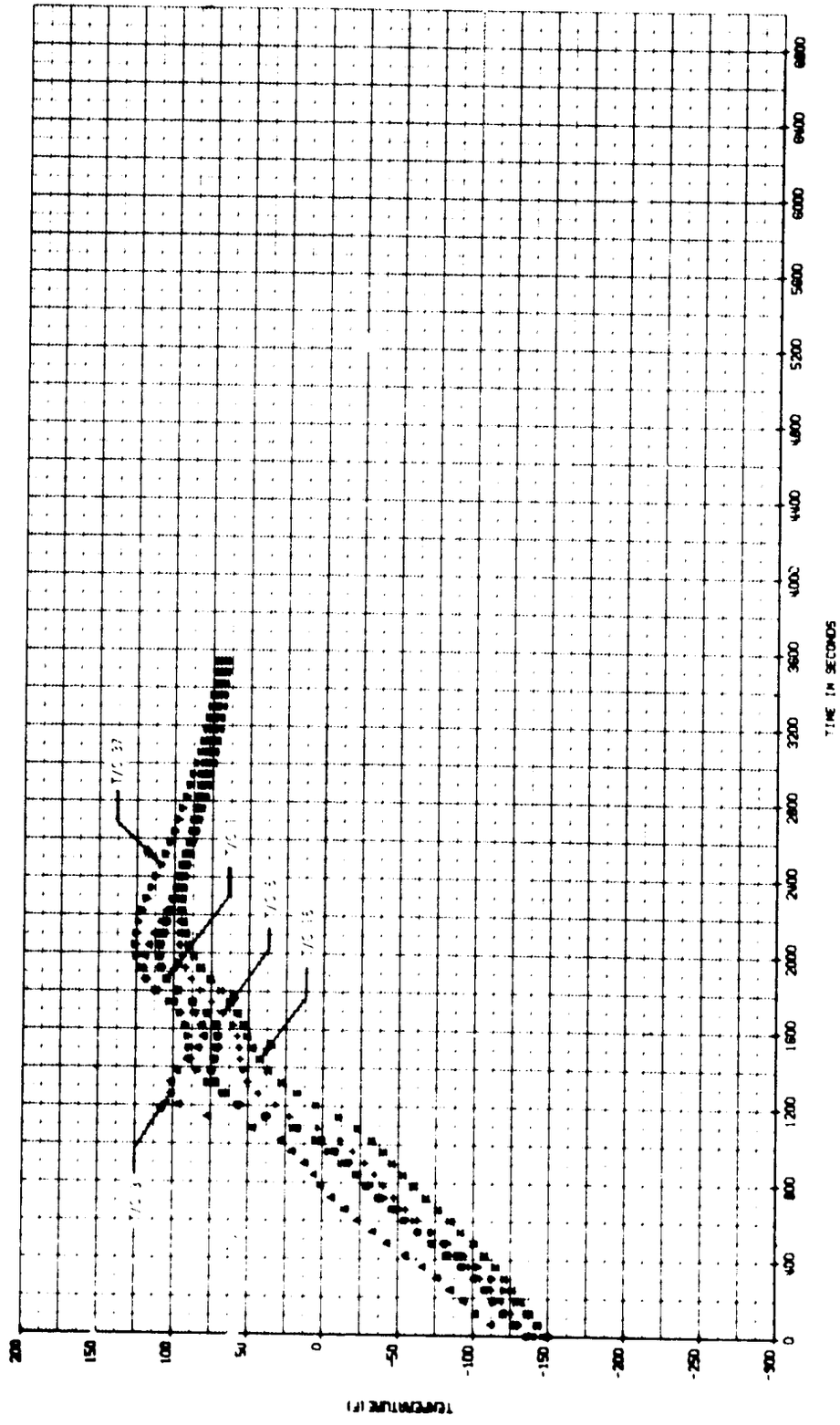

FIGURE 91 TEMPERATURE HISTORIES - TRANSCO L-BAND ANTENNA (TEST OTS-A2)

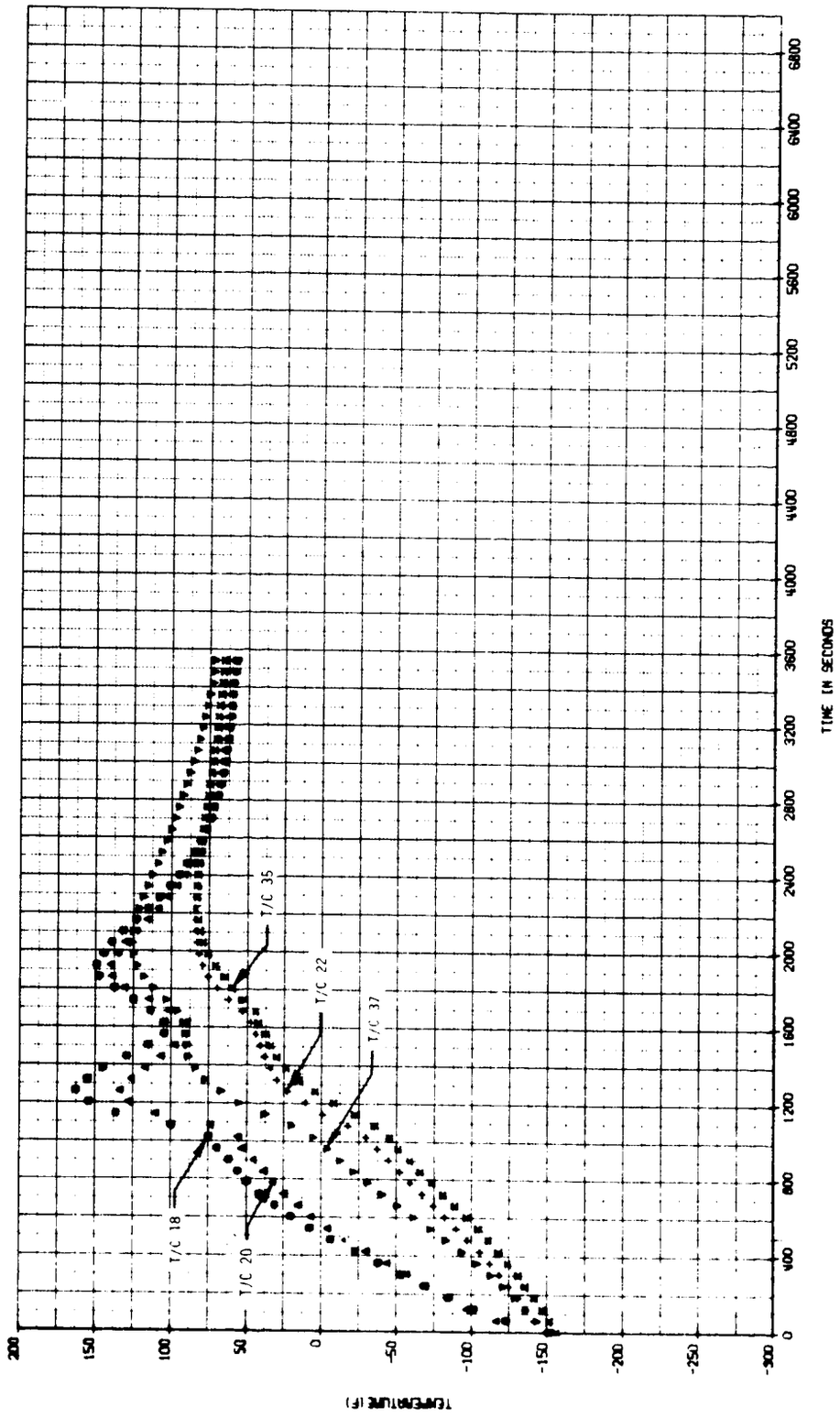

FIGURE 92 TEMPERATURE HISTORIES – RANTEC C-BAND ANTENNA (TEST OTS-A2)

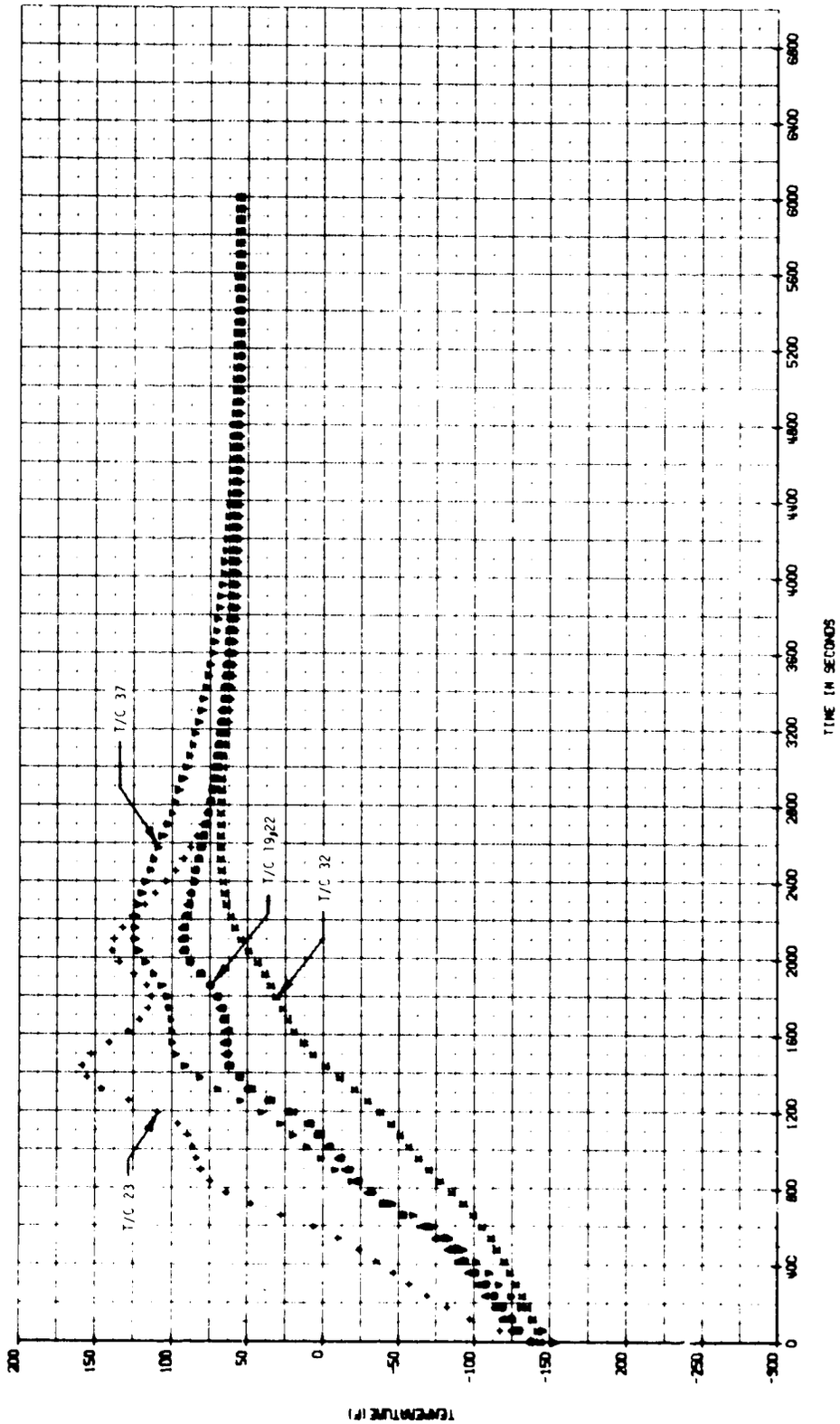

FIGURE 93 TEMPERATURE HISTORIES – D&M L-BAND ANTENNA (TEST OTS-B2)

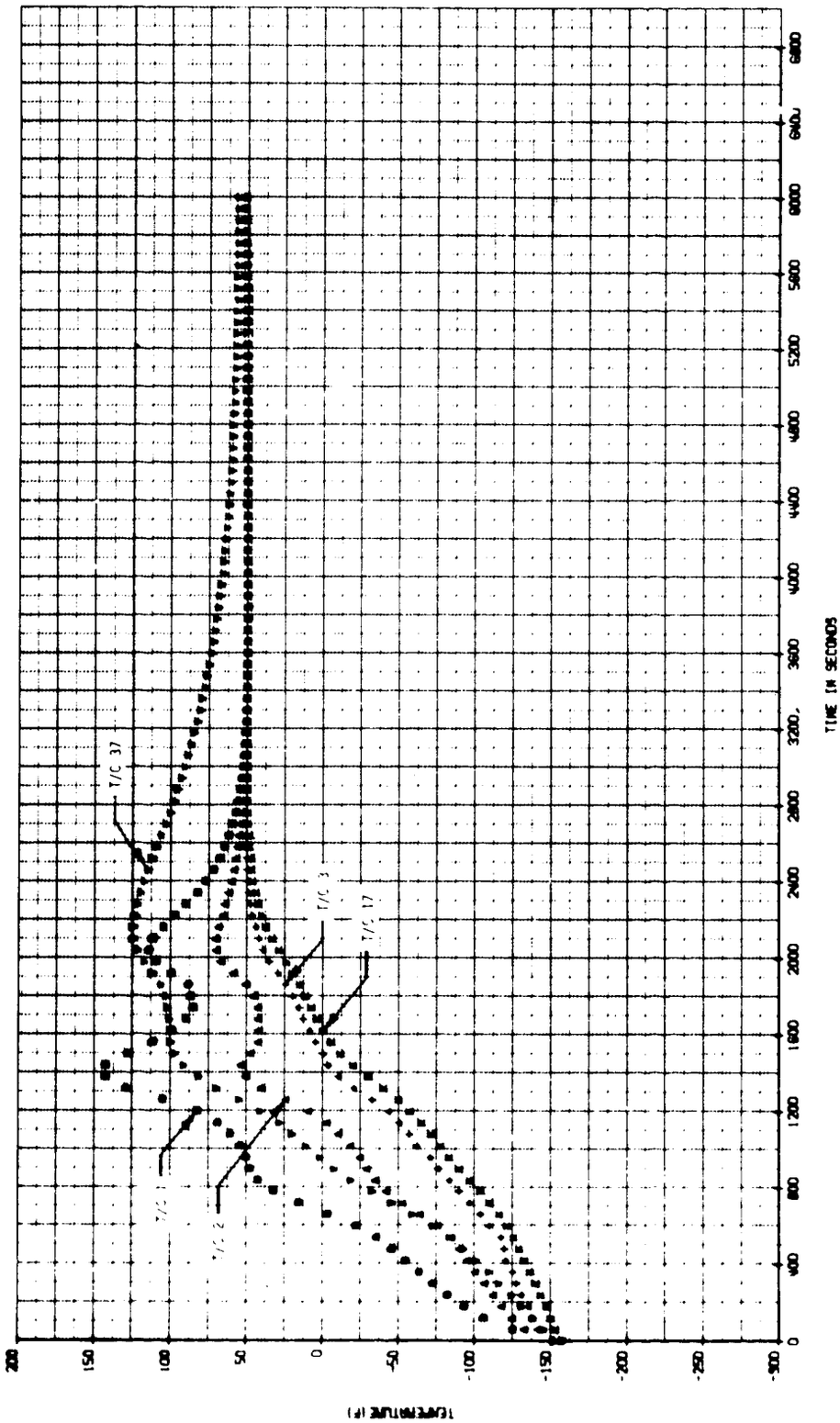

FIGURE 94 TEMPERATURE HISTORIES – D&M C-BAND ANTENNA (TEST OTS-B2)

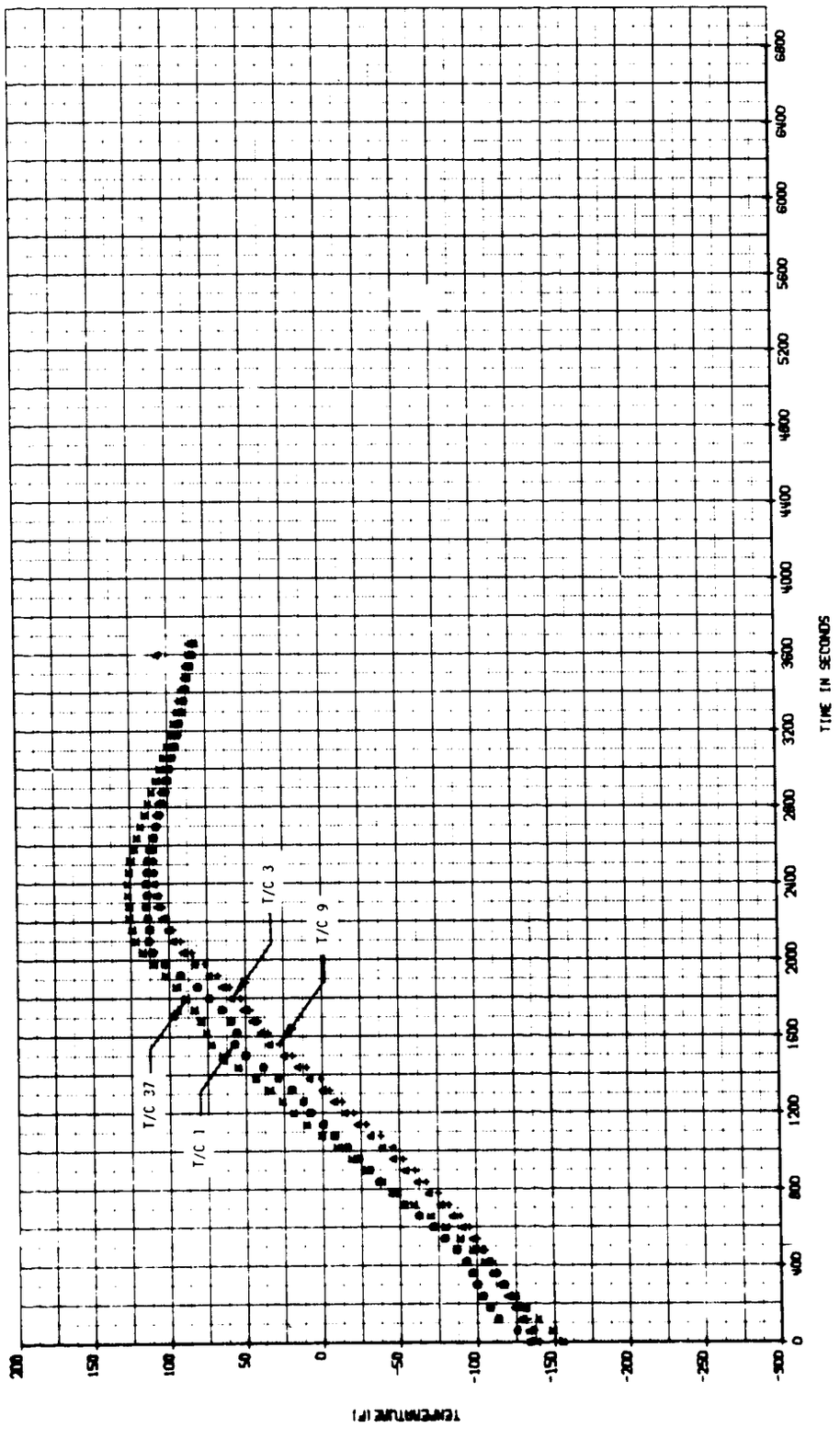

FIGURE 95 TEMPERATURE HISTORIES – SA S-BAND ANTENNA (TEST OTS-C2)

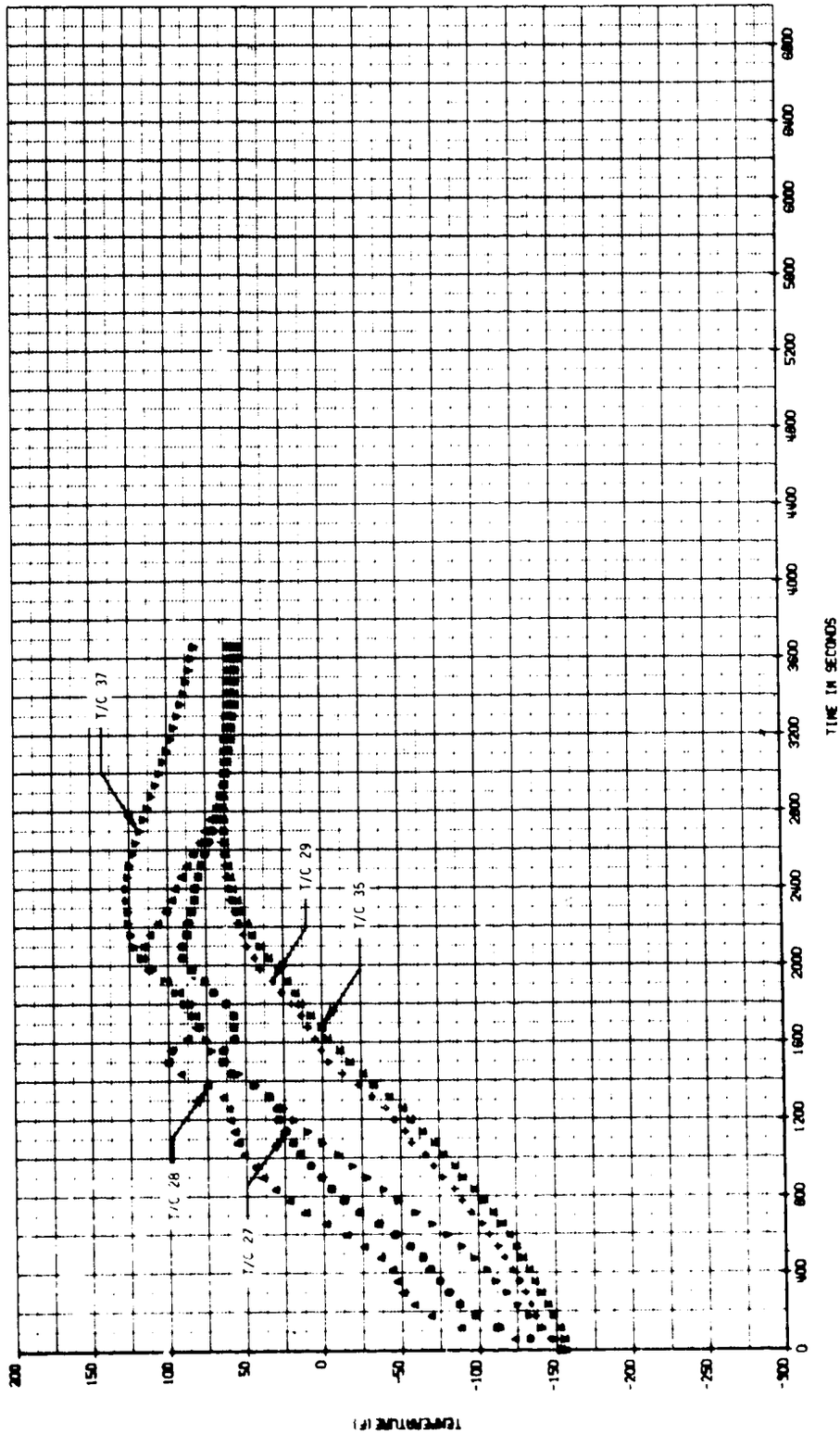

FIGURE 96 TEMPERATURE HISTORIES – AEL S-BAND ANTENNA (TEST OTS-C2)

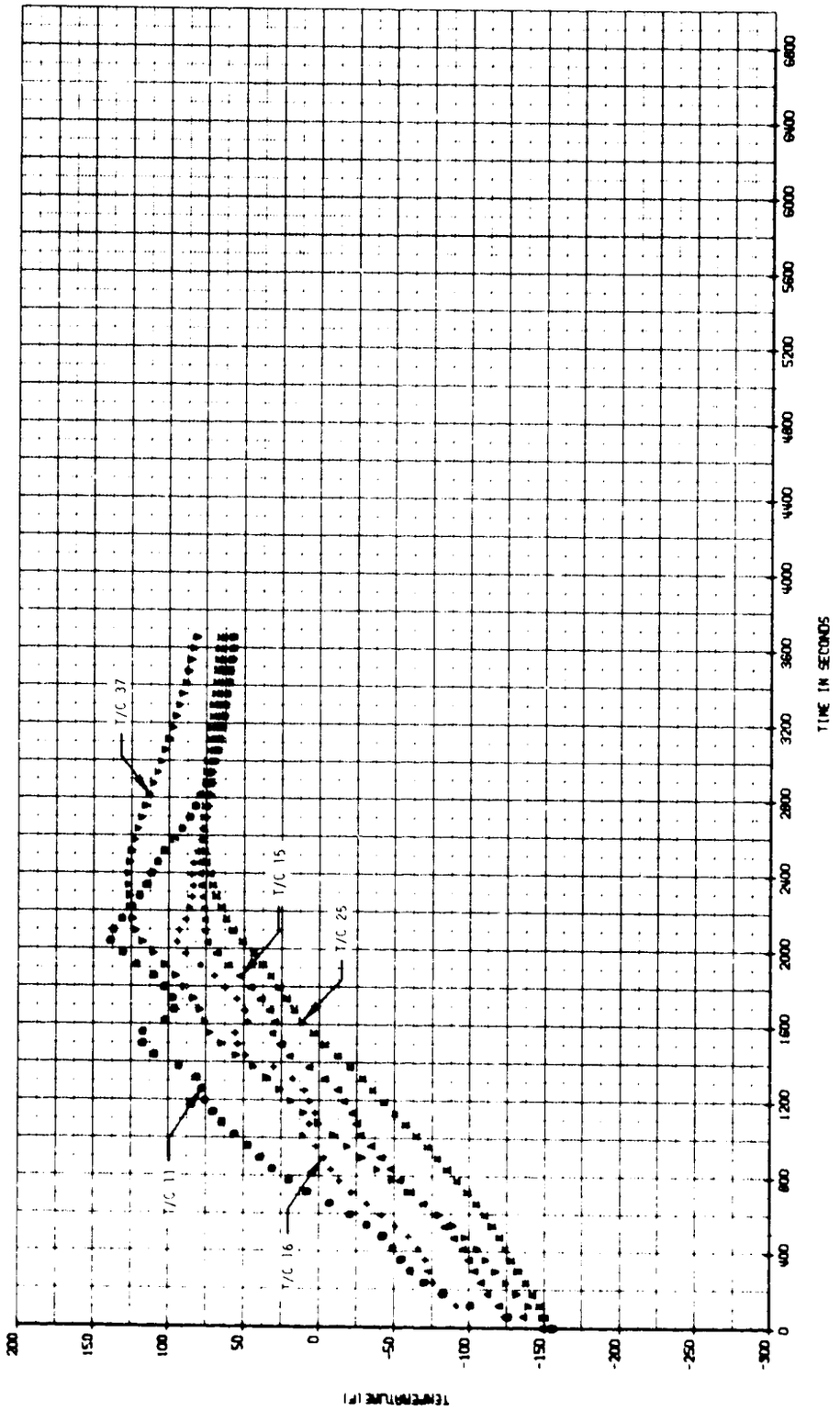

FIGURE 97 TEMPERATURE HISTORIES – TRANSCO C-BAND ANTENNA (TEST OTS-C2)

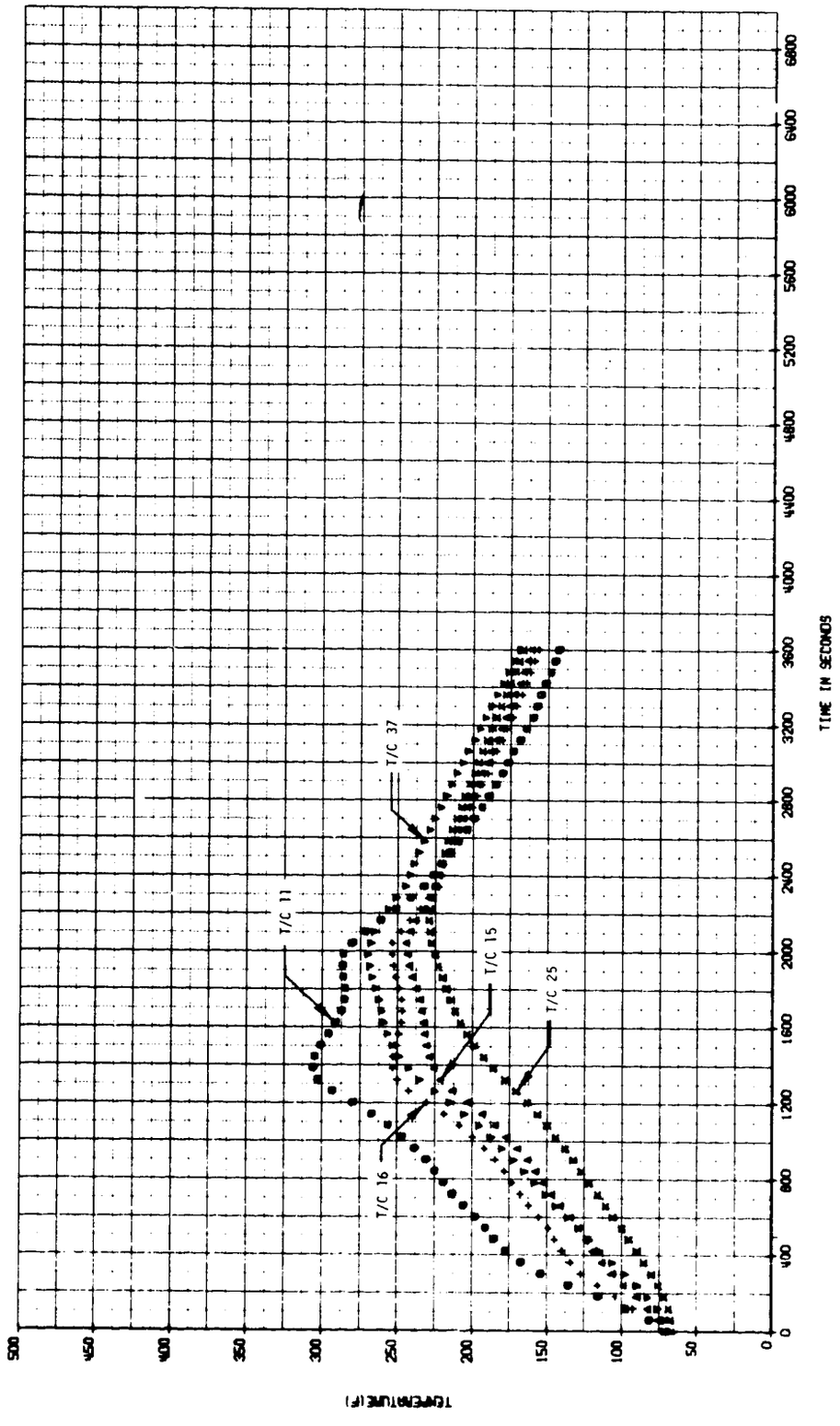

FIGURE 98 TEMPERATURE HISTORIES FOR TRANSCO C-BAND ANTENNA – TEST OTS-C3

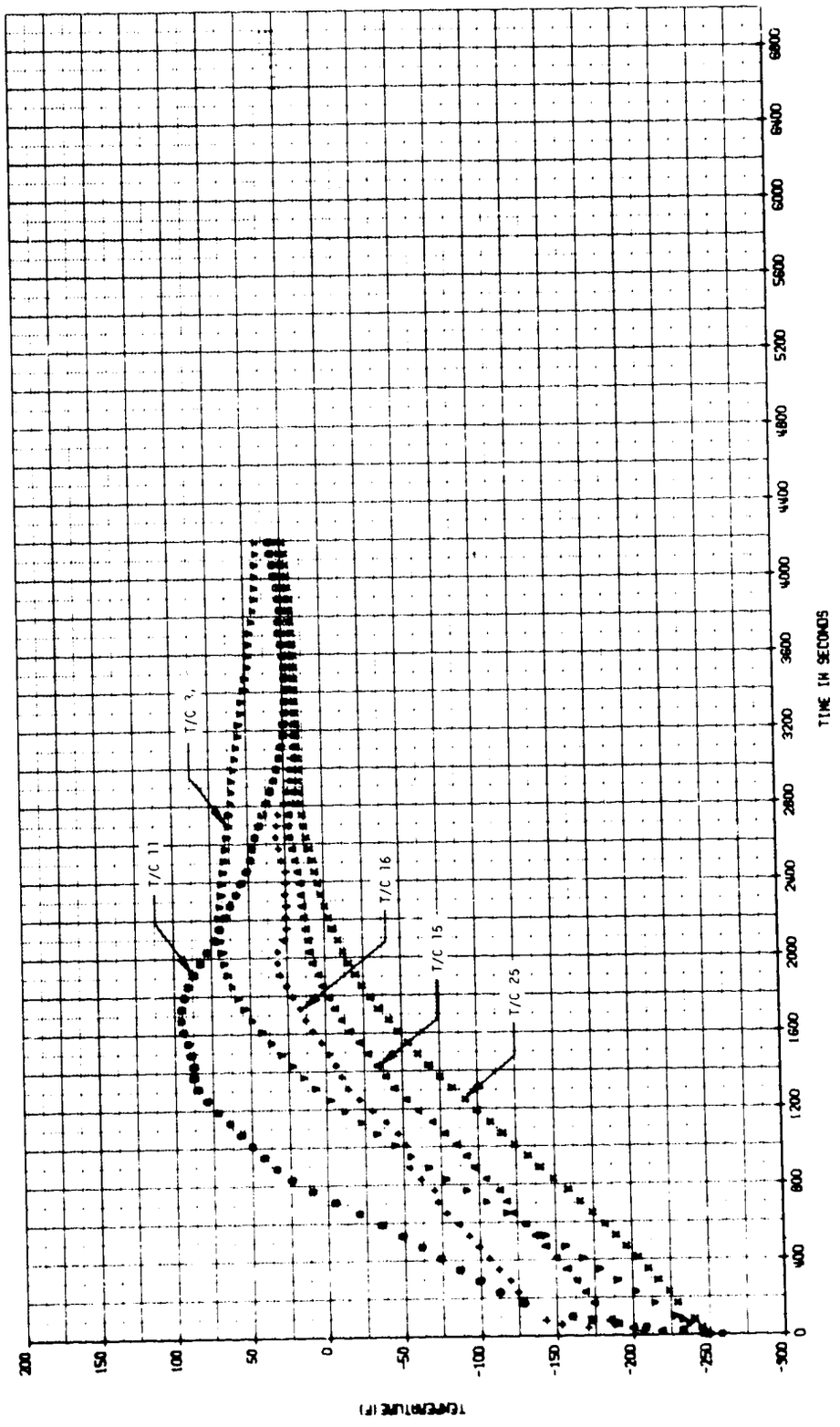

FIGURE 99 TEMPERATURE HISTORIES FOR TRANSCO C-BAND ANTENNA – TEST OTS-C4

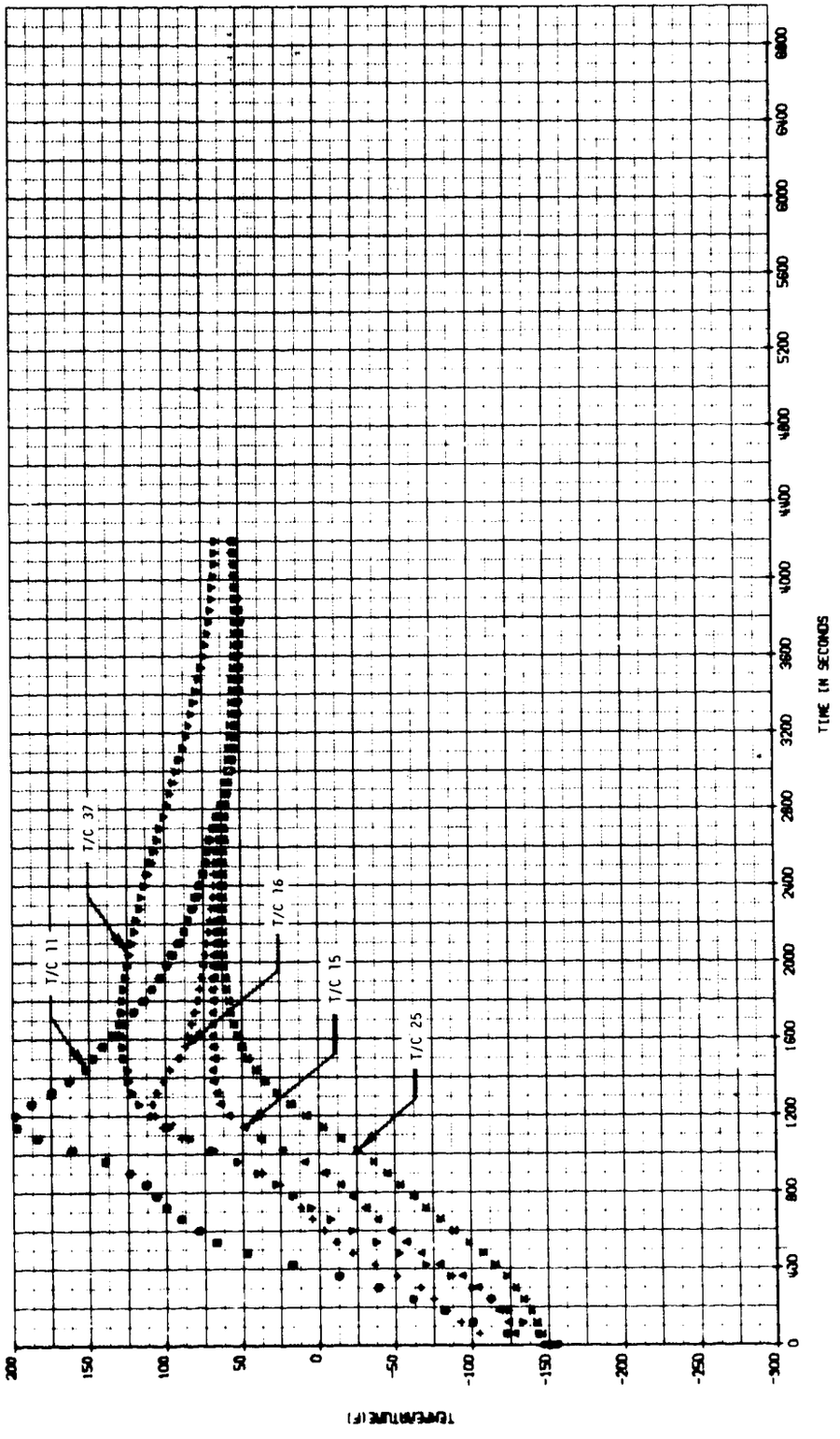

FIGURE 100 TEMPERATURE HISTORIES FOR TRANSCO C-BAND ANTENNA – TEST OTS-C5

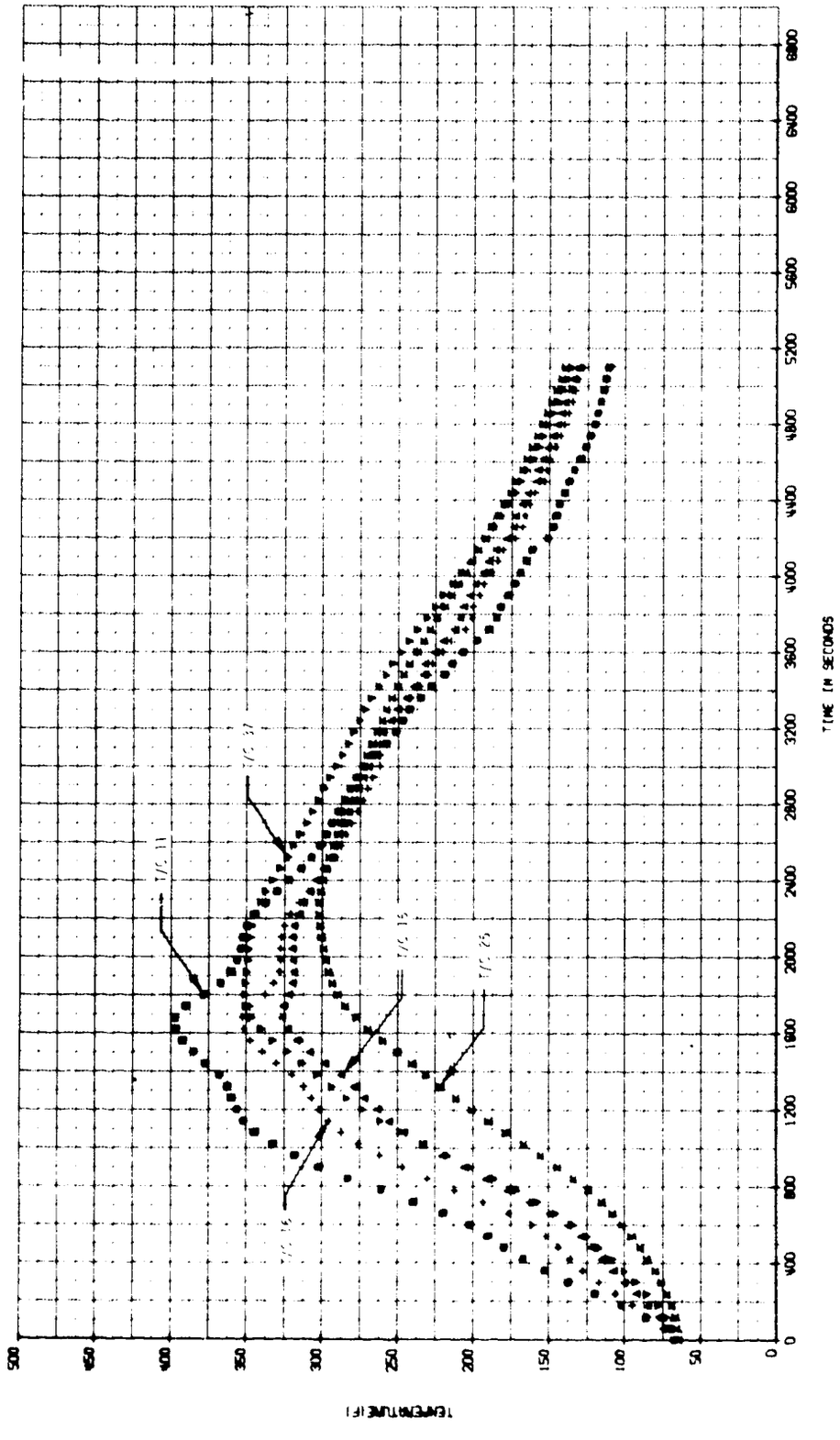

FIGURE 101 TEMPERATURE HISTORIES FOR TRANSCO C-BAND ANTENNA – TEST OTS-C6

EVALUATION

The objective of this task (Task 2.2) was to evaluate the results of the electrical and thermal tests to determine the degree of success or failure.

Electrical Test Data Evaluation

This section gives an evaluation of the electrical test results described in the selections on S-BAND ANTENNA SYSTEM TESTS and OFF-THE-SHELF ANTENNA TESTS under Electrical Testing. Comparisons are made to show changes resulting from the orbital cold and entry heating environments.

S-band antenna system. - The electrical test measurement results for Prototype No. 2 (figures 10 and 11) illustrate the deleterious effects on performance that can be caused by physical or chemical changes within the system. The carbonaceous deposit on the HRSI tile surfaces after test P2-1 caused a severe reduction in antenna gain, significant increases in axial ratio, and significant changes in input impedance. These effects occur over the antenna operating frequency range and are attributed to the losses of the carbonaceous deposit, since additional measurements showed that the S-band antenna was unaffected. It is very probable that similar effects would occur in systems which utilize the VHF, L-band, and Ku-band antennas rendering them unusable. A second test (P2-2) was run to determine if the deposit would burn off. The results of test P2-2 (figure 12) show the electrical performance was not improved, although the color of the deposit appeared somewhat lighter. Because of the degraded electrical performance of Prototype No. 2, Prototype No. 1 was used for the S-band antenna system tests as discussed in the section on S-BAND ANTENNA SYSTEM TESTS.

A summary of test results (figures 13 through 24) for Prototype No. 1 is presented in tables XVII, XVIII and XIX. The maximum difference in gain at $\theta = 0°$ and axial ratio between any two tests was 1.6 dB and 1.2 dB respectively. The input impedance showed almost no change throughout the tests. Since the electrical tests were performed at one or two day intervals, the measurement accuracy for the radiation measurements is about ± 0.75 dB. Therefore, since there is scatter in the results of the gain and axial ratio measurements and scatter is within the measurement accuracy in most cases, it does not appear that the Orbiter entry environment has a permanent effect on S-band antenna system electrical performance.

Off-the-shelf antennas. - The OTS antennas were tested in two phases. The first to determine the effects of a typical antenna window and TPS configuration, and the second to determine the effect of an orbital coldsoak environment followed by simulated entry heating. The results of these tests confirmed that the OTS antenna can perform adequately in the Orbiter TPS environment and can withstand the thermal environment within the high temperature design limits.

TABLE XVII
CIRCULAR GAIN – PROTOTYPE NO. 1

FREQ. (GHZ)	TEST	θ = 0°	θ = 60°			
			φ = 0°	φ = 90°	φ = 180°	φ = 270°
2.1	REF.	5.8	0.0	5.2	0.0	-0.6
	P1-11	5.4	0.0	5.0	1.0	-1.1
	P1-12	6.7	0.2	5.0	2.2	2.1
	P1-14	5.9	0.1	5.8	1.6	-0.2
	P1-15	5.1	-0.2	4.6	1.0	-0.4
2.2	REF.	7.2	3.2	4.0	2.0	3.4
	P1-11	7.0	2.3	4.4	2.0	3.7
	P1-12	6.0	1.6	3.0	0.8	1.9
	P1-14	5.9	1.2	3.2	1.2	2.4
	P1-15	6.1	2.0	3.8	1.2	2.9
2.2875	REF.	8.0	4.0	4.1	3.0	2.5
	P1-11	8.0	3.2	4.1	3.2	3.0
	P1-12	7.8	3.6	3.8	2.3	2.4
	P1-14	8.8	5.0	5.0	4.1	3.8
	P1-15	8.6	4.8	4.6	4.0	3.8

NOTES: GAIN REFERENCED TO LINEAR ISOTROPIC

Simulated antenna window and TPS effects: The effects of the simulated antenna windows and TPS on the OTS antennas were in general relatively minor. The evaluation of specific effects is as follows:

(a) L-band antennas – The electrical performance of the L-band antennas covered with a simulated antenna window and TPS was generally satisfactory. The radiation patterns of both the Transco and D&M antennas showed an approximate 1.0 dB decrease in peak gain at all three test frequencies. The patterns of the Transco antenna (figure 53) show an increase in gain at θ = 90° of about 1.0 dB at all three test frequencies while the D&M antenna (figure 54) showed no increase except at 1220 MHz, where it was 2.0 dB. The effects of the antenna window and TPS on input impedance of the two antennas were somewhat different. The VSWR of the D&M (figure 56) generally increased from an average of 2.7:1 but remained within 3:1 as specified by D&M. The VSWR of the Transco antenna (figure 55) increased to about 2:1 at 1090 MHz and 2.6:1 at 1220 MHz. These results are consistent with the findings of a previous antenna window/TPS study (ref. 2) for NASA-LaRC.

TABLE XVIII
AXIAL RATIO – PROTOTYPE NO. 1

FREQ. (GHZ)	TEST	θ = 0°	θ = 60°			
			φ = 0°	φ = 90°	φ = 180°	φ = 270°
2.1	REF.	5.0	1.6	8.0	21.6	0.7
	P1-11	5.0	2.5	9.4	18.0	2.6
	P1-12	6.2	1.7	9.5	13.0	6.0
	P1-14	5.3	2.0	7.5	12.8	6.0
	P1-15	5.1	1.0	7.5	16.4	3.6
2.2	REF.	2.5	6.8	6.0	8.5	4.0
	P1-11	2.0	7.0	5.0	6.8	2.2
	P1-12	2.2	4.5	4.2	7.0	3.0
	P1-14	2.7	3.6	4.5	4.5	2.0
	P1-15	2.5	4.0	4.0	4.8	2.8
2.2875	REF.	3.0	6.0	12.5	6.0	9.0
	P1-11	3.0	8.0	13.0	4.0	8.5
	P1-12	2.8	6.0	10.0	5.0	8.2
	P1-14	2.8	5.7	10.0	4.0	7.6
	P1-15	2.7	5.5	9.0	3.6	9.0

TABLE XIX
VSWR – PROTOTYPE NO. 1

FREQ. (GHZ)	REF.	P1-11	P2-12	P1-14	P1-15
2.1	1.06	1.08	1.10	1.10	1.15
2.2	1.32	1.34	1.32	1.30	1.22
2.3	1.22	1.28	1.26	1.27	1.22

(b) S-band antennas - The electrical performance of the S-band antennas was least affected by the antenna window and TPS. The patterns (figures 57 and 58) show no significant change in gain. The pattern shape is well preserved and the axial ratio increased only slightly over a 100 to 120° beamwidth. There is some evidence of surface waves in the patterns, but the effect is minor. The input impedance (figures 50 and 60) was virtually unaffected.

(c) C-band antennas - The electrical performance of the C-band horn antennas was generally satisfactory as shown by figures 61, 62 and 63. The peak gain ($\theta = 0°$) decreased by 0.5 to 1.0 dB. The H-plane patterns were virtually unchanged. The E-plane patterns developed -15 dB sidelobes at $\theta = 90°$ which are attributed to the excitation of surface waves on the TPS. These sidelobes can be eliminated by the addition of a window edge enclosure of the proper diameter expending into the TPS (ref. 2). However, that approach complicates the installation considerably and should be weighed against the system effects of the sidelobes.

The input impedance (figures 64, 65 and 66) showed some spreading and translation. However, the VSWR at the center frequency remained acceptable for all three antennas. It appears that the impedance of the respective antenna can be optimized by minor tuning with the antenna aperture covered with the appropriate window configuration.

Thermal environment effects: The results of the radiation pattern measurements for the L-band, C-band, and S-band antennas are shown in tables XX through XXVI. These tables show the change in gain relative to the previous test, and the changes relative to the reference data. In all cases, changes greater than 1.0 dB occurred during the first two runs in which the antenna was cold soaked at 172 K (-150°F). The reason for this is not clear since there were no signs of physical change to these antennas. Possible explanations include outgasing characteristics of the antenna covers and/or foam filler, and surface moisture attracted after the test due to vacuum conditions during the thermal test. The results of the S-band antenna tests were unique in that no significant changes were observed as shown by tables XXV and XXVI.

Thermal Test Data Evaluation

The evaluation of the thermal test data was made to determine the effect of cold soaking followed by a simulated orbiter entry heating pulse on the S-band antenna system and the OTS antenna. The S-band antenna system thermal data from these tests were compared with the arc tunnel data of reference 1 to correlate and evaluate the radiant and plasma heating test techniques.

S-band antenna system. - The S-band antenna system showed no significant change in thermal performance during the tests. These tests confirmed that, as predicted, the maximum temperature reached in the skin and antenna after a cold soak is much lower than the design maximum temperature of 422 K (300°F). In fact, for the 117 K (-250°F) initial temperature, the skin and antenna temperatures at the time corresponding to orbiter landing are about 255 K (0°F)

TABLE XX
TRANSCO L-BAND ANTENNA GAIN AND VSWR COMPARISONS

FREQ (MHz)	THERMAL TEST					
	1	2	3	4	5	6
CHANGE FROM PREVIOUS PEAK GAIN (dB)						
960	NC	-0.5	NC	NC	NC	0.5
1090	-2.0	-1.0	NC	NC	NC	NC
1220	NC	-0.5	-1.0	0.5	1.0	0.8
CHANGE FROM REFERENCE PEAK GAIN (dB)						
960	NC	-0.5	-0.5	-0.5	-0.5	NC
1090	-2.0	-3.0	-3.0	-3.0	-3.0	-3.0
1220	NC	-0.5	-1.5	-1.0	NC	0.8
VSWR						
	REF	1	2	3	4	5	6
900	2.35	2.80	2.80	2.00	2.25	2.25	2.05
1090	1.32	1.30	1.34	1.30	1.26	1.38	1.38
1300	2.60	2.40	2.60	2.80	2.64	2.52	1.72

NOTES: NC = NO CHANGE

TABLE XXI
D&M L-BAND ANTENNA GAIN AND VSWR COMPARISONS

FREQ. (MHz)	THERMAL TEST					
	1	2	3	4	5	6
CHANGE FROM PREVIOUS PEAK GAIN (dB)						
960	-1.5	0.5	NC	-0.5	NC	NC
1090	-1.5	NC	NC	NC	NC	NC
1220	-1.5	1.0	NC	-0.5	NC	1.8
CHANGE FROM REFERENCE PEAK GAIN (dB)						
960	-1.5	-1.0	-1.0	-1.5	-1.5	-1.5
1090	-1.5	-1.5	-1.5	-1.5	-1.5	-1.5
1220	-1.5	-0.5	-0.5	-1.0	-1.0	0.8
VSWR						
	REF	1	2	3	4	5	6
900 TO 1300	<2.8	<2.8	<2.8	<2.7	<2.8	<2.9	<2.8

NOTES: NC = NO CHANGE

TABLE XXII
D&M C-BAND ANTENNA GAIN AND VSWR COMPARISONS

FREQ. (GHz)	THERMAL TEST					
	1	2	3	4	5	6
CHANGE FROM PREVIOUS PEAK GAIN (dB)						
4.25	1.5	NC	-1.0	-0.5	1.0	NC
4.30	1.5	1.0	-1.5	NC	1.0	0.5
4.35	1.5	NC	NC	NC	0.5	NC
CHANGE FROM REFERENCE PEAK GAIN (dB)						
4.25	1.5	1.5	0.5	NC	1.0	1.0
4.30	1.5	2.5	1.0	1.0	2.0	2.5
4.35	1.5	1.5	1.5	1.5	2.0	2.0
VSWR						
	REF	1	2	3	4	5	6
4.2	1.38	1.60	1.62	1.58	1.22	1.38	1.41
4.3	1.26	1.30	1.20	1.19	1.28	1.22	1.22
4.4	1.18	1.28	1.25	1.29	1.10	1.28	1.28

NOTES: NC = NO CHANGE

TABLE XXIII
RANTEC C-BAND ANTENNA GAIN AND VSWR COMPARISONS

FREQ. (GHz)	THERMAL TEST					
	1	2	3	4	5	6
CHANGE FROM PREVIOUS PEAK GAIN (dB)						
4.25	1.0	-0.5	NC	-1.0	1.0	1.0
4.30	-2.0	2.0	NC	NC	0.5	NC
4.35	-1.5	1.8	NC	-0.5	1.0	NC
CHANGE FROM REFERENCE PEAK GAIN (dB)						
4.25	1.0	0.5	0.5	-0.5	0.5	1.5
4.30	-2.0	NC	NC	NC	0.5	0.5
4.35	-1.5	0.3	0.3	-0.2	0.8	0.8
VSWR						
	REF	1	2	3	4	5	6
4.2	1.38	1.30	1.20	1.48	1.16	1.32	1.40
4.3	1.14	1.20	1.25	1.15	1.02	1.17	1.14
4.4	1.16	1.06	1.20	1.18	1.06	1.14	1.18

NOTES: NC = NO CHANGE

TABLE XXIV
TRANSCO C-BAND ANTENNA GAIN AND VSWR COMPARISONS

FREQ. (GHz)	THERMAL TEST					
	1	2	3	4	5	6
CHANGE FROM PREVIOUS PEAK GAIN (dB)						
4.25	NC	NC	NC	-1.0	+1.0	NC
4.30	1.0	-0.5	NC	-0.5	+1.0	NC
4.35	NC	NC	NC	-0.5	+1.0	NC
CHANGE FROM REFERENCE PEAK GAIN (dB)						
4.25	NC	NC	NC	-1.0	NC	NC
4.30	1.0	0.5	0.5	NC	1.0	1.0
4.35	NC	NC	NC	-0.5	0.5	0.5
VSWR						
	REF	1	2	3	4	5	6
4.2	1.48	1.58	1.56	1.48	1.49	1.56	1.45
4.3	1.18	1.28	1.20	1.22	1.18	1.14	1.14
4.4	1.38	1.45	1.48	1.45	1.29	1.38	1.38

NOTES: NC = NO CHANGE

and peaked at ambient temperature (294 K (70°F)) 20 or 30 minutes later. Other evaluations of the S-band antenna system data are made in the subsequent paragraphs.

Data repeatability: Tests P1-11 and P1-12 had the same initial temperature of 177 K (-140°F) and used the same simulated entry heating environment. Except for surface temperature of the LI-1500 tiles, all temperatures of test P1-12 were $\leq$ 22 K (40°F) lower than for test P1-11. The disparities in the results from these tests were first thought to be caused by possible dissimilarities in the respective thermal environments. However, surface temperature histories for these tests (figure 102) show the environments are identical for all practical purposes. It is more likely that backside temperature differences were caused by slight uncertainties and nonrepeatables inherent with the test setup. Also, these differences are less than 10% of the overall temperature rise and, therefore, are considered within the accuracy (or scatter) of the data.

Effect of test article installation: Between the breadboard and prototype testing, the test installation was modified to achieve a better thermal isolation between the antenna system and the test container assembly. The results of these modifications are shown in figure 50 which compares maximum tempera-

TABLE XXV
AEL S-BAND ANTENNA GAIN, AXIAL RATIO, AND VSWR COMPARISONS

FREQ. (GHz)	THERMAL TEST					
	1	2	3	4	5	6
CHANGE FROM PREVIOUS PEAK LINEAR GAIN (dB)						
2.0	NC	0.4	-0.4	-0.5	0.3	-0.6
3.0	NC	NC	0.5	-0.7	0.4	-0.4
4.0	NC	-0.5	-0.5	1.0	NC	NC
CHANGE FROM REFERENCE PEAK LINEAR GAIN (dB)						
2.0	NC	0.4	NC	-0.5	-0.2	-0.8
3.0	NC	NC	0.5	-0.2	0.2	-0.2
4.0	NC	-0.5	-1.0	NC	NC	NC
CHANGE FROM PREVIOUS θ = 0° AXIAL RATIO (dB)						
2.0	-0.5	NC	0.8	-0.3	0.3	0.2
3.0	-0.2	-0.3	0.5	NC	NC	-0.2
4.0	0.5	-0.5	0.3	0.2	NC	-0.5
CHANGE FROM REFERENCE θ = 0° AXIAL RATIO (dB)						
2.0	-0.5	-0.5	0.3	NC	0.3	0.5
3.0	-0.2	-0.5	NC	NC	NC	-0.2
4.0	0.5	NC	0.3	0.5	0.5	NC
VSWR						

	REF	1	2	3	4	5	6
2.0 TO 4.0	<2.3	<2.2	<2.2	<2.3	<2.3	<2.3	<2.3

NOTES: NC = NO CHANGE

tures from comparable thermocouples on the breadboard and Prototype No. 1 test articles. This change produced a 28 to 33 K (50 to 60°F) increase in maximum skin temperatures and an 8 to 11 K (15 to 20°F) increase in temperatures on the antenna (the latter not shown on figure 50). If the test container assembly had been eliminated, these temperatures would have been even higher, and most likely at about the design magnitude.

During tests P1-13 and P1-14, with the prototype unit thermally isolated from the test container assembly, the structural skin temperatures measured were about 400 K (260°F) and 433 K (320°F) for initial temperature of room ambient and 330 K (135°F), respectively. During these two tests, thermo-

TABLE XXVI
SA S-BAND ANTENNA GAIN, AXIAL RATIO, AND VSWR COMPARISONS

FREQ. (GHz)	THERMAL TEST					
	1	2	3	4	5	6
CHANGE FROM PREVIOUS PEAK LINEAR GAIN (dB)						
2.6	NC	NC	-0.2	NC	NC	-0.8
3.9	NC	-1.0	1.0	0.2	NC	-0.2
5.2	0.2	0.8	BD	-0.2	0.2	-0.8
CHANGE FROM REFERENCE PEAK LINEAR GAIN (dB)						
2.6	NC	NC	-0.2	-0.2	-0.2	-1.0
3.9	NC	-1.0	NC	0.2	0.2	NC
5.2	0.2	1.0	BD	0.8	1.0	0.2
CHANGE FROM PREVIOUS θ = 0° AXIAL RATIO (dB)						
2.6	NC	0.2	NC	NC	0.2	0.3
3.9	NC	NC	-0.5	NC	NC	0.3
5.2	NC	NC	NC	0.5	-0.5	NC
CHANGE FROM REFERENCE θ = 0° AXIAL RATIO (dB)						
2.6	NC	0.2	0.2	0.2	0.4	0.7
3.9	NC	NC	-0.5	-0.5	-0.5	-0.2
5.2	NC	NC	NC	0.5	NC	NC
VSWR						

	REF	1	2	3	4	5	6
2.3 TO 5.5	<1.8	<1.8	<1.8	<1.6	<1.7	<1.9	<1.8

NOTES: NC = NO CHANGE
BD = BAD DATA

couples on the sides and rear surface of the test container assembly increased 44 K (80°F) and 28 K (50°F), respectively, above the starting ambient temperature. This indicates that, although "isolated," the test container assembly was still influencing the backside temperature responses.

Silicone resin exothermic reaction: Reference 1 described short term temperature peaks which were encountered on the breadboard and Prototype No. 1 units during the first test on each in the arc tunnel. These temperature peaks were attributed to an exothermic reaction associated with the silicone resin

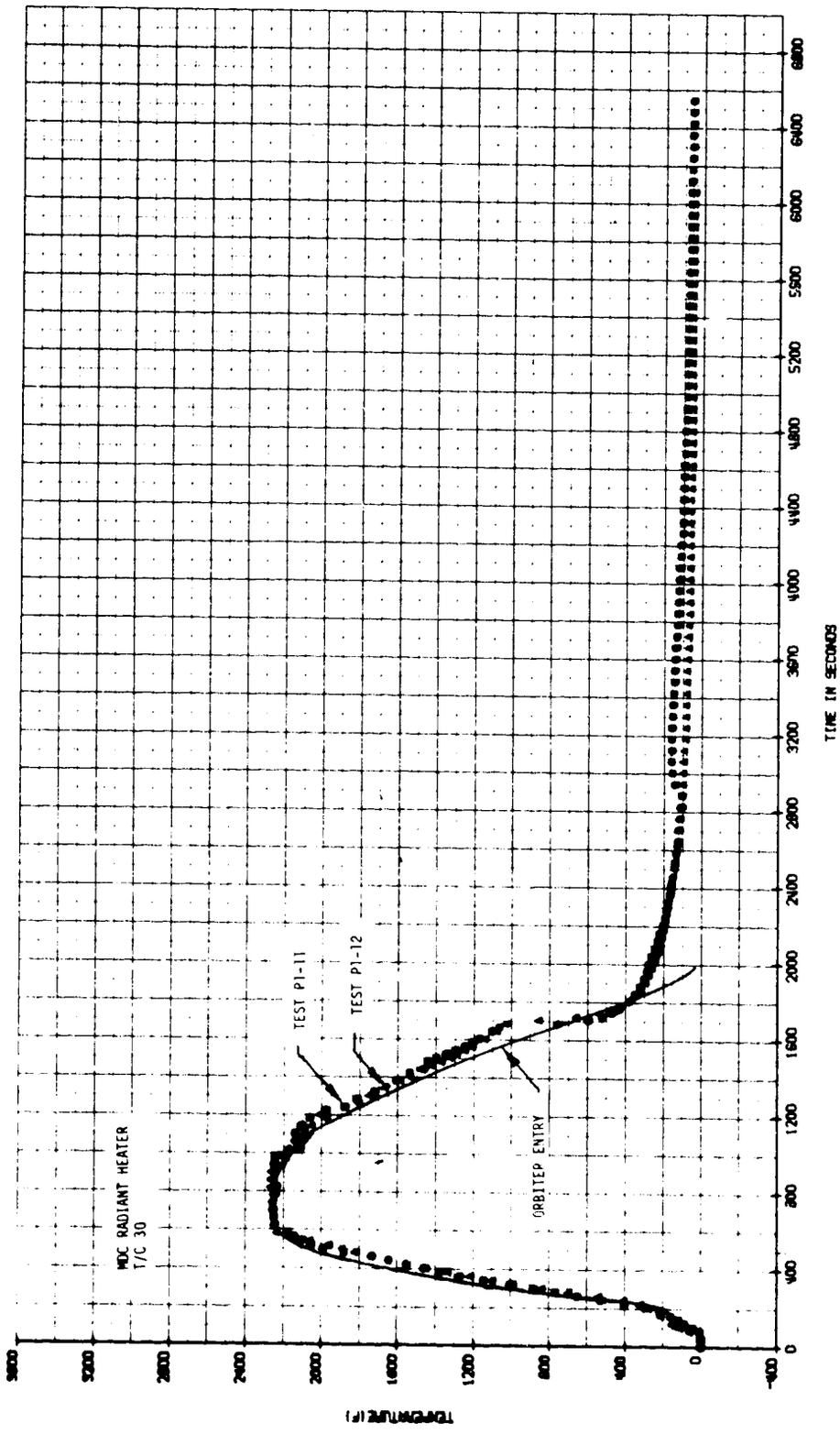

FIGURE 102 HRSI SURFACE TEMPERATURE REPEATABILITY

used for water proofing. The high temperatures experienced during the first test of Prototype No. 2 are much more significant than those of reference 1 and are also attributed to an exothermic reaction.

This exothermic reaction resulted in a black carbonaceous substance deposit on the surface and in the gaps between the HRSI tiles (figure 47), which had significant effect on the electrical performance as discussed in the preceding subsection on Electrical Tests. Deposits of this nature have been observed in other tests with LI-1500 tiles, but never of such significance. Only insignificant traces of a black deposit were noted in the gaps or window attachment holes of the breadboard and Prototype No. 1 units tested in the NASA-JSC arc tunnel. In the arc tunnel tests the plasma flow probably carried away the products of the silicone combustion as would likely be the case during Orbiter entry.

The severity of these deposits and the high temperatures during the first tests on Prototype No. 2 are attributed to a combination of factors, such as:

(a) The model was mounted face down. (In the arc tunnel it was mounted on its side.) The silicone vaporizes, outgasses and ignites on the surfaces. The products of incomplete combustion have a tendency to rise but have no place to go except onto the model.

(b) Heating was by radiation instead of convection. There was no gas flow across the model to carry off combustion products or a boundary layer to transport products away from the surface.

(c) Surface temperature and pressure (likely the most significant factor) were higher than in the arc tunnel, providing an atmosphere more conducive to ignition.

(d) The concentration of silicone was "somewhat" high.

Thus, future antenna testing should use HRSI tiles preheated in such a manner to prevent the formation of the deposit on the HRSI tiles or, if virgin HRSI is used, the test installation must be such that this exothermic reaction does not add extra heat to the test article or cause deposits on the HRSI.

Physical examination: Observations from visual inspection of Prototype No. 2 after test P2-1 are: (1) the black deposit was most severe on the edges of the outside tiles and in the tile gaps (figure 47); (2) the deposit did not extend as deep into the narrower gaps; (3) the RL-1973 strain isolator, which was exposed around the test unit periphery, was badly oxidized, decomposed, and brittle; (4) the same material around the antenna window was still soft and pliable; (5) numerous coating cracks are visible in the edges of the outside tiles; and (6) after test P2-2, the surface color was somewhat lighter.

Wet film acetaldehyde NDE tests for coating cracks were performed on Prototype No. 1 before and after run P1-15. The crack patterns obtained from these tests are shown for comparison in figure 103. It can be seen that the number of cracks and surface area affected were greatly increased after the run. It is unknown whether lowering the temperature to 117 K (-250°F), or whether the

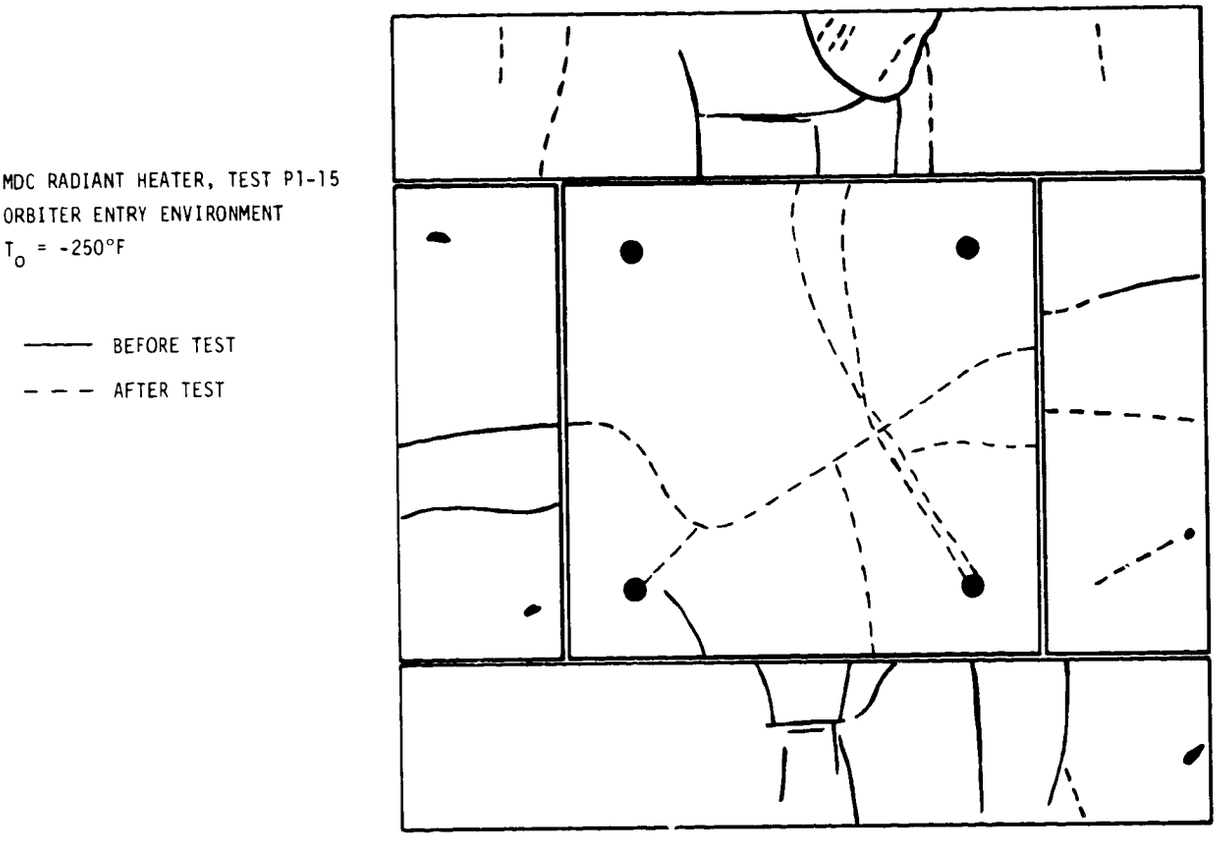

FIGURE 103 COATING CRACK PATTERN ON PROTOTYPE NO. 1 HRSI SURFACE AFTER TEST P1-15 (T_0 = 117K (-125°F))

subsequent thermal shock associated with the orbiter entry environment, was the primary cause of the increased cracks.

Heating technique comparison. - The correlation of plasma heating versus radiant heating for entry thermal environment simulation was obtained by comparing the data from test B-4 in the plasma jet with data from test B-12 in the radiant heater. Figure 41 compares the surface temperature histories (T/C 30) of the radiant heater test with those of the plasma test. Maximum temperatures measured during these two runs are presented in table XXVII. In general, the surface temperatures are similar but the peak temperatures reached during the radiant heater test are slightly lower than for the plasma testing. Some of the more significant temperature histories associated with these maximum temperatures from the radiant heating tests (table XXVII) are shown in figures 104 through 107.

The maximum temperatures of the thermal responses measured in the tile gaps (T/C 13, 15 & 16) during the respective tests differ significantly as shown in figure 104. The gap temperatures were, in general, much higher during

TABLE XXVII
COMPARISON OF PEAK TEMPERATURES FROM PLASMA AND RADIANT HEATING TESTS

THERMOCOUPLE		TEMPERATURE - K (°F)	
LOCATION	NO.	PLASMA (TEST B-4)	RADIANT (TEST B-12)
HRSI SURFACE	21	1327 (1930)	1266 (1820)
	26	1350 (1970)	1233 (1760)
	27	1377 (2020)	1272 (1830)
	28	1339 (1950)	1266 (1820)
	29	1350 (1970)	1272 (1830)
	30	1333 (1940)	1266 (1820)
HRSI IN DEPTH	18	526 (487)	534 (502)
	19	689 (780)	716 (830)
	20	-- --	955 (1259)
	23	561 (550)	597 (616)
	24	748 887	789 (960)
	25	-- --	966 (1280)
TILE GAPS	13	546 (523)	529 (493)
	14	715 (827)	714 (826)
	15	729 (853)	637 (687)
	16	795 (971)	742 (876)
	31	1302 (1885)	1175 (1655)
HRSI BOND LINE	12	376 (218)	374 (213)
	17	395 (251)	395 (252)
	22	393 (248)	410 (278)
ALUMINUM SKIN	8	340 (152)	355 (179)
	9	339 (151)	355 (179)
	10	334 (141)	353 (176)
	11	339 (150)	355 (179)
ANTENNA	3	314 (106)	329 (133)
	4	322 (120)	331 (136)
	5	327 (129)	335 (144)
	6	337 (147)	347 (166)
	7	337 (148)	352 (174)
TEST CONTAINER ASSY.	1	321 (118)	319 (115)

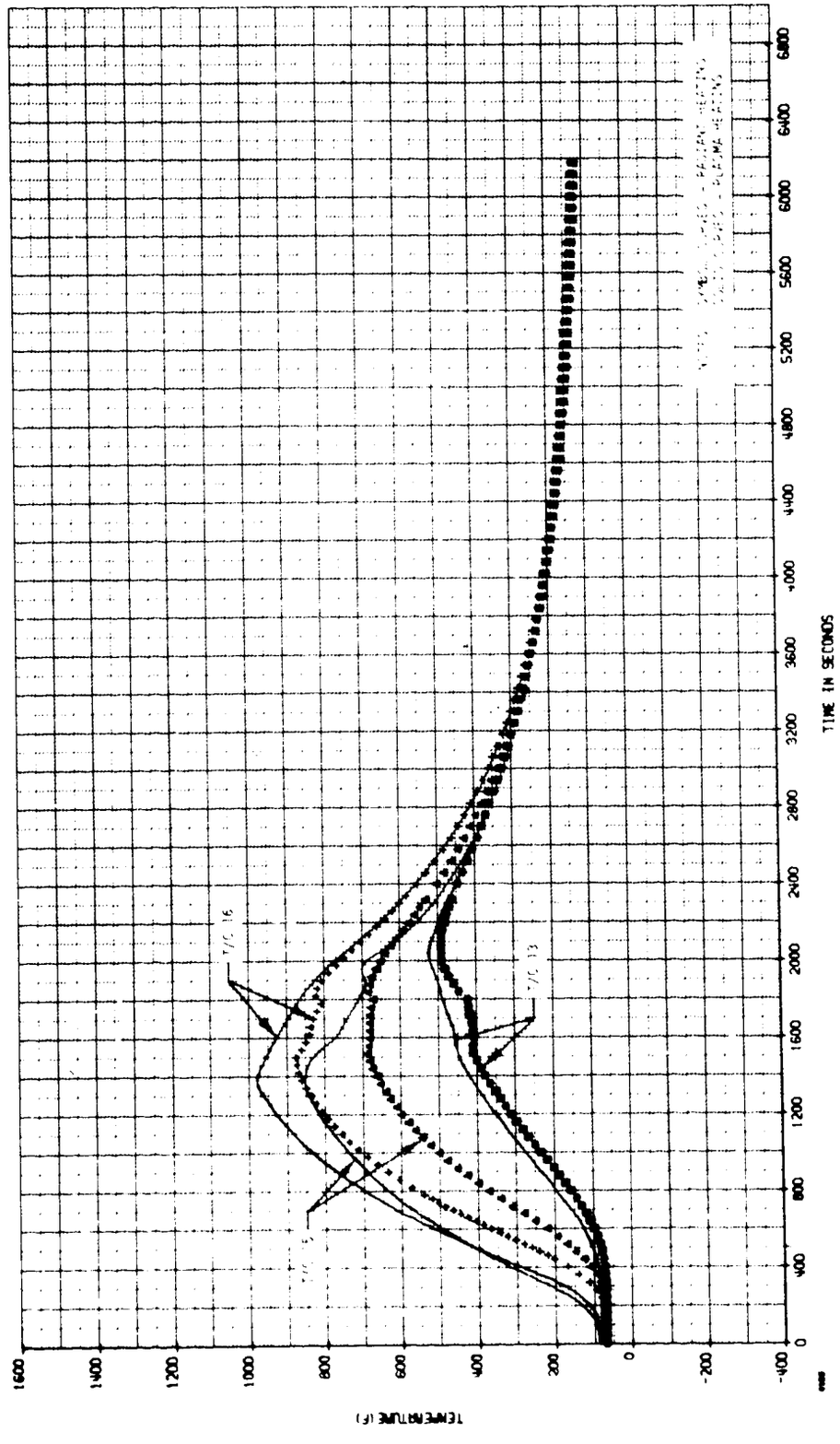

FIGURE 104 HEATING TECHNIQUE COMPARISONS - GAP TEMPERATURES

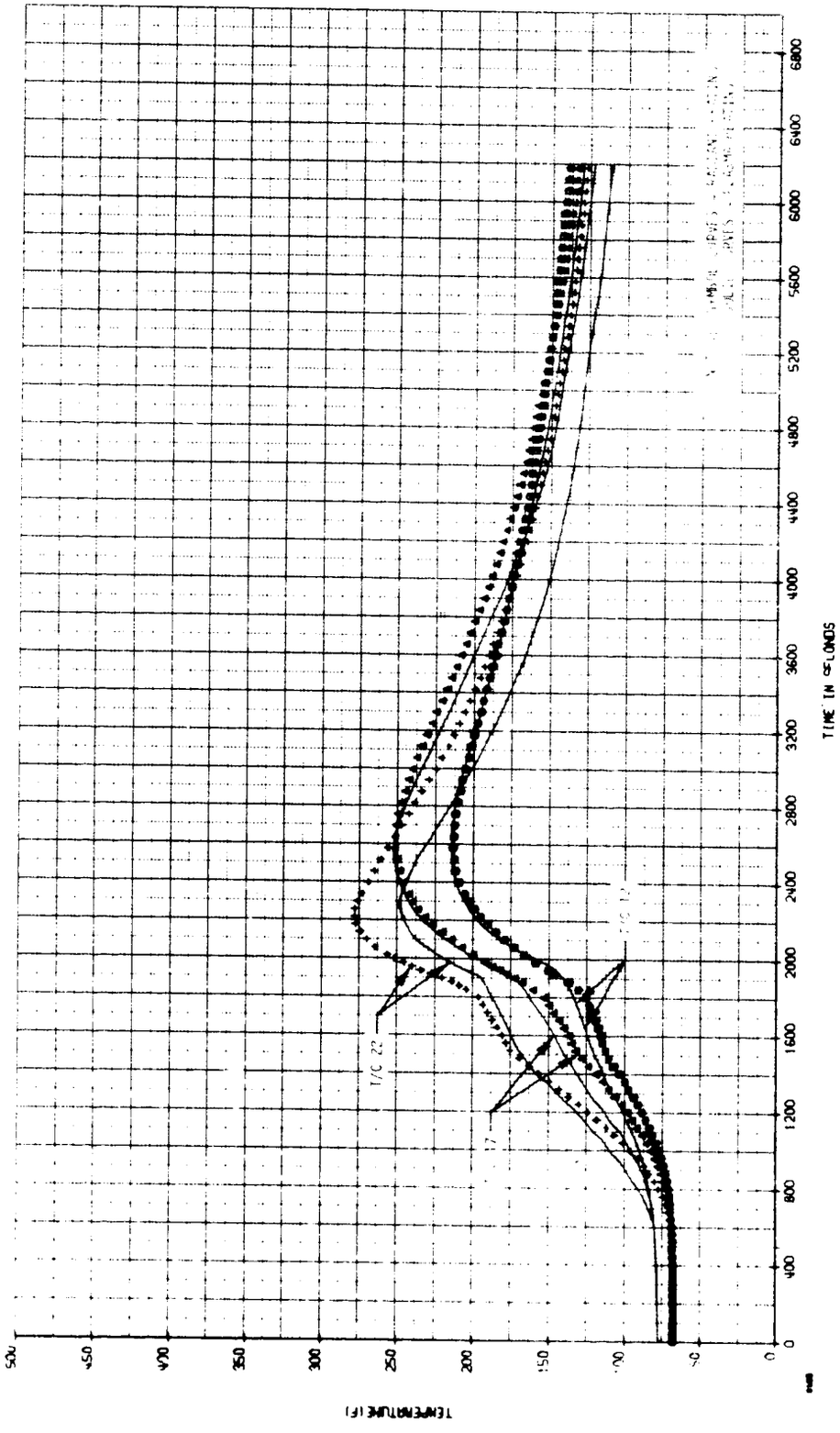

FIGURE 105 HEATING TECHNIQUE COMPARISONS – HRSI BONDLINE TEMPERATURES

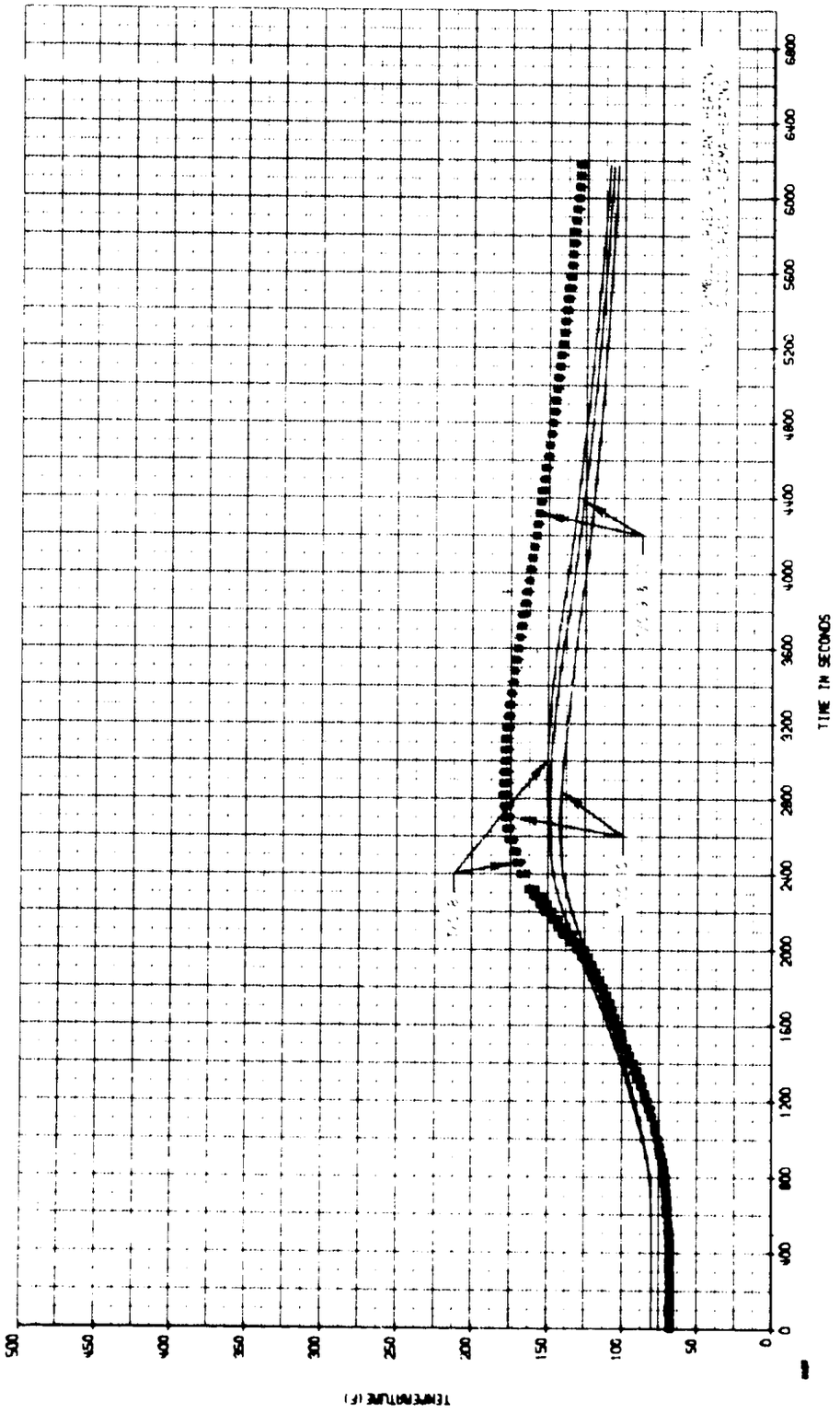

FIGURE 106 HEATING TECHNIQUE COMPARISONS – STRUCTURAL SKIN TEMPERATURES

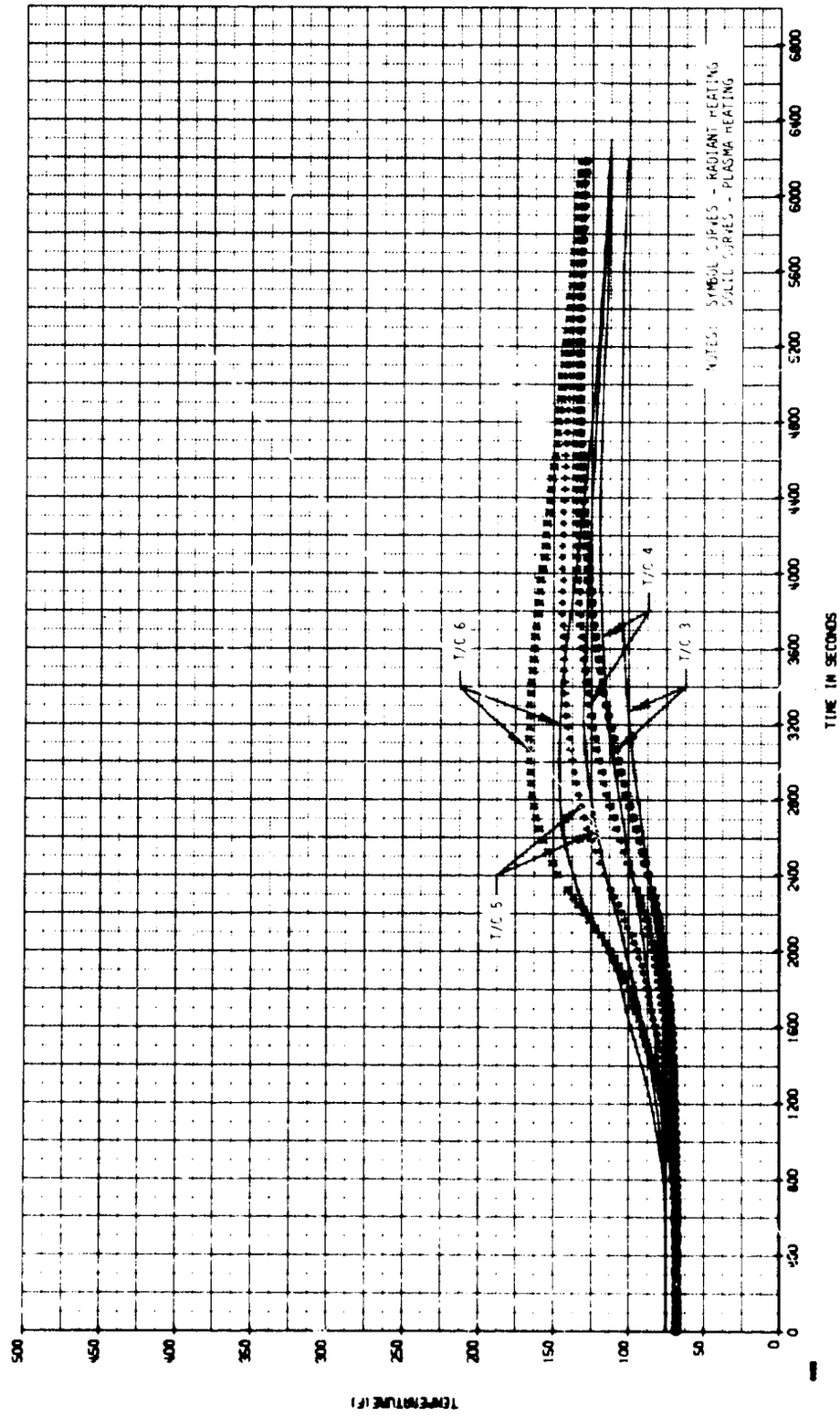

FIGURE 107 HEATING TECHNIQUE COMPARISONS – S-BAND ANTENNA TEMPERATURES

the arc tunnel test. This is to be expected since gap heat transfer is strongly influenced by local flow conditions and configuration. Some of the differences noted may also be attributed to the lower surface temperatures of the radiant heating tests. The maximum surface temperatures measured (table XXVII) were more than 56 K (100°F) lower during the radiant heating test. The maximum temperature of T/C 31, which was located in a gap stagnation region during the arc tunnel test was only about 36 K (65°F) Less than a nearby surface temperature (T/C 28). However, during radiant heating, this difference was 92 K (165°F), more than double the arc tunnel value.

Even with lower surface temperatures during the radiant test, the measurements of T/C 12, 17 and 22 at the HRSI bondline (table XXVII and figure 105) from both tests (B-4 and B-12) agree exceptionally well. Substructural skin and antenna temperatures (figures 106 and 107) were somewhat higher during the radiant test. Higher substrate temperatures during the radiant heater tests (even though lower surface temperatures were achieved) are primarily attributed to the test installation, but any transparence of the HRSI tiles could have permitted some heating of the substrate directly from the radiant source. For these tests, there was no water jacket to act as an infinite heat sink, and the test container assembly was thermally isolated from contact with the support structure.

From the preceding, it is concluded for testing of antennas or other components located under the TPS that either test facility will produce valid test results. However, the radiant heating facility can simulate the flight heat flux more accurately than the plasma facility. Further, the radiant heat facility provided a wide range of initial temperatures which are not generally available in a plasma facility and the radiant heat facility can be operated at a lower cost.

Off-the-shelf antennas. - The results of the OTS antenna thermal tests show only small temperature differences throughout the metal antenna cases and flanges. However, large temperature differences (78 K (140°F)) were measured over the antenna faces (i.e., fiberglass covers), where the effective thermal mass varied significantly. The Sanders S-band antenna, the one exception and the smallest antenna tested, did not have any significant gradient over the face.

The maximum variation of temperature over the antennas occurred at the end of the heating cycle for all tests. The peak temperatures occurred before or at the end of the heating cycle for tests 3 and 6 (initial temperature of room temperature). For tests 1, 2, 4 and 5, (initial temperatures of 172 K (-150°F) and 117 K (-250°F), the peak temperatures occurred 400 to 2000 seconds after the heating cycle ended and were approximately room temperature. The maximum and minimum peak temperatures during tests 3 and 6 (table XXVIII) show antenna case temperature variations of 0 to 8 K (0 to 15°F), antenna flange temperature variations of 1 to 18 K (1 to 32°F), and antenna face variations of 3 to 78 K (6 to 140°F). Some antenna face temperatures were higher than the control plate plate and showed more rapid response to the applied heat. The higher temperatures and rapid responses are due to the low mass and the low thermal conductivity of the fiberglass antenna faces and low density foams behind its faces.

TABLE XXVIII
MAXIMUM AND MINIMUM TEMPERATURES ON OTS ANTENNAS

ANTENNA	ANTENNA FACE						ANTENNA FLANGE						ANTENNA BASE					
	TEST 3			TEST 6			TEST 3			TEST 6			TEST 3			TEST 6		
	MAX	MIN	DIFF	MAX	MIN	DIFF	MAX	MIN	DIFF	MAX	MIN	DIFF	MAX	MIN	DIFF	MAX	MIN	DIFF
TRANSCO L-BAND	334	256	78	384	324	60	246	223	23	311	279	32	238	232	6	302	292	10
RANTEC C-BAND	335	258	77	398	342	56	254	246	8	334	322	12	254	247	7	333	324	9
D & M C-BAND	296	219	77	385	292	93	218	213	5	291	284	7	216	212	4	288	282	6
D & M L-BAND	272	224	48	440	300	140	212	186	26	280	248	32	205	193	12	271	256	15
SA S-BAND	234	228	6	320	307	13	225	224	1	301	300	1	224	224	0	330	299	1
AEL S-BAND	287	221	66	373	293	80	220	214	6	290	282	8	218	216	2	287	284	3
TRANSCO C-BAND	305	235	70	397	312	85	234	233	1	308	306	2	231	227	4	306	299	7

NOTES: MAX - MAXIMUM PEAK TEMPERATURE - °F

MIN - MINIMUM PEAK TEMPERATURE - °F

DIFF - DIFFERENCE BETWEEN MAXIMUM AND MINIMUM PEAK TEMPERATURE - °F

Temperature control technique: Typical comparisons of desired and measured control plate temperatures are shown in figures 108, 109 and 110 for tests A1, A2, A3 and C3 (note: alphabetic prefix denotes a particular test panel). In general the manual control of the heater resulted in measured temperature equal to or higher than the desired temperature and was considered satisfactory.

The temperature of the 0.15 cm (0.060 in.) aluminum control plate was always higher than the 0.15 cm (0.060 in.) aluminum ring around each antenna. This difference is due to the heat sink effect of the antennas and the mounting rings and was as expected. The control plate and skin ring measured temperatures for tests A3, B3, A6 and B6 are shown in figures 111 through 114 for comparison.

Structural skin and antenna temperatures: The skin ring temperatures were not uniform around its perimeter as shown by figures 111 through 114. The maximum and minimum peak temperatures of the skin ring and the antenna flange of each antenna for tests 3 and 6 are summarized in table XXIX. Table XXIX also includes the peak temperature of the control plate. The skin ring temperatures measured near the center of the test panels were higher than those measured on the outer edge of the test panels. This indicates heat losses around the perimeter of the test panel and/or non-uniform heating over the test article. However, resulting peak temperature differences of 24 K (43°F) or less are considered acceptable.

Physical examination: An overview of the visual inspection results is given in table XXX. The S-band antennas showed no physical changes during the tests. The Transco L-band antenna developed a slight delamination on the edge

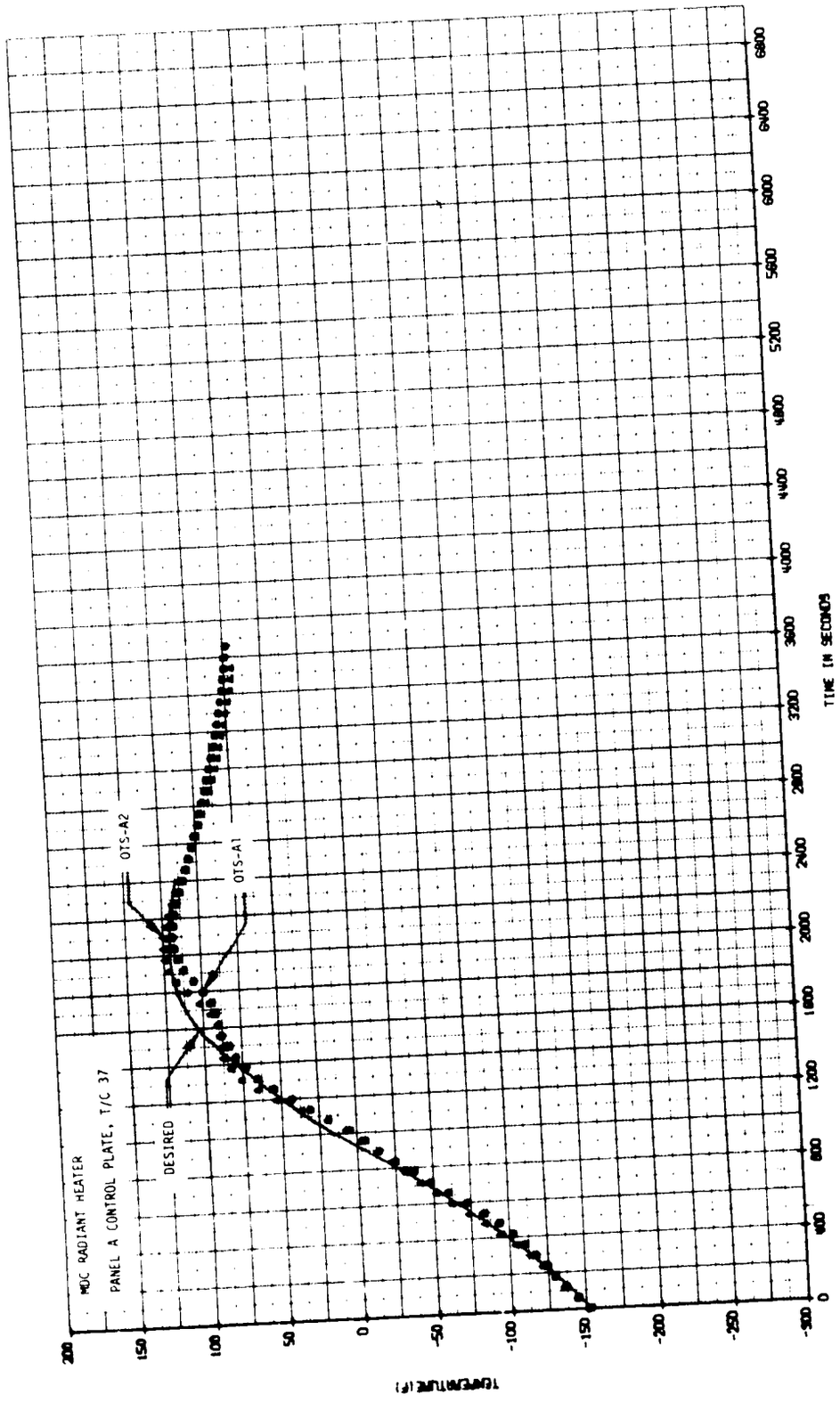

FIGURE 108 CONTROL PLATE TEMPERATURES – TEST OTS-A1/A2

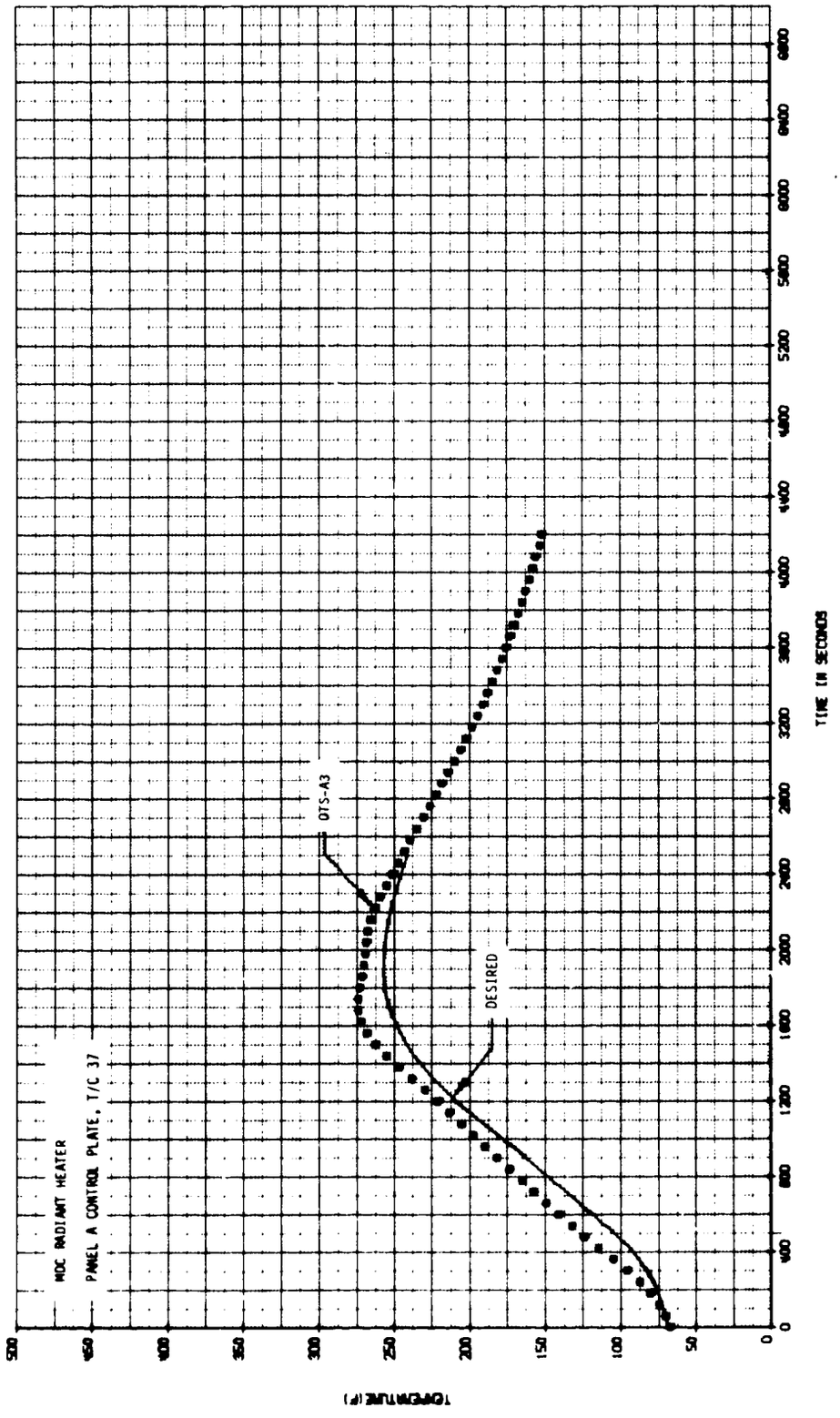

FIGURE 109 CONTROL PLATE TEMPERATURES - TEST OTS-A3

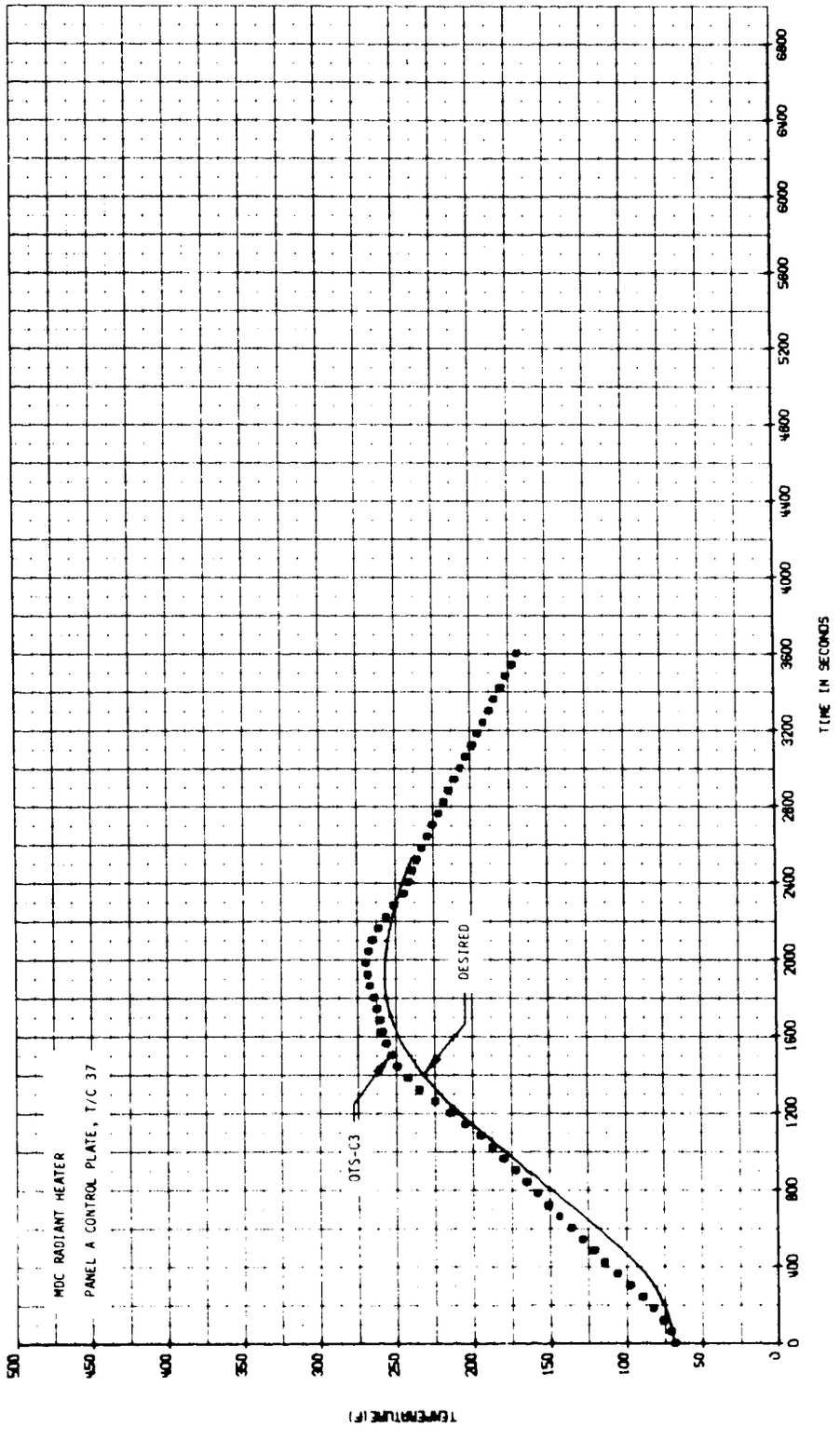

FIGURE 110 CONTROL PLATE TEMPERATURES - TEST OTS-C3

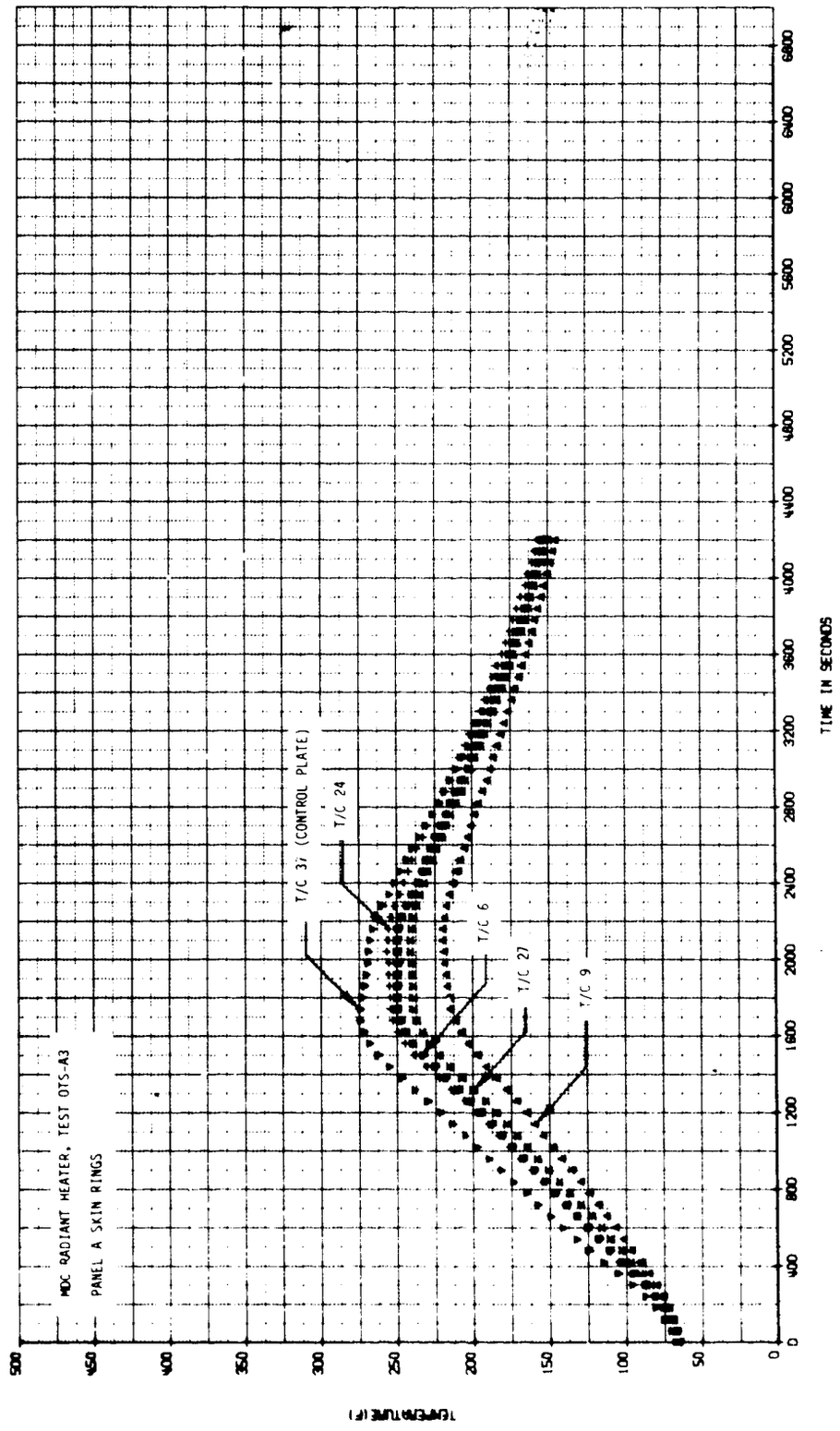

FIGURE 111 STRUCTURAL SKIN RING TEMPERATURES – TEST OTS-A3

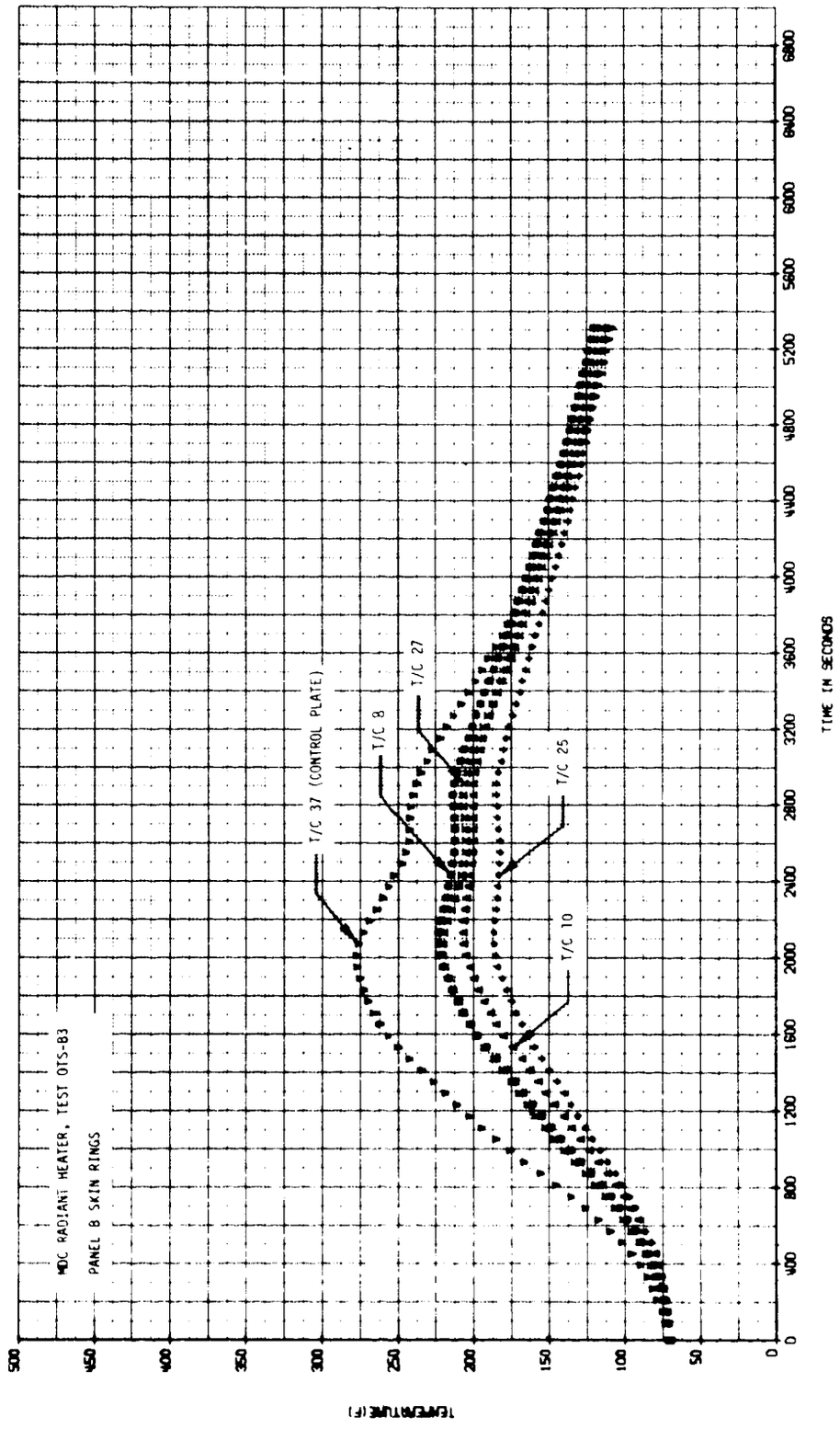

FIGURE 112 STRUCTURAL SKIN RING TEMPERATURES – TEST OTS-B3

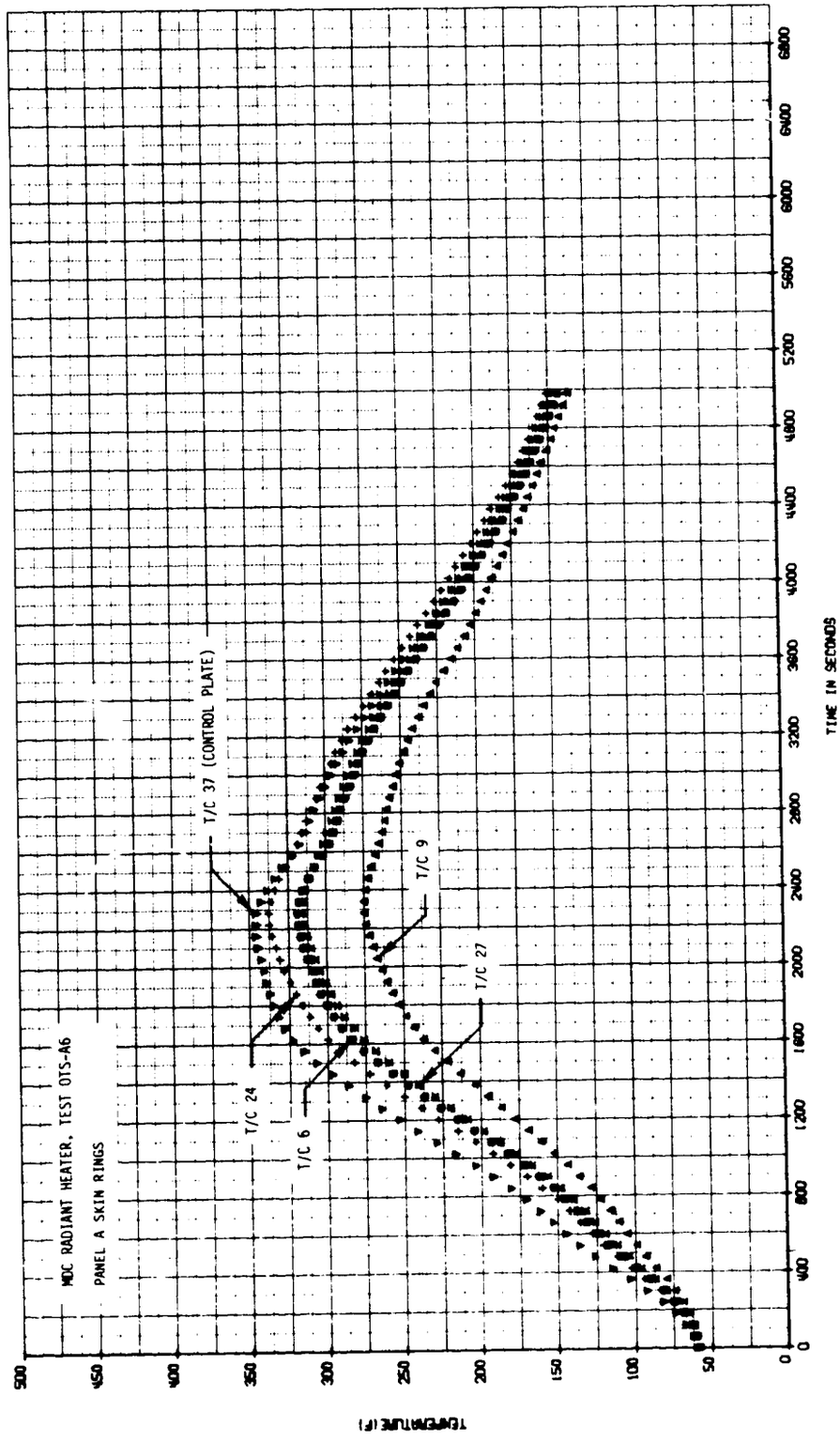

FIGURE 113 STRUCTURAL SKIN RING TEMPERATURES – TEST OTS-A6

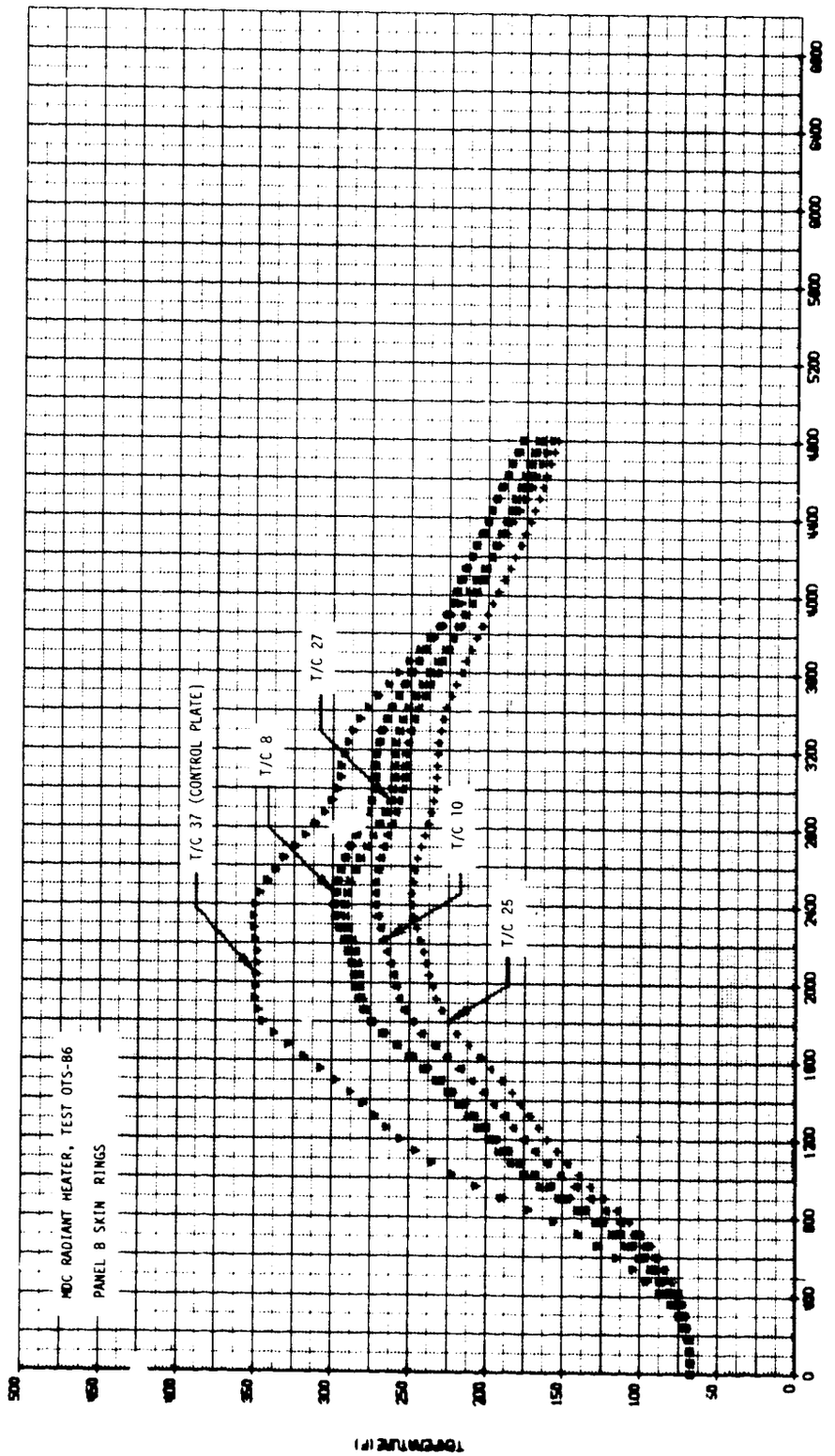

FIGURE 114 STRUCTURAL SKIN RING TEMPERATURES – TEST OTS-B6

TABLE XXIX
MAXIMUM AND MINIMUM PEAK TEMPERATURES ON PANEL SURFACE

ANTENNA	SKIN RING						ANTENNA FLANGE						CONTROL PLATE	
	TEST 3			TEST 6			TEST 3			TEST 6			TEST 3	TEST 6
	MAX	MIN	DIFF	MAX	MIN	DIFF	MAX	MIN	DIFF	MAX	MIN	DIFF	MAX	MAX
TRANSCO L-BAND	250	219	31	317	274	43	246	223	23	311	279	32	274	345
RANTEC C-BAND	256	240	16	337	315	22	254	246	8	334	322	12	274	345
D & M C-BAND	223	206	17	298	272	26	218	213	5	291	284	7	277	250
D & M L-BAND	220	187	33	291	248	43	212	186	26	280	248	32	277	350
SA S-BAND	227	222	5	304	296	8	225	224	1	301	300	1	268	350
AEL S-BAND	227	222	5	299	291	8	220	214	6	290	282	8	268	350
TRANSCO C-BAND	237	213	24	312	278	34	234	233	1	308	306	2	268	350

NOTES: MAX - MAXIMUM PEAK TEMPERATURE - °F

MIN - MINIMUM PEAK TEMPERATURE - °F

DIFF - DIFFERENCE BETWEEN MAXIMUM AND MINIMUM PEAK TEMPERATURE - °F

TABLE XXX
VISUAL INSPECTION RESULTS

ANTENNA	THERMAL TEST					
	1	2	3	4	5	6
TRANSCO L-BAND	DE-LAMINATION (a)(b)	NC (c)	NC	NC	NC	NC
D&M L-BAND	NC	NC	NC	NC	NC	BULGE (b)(d)
D&M C-BAND	NC	NC	BLISTER (b)	NC	NC	BULGE (b)(e)
RANTEC C-BAND	NC	NC	BULGE (b)(f)	NC	NC	NC
TRANSCO C-BAND	NC	NC	NC	NC	NC	BULGE (b)(g)
SA S-BAND	NC	NC	NC	NC	NC	NC
AEL S-BAND	NC	NC	NC	NC	NC	NC

NOTES:
(a) SEE FIGURE 115
(b) DEFECT ON ANTENNA FACE (OF COVER)
(c) NC = NO CHANGES
(d) SEE FIGURE 117
(e) SEE FIGURE 118
(f) SEE FIGURE 116
(g) SEE FIGURE 119

of the cover (figure 115) during the first test. However, this delamination did not worsen with the subsequent tests.

The Rantec C-band antenna developed a bulge on the antenna face during test 3 (figure 116). Electrical tests revealed no degradation in performance so it was included in the remaining thermal tests. These tests caused no change in the physical condition of the antenna. During test 6, where the design temperatures were exceeded, the Transco and D&M C-band and the D&M L-band antennas also developed bulges on the faces (i.e., fiberglass covers), as shown in figures 117, 118 and 119. Comparison of X-rays taken before testing and after the bulges developed did not reveal their cause. However, they did show that no mechanical breakage or distortion occurred. Therefore, the antennas were sectioned after electrical testing was completed. Examination of the sectioned antennas indicated that the bulges were caused by post curing of the foam in the antennas. A section of the Transco C-band antenna (figure 120) is typical and shows how the foam expanded. As noted in the subsection on Electrical Test Data Evaluation above, the physical changes due to post curing had negligible effect on the electrical performance of the OTS antennas.

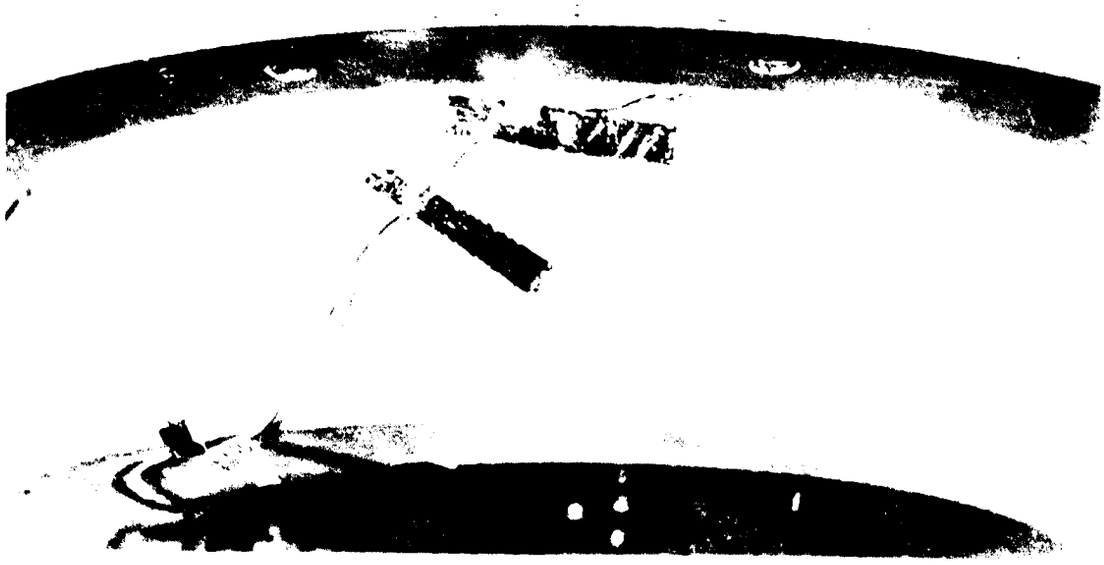

FIGURE 115 ANTENNA COVER DELAMINATION - TRANSCO L-BAND ANTENNA AFTER TEST OTS-A1

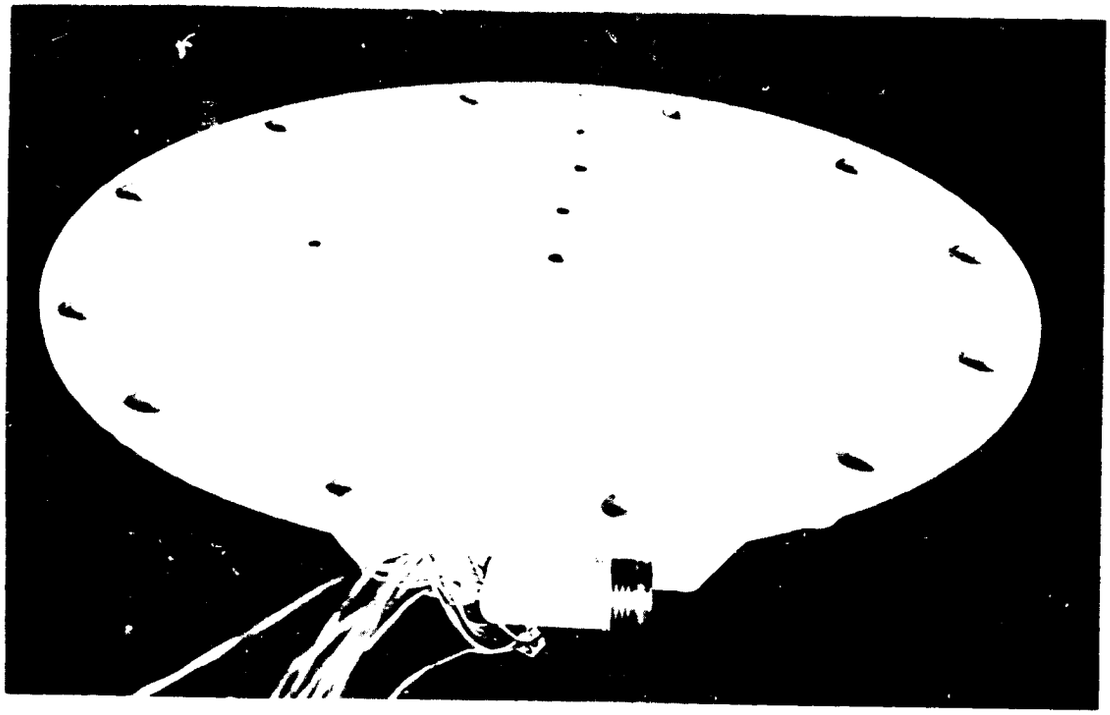

FIGURE 116 EFFECTS OF FOAM POSTCURING - RANTEC C-BAND ANTENNA AFTER TEST OTS-A3

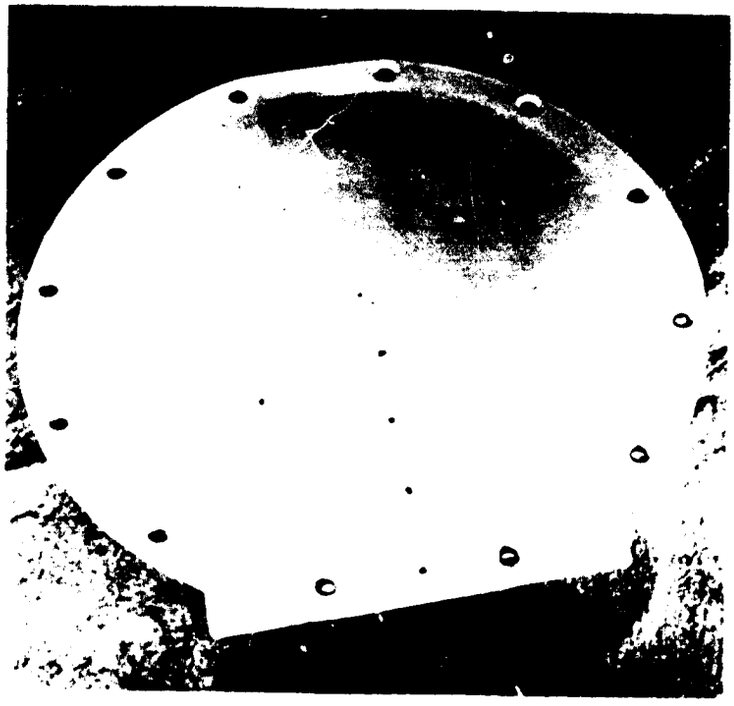

FIGURE 117 EFFECTS OF FOAM POSTCURING - D&M L-BAND ANTENNA AFTER TEST OTS-B6

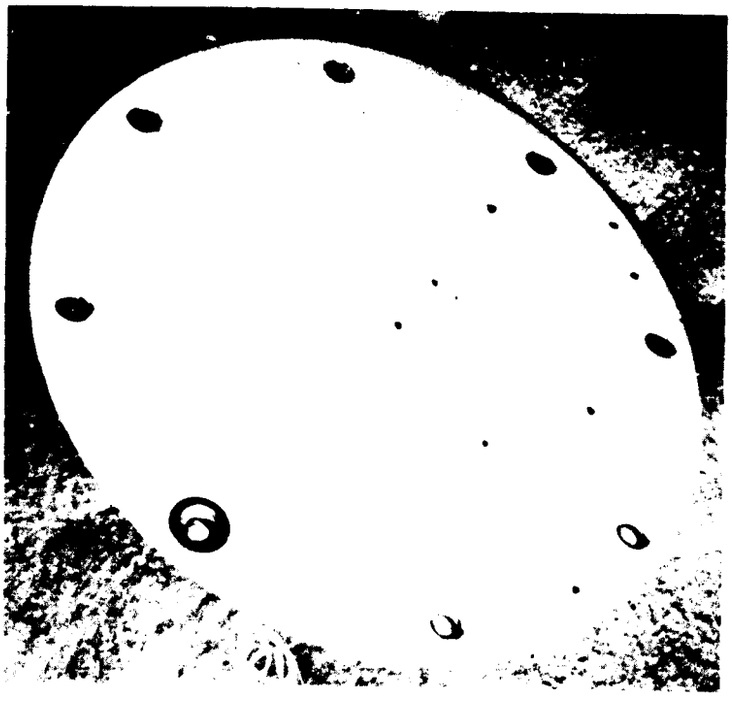

FIGURE 118 EFFECTS OF FOAM POSTCURING – D&M C-BAND ANTENNA AFTER TEST OTS-B6

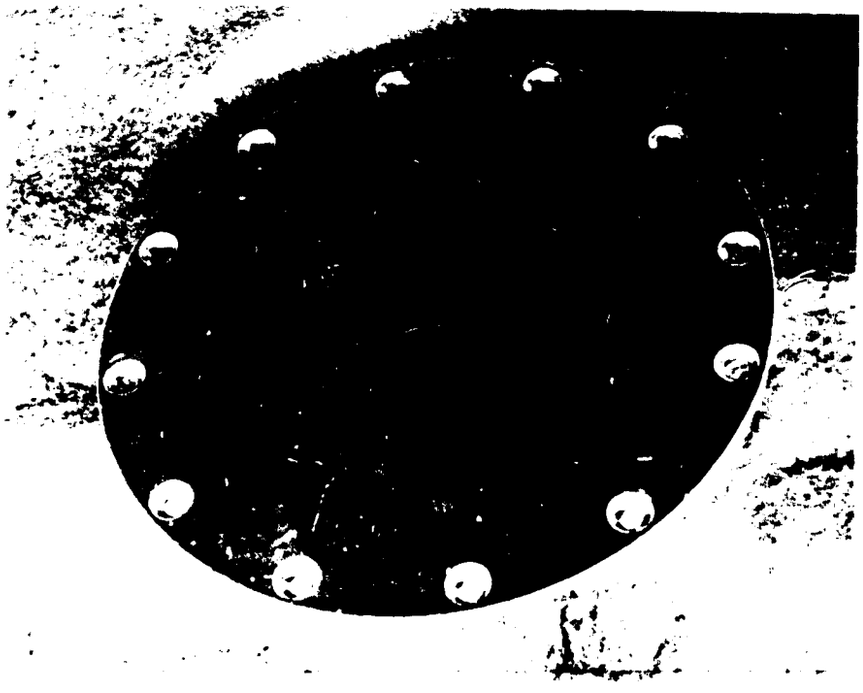

FIGURE 119 EFFECTS OF FOAM POSTCURING – TRANSCO C-BAND ANTENNA AFTER TEST OTS-C6

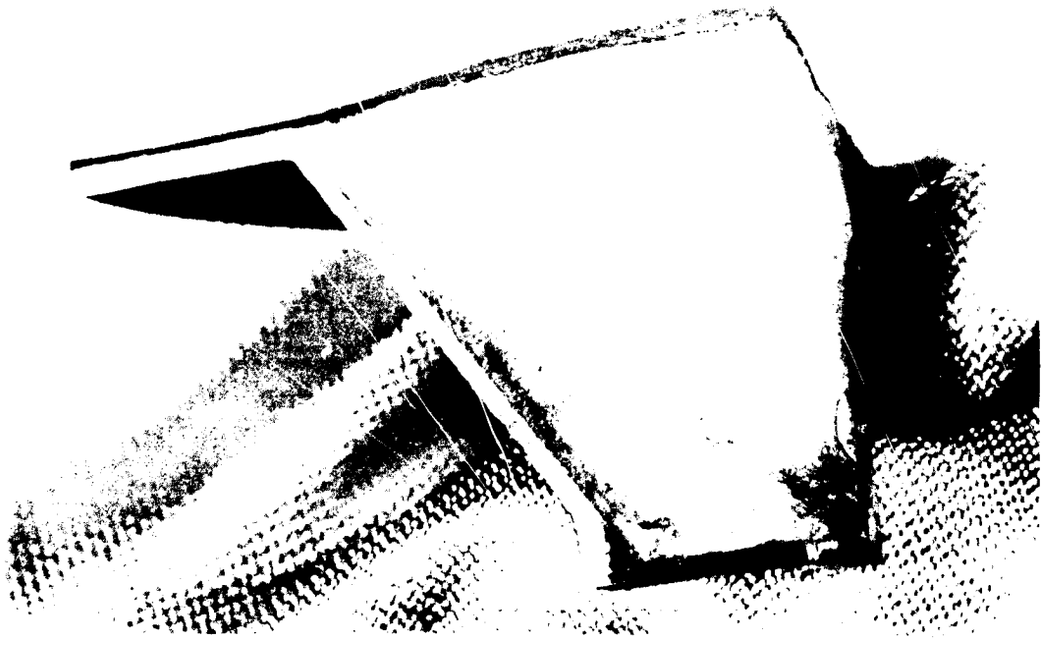

FIGURE 120 EFFECTS OF FOAM POSTCUPING – TYPICAL ANTENNA CROSS-SECTION

REFERENCES

1. Kuhlman, E. A.: High Temperature Antenna Development for Space Shuttle. (NAS 9-13004) McDonnell Douglas Astronautics Company - East, Volume I, Final Report, MDC E0896, July 1973.

2. Kuhlman, E. A.: Investigation of High Temperature Antennas for Space Shuttle. NASA CR-2294, November 1973.

END

DATE

FILMED

NOV 5 1974